Possible failure mechanisms of landslides in loess deposits

Dissertation

submitted to and approved by the

Department of Architecture, Civil Engineering and Environmental Sciences
University of Braunschweig – Institute of Technology

and the

Faculty of Engineering
University of Florence

in candidacy for the degree of a
Doktor-Ingenieurin (Dr.-Ing.) /
Dottore di Ricerca in "Riduzione del Rischio da Catastrofi Naturali su Strutture ed Infrastrutture" *)

by
Raushan Mamyrova
Born 15.10.1982
from Kochkor, Kyrgyz Republic

Submitted on	16 March 2012
Oral examination on	07 May 2012
Professorial advisors	Prof. Joachim Stahlmann
	Prof. Giovanni Vannucchi

2012

*) Either the German or the Italian form of the title may be used.

In Loving Memory of Mamyrov Ischeke

Acknowledgement

The current research was carried out in the framework of the International Research Training Group 'Risk Management of Natural and Civilization Hazards on Buildings and Infrastructure' between two Universities, namely Technical University of Braunschweig, Germany and University of Florence, Italy. It is my great pleasure to express my thankfulness to many people that supported me during the research work.

At first I would like to express my gratitude to my tutor Prof. Dr.-Ing. Joachim Stahlmann. I am thankful especially for his support and comments during the writing of this thesis. I am also thankful for the second tutor from Italy Prof. G. Vannucchi. My thanks go to Dr. Hans-Balder Havenith from the University of Liege (Belgium) for the suggestion of this research topic and his guidance and continuous support. Special thanks to Dr. Celine Bourdeau from LCPC Paris for her enormous support on numerical modelling part and for her patience, and valuable knowledge that she shared with me.

I am thankful to the technician of the Institute of Ground Construction and Soil Mechanics Uwe Zeemann for his help to conduct laboratory analyses. My thanks go to Dr. Gonghui Wang and to his students Fanyu Zhang and Lui Jin for their support to carry out the ring shear tests and to process the data at the Landslide Research Centre at Kyoto University in Japan. It was an amazing experience to work together.

My thanks are devoted to my colleagues from the Laboratory of Mining Geophysics of the Institute of Physics and Rock Mechanics of the National Academy of Sciences in Kyrgyz Republic, especially to the head of the laboratory Yuriy Georgievich Aleshin. I would like to say my gratitude and appreciation to Isakbek Asangalievich Torgoev.

At the end of my acknowledgement, I express my deepest gratitude to my parents, grandparents and my sublimes for their great support and encouragement. I would like to thank my husband for his patience and love that enabled me to complete this research work.

Abstract

Loess is a geological formation consisting of silt, clay and a small amount of sand transported and laid down by the wind. Due to the mountainous landscapes and neotectonic features, the landslides occurred in loess deposits are a major hazard in Central Asia. Ongoing field observations and investigations in Kyrgyzstan show an increasing landslide activity triggered by rainfalls and earthquakes in these regions. They indicate that the development of tension cracks in the upper part of the slope has a crucial effect on slope failure, especially in loess deposits. However, previous research studies do not clearly explain how these tension cracks impact loess slope stability. On one hand, many studies agree that existing cracks in the slope facilitate the infiltration of surface water, which may then contribute to failure. On the other hand, few have analysed the influence of the seismic response of ground cracks on slope stability. This thesis is focused on the latter effect, considering loess slope stability under dry conditions. The first part gives an overview and introduces the state of the art of current research. The second part of this research introduces the physical and mechanical properties of sampled soil that is obtained from the two landslides that are located in the Upper Mailuu-Suu Basin. Strength parameters are defined by performing of direct shear tests, triaxial tests and by using of ring shear tests. The third part presents the study of the seismic response of the slope by numerical simulations, using a 2-D finite difference code named FLAC. Tension cracks are modelled as nets of fissures and parameters as a length, direction and position within the slope crest are varied. As a case study, the Upper Koi-Tash landslide is studied.

Kurzfassung

Löss ist ein geologische Formation und beschreibt ein Sediment aus Schluff, Ton und einem geringen Anteil an Sand, das durch Wind transportiert und abgelegter wurde. Durch die Gebirgslandschaft und die tektonischen Aktivitäten, gehören Hangrutschungen in Löss-Ablagerungen zu einer der wesentlichen Naturgefahren in Zentral-Asien. Untersuchungen in Kirgisistan belegen eine Zunahme an Lössrutschungen in dieser Region, ausgelöst durch Niederschlag und Erdbeben. Zahlreiche Forschungen zeigen, dass das Auftreten von sog. Extensions-Spalten in den oberen Hangbereichen einen Einfluss auf das Böschungsversagen und somit auf das Auftreten von Rutschungen haben. Derzeit existieren jedoch keine detaillierten Untersuchungen hinsichtlich Wirkung solcher Extensions-Spalten auf die Böschungsstabilität. Zwar ist man sich in zahlreichen Studien darüber einig, dass durch das Auftreten solcher Spalten verstärkt Oberflächenwasser in den Hang infiltrieren kann und somit zum Böschungsbruch beiträgt. Diese Arbeit beschäftigt sich mit dem Einfluss von Bodenrissen unter seismischer Beanspruchung auf die Hang- und Böschungsstabilität. Im ersten Kapitel werden hierzu die allgemeinen Kenntnisse und der derzeitige Forschungsstand dargestellt. Der zweite Teil dieser Arbeit beschäftigt sich mit den physikalischen und mechanischen Eigenschaften von Lössproben, die an zwei Rutschungen aus dem oberen Mailuu-Suu Tal (Kirgisistan) genommen wurden. Für die Bestimmung der Scherparameter wurden direkte Scherversuche, Triaxialscherversuche und Ringschertests durchgeführt. Im dritten Teil der Arbeit wird die seismische Einwirkung auf die Böschungsstabilität mittels numerischer Simulation unter Verwendung des 2-D Finit-Differenz-Codes FLAC untersucht. Extensions-Spalten werden als Netz von Rissen modelliert und die verschiedenen Parameter, wie Länge, Neigung und Abstand zur Geländekante werden variiert. Als Fallbeispiel wird die „Upper-Koi-Tash“ Rutschung untersucht.

Table of contents

Chapter 1: Introduction

Mass movements are one of the geological hazards that occur in mountainous regions all over the world. The involved soil mass has a certain impact on the kinematical behaviour of a landslide. One of such soil type is loess, fine-grained yellow sediment. Landslides in loess mass can fail and travel in long distances. Historical data have shown that landslides developed in loess deposits are one of the catastrophic mass movements that cause enormous casualties and damages to the environment. Disastrous loess landslides mainly occur in mountainous regions by seismic activities. Due to the geologic features and tectonic activities, the countries of Central Asia and China are prone to the development of catastrophic loess flows.

The Haiyuan earthquake with a magnitude of M=8.5 on Richter scale that occurred in December 1920 in China caused loess landslides in three provinces of Shaanxi, Gansu and Ningxia. Gissar earthquake in Tajikistan with a M=5.5 triggered loess flows in flat slopes. About 200 people were killed. One of the notorious examples is the Kainama landslide that failed in 2004 (Fig. 1-1). Loess flow in a total volume of 220 000 m^3 covered the houses that caused to death of 33 people.

Fig. 1-1: The Kainama landslide in South Kyrgyzstan (Photograph by I.A. Torgoev, 2004)

In order to carry out disaster management in case of landslides, it is necessary to understand the main causes of these mass movements. Putting such aim forward, case studies of landslides located in South Kyrgyzstan (Central Asia) are studied in the present research work. Landslide investigations carried out in Kyrgyzstan showed that the landslides mainly develop in loess deposits with thicknesses of loess layers up to 50 m. Most of these landslides were triggered by earthquakes that occur very often in this region. One important aspect that can cause to slope instability is appearance of tension cracks. These weak zones contribute to decrease the strength of slope material. The present work aims to analyse which pattern of loess slope facilitates the slope instability.

1.1 Objectives

Landslides are one of the natural hazards that cause to excessive damages to infrastructures and fatalities (Fig. 1-2). According to the material components the mass movements can be divided into rock avalanches and debris flows and the mechanisms can be falls, topples, slides, spreads and flows (VARNES, 1978). Triggering factors of the landslide movement can be manifold (POPESCU, 1996). The most triggering factors as intense rainfall, earthquake shaking, volcanic eruption and storm wave rapidly increase the stresses and reduce the strength of slope material. In some cases, a landslide occurs by combination of variety of causes, as chemical or physical weathering of materials that gradually softens the slope material and finally leads to landslide. It is also important to identify the slip surfaces of mass movement to know the size and shape of mass movements.

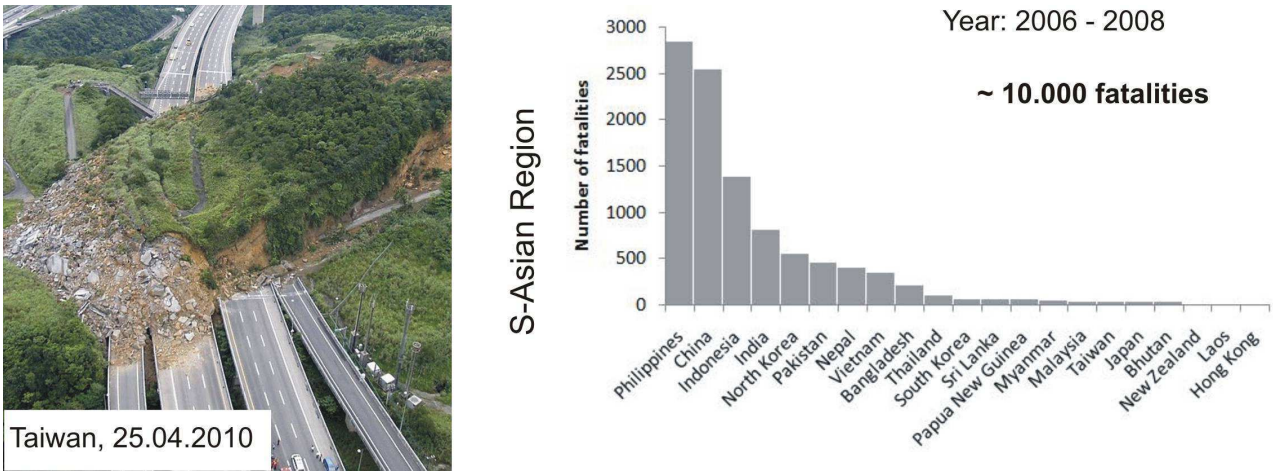

Fig. 1-2: Landslide in Taiwan in 2010 and number of fatalities of the S-Asian region for the time period 2006 to 2008 (source: Dave's landslide blog).

When the strength of slope material decreases, creeping within the slope starts and a main failure occurs. Runout of a landslide depends on the size of involving mass, on features of slope geometry and on presence of water within the sliding mass. One of the important factors of long distance runout is a slope material. Loess is concerned to have such behavior. This sediment is mainly distributed in Central Asia including Kyrgyzstan. Here, loess deposits can have thicknesses of up to 50 m.

Many areas of Kyrgyzstan are susceptible to numerous types of slope failures. Many of them are destructive. Combination of climatic and geological factors causes to development of landslides within the mountain ranges. Due to the tectonic features of the region, the most of the landslides are triggered by earthquakes. Such mass movements located in the southern part of Kyrgyzstan, which is densely settled due to the favorable climate condition to agriculture. Long-term studies of a landslide situation in the country presented the increasing amount of landslides. It is necessary to study loess landslides and possible failure mechanisms, in order to perform reliable disaster management.

Although this topic is strongly highlighted among authorities and researchers, there are still issues in terms of seismic impact on a loess slope in terms of ground motion and its anomalies. Another important problem should be taken into consideration by investigation of loess landslides. This regards impact of tension cracks on the slope. Numerous field observations presented an occurrence of tension cracks near the crest of a slope that cause to failure. However, an impact of tension cracks on a loess slope is less investigated. This research presents the behavior of loess slope in case of seismic conditions without water. Thereby it is researched if the influence of shaking is strong enough to destabilize dry slopes.

1.2 Landslide risk

Economic losses of disastrous landslides can be claimed up to several millions of US$. Every year several hundreds of people loose their lives. Statistical analyses show that geohazards, like landslides in soil and rock, which are induced by earthquakes, rainfall, flooding or human activity, are dramatically increasing world-wide (REPORT Munich Re, 2009). Landslides continue to be a major hazard and are the 7th largest killer among natural disasters after droughts, windstorms, floods, earthquakes, volcanoes and extreme temperatures. According to the CRED database (Centre for Research on the Epidemiology of Disasters*)*, landslides have claimed 800-1.000 lives per year in average during the last 20 years and also enormous economic damages. The USGS (The United States Geological Survey) describes that landslides occur in the U.S. territories, and cause 1-2 billion US$ in damages and more than 25 fatalities on average each year. Japanese annual losses are reported to be between 4 and 6 billion US$. After information of the United Nations University (UN University News Release, 2006), Asia suffered 220 landslides in the past century – by far the most of any world region – with numerous fatalities. All these statistical information shows that there is a primary importance to assess the landslide risk and to get information on an impact of such events to property, infrastructure and to people.

In general the term "risk" describes "the combination of the probability (P) of an event and its negative consequences (C)", and thus can be expressed by the formula:

$$\text{Risk (R)} = \text{Probability (P)} \times \text{Consequences (C)}$$

There are various definitions of risk exist in the world. This issue causes to difficulties in risk and disaster management, and finally in disaster response (PLIEFKE et al, 2007). A general scheme for risk management is described as "*a systematic approach and practice of managing uncertainty to minimize potential harm and loss*" (PLIEFKE et al, 2007). It consists of Risk Identification, Risk Assessment and Risk Treatment (Fig. 1-3).

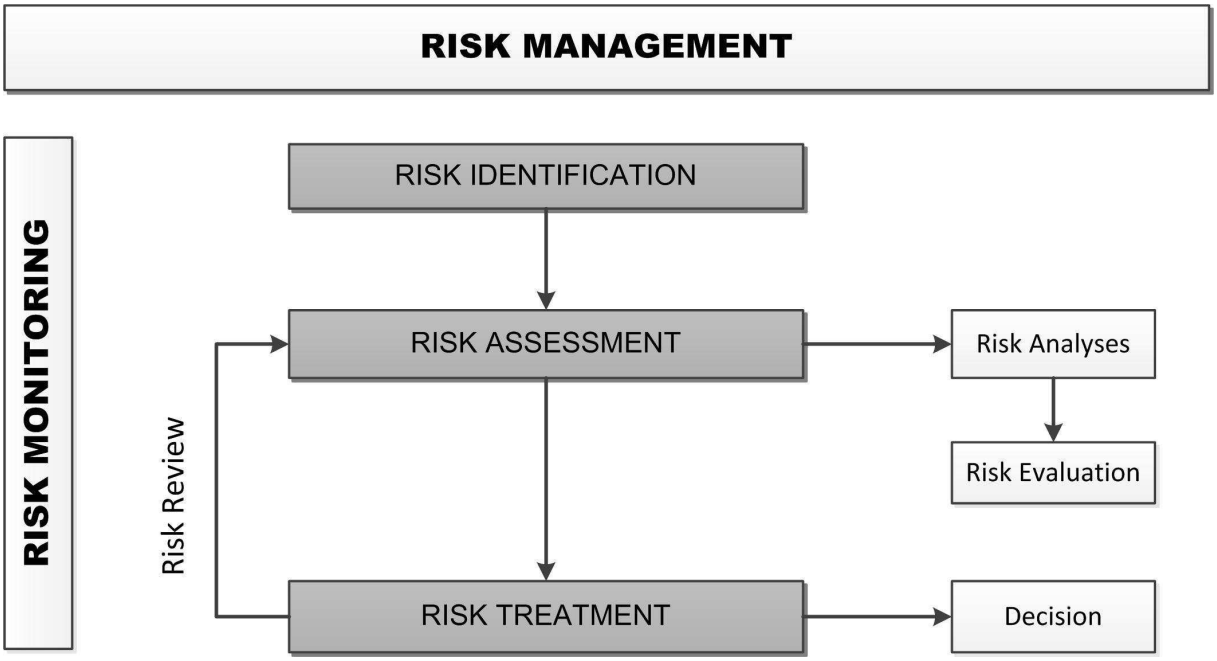

Fig. 1-3: The general risk management framework (PLIEFKE et al, 2007)

In the first element "***Risk Identification***" recognition of harms as natural hazards or man-made activities and consequences are included. (PLIEFKE et al, 2007). Concerning landslides, this step contains the identification of the movement process (falling, spreading, sliding etc.), together with the main influencing and triggering factors and the determination of endangered areas, as villages or infrastructure. Thus, in this step, it is analysed, "what" is affected by "which landslide-type".

The next element of the risk management framework is the ***Risk Assessment***. In general, risk assessment describes a methodology to determine the nature and extent of risk (UNISDR, 2009). It consists of analysing potential hazards (Risk Analyses step) and evaluating existing conditions of vulnerability (Risk Evaluation step) that together could potentially harm exposed people, properties, services, livelihoods and the environment on which they depend. The process of risk assessment determines the quantitative and qualitative value of risk related to a specific situation or scenario and tries to estimate the threat that results from this risk. It consists of a review of the technical characteristics of the hazard (intensity, frequency, probability), analyses of exposure and vulnerability (physical, social, economic and environmental conditions), and evaluation of the effectiveness of existing/alternative capacities to absorb a possible event. For landslides, DAI (2002) divides the process of landslide risk assessment in the following issues that have to be addressed:

(a) probability of a landslide
(b) runout behavior of landslide
(c) vulnerability of property and people to landslide
(d) landslide risk to property and people
(e) management strategies and decision-making

The last element of the Risk Management Framework is the **Risk Treatment**, which deals with the response to the investigated and analysed risk, how to react and how to handle it.

According to the chosen analysing tools and the current conditions, a decision whether to accept, to transfer, to reject or to reduce a given risk can be derived. Concerning landslides, this can include the decision of monitoring a landslide area, or using of constructive measures to reduce the risk in a certain location.

The **Risk Review** process is responsible for adaptations and process-updating. New information and experiences gained in the course of the risk analyses are implemented in the risk management and thus allow a constantly improvement and process-evolution over the time.

The current research contributes mainly to the element of Risk Identification and to Risk Assessment for loess landslide areas of Kyrgyzstan. By defining the probability of failure within the loess slope, it is possible to determine a probable runout. Since a landslide developed in loess slope is specified by the long runout. Features of occurrence of landslides in loess are defined in order to assess the hazard. Furthermore, the current work analyses specific elements as tension cracks in loess landslides and its influence and behaviour under ground motion. Through this, information about surface displacement and failure processes can be gained and can be used for implementations in the assessment process of the risk management framework.

1.3 Methodology of research

Aim of this research work is to understand the possible failure mechanisms in loess slope under dynamic conditions. Cases of unstable loess slopes in South Kyrgyzstan are chosen for the investigation.

After the Introduction in the Chapter 1, **the second chapter** of this research presents an overview of the studied region – Kyrgyzstan. At first, geographical location, geological and neotectonic conditions are described. Landslide situation of the mountainous landscape is outlined in order to highlight the landslide problem in the country.

The chapter three describes loess as a geological/geotechnical material. Literature review is shown to introduce the main properties of loess.

In the **fourth chapter**, the range of mass movement types developed in loess deposits is presented. Numerous cases of catastrophic failure of loess landslides are shown especially concentrating on regions of north China, Gissar in Tajikistan and Fergana Basin, Kyrgyzstan. As the research deals with earthquake triggered mass movements, **chapter five** gives an overview of methods to investigate seismic induced landslides. Based on the review on several case examples, a hypothesis about possible causes of failure in loess slope is described in the **chapter six**.

In order to address the problems of modelling of loess slope, it is necessary to collect a set of strength parameters that reflect the conditions of the material in field conditions. This aim is achieved using laboratory tests on representative samples. **Chapter seven** of this work describes two landslide sites that were selected to get undisturbed loess samples. The

landslide sites are located in Upper Mailuu-Suu basin, Kyrgyzstan, Central Asia. Physical and mechanical properties of sampled soils are determined. Strength parameters are defined by performing direct shear and consolidated drained triaxial tests and by using of ring shear tests.

Numerical analyses are presented in the **chapter 8.** The aim is to determine an impact of strong ground motion in a loess slope. To determine an amplification of seismic waves on a slope, parametrical studies are carried out. The thickness of loess layer is varied in a slope case. In addition, an impact of tension cracks as weak zones is assessed. In order to observe the behaviour of tension cracks, parameters of cracks as inclination, depth and distance from the crest are varied. To introduce the real case study, the Upper Koi-Tash landslide is analysed.

Chapter 9 presents the main results of the research and conclusion based on laboratory testing and numerical modelling and gives a recommendation based on main results.

Chapter 2: Introduction to region

2.1 General information

Kyrgyzstan is a small republic located in Central Asia, surrounded by Kazakhstan in the north, China in the east, Tajikistan in the south and Uzbekistan in the west (Fig. 2-1). The country is characterized with mountainous landscape locating 56 per cent of whole territory at the altitude of 2600 meters. Its mountain ranges derive from a large mountain belt of Tien-Shan with the highest peak of 7439 meters.

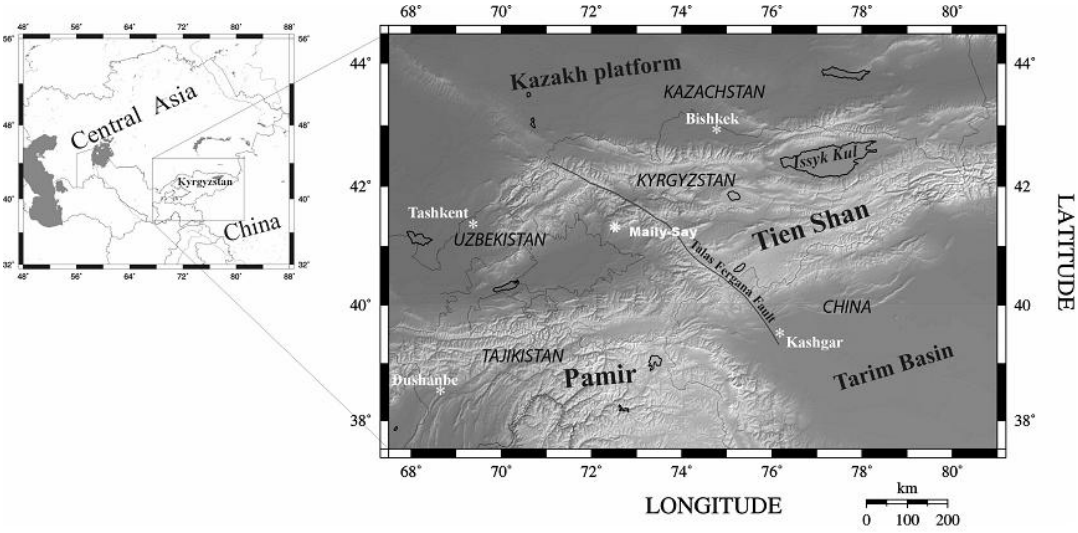

Fig. 2-1: Map of Central Asia with location of Kyrgyzstan (HAVENITH, 2002)

2.2 Geological context

The Indian sub-continent colliding with Southern Eurasia resulted in bedrock uplift by formation of world's largest mountains – Himalaya, Pamir and Tien Shan (Fig. 2-2). This collision affected the geological formation of Central Asian countries. The geology of Kyrgyzstan is complex. The mountains form an arc running through the country from west to east, with sub-parallel ranges separated by intermountain basins and valleys. The Fergana Range in south-central Kyrgyzstan runs in a northwest-southeast direction and marks the division between the principal tectonic blocks (HAVENITH, 2002) This effectively divides the Tien Shan into two; the Tien Shan in the north is made up of folded Caledonian sequences, while in the south of the lineament lie younger Hercynian rocks. This area of the country is further subdivided into the Central and Southern Tien Shan on account of their different histories of formation .

In the region where the Tien Shan Mountains lie, the crustal movements have taken place since the Archaean. In consequence, it contains a wide variety of igneous, sedimentary and metamorphic rocks, formed at different periods under different geodynamic conditions (BUSLOV, 2007)

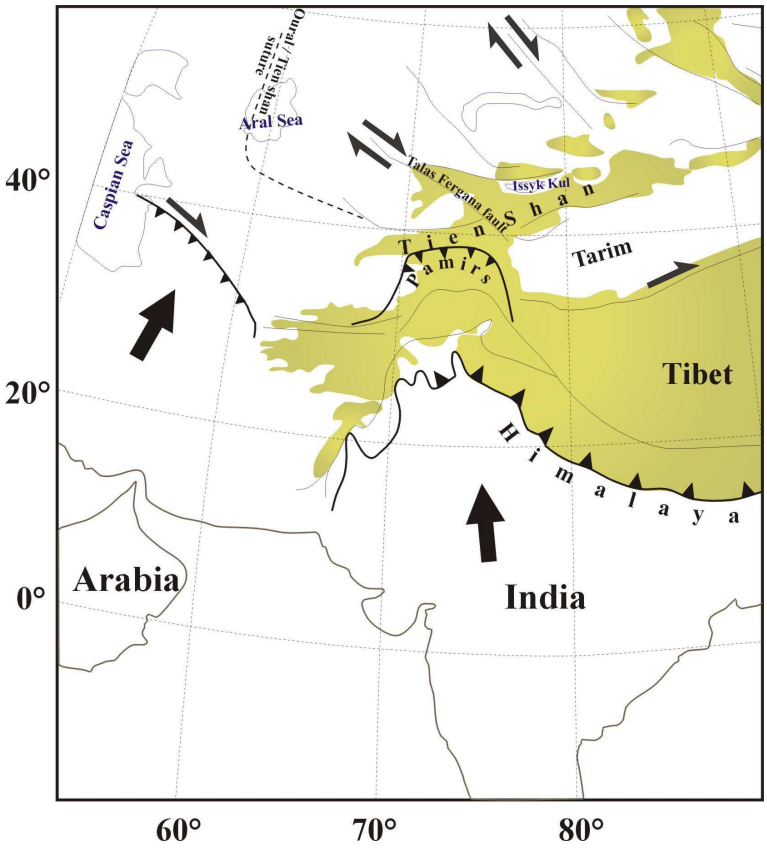

Fig. 2-2: Tectonic map of Central Asia and with the Himalaya, Pamir and Tian Shan Ranges. The regions located above 2000 m are shaded green (modified by H.-B. HAVENITH from BOSSU and GRASSO, 1996)

2.3 Seismic situation

Global Seismic Hazard Assessment Program (World Bank Report, 2008) presented that Kyrgyzstan is located in a high seismic hazard area. Every year, about 5000 earthquakes are registered by national seismic monitoring systems (ABDRAKHMATOV, 2003). Most of the earthquakes occur along the northern and southern limits of the mountain system and in the west of the Talas - Fergana fault. Fig. 2-3 shows strong seismic events in Kyrgyzstan (HAVENITH, 2002). The strongest one was the Chilik earthquake with a magnitude of 8.3 in 1889 (LEONOV, 1960) (Fig. 2-3b) and the Kemin earthquake with a magnitude of 8.2 which struck in 1911 (Fig. 2-3c). Because of this strong earthquake, 30 people were killed by a rock avalanche. The Verny earthquake with a magnitude of 7.3 took place in 1887 (Fig. 2-3a). The Chatkal earthquake with a magnitude of 7.5 occurred in 1946 (Fig. 2-3d). Among destructive earthquakes, Khait earthquake can be highlighted with a magnitude of 7.4 in 1949 (Fig. 2-3e). Although the epicenter was located in the Tajik Republic, there were strong seismic shocks felt near the border of south Kyrgyzstan (LEONOV, 1960). On October 6, 2008 an earthquake

with a magnitude 6.6 hit the Nura village in Kyrgyzstan, located northwest toward China's border. The epicenter was about 10 km from settlement and caused destruction to the whole village and the death of 75 people.

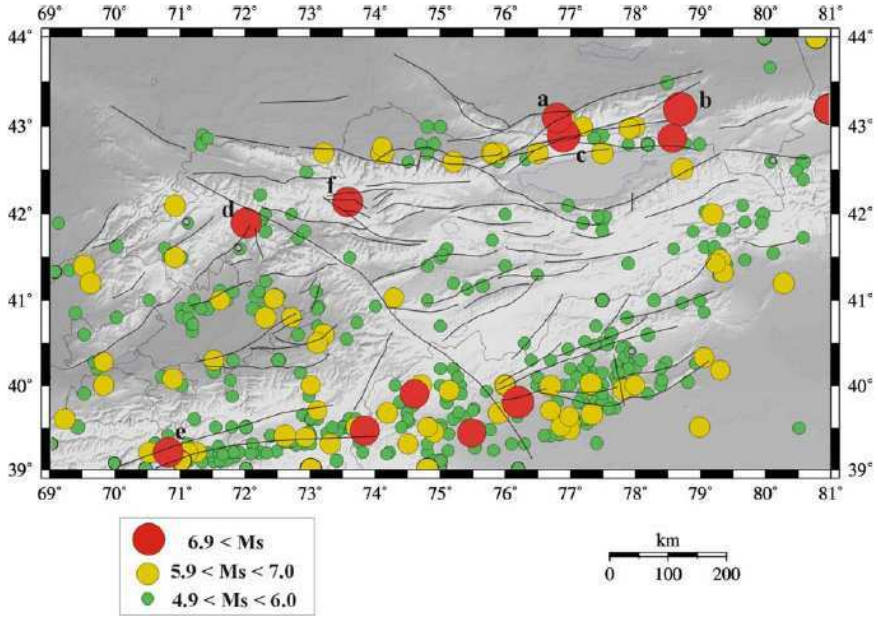

Fig. 2-3: Strong seismic events occurred in Kyrgyzstan (HAVENITH, 2002); a) Verny (1887): M=7.3, b) Chilik (1889): M=8.3; c) Kemin (1911): M=8.2; d) Chatkal (1946): e) M=7.5; Khait (1949): M=7.4; f) Suusamyr (1992): M=7.3

2.4 Landslide hazardous zones in Kyrgyzstan

Extensive areas of Kyrgyzstan are characterized by the presence of high landslide hazards. NADIM et al (2006) presented the worldwide landslide hazard map; Kyrgyzstan is counted to have medium to high landslide hazards after Tajikistan (Fig. 2-4). There are about 5000 potentially active landslide sites, about 3500 of which are in the southern part of the country. Every year landslides in Kyrgyzstan cause large economic damages (from US$2 million to 20 million) (World Bank Report, 2008). A landslide which occurred in 1992 disconnected the main Bishkek — Osh highway for several days. Therefore, communication was disrupted between northern and southern regions of the country for a long period of time. One of the major landslide disasters occurred on April 20, 2003 when a landslide near Uzgen in the Osh region killed 38 people, while 84 families lost their houses (Internal Reports of the National Academy of Sciences of Kyrgyzstan, 2003). The Kainama loess slide killed 33 people in 2003, in the Alai region. Such landslides exemplify that the southern part of the country is prone to catastrophic landslides. Because of loess deposits in south Kyrgyzstan, the landslides that developed in such loose material are characterized by their long runout and velocity.

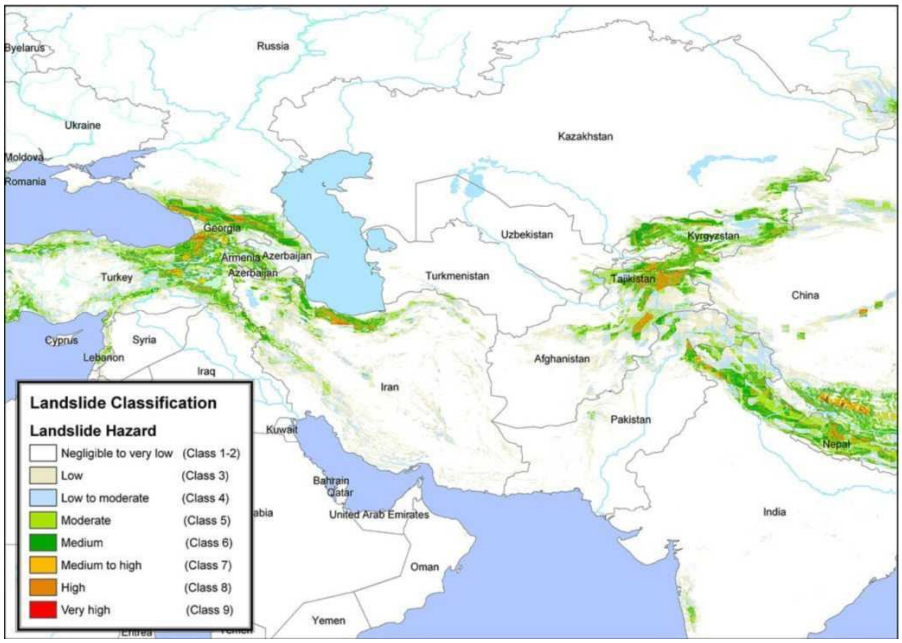

Fig. 2-4: Landslide hazard map for Caucasus and Central Asia (NADIM et al, 2006)

Landslide activity is also increased in south Kyrgyzstan due to the seismic and geomorphological conditions. An investigation carried out by TORGOEV and ALESHIN (2009) showed the large landslides in south Kyrgyzstan with a volume of 0.5 – 1 million m^3 mainly lie in river basins of upper Mailuu-Suu, Kugart, Kara-Unkur, Yassy and Kara-Darya. However, the Mailuu-Suu region should be highlighted with its density of landslide occurrences being 2 to 5 landslides per square kilometer.

There are numerous types of mass movements, due mainly to geological and geomorphological features of a slope. The northern part of Kyrgyzstan is prone to massive rock avalanches (DELVAUX, et al, 2001, STROM et al, 2006; STROM, 2004) and debris flows (HAVENITH, 2006a). In the following, examples are given on main types of mass movements within Kyrgyzstan. Moreover, the study region Mailuu-Suu is explained in detail.

2.4.1 Massive rock avalanche

One of the massive rock failures, named Belogorka "twins", is located west of the capital city Bishkek (Fig. 2-5). The right twin is a "secondary" rock avalanche with a volume of approximately 20 million m^3, and the left twin is characterized by the large block of rock inside the scar with a volume of 15 million m^3 (STROM, 1996, 2006) (Fig. 2-5). Numerous researches have been carried out to point the main trigger of the avalanche. One of the possible triggers is the Belovodsk earthquake that struck in 1885 with a magnitude of 6.9 (IGNATIEV, 1886). However, this large rock avalanche was not mentioned by Ignatiev. Only a few words were said that after the earthquake numerous slope failures had occurred.

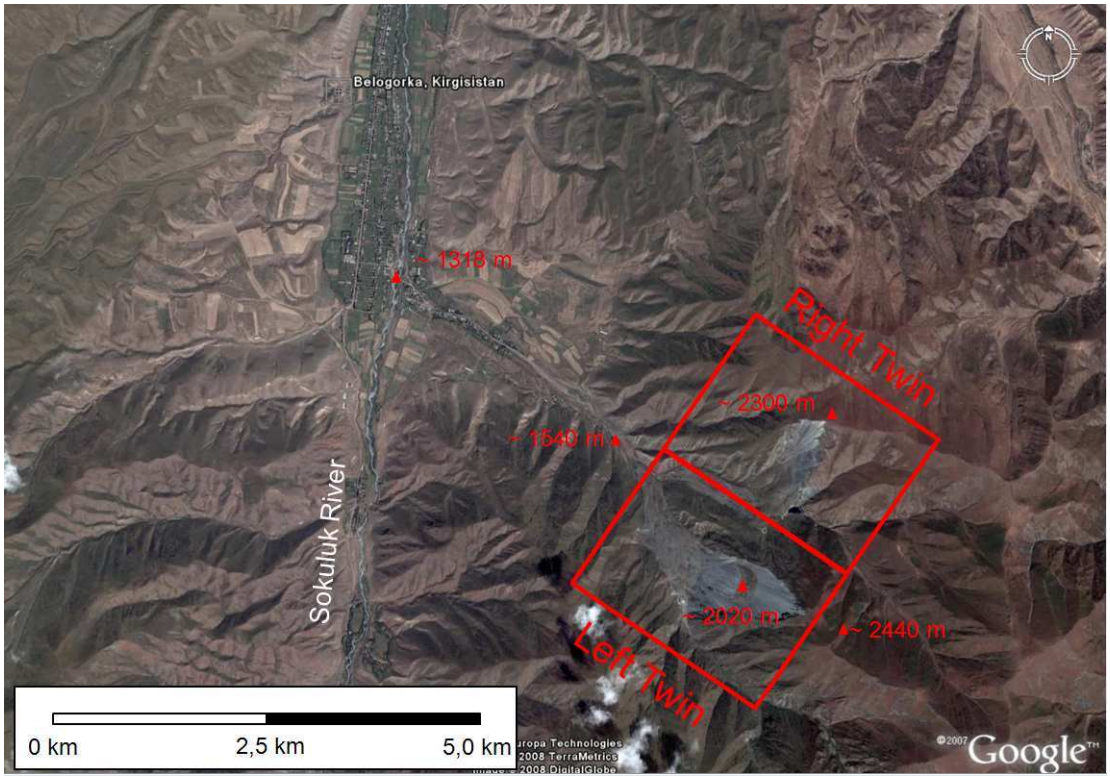

a)

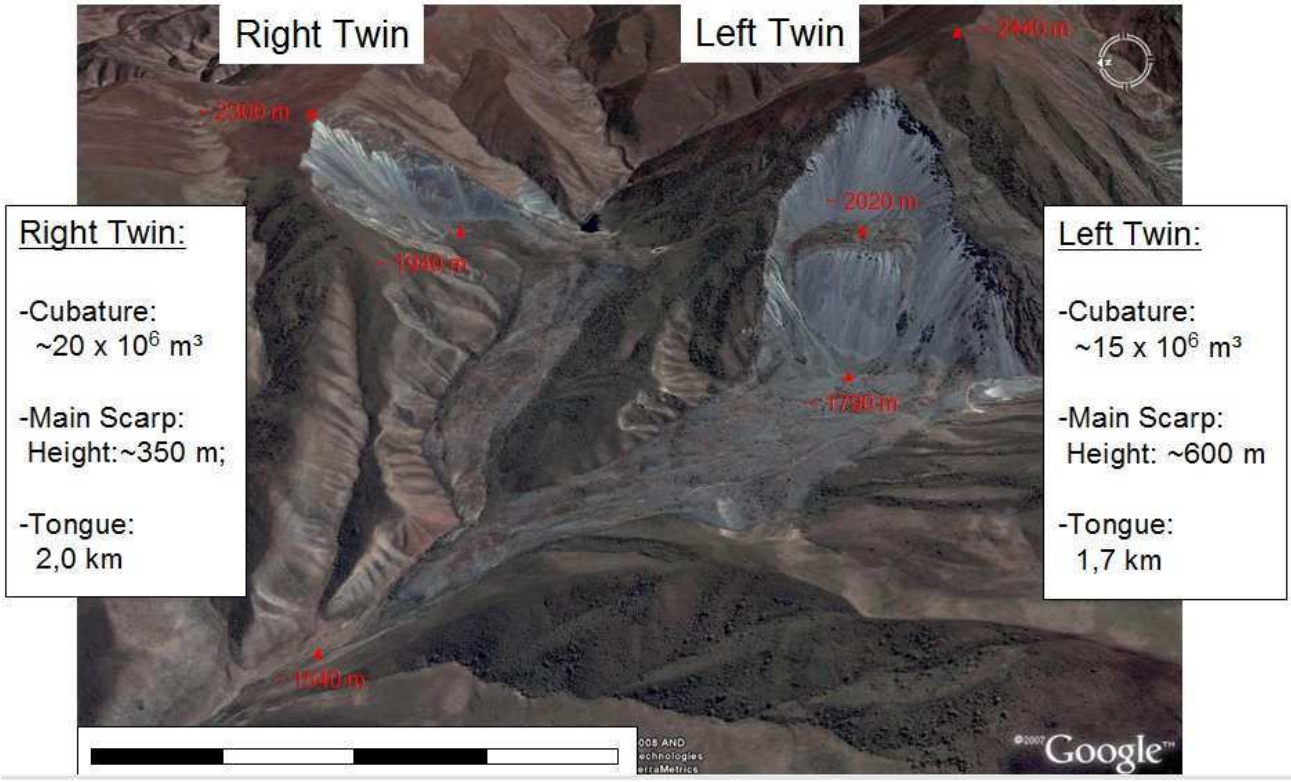

b)

Fig. 2-5: a) overall view of the Belogorka twins; b) more detailed view with approximate volume (source: Google Earth)

2.4.2 Debris flows in Chet Korumdu ridge

A second example of mass movements presented is the debris flows located on Chet-Korumdu ridge. As it is seen in the Fig. 2-6, there are numerous mass movements shown on the ridge. The main highway passes through here, as it connects the north and south of the country. The main trigger for the debris flows was the Suusamyr earthquake with a magnitude of 7.3 which occurred in 1992 and developed landslides including surface ruptures (HAVENITH, 2000). Toppling of slope was observed during a field visit and presented in Fig. 2-7.

Fig. 2-6: Debris flows occurred on Chet Korumdu ridge along the main highway

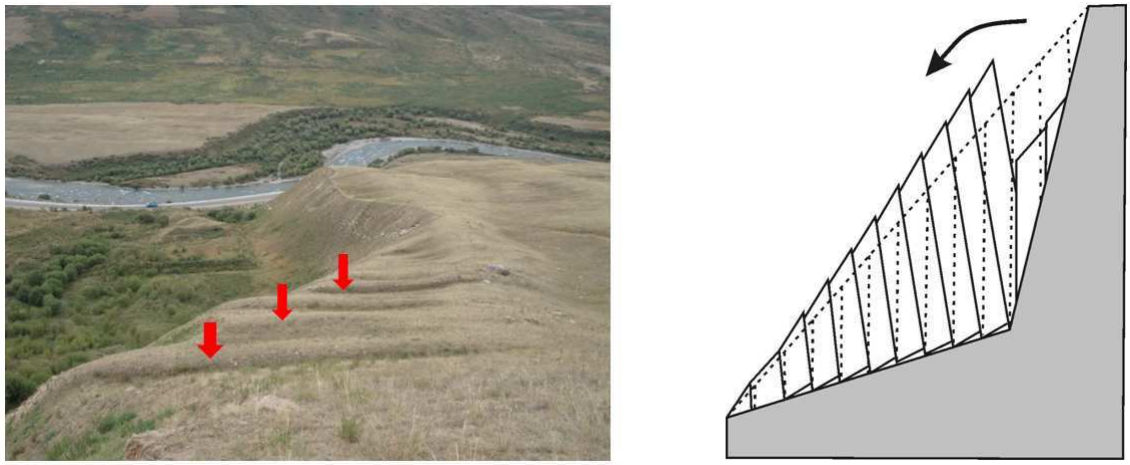

Fig. 2-7: Toppling in slope (left figure) (photo is taken in August 2008) and schematic representation of toppling (right figure) (STROM, 2004)

2.4.3 Landslide in Mailuu-Suu area

The study region Mailuu-Suu is located in the southern part of Kyrgyzstan, approximately 60 km north-west of the town Jalal-Abad and on the eastern rim of the Fergana Basin. This region is described in a detailed way because it presents the study region of the current thesis. At first, geological characteristics are given; then afterwards regional features of landslide situations are presented.

2.4.3.1 Geology of Mailuu-Suu region

The geological map presented in Fig. 2-8 was introduced by De MARNEFFE (2010). A system of faults intersects the region, related to movement of the Talas-Fergana fault (VANDENHOFE et al., 2003). The Fergana Range and north Mailuu-Suu is constituted of Palezoic rocks. Tertiary sediments and Quaternary deposits mainly constitute the smooth slopes. Silt- and sandstones constitute the cores of open anticlines and are overlay by clay- and limestone of Palaeogene and Neogene. Central anticlines cross the valley oriented from east to west and plunges into the westerly direction.

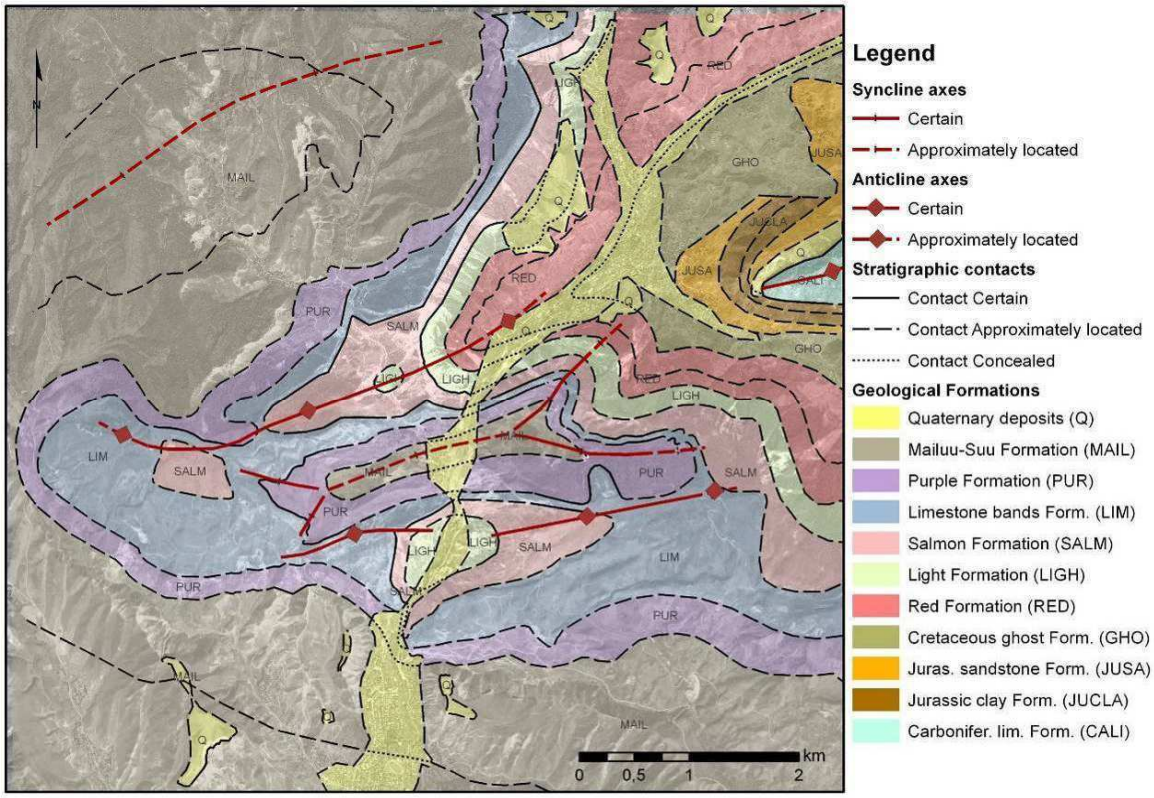

Fig. 2-8: Geological map of Mailuu-suu region (by De MARNEFFE, 2010)

2.4.3.2 Mining activity

It is important to mention that the Mailuu-Suu region is a former mining area. Uranium mining started in 1946 and continued until 1968. During these 23 years, several radioactive waste tailings were conserved in the Mailuu-Suu river basin. One of the problems that the Mailuu-Suu region faces is the waste tailings. Moreover, according to TORGOEV and ALESHIN (2002) slopes started to weaken because underground galleries with depths of 30-40 m collapsed. Such events can cause massive landslides.

2.4.3.3 Landslides in Mailuu-Suu

It should also be mentioned that before the mining activity started, 24 landslides had already existed in this area (HAVENITH, 2006b). According to ALESHIN and TORGOEV (2005) landslide activity starting from 1990 has been increasing. TORGOEV (2006) states there is a chain of disasters which can occur when landslide masses block the river. Mining waste storage space will be flooded with river water and this makes the Mailuu-Suu area one of the highest risk areas of disaster that should be mitigated. In this area, several landslides have developed and already failed. Fig. 2-9 presents the overall landslide situation in Mailuu-Suu area (SCHLOEGEL, 2009). The villages named Sart Bia, Karagach and the town Maily-Say are illustrated in pink. In red, waste tailings are presented. Landslides recorded in 2007 are illustrated in white with black dots. Two anticlines cross the Mailuu-Suu area and they are illustrated with black lines. Rivers Karagach, located on northern part of the valley and Kulmensay, located on the eastern part of the valley flow to the main river Mailuu-Suu and these are presented in blue lines. Between the two anticlines located are the three largest landslides, which are named Koi-Tash (in Fig. 2-9 specified as “Koy”), Tektonik (in Fig. 2-9 as “Tek”), Isolit (in Fig. as “Iso”).

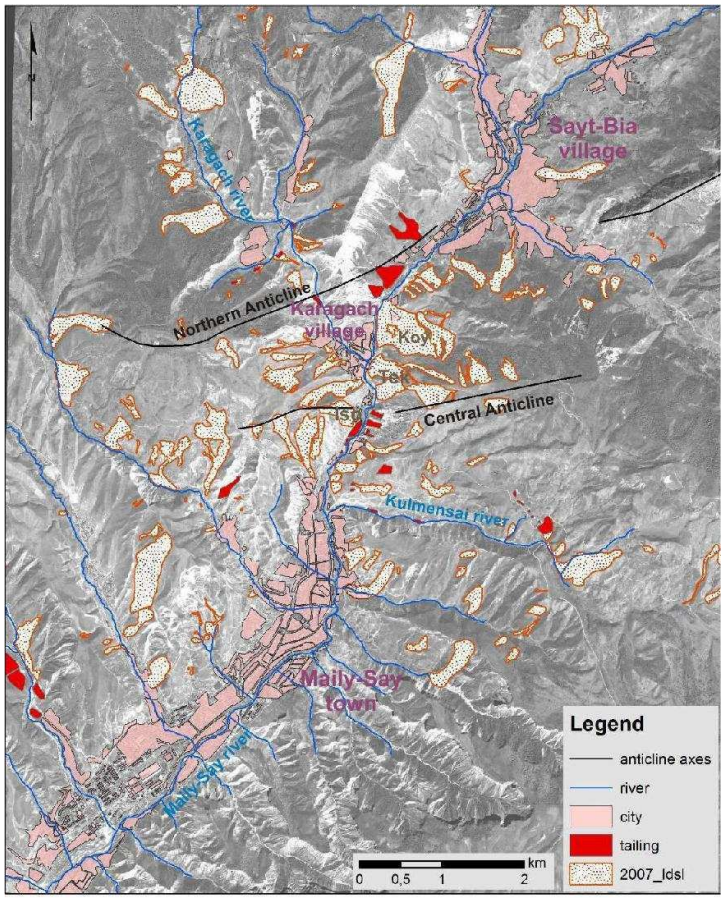

Fig. 2-9: Landslides map of Mailuu-Suu showing northern Anticline and central Anticline (SCHLOEGEL, 2009). Landslide flows are directed into the river valleys

Tektonik

The Tektonik landslide with a volume of 1.5 million m^3 formed in 1992. This case can be specified as one of the most disastrous because it buried the waste tailing #17(17 - the number of tailing) and partly destroyed the plant "Kyrgyzelektroisolith" (VANDENHOFE et al. 2003). Moreover, it has dammed the Mailuu-Suu River, though the damming of the river occurred in 1994, 2002 and 2005 (HAVENITH, 2006b). This complex landslide formed new scarps on the upper part of crest. During the field works that took place in September 2008, the scarp was observed to be 16 m as it is shown in Fig. 2-10.

Fig. 2-10: Tektonik landslide presenting scarps with 16 m

Isolit

One of the three landslides is "Isolit", that is located on the upper part of the former Uranium plant "Kyrgyzelectroisolith" and on the right bank of the Mailuu-Suu. It is estimated to have a volume of 0.4 million m^3 (Fig. 2-11). As mentioned before, the activation started in 1953 with the establishment of mining activity in the region.

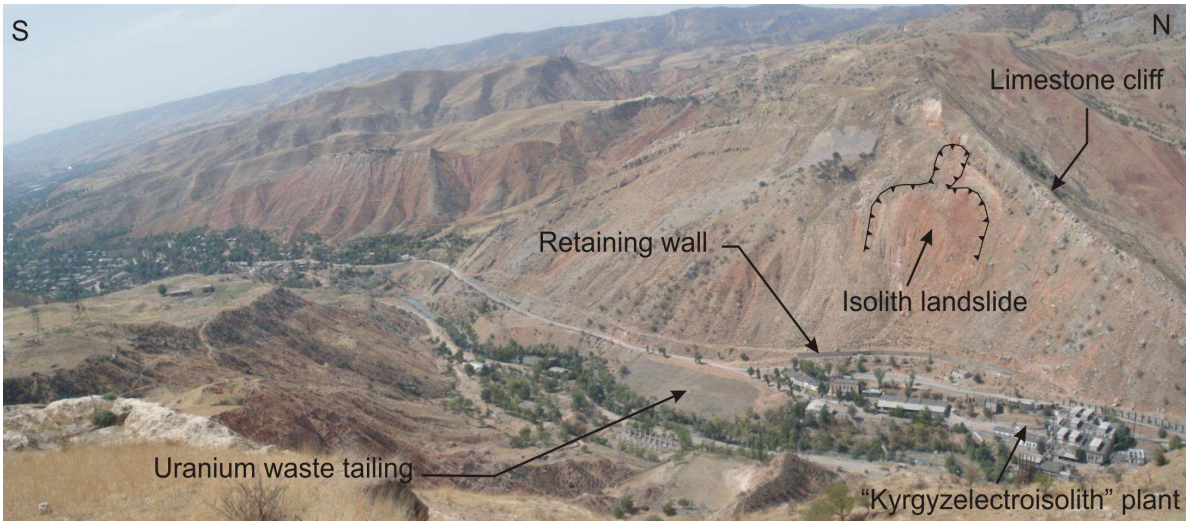

Fig. 2-11: Isolit landslide in Mailuu-Suu area and location of former plant (photo from summer 2008)

Koi-Tash

The Koi-Tash landslide is located on the left of the Upper Koi-Tash landslide, and estimated to have a volume of 3 million m^3 (Fig. 2-12). This landslide has displaced continuously since 1954; currently the displacement is 1-2 mm/day.

Upper Koi-Tash landslide

The Upper Koi-Tash landslide is located between the Tektonik and Koi-Tash landslides (Fig. 2-12). Loess overlies the top of the slope. The total length is approximately one kilometer. This landslide is located on the opposite side of settlement. Since the Upper Koi-Tash landslide is studied because loess constitutes the superficial layer, more detailed information is given in chapter six on how this landslide has developed and which major factors have had influence.

Fig. 2-12: View of Koi-Tash, Upper Koi-Tash and Upper Tektonik landslides. On the left hand side Koi-Tash Hamlet is presented; on the right hand Central Anticline (photo by SCHLOEGEL, 2009)

2.4.4 Conclusion to the chapter

As aforementioned, the Mailuu-Suu basin is influenced by mining and such activities could have reduced the slope stability. Although before the mining started, the information that landslides already existed is known from available data. Even nowadays, data about such slope instabilities is not known since large territories of Kyrgyzstan has not been investigated due to difficult accessibility. This is still one of the issues and only some efforts are being made by means of Remote Sensing tools and GIS application to study mass movements in this country of Central Asia.

Research that has been made after the mining closed has started to investigate existing landslides and predict the new ones. Investigation of largest landslides in Mailuu-Suu area has shown a link between earthquakes and development of unstable slopes, although it is difficult to determine which influence is larger: either mining activities or earthquakes. Since current research is making an effort to study landslides that are induced dynamically, only this side is taken into consideration. In order to go into detail in dynamically triggered landslides, first the nature of such mass movements are described. Due to the wide location of loess in Kyrgyzstan, and the fact that loess has a big impact on development of slope failures, loess properties have been described from wide range of literature in following chapters.

Chapter 3: Earthquake impact on slope failure

3.1 Overview of earthquake triggered landslides

Dynamically triggered landslides and their peculiarities are described and analyzed by different researchers. KEEFER (1984) has shown that the number of landslides and their dimensions are strongly dependent on the magnitude of the earthquake. Based on his investigations, the smallest earthquake magnitude that can cause landslides is about a magnitude of four. Even in areas with abundant susceptible slopes, earthquakes with a magnitude of five typically produce only few landslides, whereas events with a magnitude of 7.5 produce thousands or tens of thousands of landslides.

As many examples on the Earth show, moderate to large earthquakes trigger large numbers of landslides. For example the magnitude of 7.9 Wenchuan earthquake triggered more than 15 000 geohazards in the form of landslides, rock falls and debris flows which resulted in about 20 000 deaths (YIN et al, 2009) (Fig. 3-1).

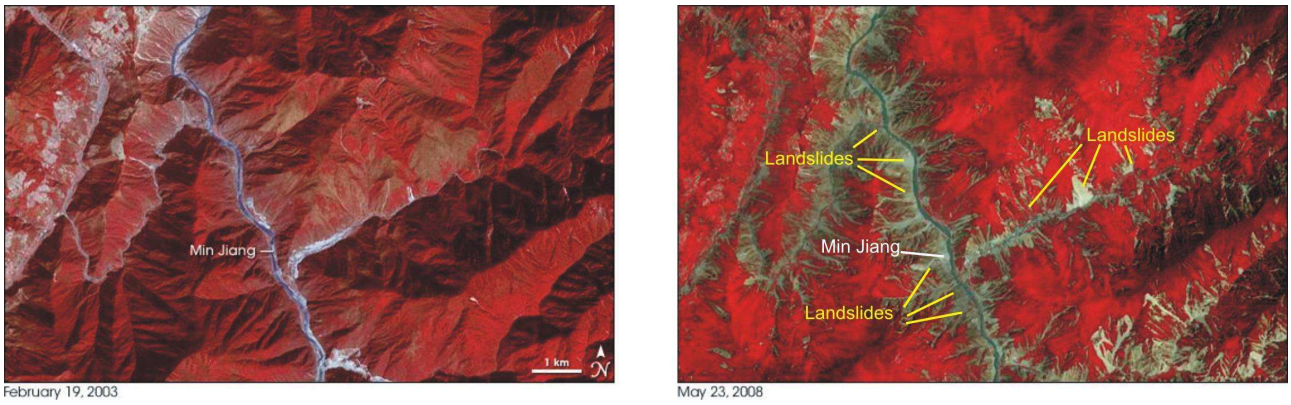

Fig. 3-1: Images from the Advanced Spaceborne Thermal Emission and Reflection Radiometer (ASTER) on NASA's Terra satellite. The images show changes in the landscape after (right picture) the May 12, 2008 earthquake struck China. The same area before the earthquake is shown in the left picture (by YIN et al, 2009)

Such earthquake-triggered landslides are studied by the pseudo-static and Newmark's displacements methods.

3.2 Conventional methods of studying dynamic-triggered landslides

3.2.1 Pseudo static method

This method involves the computation of the minimum factor of safety of a slope against sliding by including static horizontal and vertical forces representative of earthquake shaking in the analysis. These horizontal and vertical forces are usually expressed as a product of horizontal or vertical seismic coefficients and the weight of the potential sliding mass. In the pseudo static method, a force equal to the product of the design acceleration and the block weight is applied to the unstable block (Fig. 3-2). This force is usually applied horizontally. This horizontal pseudo static force decreases the factor of safety by reducing the resisting force and increasing the driving force. Other investigators (MAYES et al., 1981) have suggested also including a vertical component acting in an upward direction equal to two-thirds of the horizontal component. The resultant force is 1.2 times the horizontal force and acts in the direction 34° with respect to the horizontal.

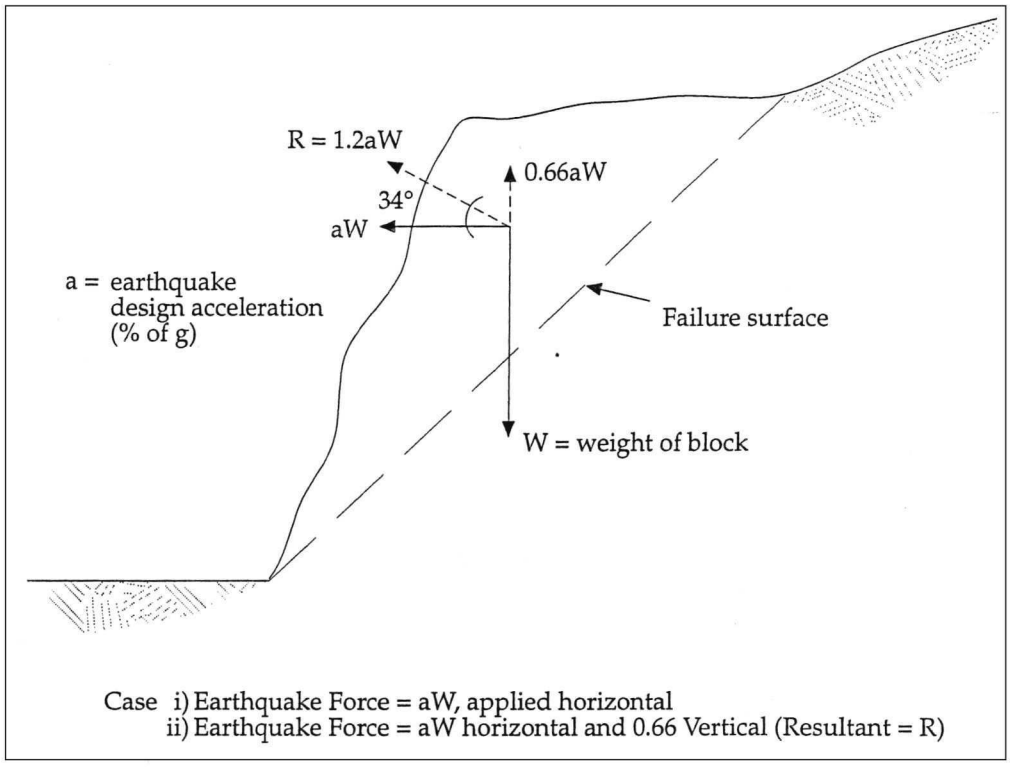

Fig. 3-2: Pseudostatic analyses (NORRISH et al., 1996)

Although this method is a common way to include forces resulting from earthquakes in stability calculations, it is very conservative, as the cyclic loading due to the earthquake shaking is replaced by a constant force. This conservatism is taken into consideration in the analyses by using a factor of safety that is lower for pseudo static analyses than for static analyses.

3.2.2 Newmark's displacements method

Newmark first proposed the important concept that the effects of earthquakes on embankment stability should be assessed in terms of the deformations they produce rather than the minimum factor of safety (NEWMARK, 1965). The method assumes rigid-plastic materials and presumes knowledge of the time history of the acceleration acting on the embankment during the earthquake. If the inertial forces acting on a potential failure mass (static plus dynamic) exceed the available resisting forces, the factor of safety is reduced to below 1 and the soil mass is no longer in equilibrium. NEWMARK (1965) used the analogy of a block resting on an inclined plane to develop a method for predicting permanent slope displacements.

Newmark's method predicts slope displacements induced by acceleration time recordings appropriate for the site. In the first step, permanent displacements of the slope only occur if the earthquake acceleration is higher than the critical acceleration for the geometry and preexisting stability condition of the slope (JIBSON, 1993). The cumulative permanent displacement of the slope is the sum of those portions of the acceleration-time history that exceed the critical acceleration value (NORRISH et al., 1996).

Thereby, a slope with a static FS close to unity has a critical acceleration close to zero and experiences movement under any earthquake motion:

$$a_c = (FS - 1)\, g \sin \Psi_p \tag{3-1}$$

Where:

- a_c - critical acceleration
- g - acceleration due to Earth's gravity
- FS- static factor of safety
- Ψ_p - angle between the horizontal and the direction of the slide first motions (equal to the inclination of failure plane)

In the second step of the Newmark analysis, the slope displacement is calculated by double integration of those portions of acceleration data that lie above the critical acceleration (Fig. 3-3).

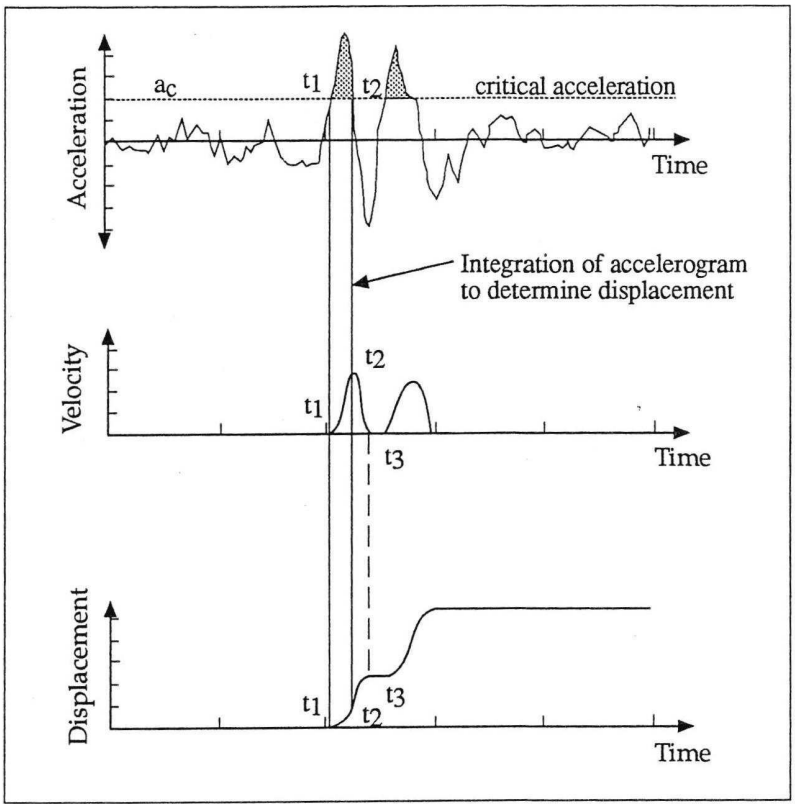

Fig. 3-3: Newmark analysis (by JIBSON, 1993)

Interpretation of the results of a Newmark analysis requires knowledge about the relationship between the materials shear strength and shear strain along the failure surface (NORRISH, et al, 1996). Materials that show ductile behaviour may accommodate the calculated displacement with little effect, whereas in brittle materials the displacement may lead to rapid loss of shear strength and failure.

3.3 Topographic and geological site effects

However, traditional methods of investigation of seismic-triggered landslides described above do not consider to wave propagation into the slope. Ground motion is an important aspect because of irregular topography and geological conditions. In this case it is necessary to talk about site effects - the local ground response, basin effects, and the influence of surface topography. “Local ground response” refers to the influence of relatively shallow geologic materials on the surface waves.

It has long been known that topography usually increases the amplitude of shaking at mountain tops and ridges, whereas valleys exhibit reduced ground motion, as is observed from records of past earthquakes (HARTZELL et al., 1994; SPUDICH et al., 1996). LEE (2001) stated that in the context of quantitative seismic hazard assessment, the Earth’s surface is an important boundary that totally reflects upcoming seismic energy and produces surface waves. An irregular free surface can further lead to complex wave propagation.

Regarding the importance of a topographical aspect, SEPULVEDA (2005) observed the decrease of peak ground acceleration (PGA). PGA of 1.58 g was recorded during the 1994 Northridge earthquake on the ridge that forms the left dam abutment. Accelerations in surrounding areas and at the bottom of the canyon, however, were generally less than 0.50 g. This localized disparity in shaking levels suggests the occurrence of topographic amplification on the ground motion, an effect caused by the interaction of the incoming seismic waves with certain geomorphic features such as steep slopes in areas of strong topographic relief. As noted by FACCIOLI (2000), geometrically irregular components such as canyons, ridges and hilltops in earth's surface cause different physical phenomena from the propagation of seismic waves. Numerous investigations on topographic effects have been made on different irregular surfaces such as ridges, canyons and slopes as illustrated in Fig. 3-4 (STEWART, 2001).

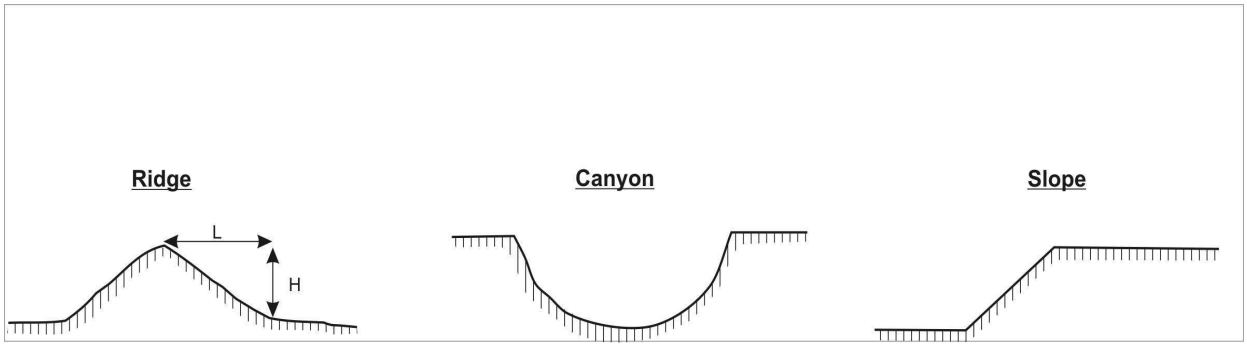

Fig. 3-4: Examples of geometries of irregular surface topography (by STEWART, 2001)

LANG (2004) reviewed different instrumental and theoretical investigations of surface topography on ground motion and presented the convex topographies which lead to an amplification of seismic ground motion, while concave topographies tend to reduce the seismic signals.

In addition to topographic site effects, the geological conditions of the site are recognized to be an important aspect to specify site effects (BARD, 1980a, 1982, TRIFUNAC, 1980). Local soil conditions can clearly impinge on the dynamic characteristics of site response during earthquake excitation.

TRIFUNAC and TODOROVSKA (1999) recognized that alluvium and soil deposits underneath the site modify the motions on the surface by interference of waves inside these deposits. The modification depends on the elastic properties of the soil and sediments underneath, the impedance contrast and the size (depth of the layers, for example), and it is frequency dependant. In general, due to the larger characteristic size, the sediments tend to affect the longer periods, while the soil tends to influence more the intermediate and shorter periods. The overall effect also depends on the impedance contrast (between the sediments and the basement rock, and between the soil layer and the sediments).

PAPAGEORGIOU (1991) stated that geologic conditions and topography at or near a site are known to exert a very significant influence on the nature of ground shaking. Such investigations have long been recognized for their importance on seismic hazard by MILNE, 1898; BORCHERDT, 1970; SANCHES-SESMA, 1987a, b; AKI, 1988, 1993. BARD (1980) presented in his studies that sedimentary deposits often has an effect on the intensity of strong ground motion.

Chapter 4: Loess

4.1 Definition

Loess has been studied by researchers from different countries for almost two centuries. Such investigations have attempted to make one definition to loess. The simple definition suggested by PYE (1995) is that loess is windblown deposit of silt consisting mainly of clay minerals, feldspar, mica and quartz. KRIGER (1969) stated in his book "Loess and its properties" thirteen definitions of loess. All these definitions listed that soil can include this or another property to be called loess. For example, BERG (1980) stated the soil should consider the following properties: the colour is light yellow, with large pores of 45-50%, and contains $CaCO_3$ and Mg and homogeneous a granular component. RICHTOFEN (1877) specified that loess slopes can stay vertically in dry conditions. He considers that loess is susceptible to vertical fracturing by developing vertical joints. By studying loess deposits in Ukraine, Russia and Central Asia, KRIGER (1965) defined two types of loess. First is loess sediment, representing yellowish porous aleurite with carbonate content. The second type is loess system. KRIGER (1965) described this loess as a natural body and can be defined by its geographic environment.

4.2 Origin

Over the period the air blown genesis is considered in the loess studies (HIGGINS et al, 1985). The main important transporters of dust from Africa over the Atlantic Ocean and Europe were recorded in the late 18th century (PYE, 1995). Apart from Aeolian origin of loess, there are some other considerations related to its origins. SMALLEY (1966, 1978) and ASSALAY, et al (1996, 1997) stated that loess can occur in alluvial deposition, i.e. river deposition. Delluvial loess occurs on slopes, prolluvial is loess on plains and elluvial is produced by soil processes. Investigations also exist regarding the soil and microbiologic origin of loess. (RAZDOLSKYI, 1962).

4.3 Geotechnical characteristics

Typical characteristics of loess are: $CaCO_3$ = 14-27%, e = 0.65-1.1, n = 39-52% (FODOR and KLEB, 1994). Loess is composed with a small amount of sand 6-18% and silt 67-92%. Clay content ranges from 6% to 30%. Being dominated by grain sizes loess can be called silty, sandy loess, loess loam and typical loess. Such a review has been presented by FODOR and KLEB (1994) in a schematic way (Fig. 4-1).

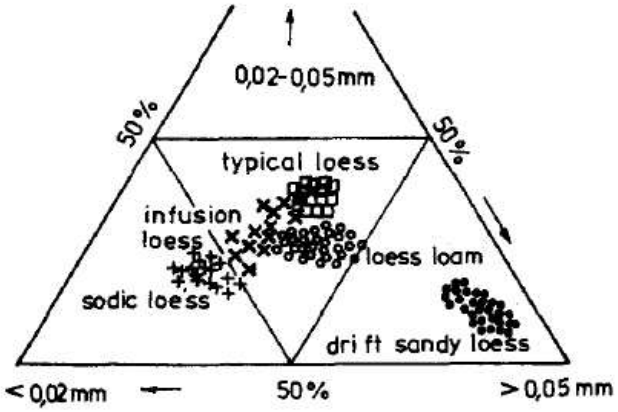

Fig. 4-1: Grain-size distribution of loess types (by FODOR and KLEB, 1994)

The liquid and plastic limits of loess are closely related to the content of clay-size grains. The liquid limit ranges 30-35 %. Loess can be characterised as a dilatant material with a low plasticity index (PI) of 10-15%.

Bulk density increases with age or degree of consolidation. DERBYSHIRE et al (1994, 2000) reported the bulk density is 1.378 ± 0.205 gr/cm^3 for the Lishi (younger age) and 1.718 ± 0.168 gr/cm^3 for the Wucheng (the oldest) loess in China. The highest bulk densities are found in the paleosols with values of 1.700 ± 0.052 gr/cm^3. According to DERBYSHIRE (2001) void ratios decrease with age.

According to TAN (1988) loess has a structure where grains of silt and sand has been covered with clay and between there are connection as bonds constitute from carbonates (Fig. 4-2). Between the grains and binders, the macropores exist. WANG (2006) studied such pores of loess and divided them according to the shape of the particle arrangement. The pores in loess can be classified into open pore, embed pore and inner-particle pore.

- The inner particle pore exists in the framework aggregate. Its deformation property depends on the rigidity of particles and has no relation to the collapse deformation.
- The embed pore is the pore between grains formed by framework particles intercrossing each other in a compact state. The bigger open pore is common in this layer.
- The open pore is the result of the framework particles depositing loosely. This spanning structure is an abnormal arrangement: When immersed in water, the joint strength is weakened. After losing the stability under a certain pressure, the particles around the open pore fall into the pore. The soil structure suddenly deforms retrievably and then collapses.

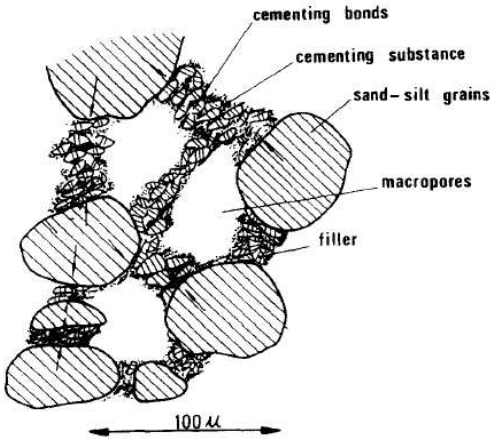

Fig. 4-2: Microstructure of loess according to TAN (1988)

Cementation bonds that are shown on Tan's structure have a great impact on undisturbed structures. It presents that calcite constructs the cementing bonds. However, GIBBS and HOLLAND (1960) stated that montmorrilonite clay with small amounts of illite is a main bonding agent and that calcite serves a secondary support structure. By studying the Kansas loess BANDYOPADYAY (1983) confirmed that the montmorrilonite constitutes the main bonding in loess structure.

Voids are always saturated in natural conditions (LARIONOV, 1963). In natural conditions, the water content of loess ranges from 5- 30%. It can vary with the seasons.

Strength parameters are a main property by studying slope stability in loess. Density and clay content and an increase in water content can cause a decrease in the cohesive strength contributed by binder. In low water content, loess can stay nearly vertical slopes. When wetted the cohesion may drop causing slope failure.

HIGGINS et al (1996, 1985, 1989) found out that determining the shear strength in loess is difficult when saturation is less than 100 %. They also concluded the friction angle constantly remains ranging between 28° and 36°, but cohesion depends on water content. HOLTZ and GIBBS (1951) observed cohesion up to 448 kPa for loess with high density, high clay content and low moisture content. Low density loess soil with high water content shows cohesion value equal to zero (HIGGINS 1996, 1985, 1989). SHEELER (1968) stated that the high cohesive strength increases with the increase of clay content. Loess can cause unexpected behaviour when the water content ranges to 20%. This state is described by DIJKSTRA et al (1994) by testing Malan loess (youngest age of Chinese loess) and named it as a critical moisture content (Fig. 4-3).

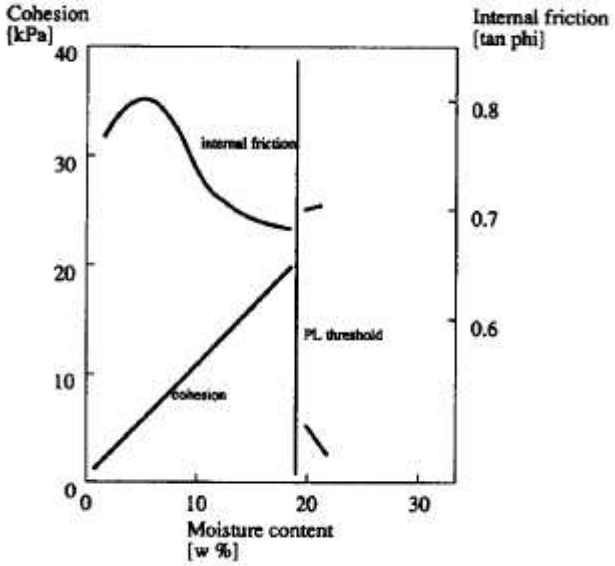

Fig. 4-3: Internal friction and cohesion in changing moisture content (by DIJKSTRA et al, 1994)

HOLTZ and GIBBS (1951), GIBBS and HOLLAND (1960) observed the complete strength of loess under the consolidation pressure of 69 kPa. They explained by stating that a minimum degree of consolidation is required to produce grain to grain contact and thus shearing resistance. In contrast to this research, KANE (1968) did not observed loss of strength.

In order to present an overview of strength parameters of loess the table is shown in the APPENDIX 1. It is obtained from wide literature review showing worldwide regions. The table presents overall properties including strength parameters of loess. It presents friction angles ranging 28-36° and cohesion 0-460 kPa.

Shear strength depends on cementing bonds and clay particles and frictional forces between particles. FEDA (1982, 1988) introduced theoretical representation of stress-strain curves for loess soil. This representation was adapted by DERBYSHIRE et al (2000) for Chinese loess and presented in Fig. 4-4. On the left side, friction and bonding are presented and the diagram on right side is adapted to Malan loess. Curves as *a* mainly represent shear strain curves of older loess since the cementing bonds are well developed. Younger loess where the bonds have degradation can show shear strain curve as *b* and *c*.

Comparison of two curves presents friction between particles and resistance to shearing are increased before reaching the strength threshold. In curve *a,* the vertical stress is great and is overshadows the frictional forces in the failure behaviour. Curve *c* presents the case when vertical stress is low; in this case cementation bonds contributed here reach brittle stage just before frictional forces lead to an increase in strength with increasing strain. Such failure behaviour has been found for wet loess of old age. Similar strain hardening for younger loess was also found and it is explained by the packing of particles due to a large void ratio.

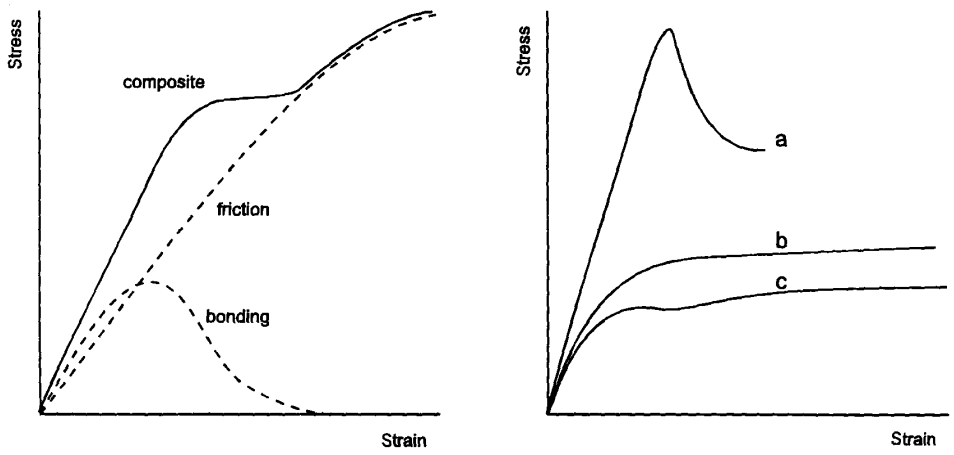

Fig. 4-4: Theoretical stress-strain relationship of cemented soil (DERBYSHIRE et al, 2000)

Moreover, the open and loose structure of loess is significant to exhibit its compressibility and strength characteristics. Clay binder is a main indication of this structure. If applied stresses exceed the binder strength, or if there is a loss in strength, the structure can collapse and large compressive deformations can occur. The primary cause for a loss in strength is the wetting and consequent swelling and softening of the clay binder (HOLTZ and GIBBS, 1951). In case cementation bonds are destroyed during the deformation, the frictional forces are mobilised at the same time, due to result of loess fabric. Shear stress is increased with strain until the maximum is reached predominantly on frictional resistance of single particles. In this case in loess can be observed dilation (*a*) and contraction (*b*) as shown in Fig. 4-5 (DERBYSHIRE et al, 2000). Such a schematic view is used to understand the behaviour of undisturbed and reworked loess samples:

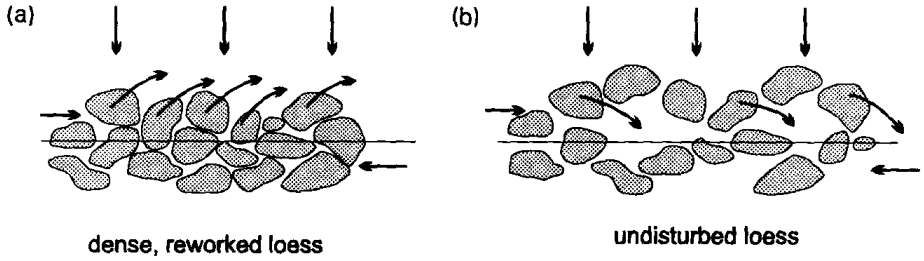

Fig. 4-5: Dilation and (b) contraction occurring in loess (by DERBYSHIRE et al, 2000)

Anisotropy of particle direction tends to have an impact on shear strength of loess. Different testing methodologies present distinctive strength values. Researchers have found different strength parameters and explained that such values can correspond to specific properties of loess as presented in following.

XIA et al (2008) carried out an investigation on cyclic variability in microstructure and determination of physical and mechanical properties for samples from Luochuan, Xuancheng

and Nanjing, China. Grain-size distribution of loess presented as silty loess with silt grains 64% and clay grains 28.3% at Luochuan, 70.7 % and 28.1% at Nanjing, and 55.7% and 39.5% at Xuancheng, respectively. Results of undrained shear tests showed cohesion is 46.9 kPa and angle of internal friction is 15.6°. They explained high cohesion value due to strong cementation bonds and low void ratio.

STROKOVA (2003) studied loess samples from Tomsk, Russia. The average friction angle varies from 16 to 27^0, and cohesion from 9 to 96 kPa. Explanation of these variables is dependant on plastic limit and density of soil.

YING et al (2006) tested undisturbed loess samples in direct shear apparatuses developed by Chen (1989). The samples were obtained from a slope in Luilin town Baota in Shanxi province. Physical properties are w=23.57%, ρ=1.82 gr/cm^3, SG (Specific Gravity) =2.72 gr/cm³, e=0.848, WL=30.2%, WP=18.4, PI=11.8%. They used vertical stress of 50, 100, 200 and 400 kPa with shear rate of 0.0032 mm/min. When shear displacement reached to 6-7 mm, the test was stopped. They found when vertical pressure was higher than the structural strength, in test case p=400 kPa, the shear – stress curve was strong rigid character. This was influenced by confined pressure and structural strength of undisturbed loess.

The anisotropy of particle direction has been observed while testing. Such behavior is explained by MATALUCCI et al (1969, 1970), by studying Vicksburg loess of the Mississippi valley. They found that shear strength is about 12 per cent greater in a perpendicular direction to grain orientation that parallel to it. This outlines the relationship between natural fabric and orientation of applied stress distribution. Results showed the fabric of Vicksburg loess is reflected by definite variation in triaxial shear strength of dry and moist specimens.

The point on the relationship of shear strength on moisture content is found by TAN (1988) by investigating loess in China. However, it is not clearly an exact age. Due to specific gravity and density, it can be considered that Malan loess was taken. Loess has tested under varying moisture content conditions using the oedometer and triaxial tests. During the triaxial test in hydrostatic stresses exceeding 1 kg/cm^2, the stresses increased with the strain. In cases of hydrostatic stresses lower than 0.1 kg/cm^2, stress strain curves show a peak followed by shear softening effect (Fig. 4-6). The strain hardening can be ascribed to the increase of frictional forces due to the increased number of grain contacts due to compression and shear.

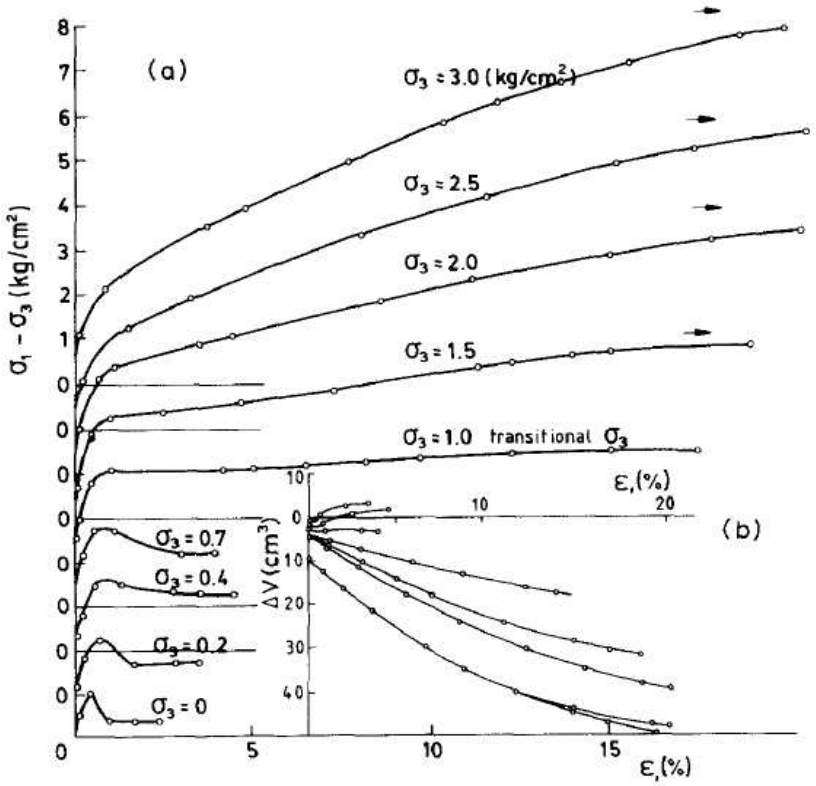

Fig.4-6: a) Stress strain curves for loess with water contents from 9.5-10.2% tested at hydrostatic pressures, b) plot of the volume deformation against the axial deformation (by TAN, 1988)

Regarding the shear hardening effect, TAN (1988) explained this as the increasing of mechanical friction between the granular particles within the bonds and the increase in overall contact between the whole assemblies of grains. Furthermore, larger grains which initially had no mutual contacts then formed increasingly more contacts as a result of the disruption of the bonds and the compaction. He found a direct relationship between tan φ and moisture content (Fig. 3-7), although moisture content of samples was up to 20% in order to compare to results of DIJKSTRA et al (1994) who found a critical threshold on moisture content (see Fig. 4-3).

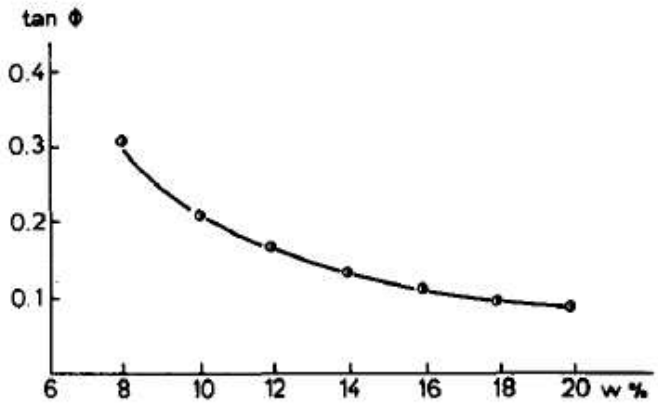

Fig.4-7: Relationship of tan φ and water content (by TAN, 1988)

KANE (1968) tested undisturbed loess samples from Mississippi with moisture content of 26-33%. Test methods included a consolidated, undrained (CU) triaxial test, the Iowa borehole shear test (IBST) in order to compare in-situ conditions. During the tests, it was observed that IBST failure envelope tends to have a higher cohesion and a lower friction angle than the CU test results. The failure envelopes tend to merge at higher-than-normal stresses. This appears to be due to the magnitude of the apparent cohesion. The disturbance of the unique loess structure by anisotropic consolidation may destroy some of the natural cohesion and perhaps even reduce the apparent cohesion by altering the position of the clay-coated silt grains so that the capillary tension is reduced (SCHMERTMANN, 1976).

The relative difference in the IBST and CU triaxial effective friction angles measured on saturated soil is due to the magnitude of apparent cohesion. Apparent cohesion is a result of both clay and moisture content. A soil which develops a high apparent cohesion will produce a significant difference between the IBST and the CU triaxial test effective friction angle. Conversely, a soil which generates a lower apparent cohesion will produce a smaller difference between the IBST total friction angle and the CU triaxial tests (HIGGINS, 1996).

4.4 Subsidence of loess

One of the behaviours of loess is susceptibility to subsidence which occurs in wetted loess and under loading. This problem of loess is widely investigated in many parts of world. Due to this, several subsidence criteria have been proposed, which are wide in range.

GIBBS and BARRA (1962) suggested that when the moisture content increases up to the liquid limit and in presence of load, the soil can collapse. This index presented in terms of liquidity index:

$$LI = \frac{w - PL}{LL - PL} \tag{4-1}$$

where, LI = liquidity index, w = moisture content, LL = liquid limit, PL = plastic limit

Large amount of investigation has been performed on loess subsidence. DIJKSTRA (2000) carried out a review of criteria on subsidence and could present that a wide range of research has been done in order to study loess subsidence issues.

4.5 Seismic subsidence of loess

When the loess is of an older age, the cementation bonds are well developed and loess have lower void ratios. Collapse takes place when the loess is subjected to additional pressures either in the form of static as additional overburden, or dynamic stresses such as seismic shaking (DIJKSTRA et al, 1994, SMALLEY, 1996).

KRIGER (1969) stated that during dynamic loading loess can subside. In order to investigate this question, explosion tests carried out in Yavan region, Central Asia. Results presented that during the explosion loess subsidence was 7-24 mm, but after the explosion it continued and

after one month was 28-36 mm. The moisture content of loess was 14-18%. KRIGER (1983) referred to researches from Popov and Nazarov, which stated the decrease of P - wave velocity is due to moisture content level in loess. KRIGER et al (1983) supported this point and named it as a "paradoxical interval". In loess loam this threshold is 10-18 %. In this value of water content the P- wave velocity decreases from 700-1000 m/s to 350-650 m/s. Investigation showed while increasing clay content this threshold displaced more moisture content.

4.6 Liquefaction in loess

By investigating loess flows in Tajikistan, ISHIHARA et al (1990) stated the loess with PI=10 causes liquefaction under seismic excitation. In order to investigate dynamic loading impact on loess liquefaction, WANG et al (2006) carried out explosion tests in loess sites near the village Ligiagou in Lanzhou, China. They simulated earthquake effects by using nine explosive compartments. Before the explosion test the loess site was saturated. Pore pressure and residual strain developed in saturated loess, which verifies the liquefaction in Malan loess.

Not only the water content is a main factor to cause liquefaction, but also the other specific properties of loess are responsible. HWANG et al (2000) studied liquefaction potential of loess from Lanzhou, China and Memphis, USA. Index properties of loess samples are different. Plasticity index for Lanzhou is 9.9 and Memphis is 11. Grain-size distribution indicated that the Memphis loess has clay content that equal to 19, and Lanzhou loess has 10.5. Sand content is 13 and 4.7 and e = 1.022 and 0.632, respectively. They tested by using dynamic triaxial tests. As the dynamic loading, the synthetic earthquake time history is used in the study. Results presented as the same time histories of dynamic stress (σ_d), pore pressure (u_d), and dynamic strain (ε_d) for samples of both regions (Fig. 4-8; Fig. 4-9). Results of the tests show the Memphis loess is less susceptible to liquefaction. In the case of ground shaking, the pore pressure in Lanzhou loess increases and a large amount of residual pore water pressure generated and residual strain is developed (Fig. 4-8). When the Memphis loess is subject to ground shaking, only an elastic pore pressure is generated, that is, no residual water pressure is observed (Fig. 4-9). They explained different liquefaction potential of two loess samples by different microstructures, physical properties and dynamic parameters of loess. Another important factor is clay content, pointed out as a significant attribute that has an impact to liquefaction potential.

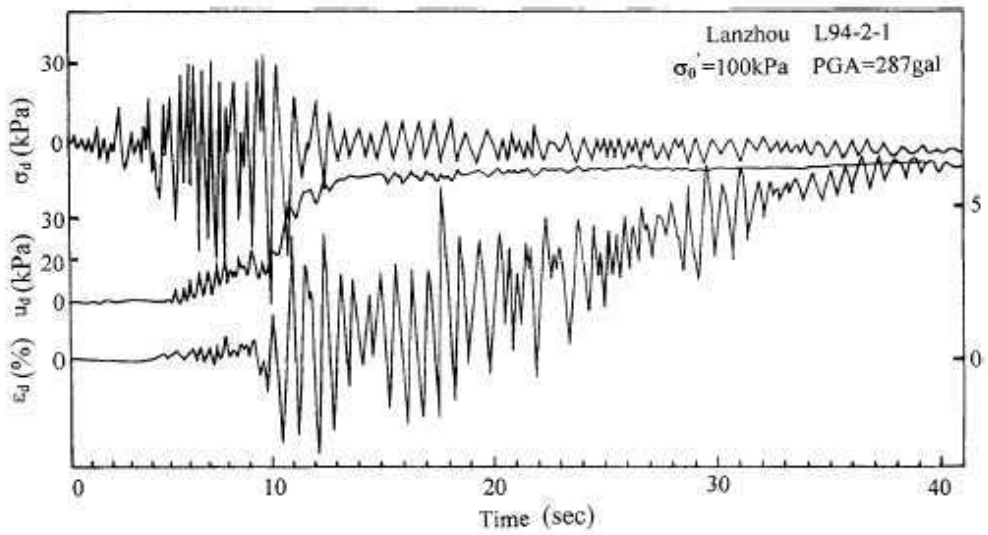

Fig. 4-8: Pore water pressure, dynamic stress and strain for the Lanzhou loess (HWANG, et al, 2000)

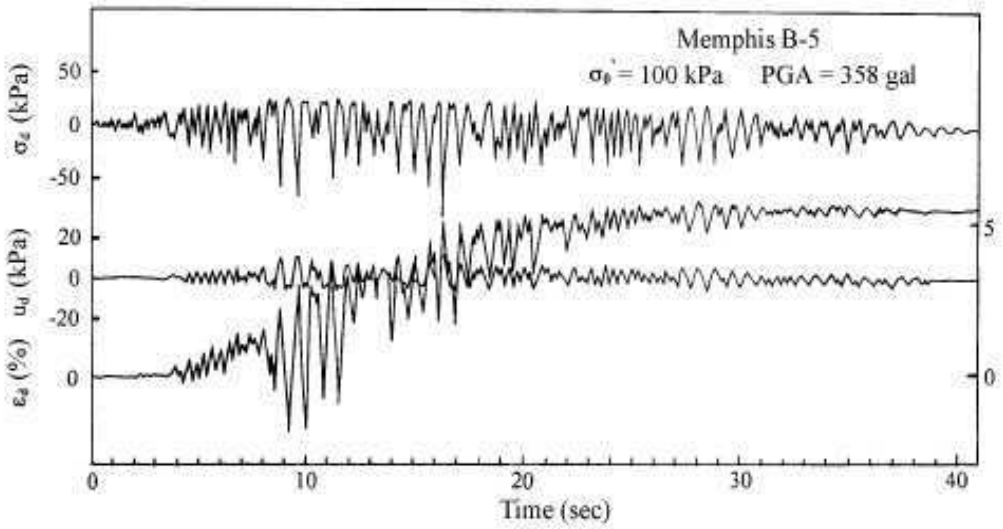

Fig. 4-9: Pore water pressure, dynamic stress and strain for the Memphis loess (HWANG, et al, 2000)

Chapter 5: Loess landslides

5.1 Landslides in loess

Landslides in loess are defined as earth flows by the classification of Varnes (VARNES, 1978, CRUDEN and VARNES, 1996). However other descriptions can be found on mass movements in loess as loess landslides, loess falls and loess flows in literature. To introduce the reader to how the slope movements can occur and to give a brief overview on landslide types, the following three types of landslides are described. At first, earth flow is illustrated on Fig. 5-1a). These types of mass movements can occur in wet and loose soil, and are characterized by rapid movements. Earth slides are defined by a distinct zone of unstable slope that separates underlying and sliding material (Fig. 5-1 b). Earth fall can be characterized by abruption of soil masses from the steep slopes (Fig. 5-1c)

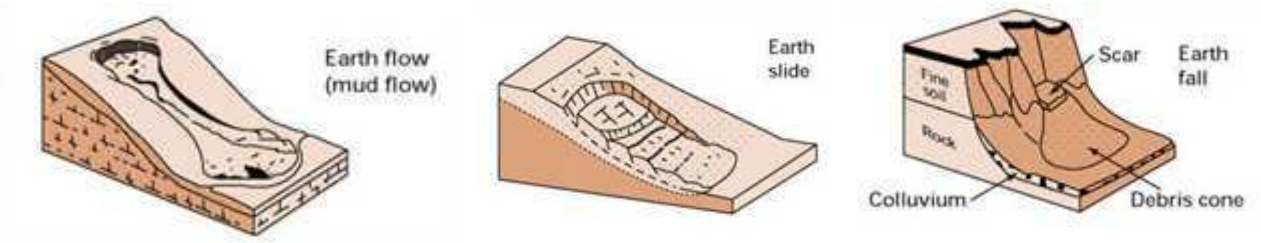

a) b) c)

Fig. 5-1: Classification of mass movements (by CRUDEN and VARNES, 1996):
a) earthflow; b) earthslide; c) earthfall

5.1.1 Loess landslide classification

Landslides in loess deposits mainly concentrate in the mountainous regions of the northern part of China and Central Asia. Many researchers consider issues related to failure mechanisms in loess slope. Based on broad field studies related to loess mass movements in Gansu Province in northern China, DERBYSHIRE (2001) referred to MENG et al (1998) that provided a detailed classification on loess landslides. According to this classification, mass movements in loess are divided into six types (Fig. 5-2).

1. Bedrock contact landslides. These types of landslides involve sliding of a loess mass on or within the numerous palaeosols found in the Chinese loess. Vadose waters are impeded by this clay - enriched and less permeable layers. The likelihood of failure is even greater where slopes are undercut by river incision or artificial excavation.
2. Palaeosol contact landslides. Palaeosol within loess has a finer mean grain size, low permeability and is more compacted than loess. Occurrences of fissures on the upper part of the slope contribute to water infiltration and the decrease of soil strength.

3. Mixed landslides. Loess covers permeable bedrock and develops mixed landslides. Such slopes overlaid by loess are stable. However the presence of intercalated mudstone may cause sliding.
4. Slides within loess. These types of landslides are not very common in the Loess Plateau in China since the moisture content is lower than 12%. Earthquake shock and slope cutting causes slopes to fail.
5. Terrace landslides. Landsliding occurs in margins of river terraces.
6. Tan-ta. This type occurs in upper reworked layers which are steeper than the loess slope.

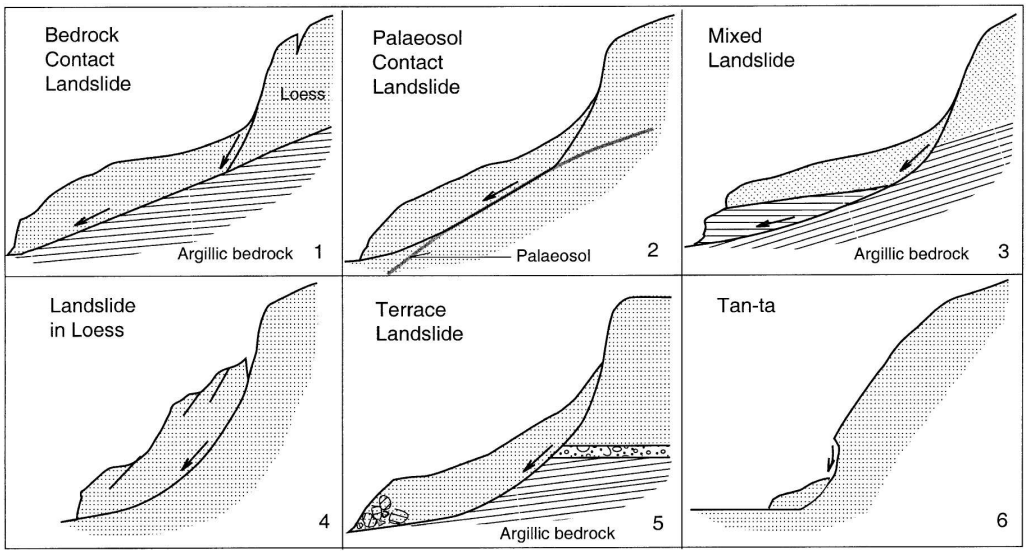

Fig.5-2: Principal types of landslides in the thick loess terrain of Gansu Province (by MENG et al, 1998)

Moreover, DERBYSHIRE (1995) described the loess landslide types in the same area in China according to geometry and movement mechanisms. For example, the Saleshan landslide which occurred in 1983 in Lanzhou belongs to flow and complex mass movements. The thickness of loess was 150 m, mass was 1000 m wide and 170 m high, and it moved a distance of 1600 m (DERBYSHIRE et al, 2000). The mass of 50 million m^3 failed within several seconds. 220 people were killed and four villages were destroyed. The trigger of this loess slide is not clear since there had been no intensive rain or earthquake at this time. ZHANG (1989) emphasised the importance of human influences on the stability of Saleshan loess slope. Another type of loess failure is large rotational mass movements distributed within loess slopes. Such large movements cause disastrous events. Minor hazards contributed by planar slides that move on shallow slip surface. Types of mass flows described in the Lanzhou area in China are debris flows where bedrock lies close to the surface. These flows are a mixture of loess and bedrock fragments DERBYSHIRE (1995).

5.2 Loess failure and triggering mechanism

5.2.1 Geomorphological aspects

Geomorphological features of slope have a significant impact on the occurrence of loess failure. ZHANG et al. (2007) investigated thirty-nine landslides with widths of more than 500 meters, which could be recognized from aerial photographs that were triggered by the Haiyuan earthquake. Investigations presented most landslides developed within the slope with angles of 30-35° (Fig. 5-3).

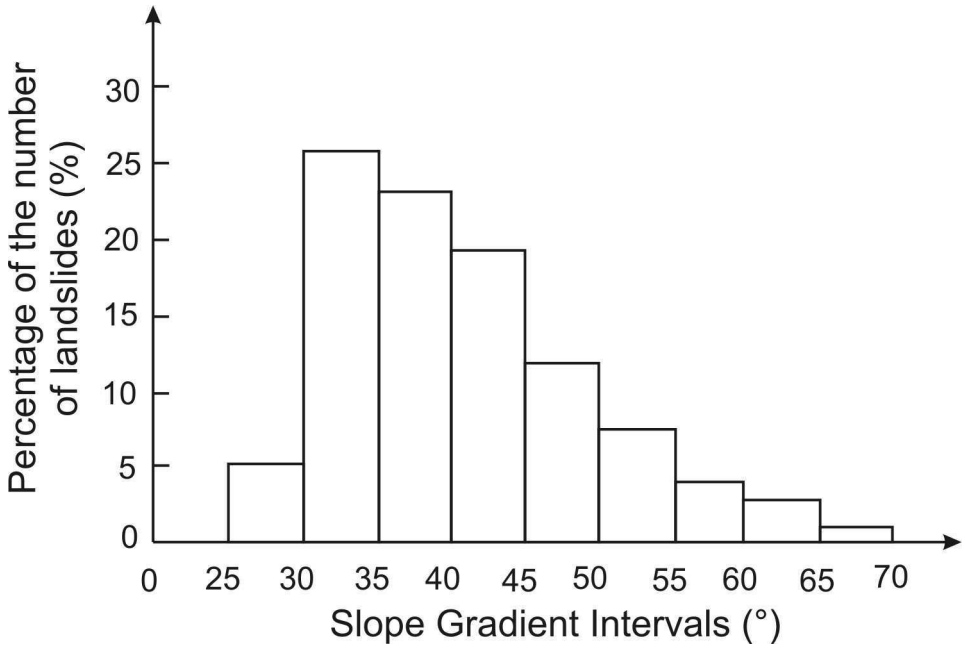

Fig. 5-3: Percentage of the number of landslides in different slope gradient intervals (by ZHANG et al, 2007)

Slope height also controls the development of mass movements. Loess landslides occur commonly in slopes with the height of 50-120 m and loess mostly falls on a slope height of 10-20 m (ZHANG et al, 2007). The higher the slope, the lower the ratio of loess falls. The reason is that through long term weathering, high slopes have reached a stable condition and the slope angle is low. On the contrary, lower slopes are readily eroded by river action and erosion, and are also susceptible to human engineering activities (DIJKSTRA et al, 1994, ZHANG, 1989).

5.2.2 Precipitation induced loess landslides

Apart from the geomorphological aspects of landslide development in loess, the climatic condition has a significant impact. ZHANG et al (2004) studied loess landslides in the Baota district in China. They presented annual precipitation as 496.2 mm, however, the distribution within the year is occasional as is shown in Fig. 5-4. Much precipitation is concentrated between June and September. The types of mass movements developed within loess mainly

are distributed in July and September. The highest amount of loess landslides and flows was observed in September.

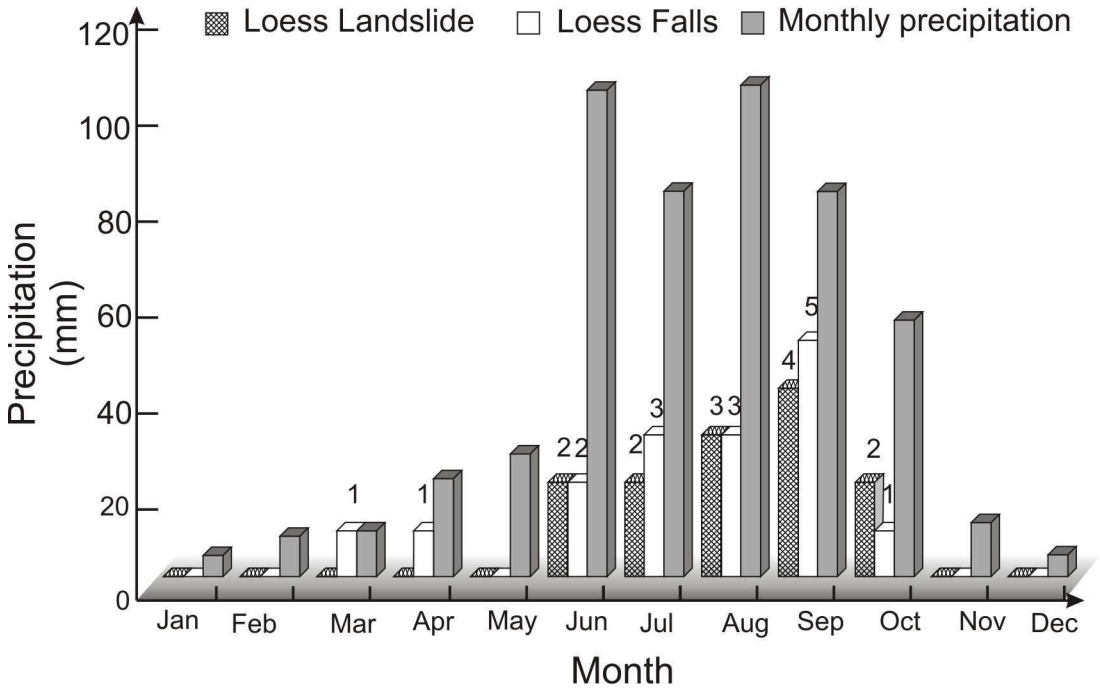

Fig. 5-4: Relationship between precipitation and landslide in numbers (by ZHANG et al, 2007)

An investigation regarding climate condition and loess mass movements was carried out by Niyazov in Uzbekistan (Central Asia) during the 1969-1972 (NIYAZOV, 1984). According to this research, the precipitation has an impact on the development of shallow landslides.

5.2.3 Earthquake and loess landslides

When precipitation is infiltrates into the loess layer, the strength of slope material decreases. Seismic events occurred during this time increase the instability of slope that causes failure. Due to the location of the Tibetian Plateau, the areas of China and Central Asia are affected by strong earthquakes.

Numerous strong earthquakes have been recorded with magnitudes of 6.5 – 8.5 in the Gansu area of China. The most disastrous was the Haiyuan earthquake, which occurred on December 16th 1920 with a magnitude of 8.5. About 230 000 people were killed and 180 000 of these were buried under the landslides (CLOSE and McCORMICK, 1922). This earthquake triggered landslides that extended more than 50 000 km^2 and 657 of them more than 500 m in width (DERBYSHIRE et al, 2000; LI 1989). DERBYSHIRE et al. (2000) sited that such large earthquakes triggering landslides at a great volume, large scale and can cause serious impact to a population. ZHANG and LIU (2009) presented that earthquakes have a close relationship with loess landslide development.

Regarding Central Asian countries, NADIM et al (2006) showed that Tajikistan is the seismically active region. The Khait earthquake with a magnitude of 7.4 that occurred in July 1949 is one of the most disastrous earthquakes that has triggered mass movements in Tajikistan (LEONOV, 1960, EVANS, 2009). Loess landslides with an estimated volume of 245 million m^3 formed to loess flow that travelled up to 20 km in the Yasman valley (EVANS, 2009).

Another Tajik earthquake occurred near the town Dushanbe with a magnitude of 5.5 in December, 1989. ZOLOTAREV and ZERKAL (1996) carried out an investigation in loess flows in Tajikistan which were caused by this earthquake. These studies allowed the defining of the following factors that determine the slope stability in loess:

- Construction of loess mass
- Moisture content level of loess layer
- Geomorphological conditions and features of relief
- Seismic conditions of the region

In contrast to ZHANG (2007), this research says the slope angle has no affect in the development of loess flows, since the loess slope that occurred in Tajikistan was only 4°. However, ZERKAL (1994) pointed out that the slope angle is an important factor for estimating kinematic characteristics of mudflows, such as velocity and distribution. Nevertheless, the failure mechanisms of loess flow in Tajikistan were different relating to liquefaction (ISHIHARA, 1990). This is well documented in cases of loess liquefaction.

5.2.4 Combination of earthquake and precipitation on loess slope stability

In order to make a relationship between precipitation and earthquake impact to failure on loess slope, it is attempted to show three examples. These are related to three loess landslides located in the southern part of Kyrgyzstan.

5.2.4.1 Kochkor Ata Landslide

The Kochkor-Ata landslide failed in April 13th, 1994. Due to the remote location of the area, there were very few people living in this zone and therefore only one man died under the flow. Only few data are available from this landslide. Kochkor-Ata is a complex rotational slide that had developed in Quaternary and Tertiary sediments and is one of the biggest landslides in the Mailuu-Suu River basin with a total volume of more than 10 million m^3 (ROESSNER, 2005).

Precipitation data is obtained from meteorological station of the country (Report of the Meteorological station, 1930-2010) and earthquake data is taken from USGS database (Source: United States Geological Survey, www.usgs.com). Precipitation data for this region has been observed for the last 71 years. Over these years, the least amount of precipitation, 633.3 mm/year, was observed in 1944. The highest amount, 1716.4 mm/year, was observed in 1969. The second highest data of 1639.2 mm/year was in 1987 (Fig. 5-5).

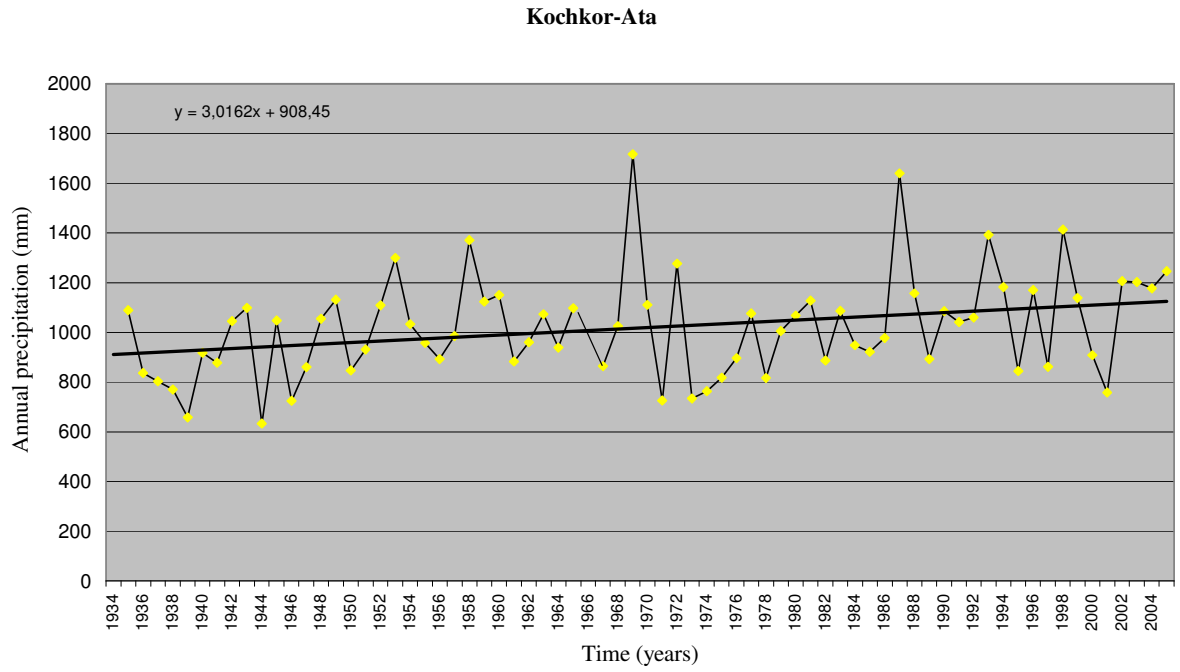

Fig. 5-5: Annual precipitation in Kochkor-Ata region

Fig. 5-6 presents earthquake data from USGS data source. An earthquake with a magnitude of 4.6 occurred on December 26th in 1987. The epicentre was 23 km from the landslide area. The most recent, strongest earthquake with a magnitude of 6.2 occurred in May 1992 with a distance of 17 km. Aftershocks followed for one month. An earthquake with a magnitude of 5 was registered in distance of 19 km on November 6th 1992. In 1993 two earthquakes in March and May registered with magnitudes of 4.4 and 4.8, respectively. In the year when failure occurred there were two earthquakes with a magnitude of 4 with a distance of 76 km on January 25th and with a magnitude of 3.9 and depth of 17 km on 16th of February. The failure occurred on April 13th, 1994.

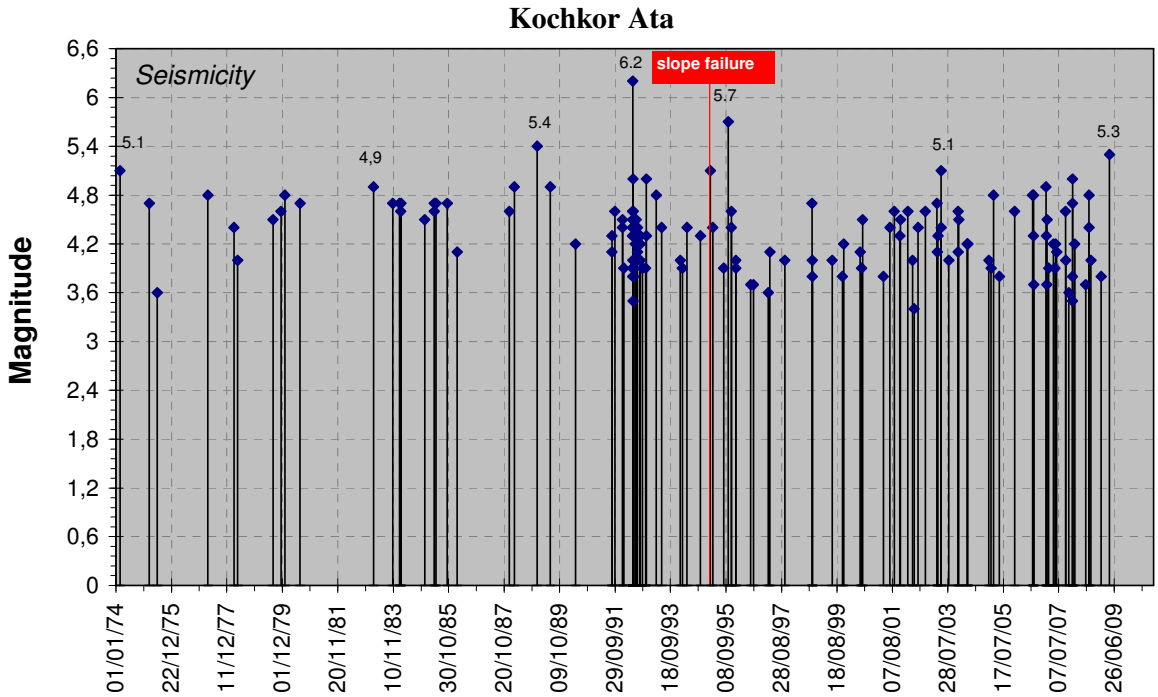

Fig. 5-6: Earthquake data in Kochkor-Ata region showing the strong earthquakes

The satellite image CORONA from 1989 shows the slope degradation on the upper part of the slope. It presents the development of tension cracks before 1989 (Fig. 5-7a). The next CORONA image obtained was after the failure occurred in 1995 (Fig. 5-7b). It can be said that the strongest earthquake, with a magnitude of 6.2, registered in this region in 1992 caused to widen the tension cracks to make this slope unstable.

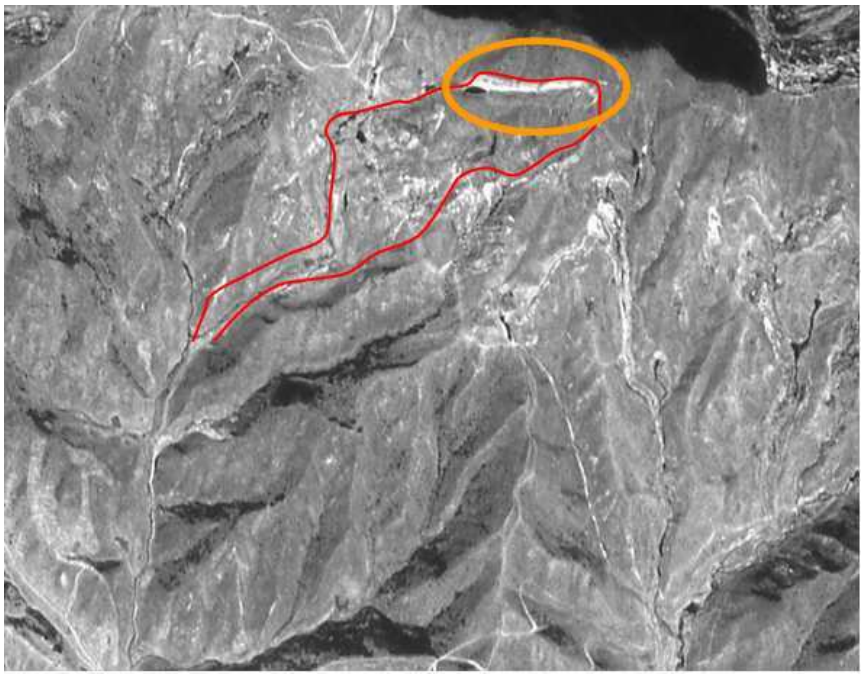

a)

b)

Fig. 5-7: CORONA images a) presenting tension cracks on the upper part of the slope; b) after the failure in 1994

5.2.4.2 Kainama landslide

This loess flow failed in April 2004 causing the death of 33 people and destruction of 12 houses. The development of loess flow is shown in the Fig. 5-8. Satellite images in September 2001 show a small failure on the right part. In August 2003, there were eroded areas on the upper part of the slope and failure in the middle parts was also observed. Images that were obtained in August 2004 presented the case after the failure.

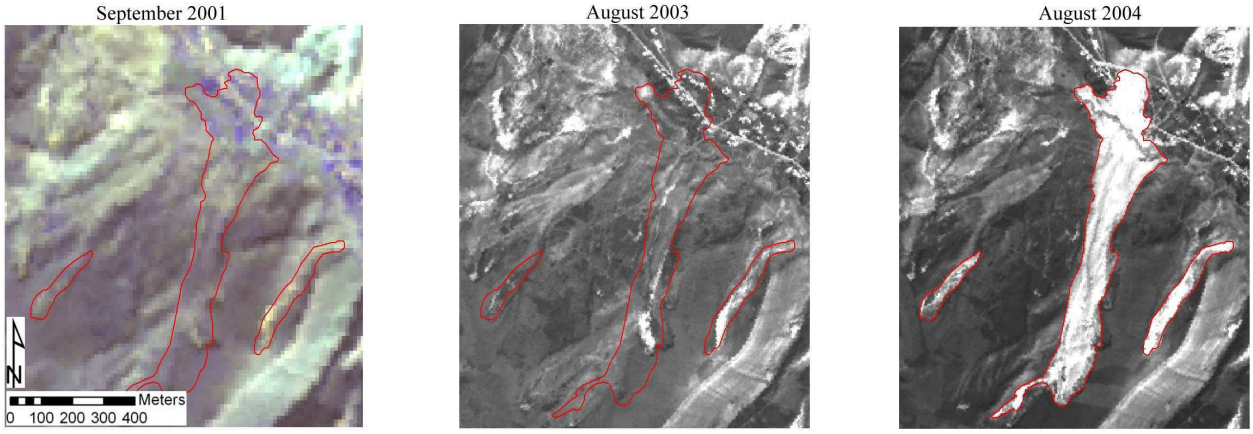

Fig. 5-8: Development of Kainama slope (HAVENITH and BOURDEAU, 2010)

In order to find out the relationship between earthquakes and precipitation impact, first precipitation data was obtained. Gulcha meteo station is the nearest station to the Kainama region, and worked from 1938 to 1991. Observation was carried out over 53 years. Unfortunately due to the closing of the station there is no longer any data available. However the data shown presents the highest amount registered in the Kainama region (Fig. 5-9). Precipitation amounts observed within the 53 year period shows the least amount was 305.2 mm/year and registered in 1939. The highest amount was 942.8 mm/year in 1987. The next observation started to measure the precipitation in the station from 2003. Amount of 923 mm/year was registered in this year, mainly concentrating in April and May.

Earthquake data from 1973 shows the strongest seismic event with a magnitude of 7.3 occurred in 1973 (Fig. 5-10). An earthquake with a magnitude of 5.2 occurred in September 2002. Before this time several seismic events had been registered with magnitudes from 3.4 to 4.6. Three earthquake events were registered in 2004 before the failure: one seismic event with M 4.7 on March 26, the second one with M 4.2 in April 8 and one earthquake with M 4.2 in April 9. These earthquakes probably had an impact on slope instability. The relationship of these seismic events and highest amount of precipitation caused slope failure.

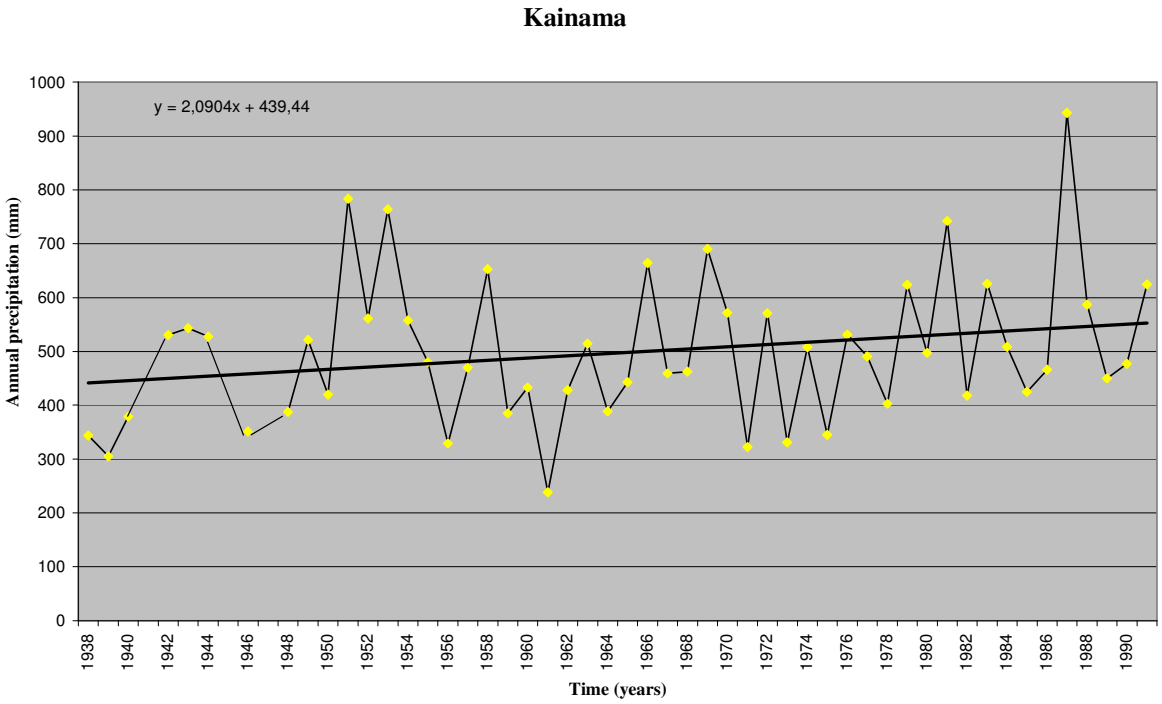

Fig. 5-9: Graph presenting the highest amount of precipitation registered in the Kainama region

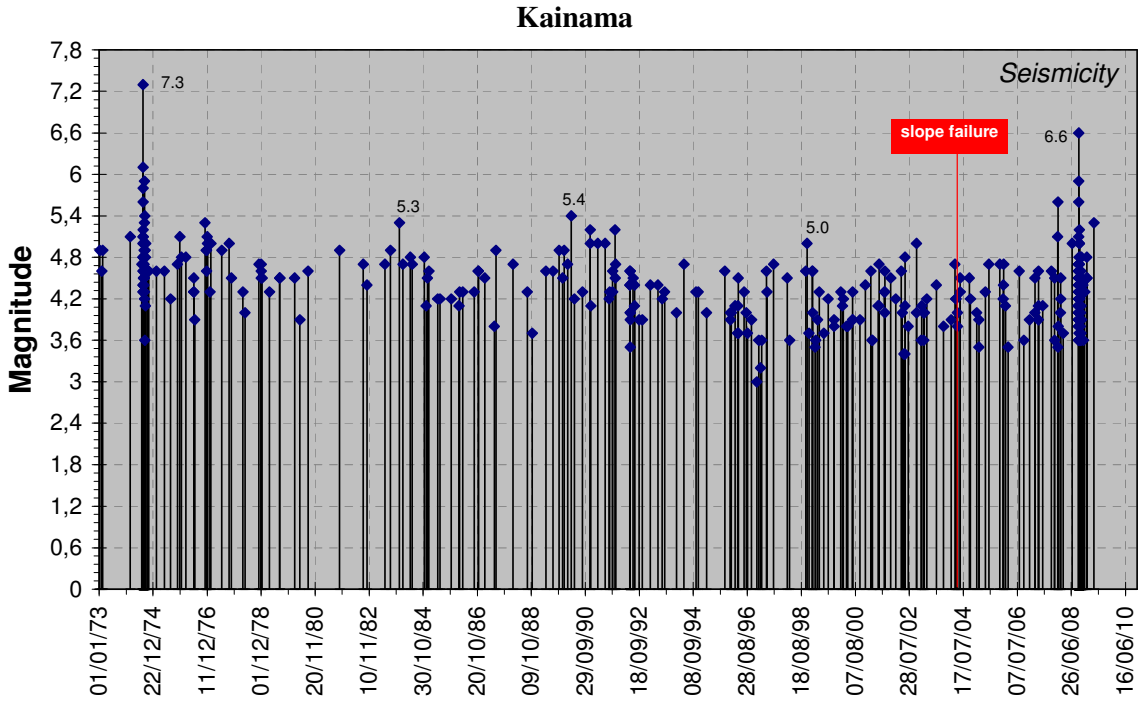

Fig. 5-10: Earthquake data for the Kainama region (source USGS)

5.2.4.3 Upper Koi-Tash

The Upper Koi-Tash landslide is located on the right bank of Mailuu-Suu river. In this area a loess layer covers the top of the slope. Displacement data from extensometers available from 1996 show a correlation between seismic activity and precipitation (Fig. 5-11). However, displacement of 60 cm was observed after the earthquake in 1997 with a magnitude of 5.9 at a distance of 150 km from the site (HAVENITH, 2002). Apart from this earthquake, there is a correlation between snow cover and temperature rise. During the spring time the snow thaws due to the temperature rise, and this induces small displacements.

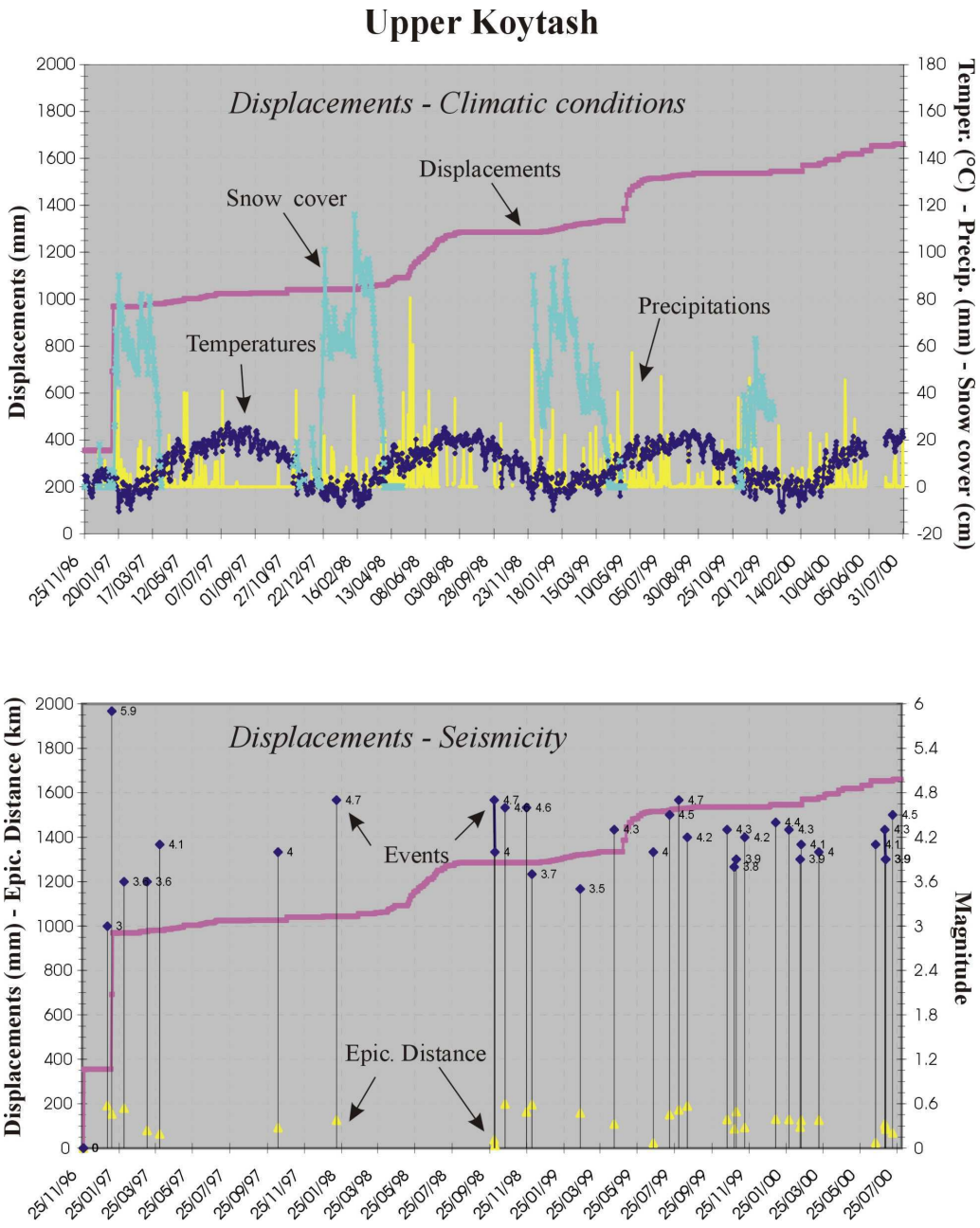

Fig. 5-11: Displacement from extensometer data in Upper Koi-Tash landslide (HAVENITH, 2002)

5.3 Failure mechanisms

Identification of failure mechanisms of slope is necessary to define the potential for unstable conditions. Different failure modes in loess slopes exist depending on sedimentological properties, the stress history and the thickness of the deposits (DERBYSHIRE et al 1994). Loess deposits located in Missouri and Washington presented failure mechanisms as erosion including piping. This type of slope degradation is mainly observed in silty loess (HIGGINS, 1985, 1989). Piping failures can be originated 2 to 3 m behind the top of cut surface. These pipes are initiated by animal burrows and then enlarged, forming gullies. Shallow types of movements and rotational slides in Washington have also been observed (KANE, 1968). Studies carried out in Lanzhou loess slopes show the main failure modes can be progressive failure. Slope analyses show that in Lanzhou loess, stresses concentrate at the toe and central part of slope as is shown in Fig. 5-12 (DIJKSTRA et al, 1994).

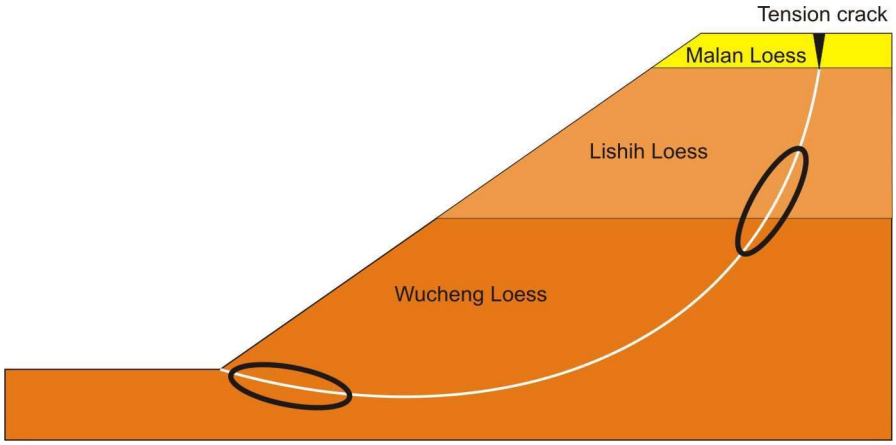

Fig. 5-12: Stress concentration in loess slopes occurs in the central part and toe of the slope (DIJKSTRA et al, 1994).

NIYAZOV (1974) carried out field investigations related to loess landslides within Central Asian countries Kyrgyzstan, Uzbekistan and Tajikistan. These studies show that in Uzbekistan and Tajikistan, loess flows dominate. Sliding type of movements are mainly distributed in Kyrgyzstan.

5.4 Tension cracks

DIJKSTRA (1994) stated that tension cracks are a main catalyst for slope failure. Furthermore some researchers indicated that the tension cracks can cause to damages. SUN (2009) described the ground fissures are geological problems that destroy buildings, infrastructure and threaten people's lives.

NIYAZOV (1974) referred to the research of appearance of cracks related to seismic shaking which has been studied by Dedova et al. They stated that in dry loess deposits, tension cracks appear in 7 ball of intensity of MSK scale (for more details of this scale see APPENDIX 2) tension cracks appear with width of 1-5 mm, 8 ball 6-15 cm, in 9 ball 15-20 cm. In the case of seismic impact more than 9 ball, cracks have widths 0.5 m and more. The seismic impact of

more than 9 ball can develop nets of cracks, blocks of sliding, and subsidence with vertical amplitude of 15-25 m. These 9-10 ball of earthquakes can impact the bedrock, then seismodislocation appears in depths of up to 3 m and more, developing nets of cracks.

Some points of initiation of tension cracks due to water effects are considered in loess slopes in Gansu Province. Research related to this issue presents the effects of the through-flow of groundwater. The resulting solution of salts and carbonates result in a progressive failure of the loess structure within the slope. Subsequently, the tensional forces of the whole slope are distributed over an increasingly smaller proportion of undisturbed loess. At this stage, plastic deformation in the loess slope begins, resulting in tension cracks.

Few research works have been carried out on the behavior of tension cracks. KRIGER (1965) studied loess slopes in Central Asia and some parts of Ukraine. According to him, the cracks in loess can be as prismatic discontinuities. He defined the cracks developed as networks of fissures and this assumption is supported by RUSSEL, (1944a). RICHTOFEN (1877) described tension cracks developed in loess with a length of 60m, width in the lower part of up to 3-5 m; the width on the upper part is up to 30-40 m. PECSI (1994) observed cracking in Dunaföldvar loess bluff near the Danube River in Hungary.

Networks of cracks in loess slopes are also observed in Chinese loess landslide. The landslide is located on Heifangtai, which lies to about 25 km west of the Lanzhou basin in the Gansu province, China. The landslide is a typical loess flow. The crack on the crown of the landslide gradually expands away from the scarp of the landslide after the failure.

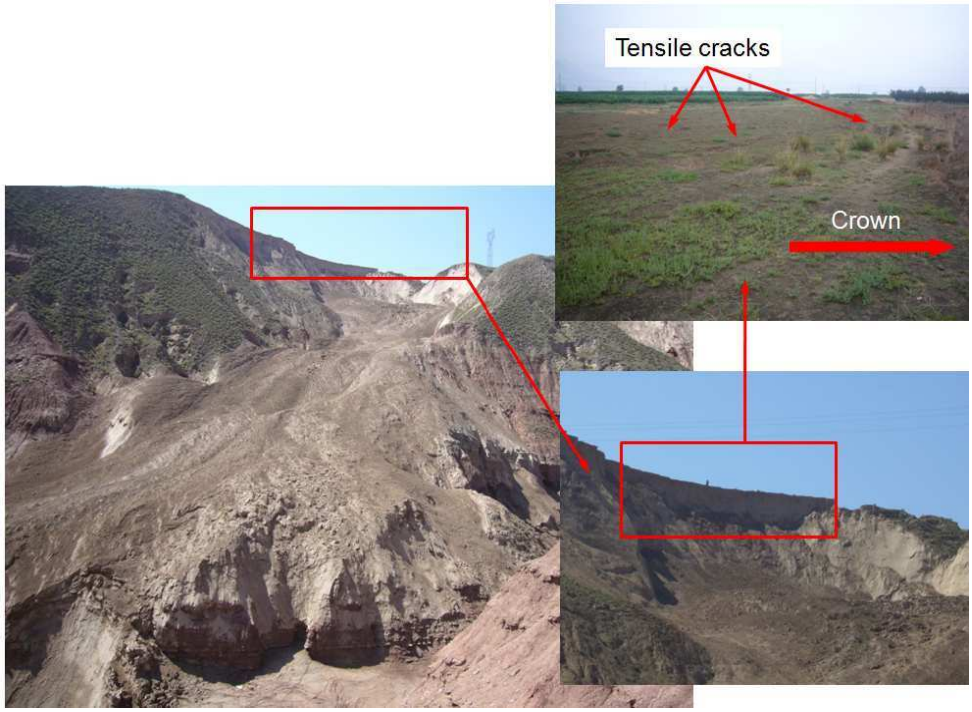

Fig. 5-13: Landslide located on Heifangtai in Gansu Province, China (Photo by Fanyu Zhang)

Chapter 6: Hypotheses of occurrences of loess landslides

6.1 Slope failure development within the loess slope

Previous chapters illustrated that loess landslides are mainly occurred in seismically active regions and therefore earthquakes have a direct impact on the loess failures. The researches on loess landslides revealed various aspects that caused to occurrence of slope failures. Regarding to geomorphological factors, slope inclination of 30-35° was defined to be the most susceptible in investigations carried out in landslides triggered by Haiyuan earthquake in China that occurred in 1920. An obvious effect of seismic shaking on loess slope stability can be presented in example of Upper Koi-Tash that located in Mailuu-Suu region, Kyrgyzstan (Fig. 5-11). As recorded by means of landslide registration systems at the unstable slope, the displacement of 60 cm is an argument of an earthquake effect on this landslide. Another important feature that made it susceptible to failure, is the tension cracks located on the upper part of a slope. Satellite images that obtained from the landslide prone areas in Kyrgyzstan showed the presence of tension cracks on the upper part of a slope. These cracks facilitated the slope failure by often occurrence of seismic shaking; the tension cracks spread out and made possible to further water infiltration into the slope. The researches related to water effect by precipitation and ground water in loess slope have been performed in the loess landslide cases in Northern China and Central Asian countries, as Uzbekistan, Tajikistan and Kyrgyzstan.

Mainly development of landslides depends on soil characteristics and environment of location. Such conditions define the occurrence of failure also in a loess slope. Due to specific characteristics of loess, the properties obtained from different literature have not presented a tendency to show one definite property for loess soil (See APPENDIX 1). However it can be pointed out some common properties of loess as big pores and cementing bonds. Strength parameters of loess depend mainly on water content, density and clay content. Determination of the strength properties of loess depends on apparatuses and test procedures.

The factors that facilitate loess slope to fail are dynamic loading, soil characteristics and climate conditions of specific region. But another important aspect as presence of tension cracks needs to be accounted in order to make slope stability works. To figure out which factors facilitate the loess slope, aspects on possible cases of appearance of tension cracks in loess slope and further slope failure development are discussed in the following sections.

6.2 Water infiltration into the slope

It is well known that loess material has a low permeability coefficient (WANG et al, 2004). Nevertheless, precipitation features and its amount can be an aspect to cause the slope failure.

The correlation between slope displacement, snowmelt and increasing of temperature are recorded at the Upper Koi-Tash landslide based on extensometer data.

To investigate the rainfall intensity impact on loess slope, numerous tests have been performed by WANG et al (2004). According to their research, landslides mainly occur during two seasons. In years characterized by a normal precipitation rate, landslides usually take place in July to September. While in years characterized by heavy rainfall, landslides occur mainly in February to April and July to September. WANG et al (2004) carried out infiltration tests to find out rainfall intensity impact. Test results presented that short-term intensive rainfall has less impact on loess slope stability than long-term continuous light rain. Besides, the response of water content and suction is limited within the top 4 m. This is due to the fact that landslides in this area usually occur at shallow depths even during heavy rainfall, in the absence of deep seated cracks or other weak planes.

6.3 Progressive failure

During repetitive wetting from precipitation and groundwater increase, the loess structure weakens and cementation bonds are destroyed. According to the theory of DIJKSTRA et al (1998), soluble salts are dissolved and flow away leading to salt efflorescence's near spring zones at the toe of the slopes. Such observations considered to be evidence that the structure of loess is decreasing. In this case, the progressive decreasing of slope stability is observed and loess mass experiences the creep deformation and relaxation. Under compression the internal structure of loess may collapse and grains may be squeezed into the pore spaces resulting into mutual interlocking (DIJKSTRA et al, 1998, 2000, DERBYSHIRE et al, 2000).

Another view of progressive development of failure and appearance of cracks presented by NIAYZOV (1974) is illustrated in Fig. 6-1. This failure is related to water infiltration and further subsidence. In further, this case is depicted because of detailed explanation of appearance of cracks in case of water effect. By investigating the loess landslides in Central Asia, Niyazov divided two stages of slope failure. The first stage involves the preparatory stage that consists of three phases: phase of preliminary compaction, phase of subsidence, phase of secondary compaction. The second stage named as a stage of movement that includes phase of displacement, phase of flow and phase of secondary displacement.

During the **preparatory stage (I)**, first of all compaction take place due to the decreasing of pores. However the loess structure is not destroyed. This case is characterized by the appearance of tension cracks on the top the slope. Tension cracks length is approximately 15-30 cm and depth is 2-3.5 m. About 30% of whole mass of loess layer is wetted and vertical deformation occurs. In **phase of subsidence (Ia),** increasing of subsidence occurs in deep wet zones. In this case, the scarp of the landslide formed and the nets of tension cracks developed on the top of the slope. Further subsidence caused to destruction of loess and further compaction. This compaction takes place due to vertical and horizontal deformation. Maximum deformation takes place when the critical moisture content achieved, but not only in case of saturation. **Phase Ib** is formed by a longer time and depends on further saturation.

During the stage of movement, at first the **phase of displacement (II)** takes place with forming of sliding surface afterwards the **phase of flow (IIa)** is followed. In this case heave formed on the lower part of the slope, where the upper part of slope mass starts to move downwards. **Secondary displacement phase (IIb)** caused to formation of further displacement on the upper part of slope mass than caused to expansion in loess soil.

This Niyazov's theory on failure development in loess slope mainly considers the influence of underground water and precipitation. However, he stated that in case of external stress, as dynamic loading, the loess slope can fail without the first stage. In this point, NIYAZOV (1974) mentioned the investigations carried out by Dedova et al. The studies included impact of earthquakes on appearance of tension cracks in loess slopes and stated in the Chapter five. This investigation is an argument of crack development by effect of earthquake.

Combination of different factors and trigger mechanisms stated in previous chapters brings to make a hypothesis on the mechanisms of development of slope failure in loess deposits.

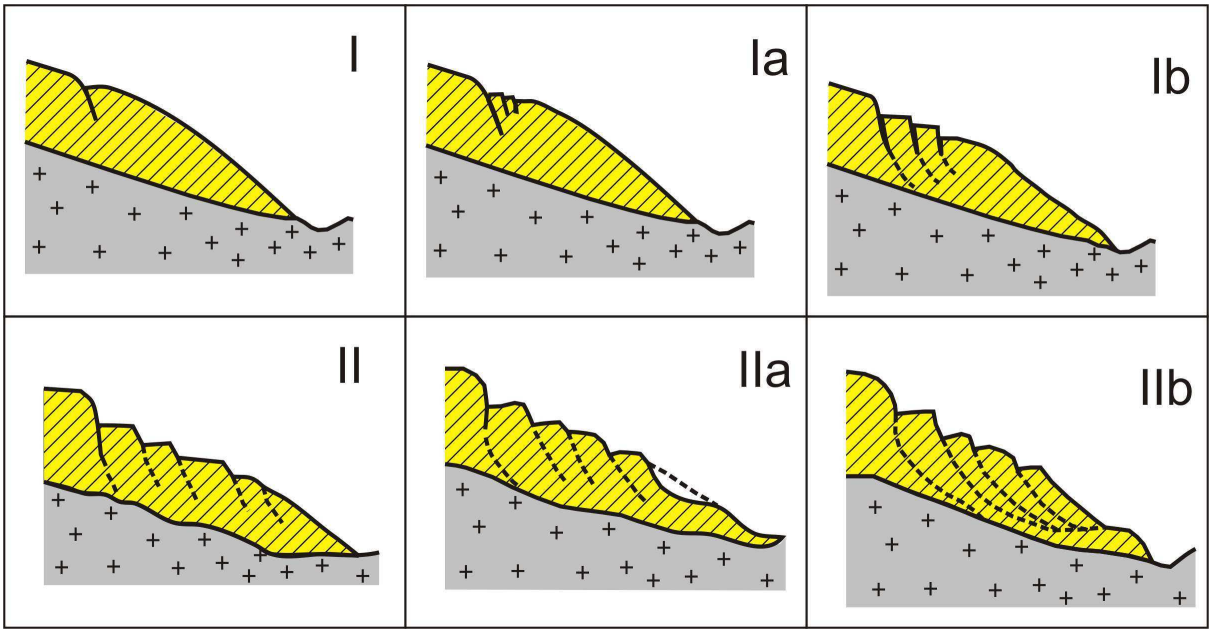

Fig. 6-1: Progressive loess slope failure (by NIAZOV, 1974). *Preparatory stages*: I – phase of preliminary compaction; Ia- phase of subsidence; Ib – phase of secondary compaction. *Stages of movement*: II – phase of displacement; IIa - phase of flow; IIb – phase of secondary displacement.

6.4 Hypotheses regarding to the formation of tension cracks and the development of loess slope failure

Besides the abovementioned cases concerning of appearance of tension cracks with impact of precipitation, the development of failure mechanisms in loess slope in terms of seismic factors need to be taken into account. Reviewing the results and investigations from researches related to loess slope, the following hypotheses regarding the formation of cracks

in the landslide body and the development of slope failures in loess material can be drawn by dividing into three stages (Fig. 6-2):

- Seismic shaking has a direct impact on loess slope stability. Due to the strong seismic shaking, small cracks appear on top of the slope.

- After the appearance of small cracks, rainfall and snowmelt infiltrates into the slope. Through this, the internal loess structure becomes destructed and the subsidence in loess mass appears. Through this, progressive failure occurs. As a result, the slope starts to fail gradually. One hypothesis regarding to the formation of tension cracks in slopes located in river valleys is erosion processes. The toe of the slope is weakened by river erosion favoring the decrease of slope foot stability. Due to erosion, the upper soil mass starts to move downwards. This effect causes to weakness on top of the slope, leading to tension cracks.

- Further disturbances of loess fabric may take place on the upper part of the slope due to combination of various environment factors. One of such processes, as snowmelt can cause water infiltration into the loess fabric, breaking down cementing bonds and making the soil fabric compacted. Plastic deformation takes place within the slope inducing further decrease of the factor of safety of the slope leading to failure.

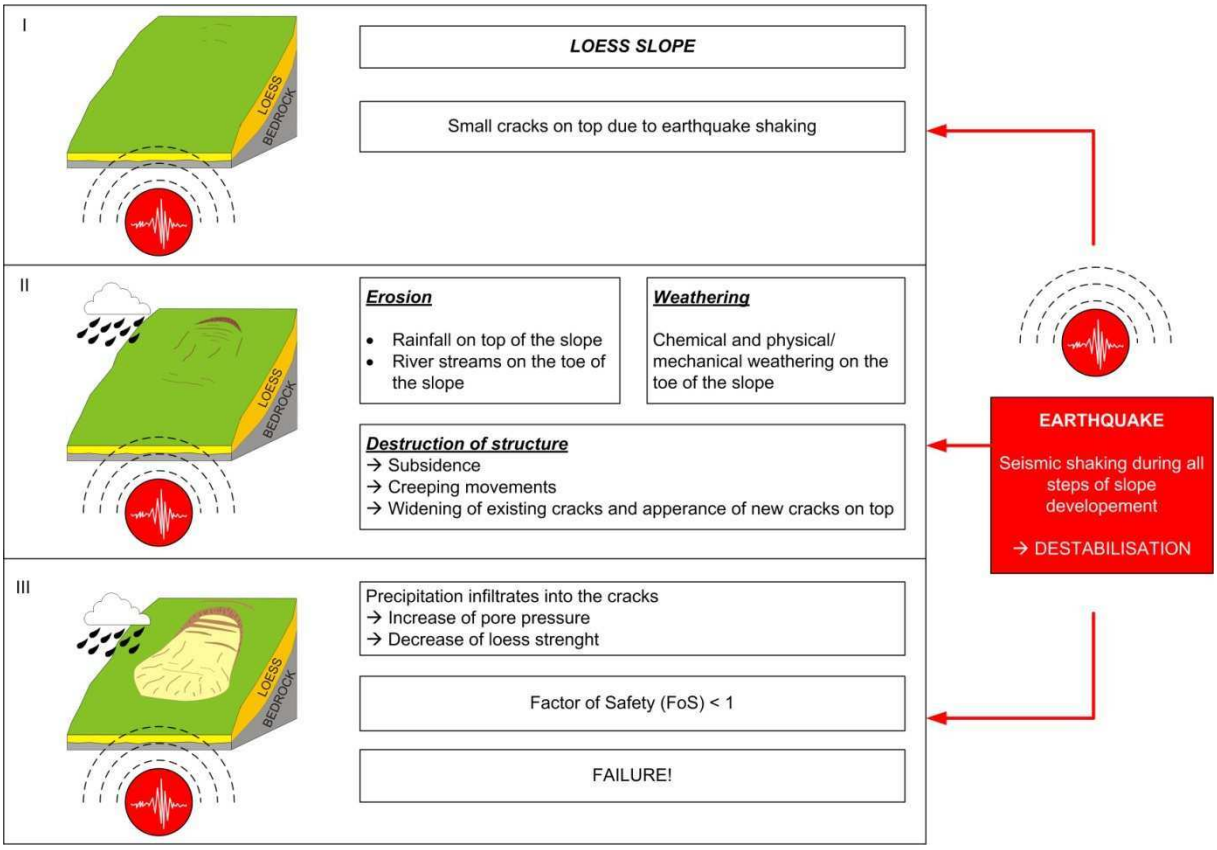

Fig. 6-2: Hypotheses to explain loess slope failure development in Central Asia.

Fig. 6-2 can be explained as follows:
1.) Top block: Small cracks appear on top of the slope due to seismic shaking
2.) Middle block:
- Erosion: Rainfall may erode the surficial layers
  River streams may erode the toe of the slope
- Weathering: Weathering affects the slope, an evidence of such weathering presented as salt efflorescence's on the toe of the slope
- Destruction of slope structure: Global subsidence; Widening of existing cracks and development of new cracks on top of the slope

3.) Lower block: Precipitation infiltrates into the cracks that caused to decrease of loess strength. Factor of safety gets lower causing to failure.
4.) Earthquake block: seismic shaking may occur during all steps of slope failure causing destabilization

It is illustrated on the hypothesis, the earthquake effect considered in development of loess landslides. During the process of loess slope failure, seismic shaking due to the earthquake activity is likely to take place. Thus, loess slope failures in Central Asia need to be considered as dynamic triggered loess landslides.

6.5 Earthquake impact on loess slopes

To study dynamic triggered landslides, the traditional methods exist. However, it is necessary to consider the case of complex topographical features in ridges and seismic wave propagation. In addition, seismic wave components, as refraction and diffraction within complex topographical reliefs and different geological units are important aspects. Because of these factors, seismic wave arrival can get complex characteristics. Most studies on seismic slope stability in loess deposits have been carried out by using of traditional methods. Nevertheless, effect of local condition on seismic waves has not deeply investigated. To study the ground shaking and site effects in a loess slope, at first the behavior of a dry slope need to be considered. DANNEELS et al (2008) observed strong amplification in a thicker cover of loess on top of a slope. This study showed that it is important to investigate the loess thickness because it controls site amplification.

6.6 Tension cracks in loess slopes

As presented on Chapter five, the tension cracks have an important role on slope instability. In other words after appearing the cracks on the crest of a slope, the loess slope intensifies its development to fail. Although the presence of cracks plays an important role within loess slope failure, there are not clear investigation which parameter of crack the most critical. There are some components as location within the slope body, depth and inclination of crack can be probable critical components to intensify the slope to fail. But these possible characteristics of crack have not investigated. In this case, it is necessary to carry out parametrical studies to find out a critical component of tension crack parameters (distance from the crest, inclination, width and length). Here, it is necessary to note that the tension cracks introduced as **weak zones** in numerical slope models, the properties are given as lower

values than the slope materials. These weak zones present not only one specific crack but the nets of cracks.

6.7 Laboratory testing

In order to simulate slope cases by means of numerical software, it is necessary to get insight parameters of loess soil. Extensive overview of loess properties from literature has not shown a tendency to present one appropriate strength property to attribute on a slope model. The reason is the loess properties depend on environment of location, genesis and age of deposit. Since this research involves the loess landslides in Central Asia, two landslide sites were chosen in order to get loess samples. At first the soil characteristics are determined in order to better explain the insight strength parameters. By using of laboratory testing, strength parameters as cohesion and friction angle are defined.

6.8 Investigation of loess slope with presence of tension cracks

Several components of a slope such as height and angle may have an influence on topographic site effects. Geological site effects may be induced by the presence of the weak loess layer overlying bedrock. Because of the slope cases from Central Asian countries are considered, slope inclination is taken equal 15° to 30° and loess thickness is ranged to 20 m and 50 m. By applying the seismic shaking, the slope with superficial loess layer is studied. Certainly the tension cracks that are located on the top part of the slope can cause complex site effects in both topographical and geological patterns. In order to find out an impact of tension crack on local site effects in a loess slope the crack cases are investigated. The way of investigation can be presented schematically in Fig. 6-3.

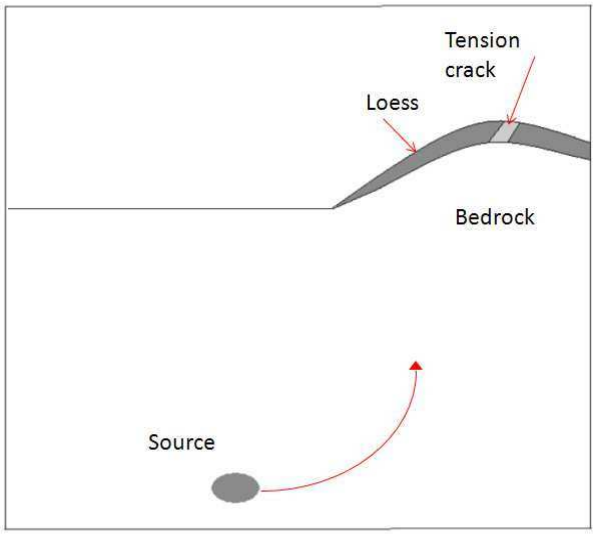

Fig. 6-3: Investigation of local site effects within the loess slope

6.9 Conclusion to chapter

Many different factors exist that have influence on slope stability and can trigger landslide movement. POPESCU (1996) summarized the most important triggering factors. By definition a trigger is an external stimulus such as intense rainfall, earthquake shaking, volcanic eruptions, storm waves or rapid stream erosion that causes a near-immediate response in form of a landslide by rapidly increasing the stresses or by reducing the strength of slope materials (WIECZORECK, 1996). In some cases it seems that landslides occurred without any apparent attributable trigger. The reason can be the combination or variety of causes that gradually softens the material and finally leads to landslide. Often not only one, but rather the interaction of various triggers is the reason for the landslide movement. The Kainama landslide in Kyrgyzstan that killed 33 people in April 2004 (see CHAPTER 1, Fig. 1-1) occurred due to the combination of earthquake ground shaking, which opened cracks and fissures and then heavy spring rain and snow melting that leaded to a further destabilisation and finally to the slope failure (DANNEELS, 2008). But this is also the complex part. Even though many research works exist, in which the influence of water and rainfall is described, detailed analyses about earthquake waves and ground shaking on slope stability is still in its infancy.

Therefore, this research investigates the ground motion and its anomalies in a loess slope. Detailed parametrical studies allow understanding the behaviour of slopes in dry conditions. Another aspect that analysed in this work is an influence of existed tension cracks on slopes due to earthquake shaking.

Chapter 7: Laboratory analyses

7.1 Introduction

Laboratory measurements were made to collect important information and parameters about loess material in Central Asia and to use these data for further modelling analyses. Cemented bonds and low moisture content enable loess slopes to sustain nearly vertical slopes. Slopes in loess mass can stay for a long period influenced by geomorphological and geological processes. These processes disturb the cementation bonds of loess fabric and consequently lead to a decrease in the strength parameters. Such kinds of modifications cause a collapse of material and this leads to catastrophically slope failures. In order to study deformations of loess slope by means of numerical model, it is necessary to collect the strength parameters of soil that present the conditions of loess mass in field conditions.
Therefore, different methods and analyses were made as follows:

- Sampling: Taking numerous specimens from loess material in two different landslide sites in Kyrgyzstan
- Analyses of mineralogy, chemistry and microstructure: Investigation of the mineralogical composition and structure of material with X-ray diffraction analyses and Scanning Electronic Microscope (SEM)
- Geotechnical tests: In this context various tests were made for characterizing the soil material. Furthermore, the following tests were executed:
  - Direct shear tests
  - Triaxial tests
  - Ring shear tests

In the following the methodology of laboratory analyses, sampling sites and results are described.

7.2 Methodology and Analyses

7.2.1 Sampling

Two different landslide areas were selected in South Kyrgyzstan in order to obtain loess samples (Fig. 7-1). The first is the Upper Koi-Tash landslide located in the Mailuu-Suu basin. The second area is the Kochkor-Ata landslide and is located approximately 15 km to the north-east of the first landslide site and located in the Upper Mailuu-Suu river basin (Fig 7-1).

Fig. 7-1: Location of sampling areas: Upper Koi-Tash and Kochkor-Ata landslides (Source: Google Maps)

7.2.1.1 Landslide Kochkor-Ata

Failure of the Kochkor-Ata landslide occurred on 13th April 1994. As it is illustrated in Fig. 7-2 the total runout is more than 3.6 km. A small spring that local people used as a drinking water is observed near the tongue of the slide. A small lake is located on the opposite side of the spring.

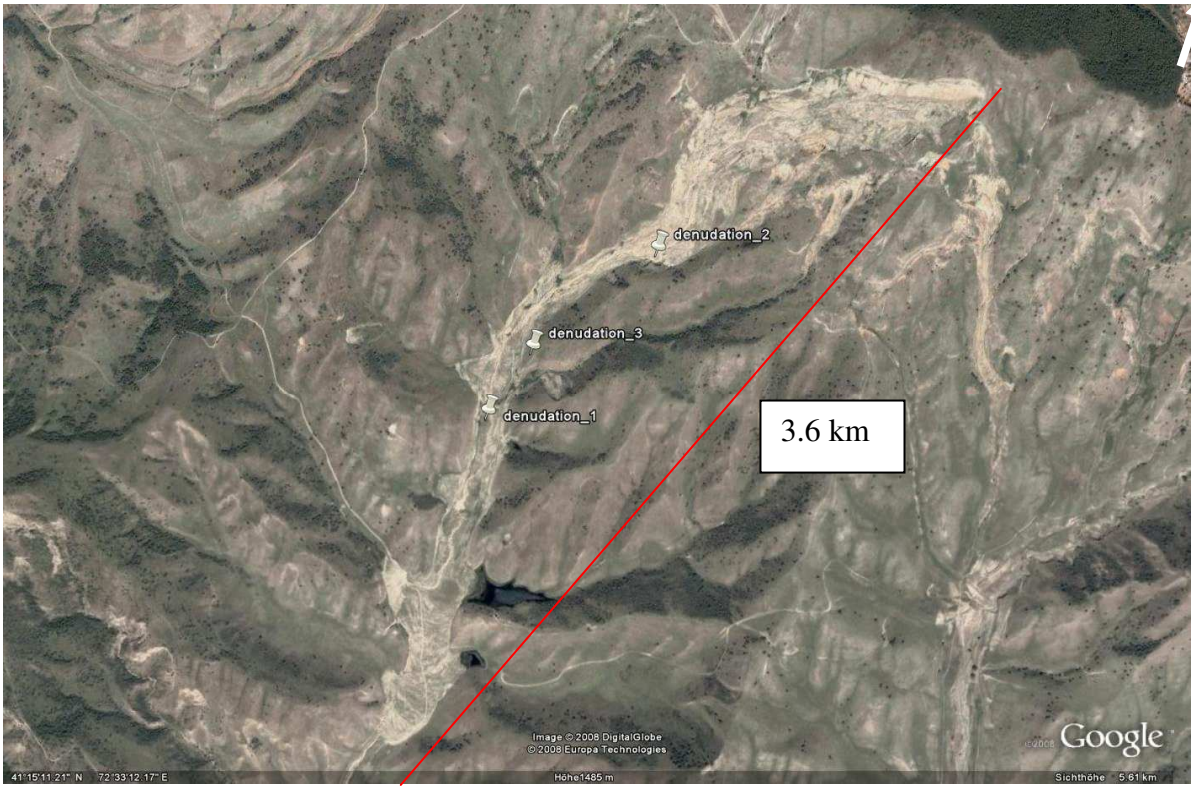

Fig. 7-2: Google earth image showing the whole landslide area Kochkor Ata and the denudation areas, where different samples were taken.

Three denudation areas were chosen for loess samples. Due to limited accessibility of this landslide area (it cannot be reached by car), the sampling was carried out manually. Fig. 7-3 illustrates the taking of undisturbed loess samples for laboratory investigations and the sealing of the outer sample layer with paraffin for preserving the water content inside the loess soil.

Fig. 7-3: Sampling of loess (left), and preservation of the sample to enable transport to laboratory (right)

The surface of the first denudation area is eroded by precipitation. During the sampling, small layers of carbonates are observed in samples from the second denudation area. In the middle part of the slide (denudation area three), roots of canes were observed. This is an indicator of wet conditions in the area. Table 7-1 shows the location features of sampling that were carried out in Kochkor-Ata landslide.

Table 7-1: Coordinates of sampling areas at the Landslide Kochkor - Ata (Soil sampling carried out on 09.09.2008)

Trench (Denudation)	Coordinates		Altitude, m	Remarks
Spring with pure water	41° 15' 04" N	72° 32' 52" E	1370	Local people use as drinking water
Denudation 1 (western part)	41°15' 04" N	72° 32' 52" E	1373	
Denudation 2 (7 soil samples were taken)	41° 15' 30" N	72° 33' 14" E	1442	
Denudation 3 (eastern part) 4 samples	41° 14' 59" N	72° 32' 59" E	1382	There is a marsh nearby the soil sampling
Spring with salty water	41° 15' 14" N	72° 32' 57" E	1384	450 m north of denudation 3

7.2.1.2 Upper Koi-Tash landslide

For a second sampling, the site Upper Koi-Tash landslide was selected. This landslide is located on the left bank of the Mailuu Suu river in the south of Kyrgyzstan. The whole landslide is part of the much bigger landslide named Koi-Tash (Fig. 7-4). Movement of the Upper Koi-Tash started in 1954 with minor mudflows. In 2004 the landslide came down after a combination of earthquake and rainfall. The height of the main scarp is about 15 – 20m, with a length of the tongue about 500m. The main threat of this landslide is on one side, danger to the small village on a foot of the landslide and on the other side the uranium tailing located beneath the sliding area. Destruction of the uranium tailing due to landslide movement can directly lead to pollution of this area itself, but also pollution of the fertile Fergana Valley due to river transport of uranium waste.

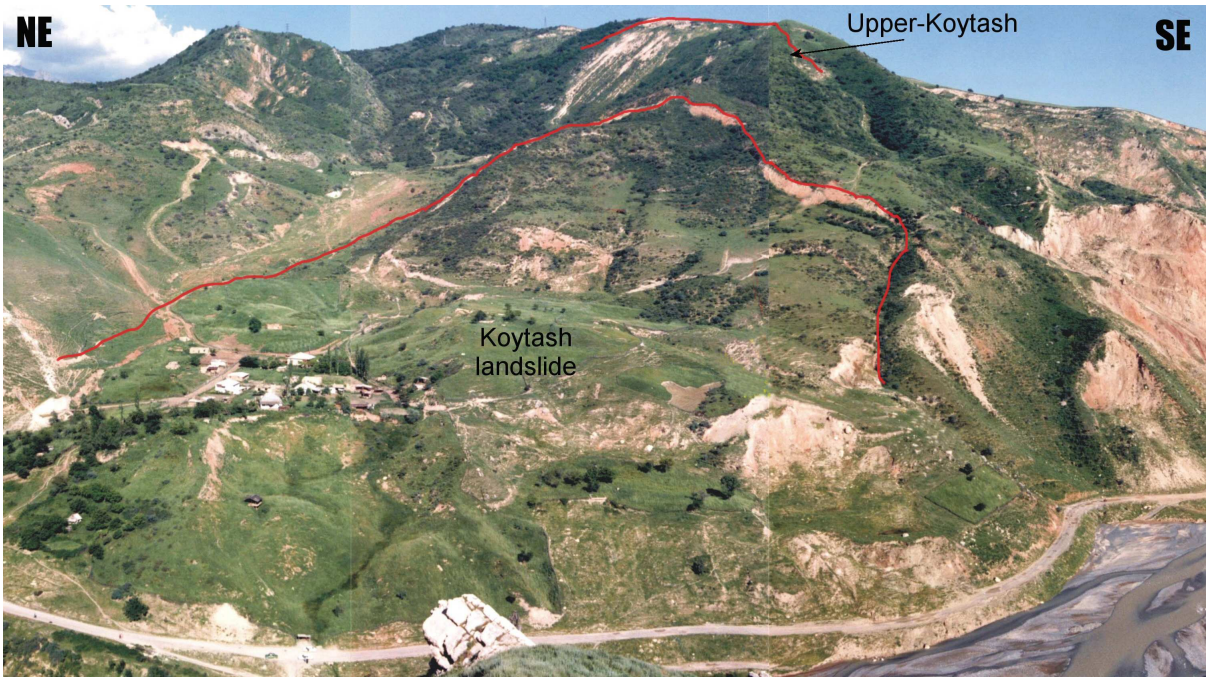

Fig. 7-4: Overview of landslide area Upper Koi-Tash (The name Koytash is the same as Koi-Tash) (DANNEELS, 2004)

During a field campaign in 2008, different loess samples were taken from the main scarp area and the flank areas of the landslide of the Upper Koi-Tash. Loess specimens were obtained from four denudation sites located on the scarp of slope (Fig. 7-5). During the sampling the gypsum layers have been observed in specimens. Table 7-2 gives the description of soils obtained from the landslide. Depth of samples taken varied from 1-12 m.

Table 7-2: Description of soil samples obtained from Upper Koi-Tash landslide

Number of sampling area	Samples number	Depth, m	Description
Denudation 1	1	6	N-S argillaceous soil (clayey soil) with small layers of Gypsum
Denudation 2	1	12	Eastern part 0/70 W
Denudation 3	1	3	Northern part, 132/82 SW
Denudation 4	1	1	Western part, 70/85 NNW, 83/80 NNW

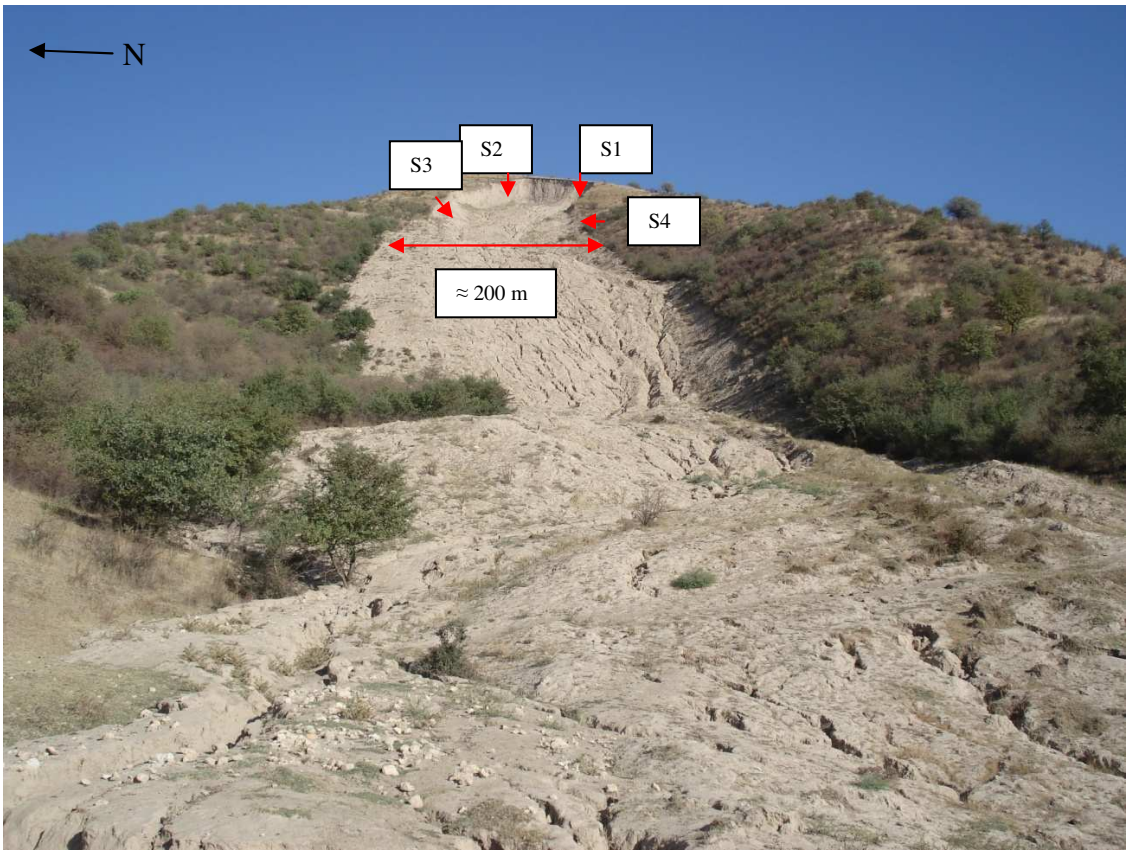

Fig. 7-5: Location of sampling places in the landslide Upper Koi-Tash in Mailuu-Suu area. S1-sample 1, S2- sample 2, S3- sample 3, S4-sample 4

7.2.1.3 Undisturbed and remoulded loess samples

Undisturbed and remoulded loess samples were used in the testing by using direct shear box, triaxial apparatuses and ring shear apparatuses. Undisturbed samples represented *in situ* natural condition of loess. Due to collapsibility of loess material with a low cemented strength, it is difficult to get truly undisturbed samples. Blocks of specimens are wrapped into the material and mantled with a wax in order to transport to laboratory (left picture of

Fig. 7-6). The photo on the right side in Fig.7-6 shows the collapsibility of some samples during preparation in the laboratory. Remoulded loess samples are used in the testing of ring shear apparatuses. Cemented bonds of reworked samples are destroyed and cannot present the natural *in situ* conditions. Due to this it is assumed that these samples are representing the slopes where the sliding has already occurred. In this case the failure depends on exceeding of failure thresholds of rearranged loess particle (DIJKSTRA, 1994).

Fig. 7-6: Loess sample after removal of the paraffin wax (left photo) and collapsibility of loess observed during the preparation of sample to testing (right photo)

7.2.2 Analyses of mineralogy, chemistry and microstructure

X-ray diffraction analyses have been performed to determine mineralogical composition of the samples. This analysis is widely used for the identification of unknown minerals and inorganic compounds. X-ray diffraction analyses were carried out at the Geological Department of the Liege University in Belgium.

7.2.3 Geotechnical analyses

In this study the geotechnical behavior has been analyzed by using direct shear, triaxial, and ring shear tests. Additional tests were made to characterize the soil material, such as density of soil or water content. The following describes the different methods in more detail.

7.2.3.1 Soil characterization

At the beginning of a geotechnical study, the general characteristics of the sample must be analyzed to describe and to classify the soil. The density of the soil, water content, porosity, void ratio, permeability, particle size distribution and the Atterberg limits are common properties in characterizing soils. All of these parameters have been obtained for the samples by using German standards for geotechnical laboratory analyses.

7.2.3.2 Direct shear tests

The direct shear test is one of the popular tests that is easy to perform and to obtain rapid insight to the shear strength parameters (HEAD, 1982). However there are drawbacks, such as

influence of the location, shape of the failure surface and a change of failure surface area during shearing (TERZAGHI and PECK, 1967). By using the direct shear box, cohesion (*c'*) and friction angle (φ) parameters are obtained.

7.2.3.3 Triaxial tests

Among various methods, triaxial testing is the most widely used procedure for determining the stress-strain and strength characteristics of soils. The outstanding advantages of this method are the control of drainage conditions, well-defined boundary conditions and control over stress paths. Consolidated drained (CD) triaxial tests for four undisturbed samples were conducted. The cylindrical sample is wrapped in a rubber membrane inserted between the rigid upper and lower loading platens and enclosed in the pressure cell. The specimens were consolidated and tested in cell pressures ranging from 25 kN/m^2 to 85 kN/m^2.

7.2.3.4 Ring shear tests

Ring shear tests were carried out by using apparatuses developed at Disaster Prevention Research Institute (DPRI) at Kyoto University. There are seven generations of these apparatuses (SASSA 1986, 1996, 2002, 2004). For testing, the fifth generation – DPRI – 5 – is used. Main features are shown in the Table 7-3. Fig. 7-7 shows a general view of ring shear apparatuses. It is possible to simulate the shear displacement in long distances in order to observe the liquefaction.

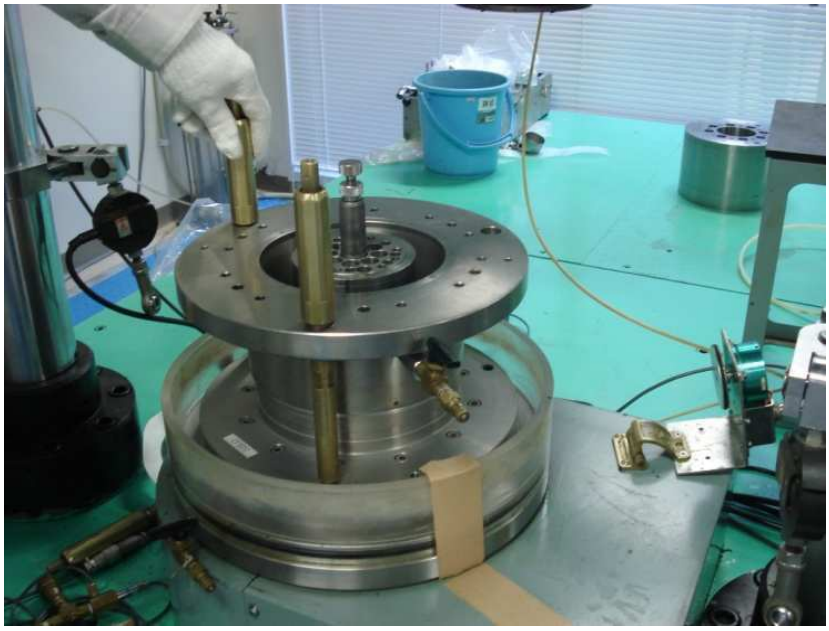

Fig. 7-7: General view of ring shear apparatuses

Fig. 7-8 shows the concept of the stress-controlled dynamic-loading ring-shear apparatus. This device aims to geotechnically simulate the formation of a sliding surface and the resulting post-failure motion by reproducing the stresses acting on the potential sliding surface in the slope: the static stress due to the self-weight of the soil layer, seismic stress due

to an earthquake, and pore-pressure increase due to rainfall. (SASSA, 1998, FUKUOKA, 2004. 2007, WANG, 2002, WANG, 2006).

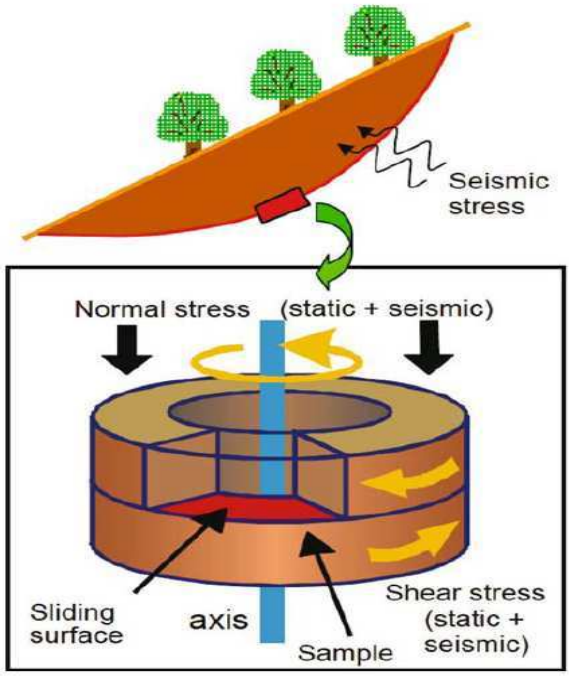

Fig. 7-8: Concept of stress controlled dynamic loading ring shear apparatuses (SASSA, 2002)

Table 7-3: Main features of DPRI – 5

Shear box	**DPRI - 5**
Inner diameter, cm	12.0
Outer diameter, cm	18.0
Max.height of sample, cm	11.5
Ratio of max. height/width	3.83
Shear area, cm^2	141.37
Max. normal stress, kPa	2,000
Max. shear speed, cm/sec	10.0
Cyclic torque control testing (max. frequency)	Yes (5 Hz)
Undrained testing and pore pressure monitoring	Yes
Max.data acquisition rate, readings/sec	200

The testing procedure in ring shear apparatuses can be described as follows (source: SASSA 1988, 2002, 2004):

Sample setting

The samples were placed in natural moisture content condition. However, to make dense samples, each layer was tamped or the samples were over consolidated after the setup. To make a very loose sample, the moist placement method was used.

Sample saturation

The samples were saturated with the help of carbon dioxide and de-aired water. After a sample was packed, CO_2 was percolated through it to expel the air from the sample pores. The CO_2 was very slowly introduced into the sample through the lower drainage line, and discharged from the upper drainage line. Usually, this process takes 4 to 12 hours. After hours of percolation of CO_2, de-aired water was infiltrated into the sample from the lower drainage line to expel the CO_2 in the sample pores from the upper drainage line. This infiltration process was kept at a very slow rate by using a very small water head.

Checking degree of saturation

The degree of saturation was checked by using of B_D. B_D is a pore pressure parameter, related to the degree of saturation in the direct-shear state, which was proposed by SASSA (1988), and is defined as:

$$B_D = \Delta u / \Delta\sigma, \qquad (5.3)$$

where, Δu and $\Delta\sigma$ are the increments of pore pressure and normal stress, respectively. Undrained tests are usually carried out with $B_D = 0.95$.

Sample consolidation

In most cases, the soil layers in which sliding surfaces were formed were weathered or fully softened. Therefore, samples taken from the landslide sites were normally consolidated before the test. However, sometimes, samples were over-consolidated to reproduce the over-consolidated or dense soil layer condition. Thereafter, the initial shear stress due to the weight of the soil mass above the sliding surface was applied slowly to reproduce an initial stress state the same as field conditions.

Loading

Additional seismic shaking or pore-pressure increase corresponding to rain storms was applied onto the sample in the undrained condition, or sometimes in the naturally drained condition, keeping the upper drainage valve open.

Monitoring of shearing

Change of mobilized shear resistance is measured by two load cells (S1 and S2). Pore pressure, resulting in shear displacement and shear speed are also monitored. The shear resistance mobilized during shearing is obtained by subtracting the rubber-edge friction from the monitored shear resistance.

7.3 Results

7.3.1 Analyses of mineralogy and microstructure

Clay particles contribute to the tensile strength depending on water content (SMALLEY, 1966, DERBISHYRE, 1983b, TAN 1988). Therefore it is important to determine the dominant clay - size fraction. X-ray diffraction analyses were performed on specimens of both sites. The results show that the dominant minerals are quartz, calcite, chlorite, plagioclase and illite. Mineral compositions of Kochkor-Ata and Upper Koi-Tash landslides are similar except the larger amount of illite in the soil specimen taken from the middle part of the Kochkor-Ata.

Fig. 7-9 presents the typical results of X-ray diffraction results of loess samples. Fig. 7-9 a) and b) represent the samples from Kochkor-Ata landslide; c) and d) represent the Upper Koi-Tash

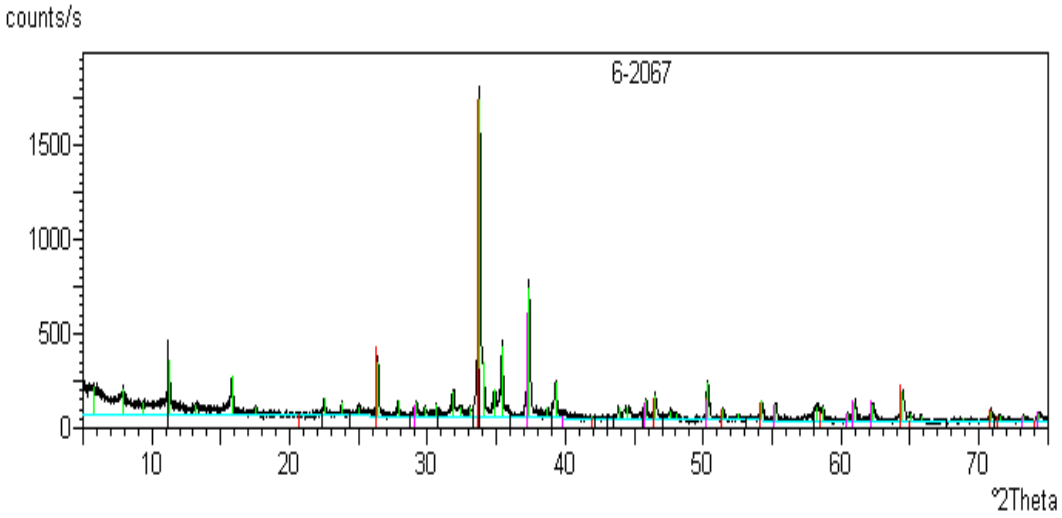

a) Red = quartz, black = illite, purple = calcite.

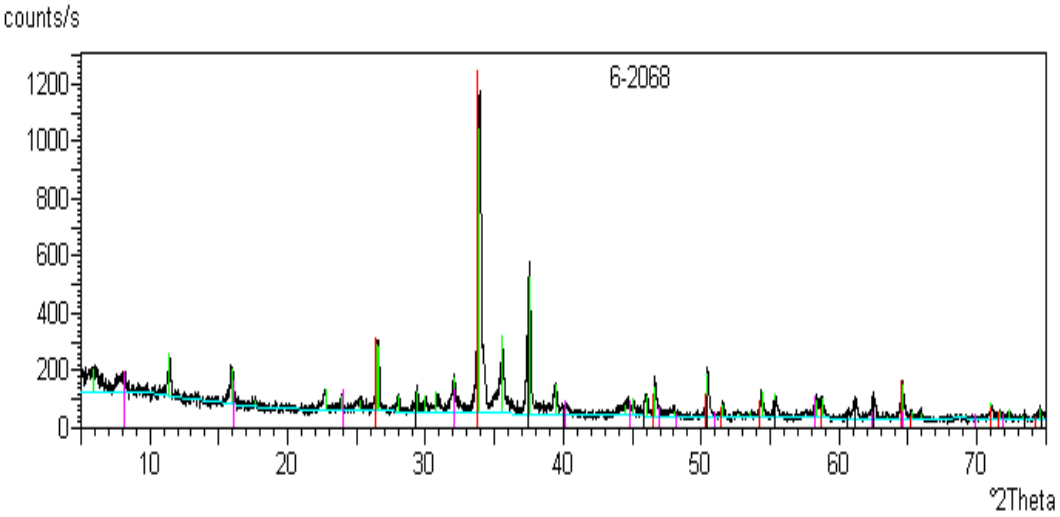

b) Red = quartz, purple = chlorite, black = calcite

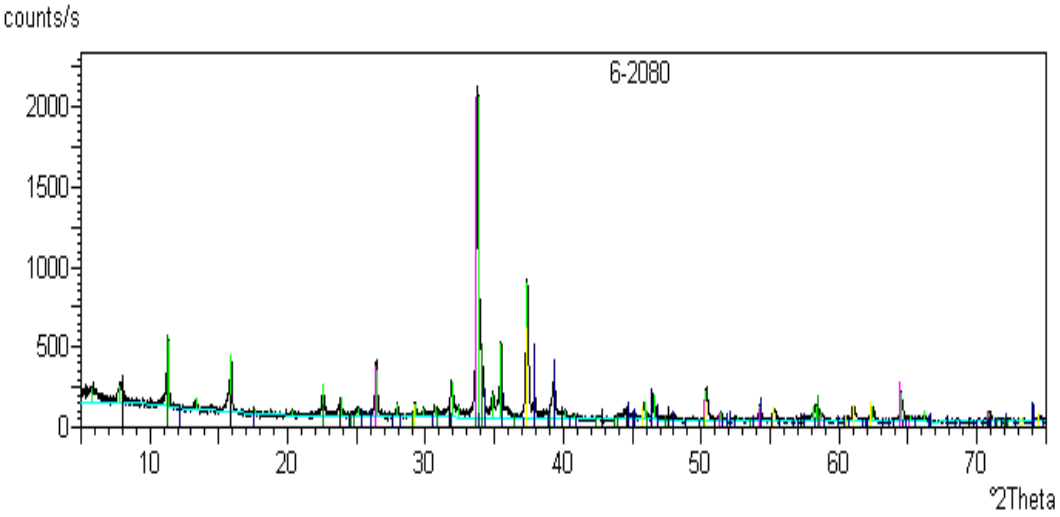

c) Purple = quartz, yellow = calcite, black = chlorite

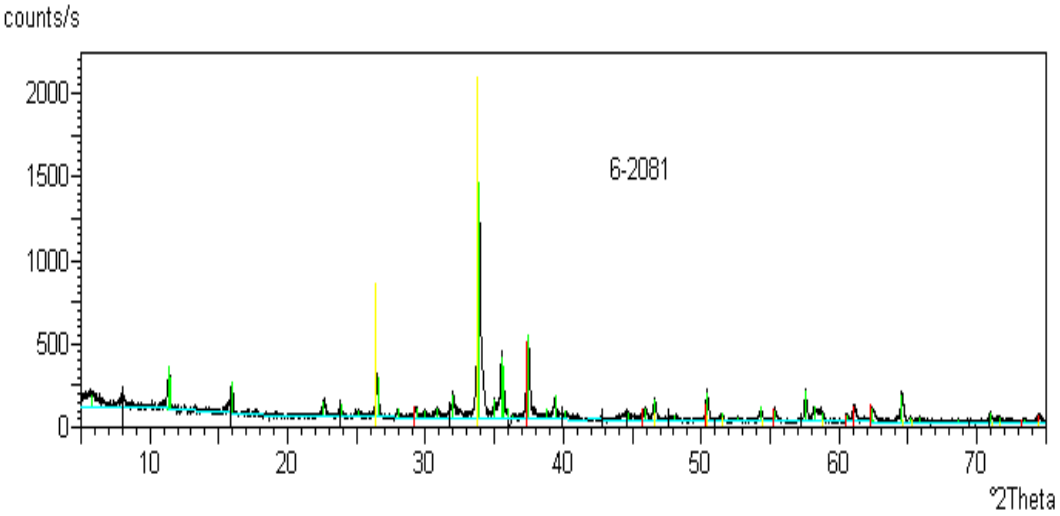

d) Yellow = quartz, red = calcite, black = illite

Fig.7-9: X-ray diffraction analyses a) and b) results of samples from Kochkor-Ata; c) and d) results from Upper Koi-Tash

Microstructure

By using a scanning electronic microscope (SEM), the structure of undisturbed loess from the Upper Koi-Tash landslide was investigated. Natural water content of the sample was 13.1 % and the depth of sample was 3m. Fig. 7-10 presents the aggregates in different scales. SEM images show the relatively compact fabric of loess.

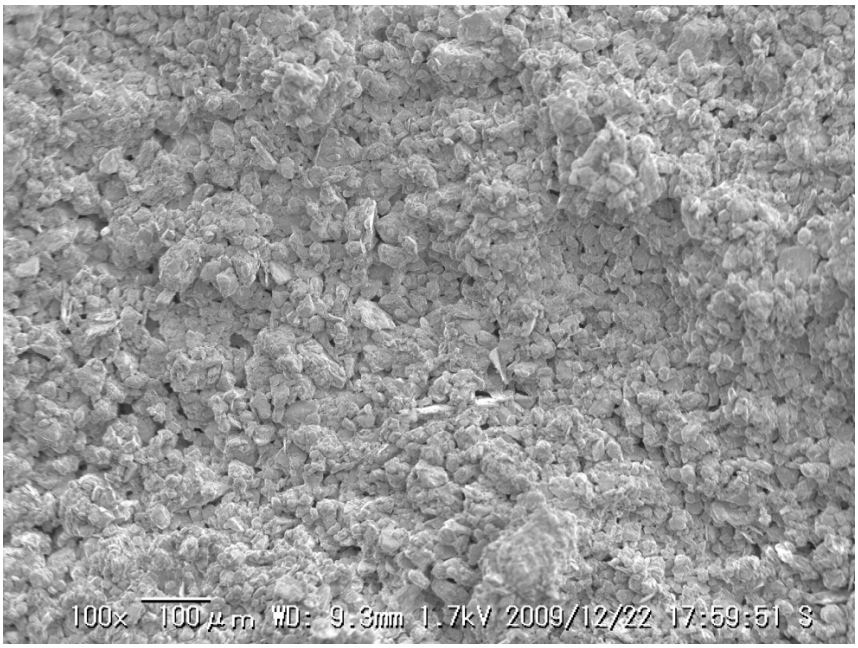

a) 100x

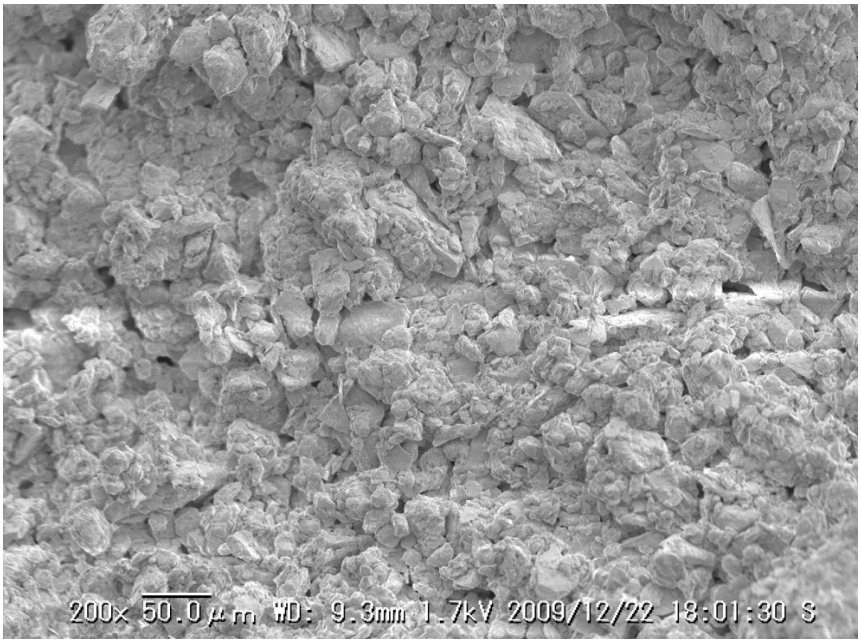

b) 200x

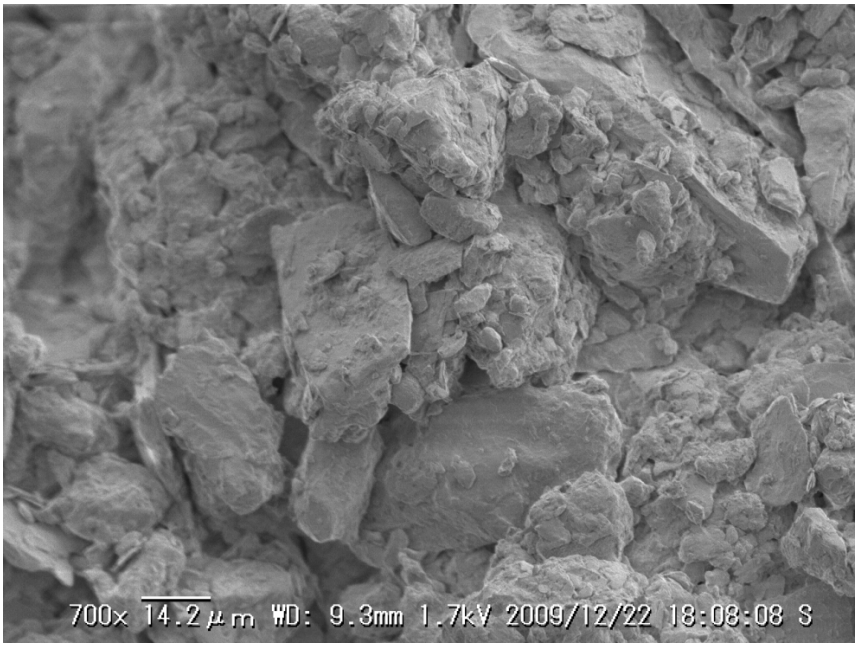

c) 700x

Fig. 7-10: SEM examination of loess aggregates from the sample obtained from Upper Koi-Tash in scales a) 100x, b) 200x and c) 700x. Water content of the sample is 13.1 %.

Loess fabric mainly consists of coarse silt grains. Pores within the grains are small. Comparison has been made with undisturbed Malan loess taken from China (ZHANG, 1995) and presented in Fig.7-11. As it can be seen, the loess sample from China has large pores.

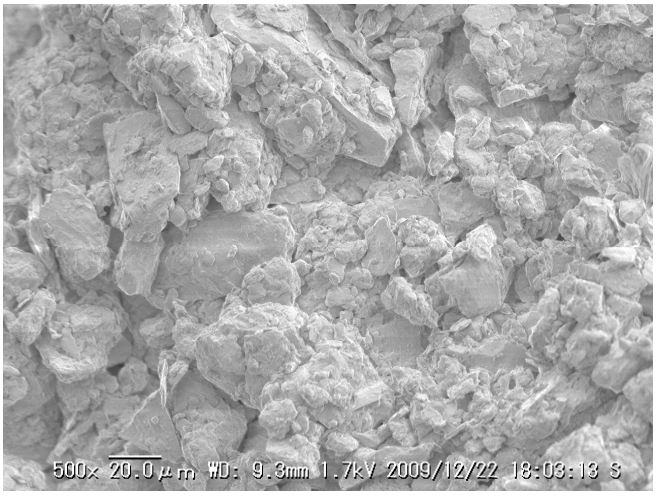

a) Upper Koi-Tash with a scale 500x

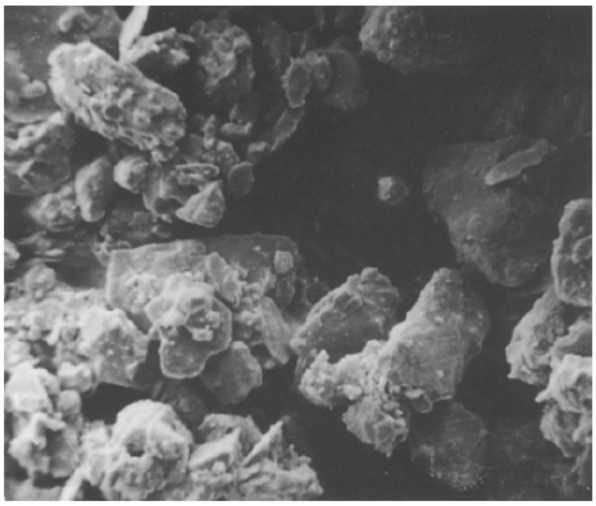

b) Malan loess with a scale 500x (by ZHANG, 1995

Fig. 7-11: Loess fabric of Upper Koi-Tash sample in comparison to Malan loess, China (by ZHANG, 1995)

7.3.2 Geotechnical tests

7.3.2.1 Soil characterization

Index properties of samples are presented in the Table 7-3. Dry density values for the Upper Koi -Tash site are in the range of 1.5-1.7 gr/cm^3 and for Kochkor-Ata landslide 1.20-1.29 gr/cm^3; void ratios range from 0.73 to 0.87 and 1.06 to 1.22, respectively. Plasticity indexes are in the range 12-15 % for the samples of both places. Liquid limit was found to be 33-35%. These values are comparable to the liquid limit indicated by GIBBS and HOLLAND (1960) for silty loess (25-35%). Fig. 7-12 shows the grain size distributions of the samples. Silt composition is about 68-77%, clay composition is 20% and sand composition ranges from 0 to 5%. The values of specific gravity of loess are between 2.66-2.68 gr/cm^3. These values are smaller than values stated by KOJOBAEV (2002), who determined the index properties of loess samples from Osh region (Kyrgyzstan). According to KOJOBAEV (2002) an average value of specific gravity was 2.71 gr/cm^3.

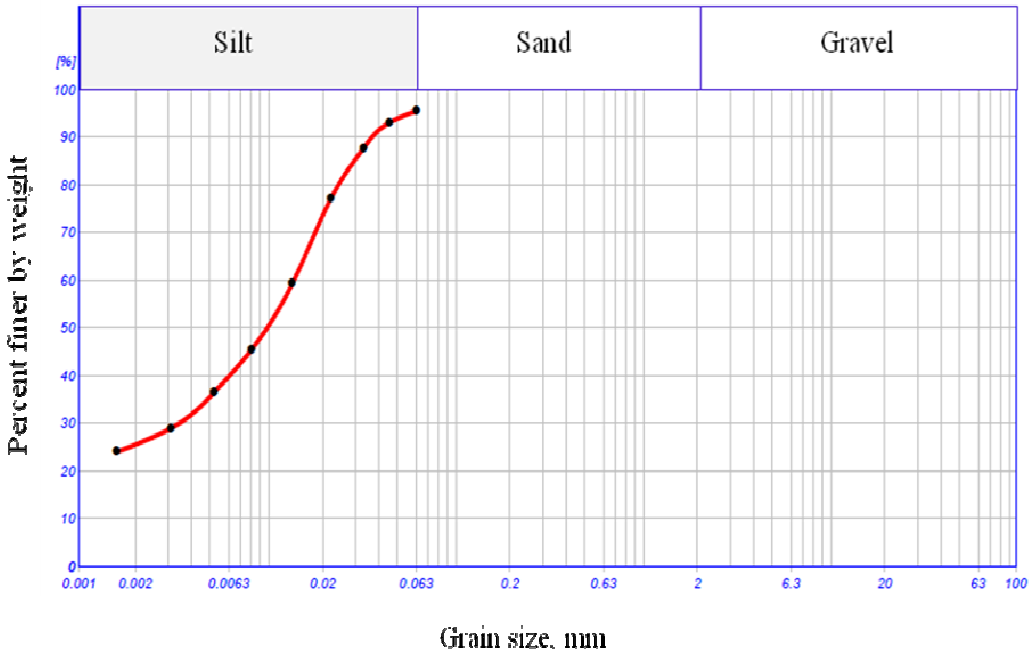

a) Kochkor-Ata landslide

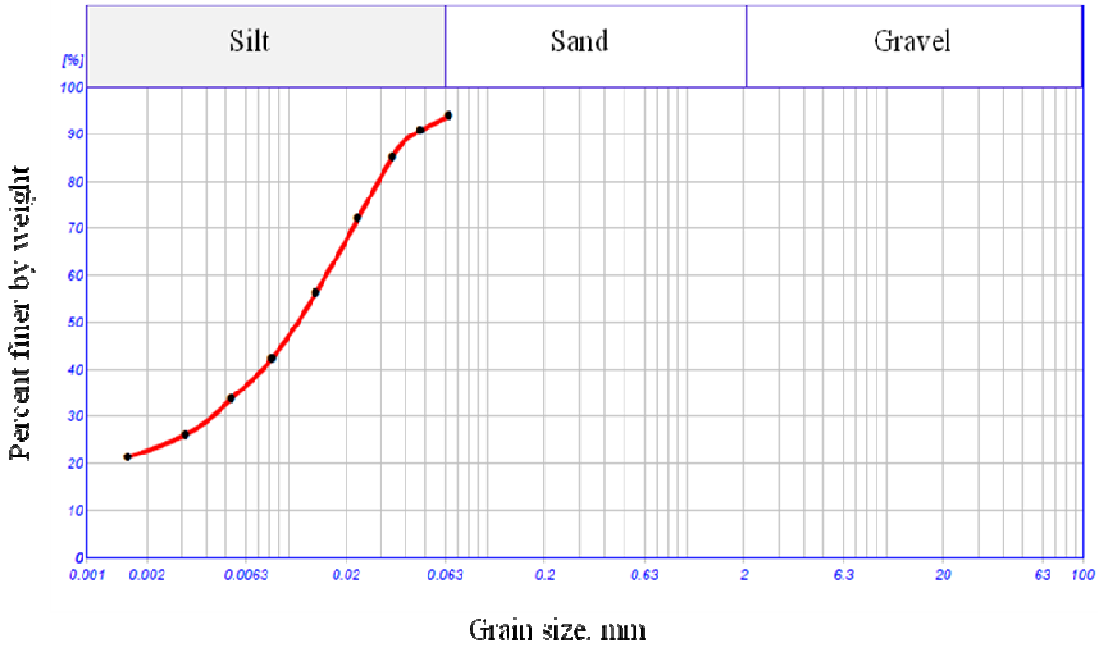

b) Upper Koi-Tash landslide

Fig. 7-12: Grain - size distribution of soil samples from a) Kochkor-Ata landslide; b) Upper Koi-Tash landslide

Table 7-3: Index properties from the laboratory tests

	Laboratory sample number	**Depth, m**	**ρ gr/cm^3**	**ρ_d gr/cm^3**	***w*,%**	***n* porosity**	***e* void ratio**	***Sr* degree of saturation**	***LL***	***PL***	***PI***	***CaCO$_3$***
1	2068	1.3	1.365	1.206	12.8	0.550	1.223	0.29	34	22	12	27
2	2069	5	1.555	1.272	22.2	0.525	1.111	0.539	36	21	14	29
3	2071	7	1.576	1.262	25	0.529	1.124	0.595	35	23	12	27
4	2073	4	1.579	1.295	21.9	0.516	1.069	0.549	34	20	14	28
	Upper Koi-Tash											
1	2080	6	1.875	1.547	21.2	0.422	0.733	0.776	33	21	12	23
2	2081	11	1.715	1.427	20.1	0.467	0.878	0.616	32	21	11	22

7.3.2.2 Direct shear tests

Direct shear tests were performed on two samples which were taken from the exposition site of two different positions, located in the middle part of the landslide Kochkor-Ata. The depth of the first specimen is 1.3 m and the second, 5 m. Water content of samples were 12.8 and 22.2%. The first test sample with water content 12.8 % can be explained by the relatively dry time of sampling since the sample was taken from the depth of 1.3 m. Regarding direct shear test data, the height of specimen is 19.9 mm, a= 80 mm and A=50.3 cm^3 and the volume is

99.8 cm^3. The shear displacement velocity used during the direct shear test was 0.005 mm/min. The stress was 25, 50, 75 kN/m^2 for the specimen taken from the depth of 1.3 m and 33, 66, 99 kN/m^2 for the sample from the depth of 5 m. Dry density ρ_d is 1,198 gr/cm^3. Specific gravity was estimated to be 2.68 gr/cm^3. Shear box that is used during the test can be characterized as follows: diameter 8 cm, height is 1.97 cm and volume is 99,023 cm^3.

Fig. 7-13 shows the behaviour of the loess specimens. The graph of shear stress versus shear displacement shows a shear hardening behaviour of the soil (Fig. 7-13 a). The sample very quickly displaced to 1 mm and constantly stayed in a displacement range of 3 mm.

The sample with a water content of 22.2 % presented similar behaviour to the first sample with a water content of 12.8%. Shear hardening behaviour is observed without showing peak strength (Fig.7-13b)). To obtain peak strength of such a loose soil, German standards are used to obtain Mohr Coulomb failure line. Fig.7-13 a) presents a failure line that was obtained from a soil with a water content of 12.8%. Cohesion in this case is estimated to be 1.7 kPa and friction angle to 29.6°.

Fig. 7-13b) presents the cohesion for a sample with a water content of 22.2% is 0.3 kPa and friction angle to 30°.

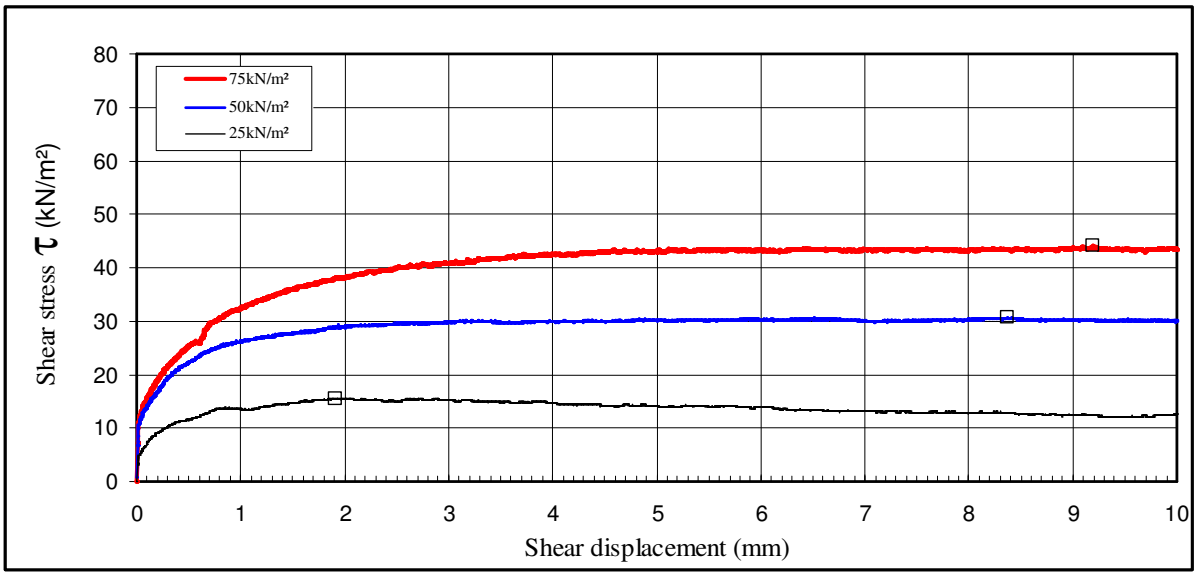

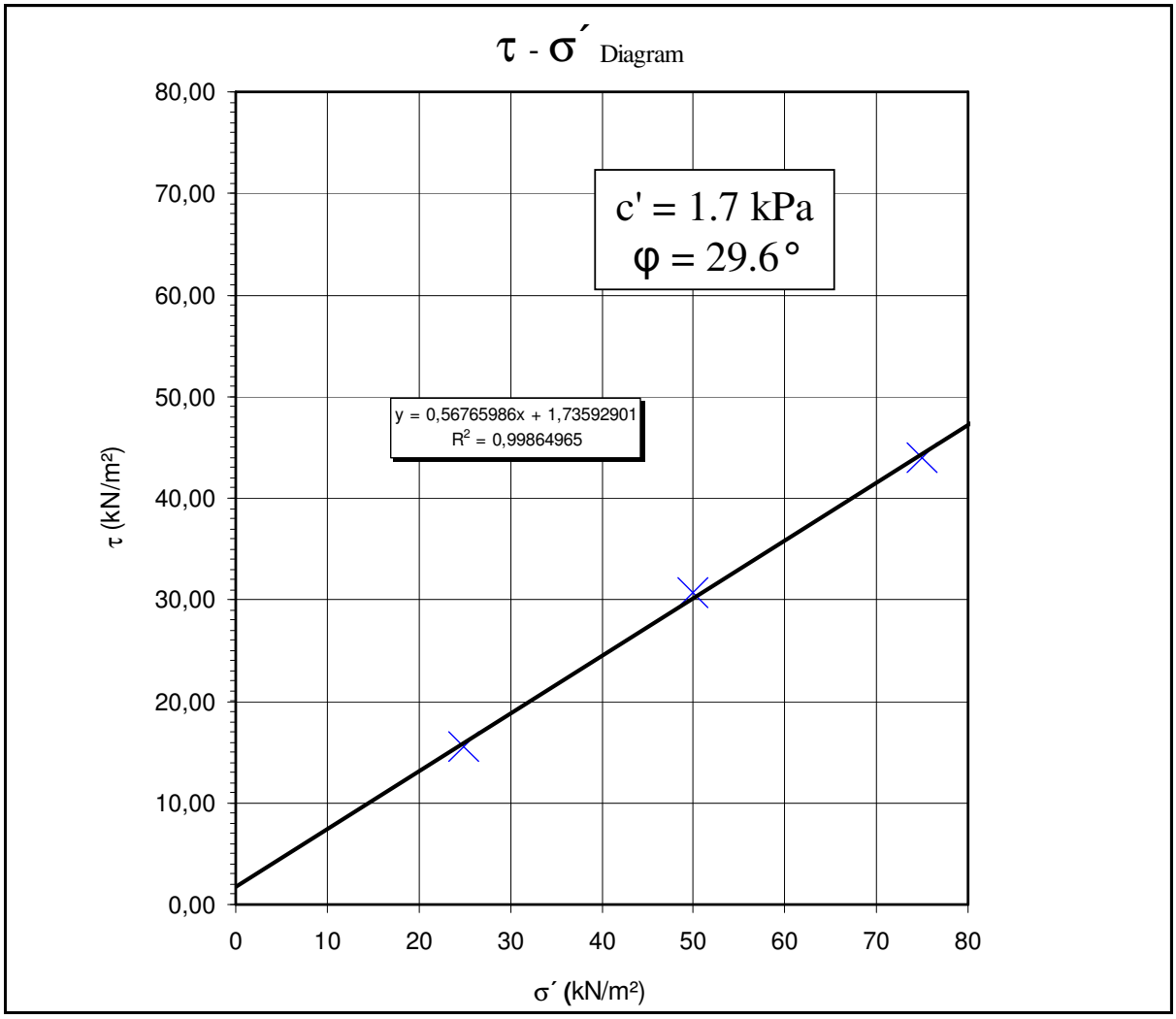

a) Water content: 12.8%

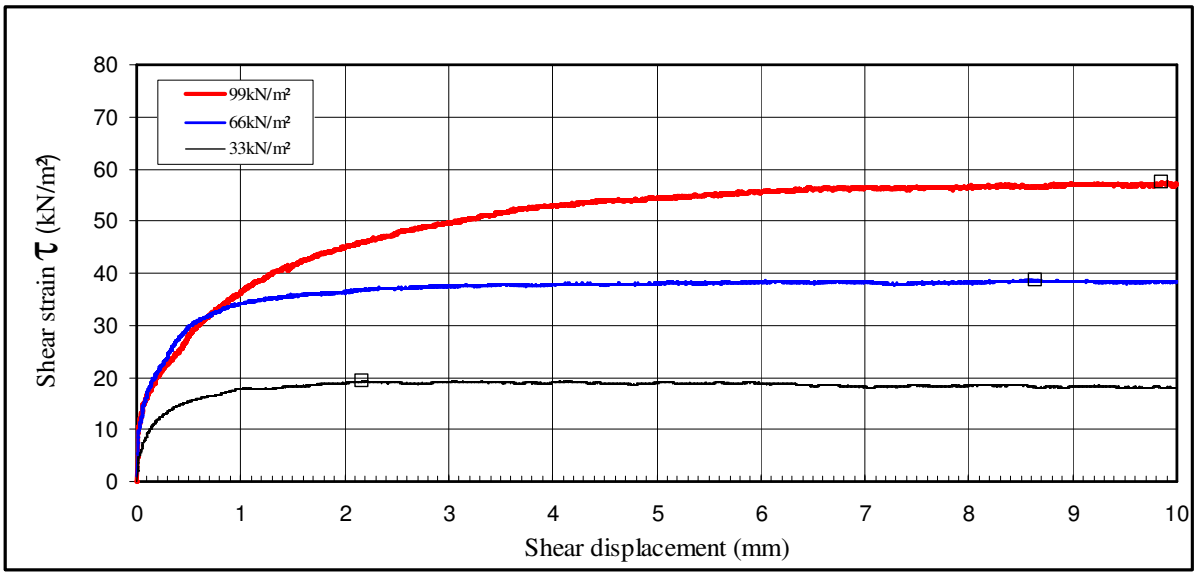

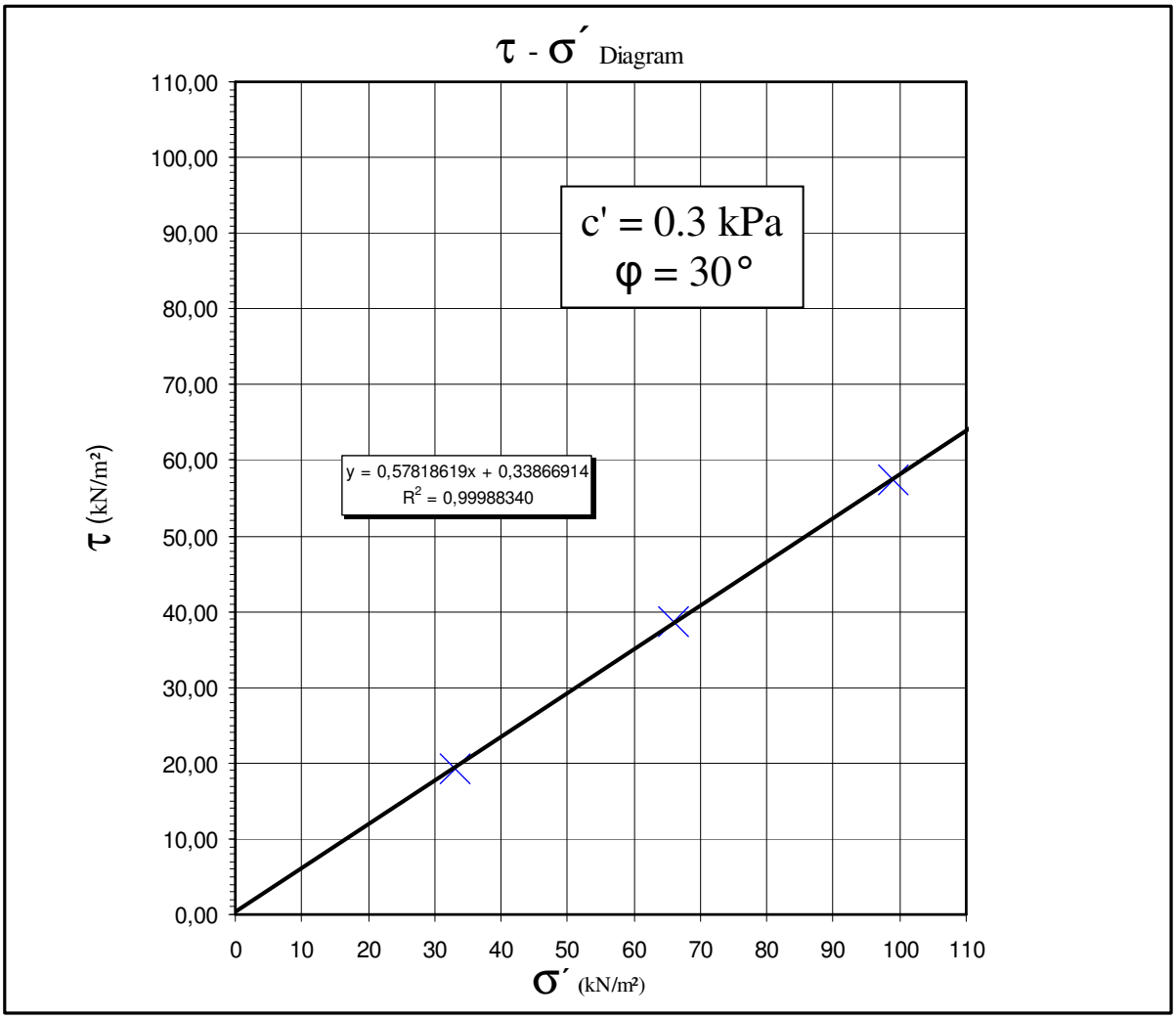

b) Water content: 22.2%

Fig. 7-13: Shear strain curves for the direct shear tests for samples with water contents a) 12.8%; b) 22.2%

7.3.2.3 Triaxial tests

Fig. 7-14 and Fig. 7-15 present the test results in the form of axial stress against axial strain. For applied cell pressures no peak was observed and the stresses increased with the strain. When the pressure increases the loess structure suffers and stress-strain curves appear to be of the hardening type. Shearing resistance increases with increase in the shearing deformation.

In the sample (2073) with moisture content of 21.9 %, it is observed that the shear stress increases in the pressure of 25 and 50 kN/m^2 (Fig. 7-14). In a higher value pressure of 85 kN/m^2, the loess deformation is observed at 0.0019, after it behaves straight then starts to deform at 0.0049.

In the case of the sample with moisture content of 25%, the stress-strain behaviour in pressures of 25 and 50 kN/m^2 gives a stress–strain graph similar to the sample with the moisture content of 21.9 % (Fig. 7-15). For the sample with moisture content of 25%, the vertical stresses 25, 50 and 75 kN/m^2 have been applied. The depth of sampling is 7 m. By applying the vertical stress in 75 kN/m^2 the deformation increased until 4.7 kN/m^2, then there was no change from 0.00096 to 0.01.

The cohesion parameter obtained from the consolidated drained triaxial tests is 35.5 kPa and a friction angle is 24.7° for the soil with water content of 21.9%. Cohesion is 27.6 kPa and friction angle is 32.3° for the soil with a water content of 25%.

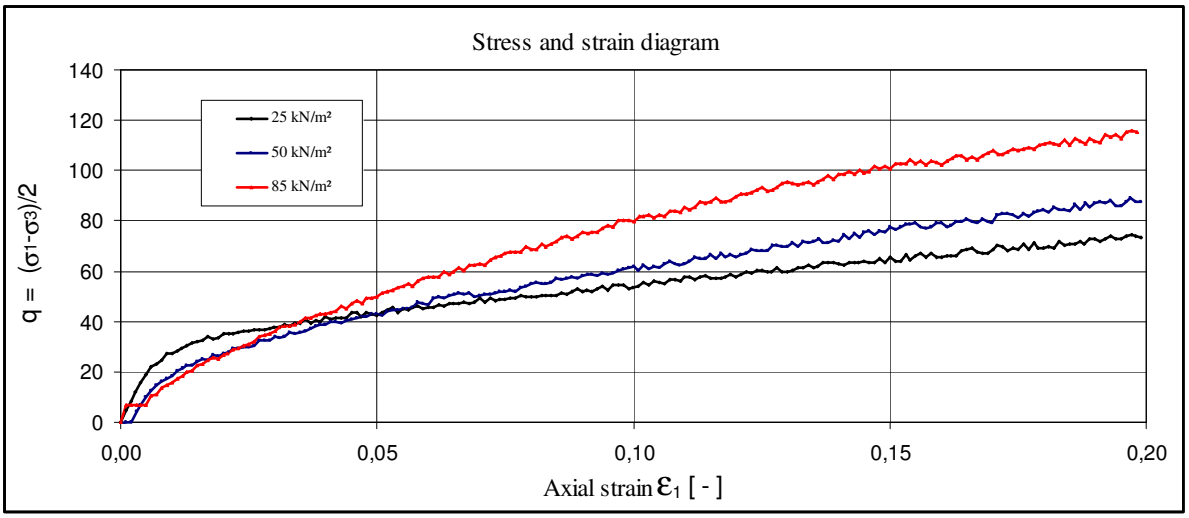

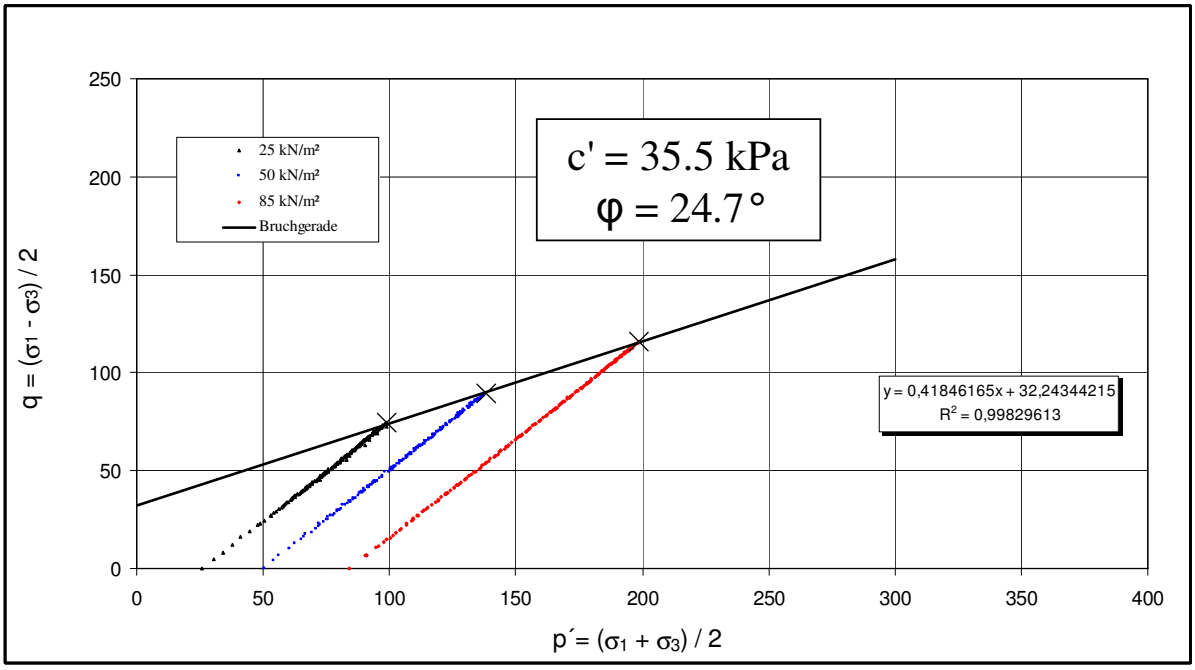

Fig.7-14: Results from consolidated drained triaxial tests, w =21.9 %

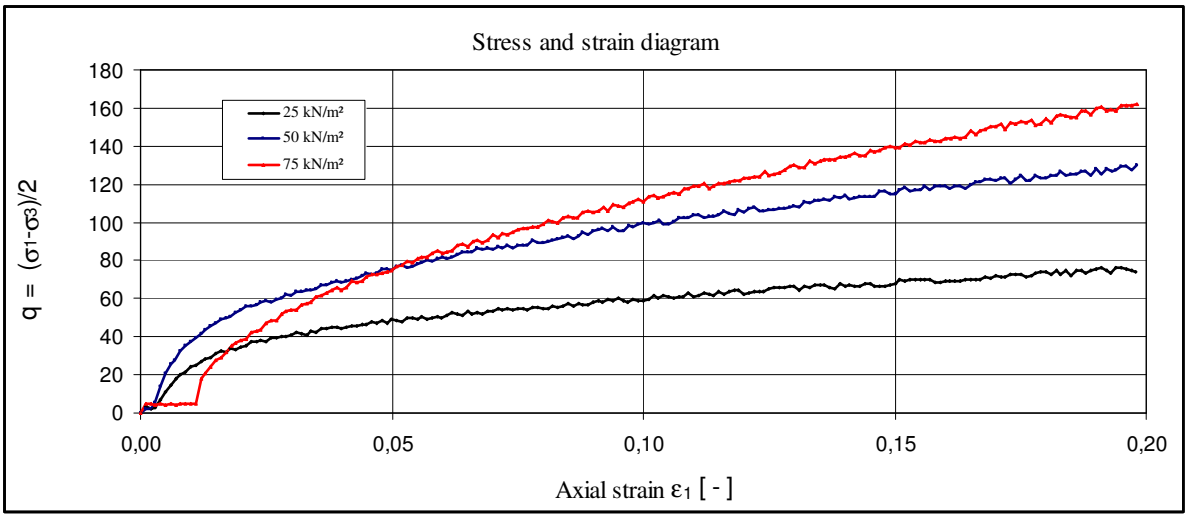

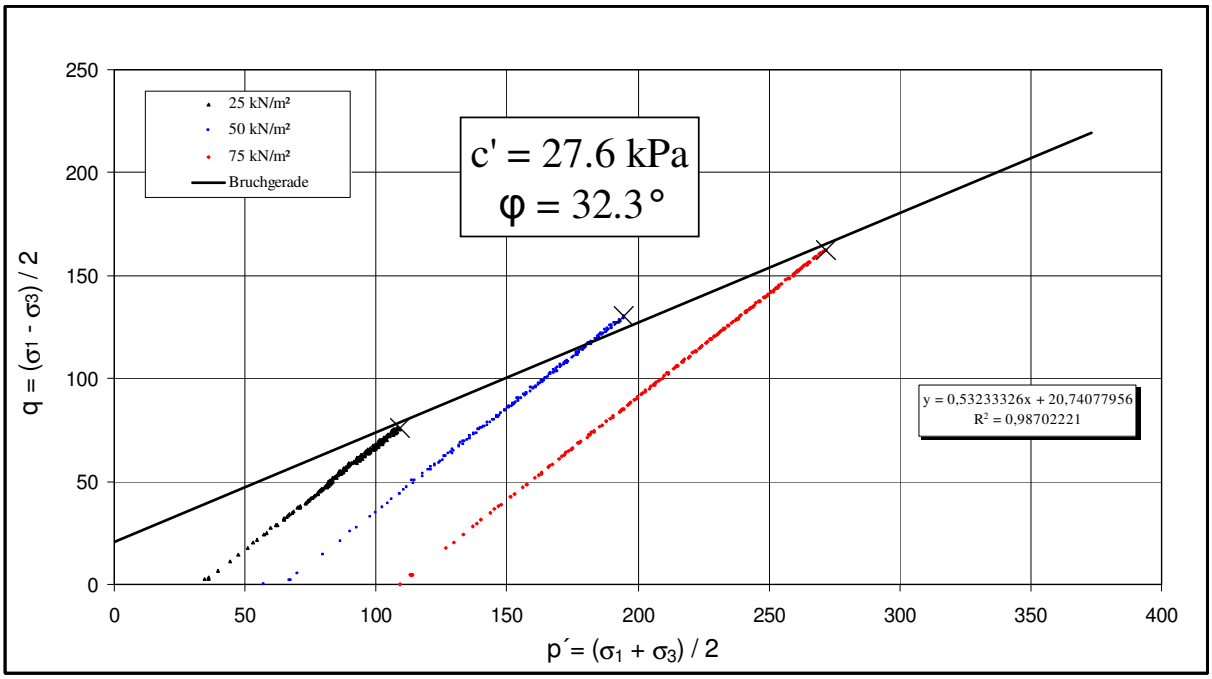

Fig.7-15: Results from consolidated drained triaxial tests, w =25 %

7.3.2.4 Ring shear tests

There are 14 samples tested in ring shear apparatuses. Two of them tested for liquefaction analyses. After the testing in drained conditions, the shear zone of the loess samples was analysed to observe the microstructure.

In Fig. 7-16 a) the shear zone at the end of one test is presented. It shows the compacted structure of loess and grain crushing has occurred. SEM images obtained after the testing were finished to observe the loess structure. The images of these analyses also show the compacted structure inside the shear zone (Fig. 7-16 b) and c)).

a)

b) above the shear zone

c) shear zone

Fig.7-16: SEM photos of the samples after the testing in ring shear apparatus; a) photo showing a shear zone; b) structure of loess above the shear zone; c) shear zone

To get strength parameters of soil, multistage testing procedure is carried out that is shown in Fig. 7-17. Each sample was initially consolidated at a normal stress of 50 kPa, and then was sheared up to certain shear displacement under drained condition. After that, the sample was reconsolidated at 100 kPa, and was sheared again for another shear displacement under drained condition. The procedure was repeated on the sample for the normal stresses of 200, 300, 400 kPa. As it is illustrated the shearing took place until peak strength was reached. In the case where no deformation was further observed, this point was taken as a peak value.

These values eliminated rubber edge friction to get a true strength parameter. After obtaining peak strength parameters, it is possible to present the σ - τ diagram to get c´ and φ.

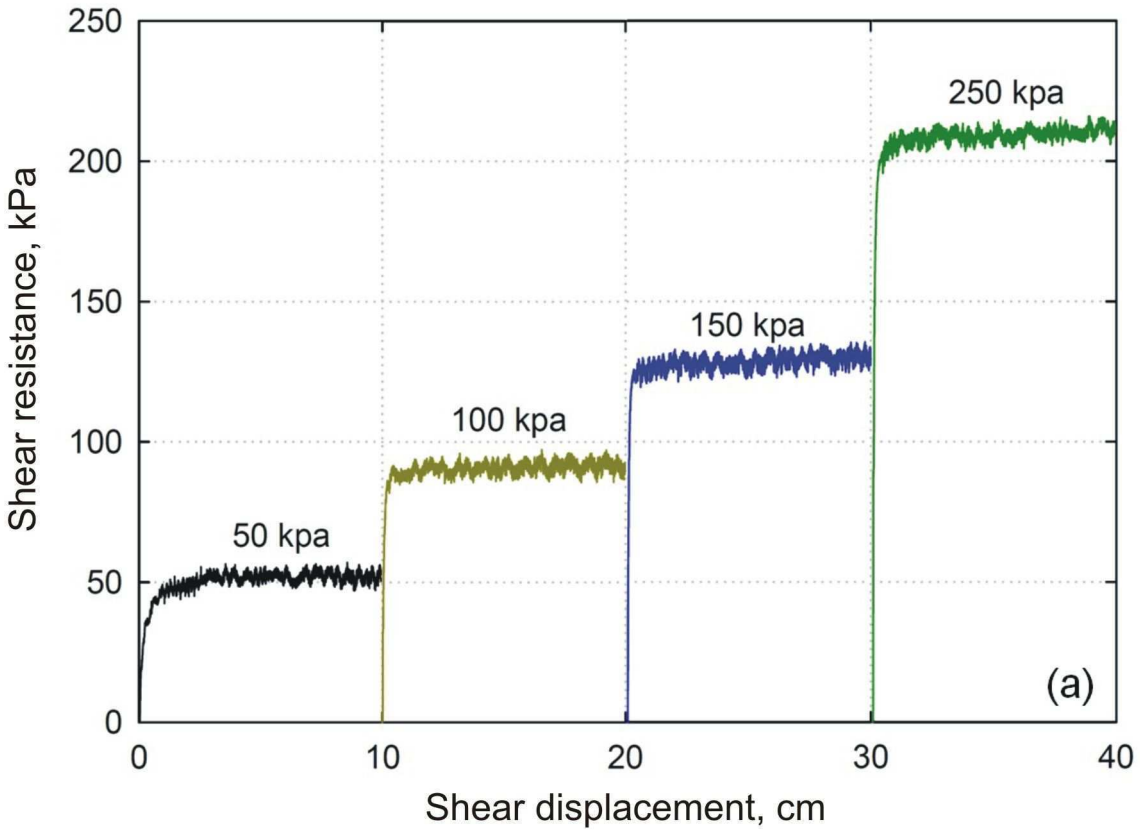

Fig.7-17: Multistage data processing in ring shear tests.

7.3.2.5 Liquefaction analyses with ring shear apparatus

Fig.7-18 shows the results of the test of the liquefaction analyses. This sample presented the condition of remoulded soil in natural condition without drying. After saturation and normal consolidation, the sample was sheared in undrained condition to a displacement of 12 m. As presented, in the initial period after undrained shear stress was applied, with increasing shear displacement, pore pressure built up gradually. Shear resistance decreased from 80 kPa to 30 kPa. After the elapsed time reached approximately 120 seconds, the pore pressure decreased. After this time, the pore pressure decreased in stress from 80 kPa to 60 kPa. However, pore pressure did not reach normal stress; in this case it can be said that no liquefaction appeared in this soil. A possible explanation for this is the high clay content.

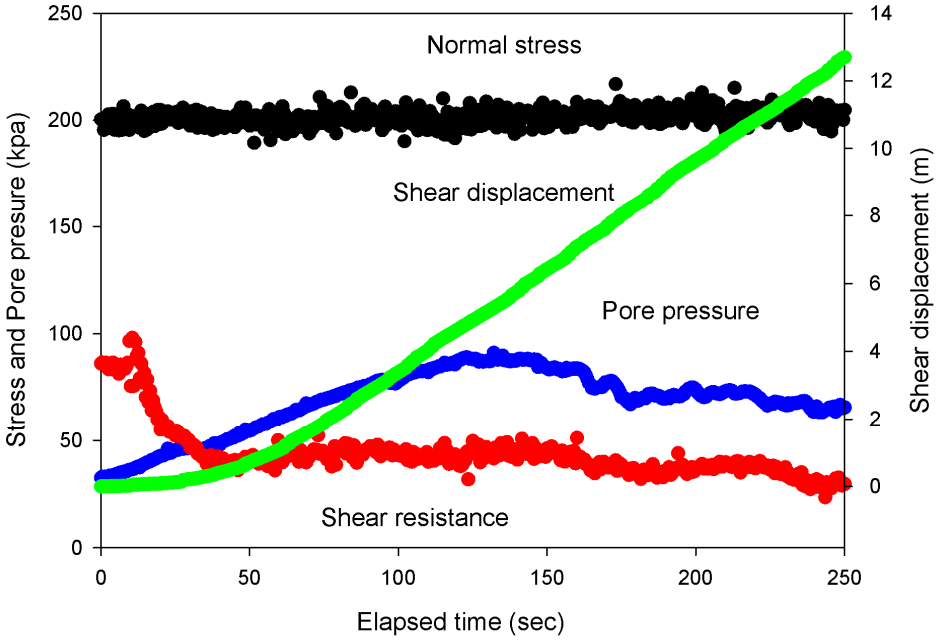

Fig. 7-18: Liquefaction analyses for loess samples from Upper Koi-Tash landslide

7.3.3 Strength parameters obtained from tests

Table 7-4 presents the strength parameters obtained from the laboratory analyses in order to determine strength properties of loess samples. Direct shear tests give the values of cohesion 1.7 kPa and 0.3 kPa and friction angles are 29.6° and 30°. Triaxial tests presented cohesion from 22.7 to 35.5 kPa; the friction angle ranged up to 38°. The strength values obtained from ring shear tests presented the large range of values of cohesion starting from 8.76 kPa, and up to 25.79 kPa. The highest friction angle was observed to be 40.7° with the cohesion 8.76 kPa.

Regarding strength characteristics of loess obtained from tests as it is shown in Table 7-4**,** it may be concluded that failure behaviour depends on the levels of vertical stress and the conditions of the cementation bonds. In direct shear tests, the cohesion values equal 0.3 – 1.7 kPa. Such behaviour of loess soil can be explained in the following way. Since the particles of loess consist of clay particles, covered silt and cementing bonds connect the particles. When vertical stress is applied in direct shear tests, the particles slide against each other. Triaxial testing presents the inherent structural anisotropy in loess, and as result of skeletal grain orientation, this affects the strength properties considerably. Ring shear tests are carried out on disturbed samples. These loess samples are representative of collapsed, residual loess deposit. However, strength parameters show the friction angle ranging from 24 – 40.7°, which is similar to two other tests.

Table 7-4 Strength parameters of loess

Type of the test	Depth of the sample, m	Water content, %	c', kPa	φ, °
Direct shear test (for undisturbed specimens)	1.3	12.8	1.7	29.6
	5	22.2	0.3	30
Consolidated drained (CD) triaxial test (for undisturbed specimens)	7	25	27.6	32.3
	4	21.9	35.5	24.7
	4.9	20	22.7	25.4
	1.2	10.5	31.7	38
Ring shear test (for remoulded specimens)	8	15.78	25	36
	9	20	17	33
	10	19	50	30.8
	8	16.58	49	35.3
	2	8.76	19	40.7
	12	25.79	35	24
	13	24	65	23.7
	3	13.74	28	38.1
	12	20.67	30	38
	3	18.32	12	36.8
	12	15.76	9.5	35.8

7.3.4 Comparison to literature

It can be concluded that undisturbed loess specimen can be referred to as structural strength when the cementing bonds are involved in the shearing. If the vertical stress is smaller than the structural strength, the loess structure survives until the stress threshold occurs. Remoulded material can be considered as a particulate material that is described by FEDA (1982). However, stress direction has a considerable impact on strength of loess as showed by MATALUCCHI (1970). Triaxial tests give a natural insight to structural strength of loess material.

As it is shown in investigations of Wucheng loess (the oldest) from China, it has stronger cemented bonds than younger loess. The porosity *n* of Wucheng and Lishi loess ranges up to 0.48, and the void ratio is 0.9. In comparison to these data, Upper Koi-Tash loess samples present values lying in a range of porosity 0.42-0.46 and void ratio 0.73-0.87. With some contrasts to the values from Kochkor-Ata, loess specimens presented void ratio ranging from 1.07 to 1.22 and porosity 0.51 – 0.55. These values from Kochkor-Ata loess specimen lie in the range from Malan loess. As it stated by DIJKSTRA (1995) and DERBISHYRE et al (2000) the Malan loess is a collapsible soil.

The theoretical stress–strain relationship presented by FEDA (1988) has shown that well developed cementing bonds in older loess can form peak strength. Young loess is dominated, bonds are gradually destroyed, and at the same time frictional forces are mobilized as a result of the collapse of the loess fabric. This can explain the behavior presented by direct shear tests for Kochkor-Ata samples.

7.3.5 Conclusion to chapter

In this study, undisturbed and remoulded loess samples have been analyzed. In order to obtain such samples, two loess landslides in South Kyrgyzstan were selected. One of them is also used as a case study for numerical simulations. Extensive literature reviewing engineering properties of loess presenting the behavior of this soil can depend on location, water content and grain size distribution. A particular feature is a cementing particle that consists on clay grains coated in silt material. This study reveals peak strength parameters and compares other loess deposits.

The mineralogical study of the soil using X-ray diffraction has revealed the main mineral present is quartz; the secondary minerals are calcite, chlorite, plagioclase. Illite was found to be a clay mineral in almost all samples. Analysis of the microstructure has shown that in its undisturbed condition, the pores are compacted and have a dense microstructure.

The soil's characteristics obtained from the first step of the geotechnical analyses indicate the soil can be classified as low plasticity silty loess.

After the vertical loading, undisturbed soil collapses and starts to deform by the increase of vertical loading. The shear stress-strain curves obtained by the direct shear tests are characterized by a lack of clear peaks and a further increase of deformation by low stress

loading. The peak shear strengths obtained from normal stresses up to 99 kN/m^2 give a friction angle of about 30° and cohesion is 0.3 to 1.7 kPa. This high angle of friction and low cohesion stress reflects the effect of consolidation processes in breaking down the particle bond and fabric structure, thus allowing for closer particle content. This contact becomes more pronounced in the soils containing higher coarse material contents, such as the silty clayey sand with gravel and the sandy silty clay with gravel. The peak strength parameters achieved from the ring shear tests indicate a larger cohesion value than direct shear tests. Strength parameters obtained from triaxial tests are considered to present insight to the properties of loess samples and attributed in numerical modelling part.

CHAPTER 8: Numerical analyses

8.1 Introduction

The numerical part of this research is carried out to understand the possible failure mechanisms of loess landslides particularly concerning Central Asian countries. As the country is prone to earthquakes, the main focus is on the seismic impact on a loess slope. This part of the research considers several studies in order to study the earthquake effect on loess landslides.

As discussed in chapter six, most research on earthquake-triggered landslides has used traditional methods such as pseudo static and Newmark's displacement methods. One important factor is the ground motion and its anomalies caused by local sites, which is named site effects. These site effects can be investigated analytically and numerically. In order to carry out analytical research, field experimental prospecting is necessary. Such techniques are usually time-consuming. In addition, experimental studies can be carried out in one location, thus investigation in large scale areas is difficult. Therefore, the objective of this chapter is to investigate the influence of ground motion numerically and find out which parameters of slope can cause to failure.

As already stated in chapters five and six, the patterns of a loess slope, thickness of loess layer and presence of cracks facilitate the instability of a loess slope. In addition, the seismic factor as Peak Ground Acceleration (PGA) also has a significant influence on seismic slope stability. By taking these slope parameters into account and considering seismic factors, the parametrical studies are carried out.

The first study considers site effect analyses for two configurations of loess thicknesses in a slope: 20 m and 40 m. The first value of thickness is related to loess slopes located in South Kyrgyzstan. The thickness of loess larger in the neighbouring countries: Uzbekistan and Tajikistan. The second value of 40 m considers loess slopes in such regions. Slope degrees are varied respectively to each loess thickness case in each country. As stated, one important factor that can cause to slope instability is the presence of cracks.

To study this case, tension cracks are constructed within a loess slope model to find out its influence on the site amplification. Since tension cracks are of particular interest to study in terms of slope instability, the parametrical studies on tension cracks are carried out as a second case of study. The output of this investigation is presented in terms of unstable mass. Since several slope parameters are important to include in this parametrical study, two configurations of slope degrees and two values of loess thickness have been taken.

The third study, in which a real case is considered, is introduced by the Upper Koi-Tash landslide that is located in the Mailuu-Suu area in South Kyrgyzstan (for more details see the chapter five). Although it is presented as a "real" slope case within this thesis, this case of research is considered one of the parametrical studies. The reason for this is the severe limited data available in terms of material properties and the exact location of tension cracks. There is also no recording of seismic signals. However, this case of study is considered to be as 'real' as possible. In this case, tension cracks are not included in the studies. As a first step, the analyses of site effects are carried out to identify the ground motion on thin superficial loess in the Upper Koi-Tash landslide. The results are interesting to compare with results of the first parametrical studies where two loess thicknesses are presented, moreover when a loess layer covers a total slope. In the Upper Koi-Tash case, a loess layer is located only on the top of the slope.

Regarding loess landslides, chapter two showed several earthquakes with weak seismic shaking have occurred in the region where the Upper Koi-Tash is located. To see the influence of such small earthquakes on this landslide, seismic shaking values are varied as a second step. Outputs are presented by way of shear strain increment and maximum displacement, because these parameters are important to know while analysing slope stability.

Since the investigation is carried out numerically, it is important to choose software that is suitable to simulate in the dynamic conditions. For this reason, the Finite difference code named FLAC in 2D domain is used for the numerical analyses.

8.2 Introduction to FLAC software

FLAC is a finite difference code which was developed by Peter Cundall in 1986. It can simulate the behaviours of three-dimensional structures built of soil, rock or other materials that undergo plastic flow when their yield limits are reached (ITASCA 1997). It offers a wide range of capabilities to solve complex problems in mechanics and particularly in geomechanics.

8.2.1 Generation of the numerical slope model for dynamic analyses

In order to start, it is need to setup a model. Fig. 8-1 presents the generation of a numerical model in FLAC within a dynamic domain. Primarily, a grid needs to be generated that fits into the desired shape. After this step, the constitutive behaviour of a model is defined and material properties are introduced. Then, an equilibrium state is reached in static conditions. After this step, dynamic analyses can be carried out. In order to introduce possible natural conditions, boundary and initial conditions are necessary for dynamic analyses. Damping is applied in the model, then a seismic signal is defined. After defining a signal, the wave is propagated through a model.

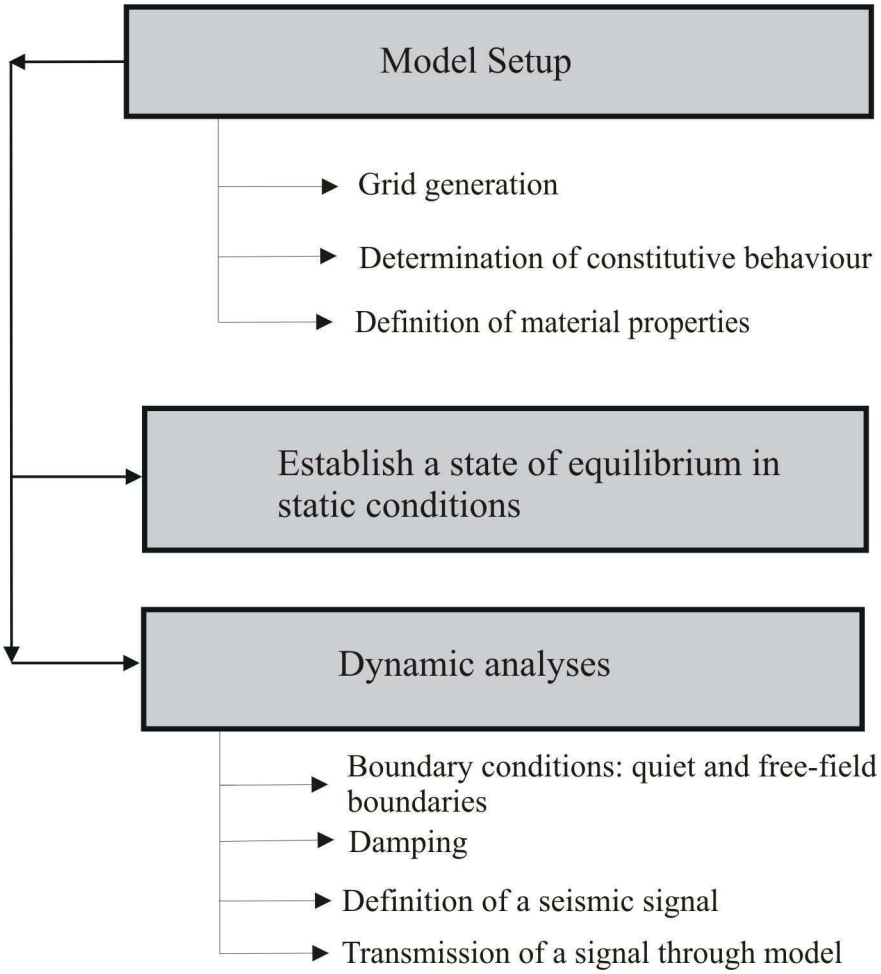

Fig. 8-1: Generation of a numerical model in FLAC software

8.2.2 Model setup

8.2.2.1 Grid generation

A grid is generated by using quadrilateral meshes for a slope as in Fig. 8-2 (left plot). However, a FLAC grid can be distorted into uniform shapes, arbitrary in more complicated shapes of model (Fig. 8-2 right plot). To reduce time-consuming calculations, the element size in the zone of interest can be set to size that allows propagating in definite frequencies. Detailed, the element size is smaller than one-tenth of the wavelength associated with the maximum frequency value of the input wave. In addition, the aspect ratio of zone ranges is to be 4:1.

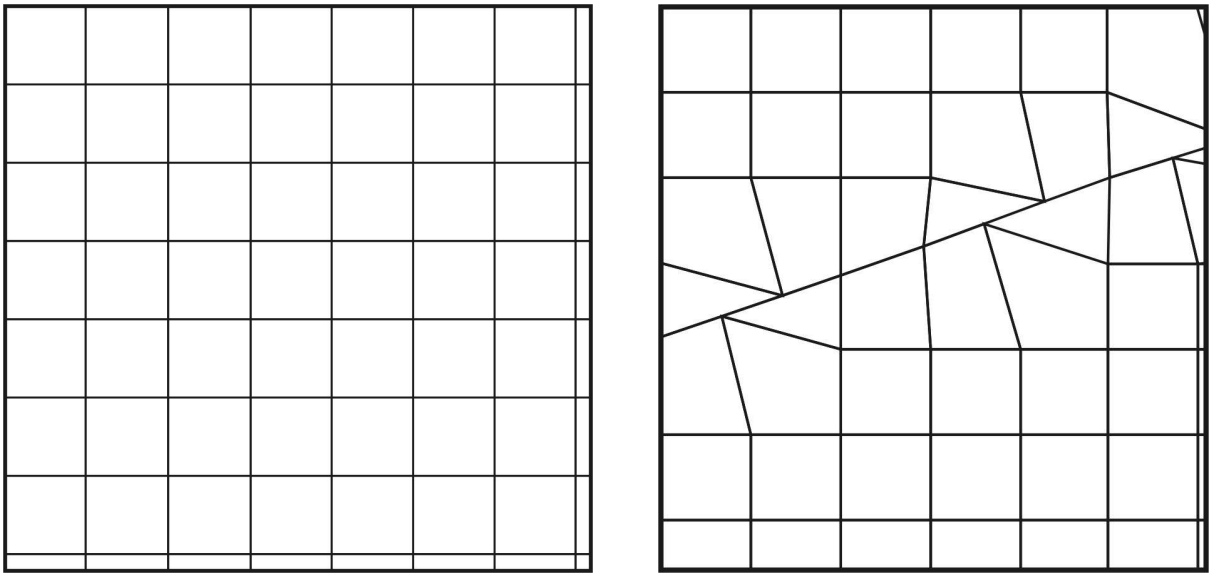

Fig. 8-2: Regular (on the left) and irregular shape (on the right) of a grid

8.2.2.2 Constitutive models

There are ten constitutive models within the FLAC software. It is possible to constitute models in elastic and elasto- plastic domain. Numerical slope models that are used in the current research are Mohr-Coulomb models.

8.2.2.3 Definition of material properties

Material properties defined by use of laboratory experiments. Shear modulus (G) determined by using of equation:

$$G = \frac{E}{2(1+\nu)} \tag{8-1}$$

where E- modulus of deformation

ν- Poisson's ratio

Bulk modulus (K) is defined by using formula:

$$K = \frac{E}{3(1-2\nu)} \tag{8-2}$$

8.2.3 Equilibrium state

Before starting to run a model in dynamic analyses, an equilibrium state is reached in static conditions (ITASCA, 1997).

8.2.4 Dynamic analyses

8.2.4.1 Quiet boundaries

In dynamic analyses, the application of boundaries to the model may cause the applied propagating waves to reflect back into the model. In order to overcome this problem, quiet boundaries are used, as suggested by LYSMER and KUHLEMEYER (1969). These boundaries run in the time domain and were based on the use of independent dashpots in the normal and shear directions applied at the model boundaries. The formulation of quiet boundaries can be written as:

$$t_n = -\rho C_p v_n \tag{8-3}$$

$$t_s = -\rho C_s v_s \tag{8-4}$$

where
t_n , t_s - the normal and shear stresses at the model boundary
ρ - density of mass
C_p, C_s - the *p*- and *s*- wave velocity
v_n , v_s - the normal and shear component of the velocity at the model boundary

P-wave velocity (C_p) and S-wave velocity (C_s) can be defined by using the following equations:

$$C_p = \sqrt{\frac{K + \frac{4G}{3}}{\rho}} \tag{8-5}$$

$$C_s = \sqrt{\frac{G}{\rho}} \tag{8-6}$$

where G is shear modulus and K is bulk modulus

8.2.4.2 Free field boundaries

Free field boundary is used to absorb outward waves by the side boundaries. Free field boundary is similar to that of an infinite model. A one-dimensional column width is created adjacent to the side boundaries of the model which are connected to each other by viscous dashpots. Fig. 8-3 presents the free field boundaries used for a loess slope.

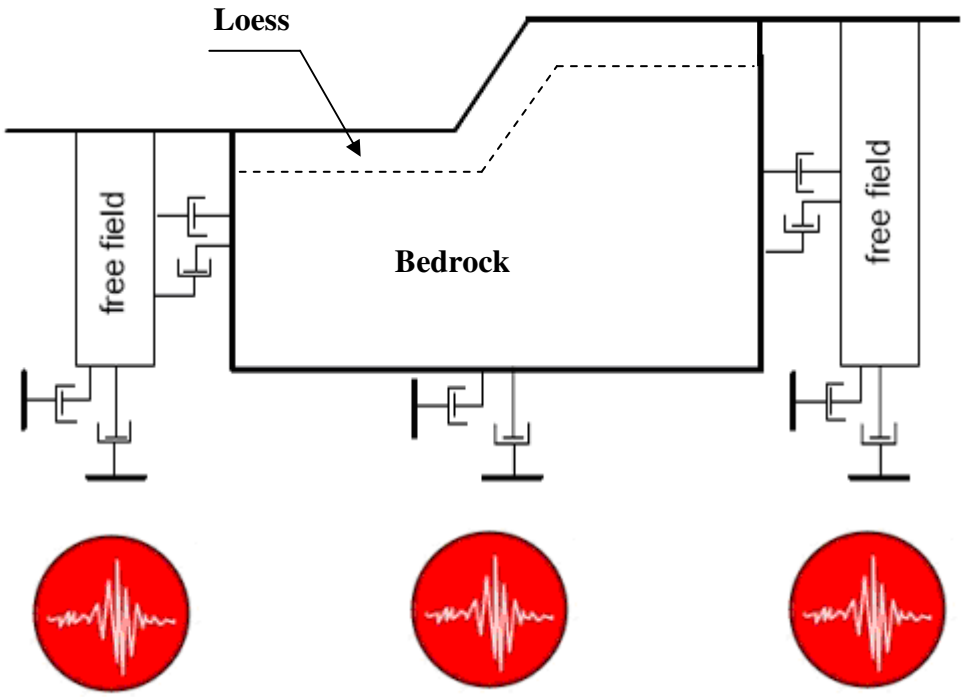

Fig. 8-3: Free field boundaries used for a loess slope

8.2.4.3 Damping

Damping is applied when the slope models are subjected to dynamic loading because the slope oscillates indefinitely. In numerical simulation, Rayleigh damping is used (ITASCA, 2000)

8.2.4.4 Ricker wavelet

As a seismic signal, the Ricker wavelet is used. Ricker wavelets are zero phase wavelets with a central peak and two smaller side lobes. The mathematical formula for a Ricker wavelet is given by:

$$f(t) = A * \left[1 - 2 * g\left(t, f\right)\right] * e^{-g(t,f)} \tag{8-7}$$

The reason for using such a type of wave is there are no ground motion recordings in the investigation site. One advantage of this signal is that it can cover all frequency ranges. This signal is a plane elastic wave propagated vertically towards the slope and polarized horizontally.

In the parametrical studies, the Ricker wavelet with amplitude of 0.05 g is used with time duration of 5 s. In a real case of the landslide Upper Koi-Tash, the amplitudes are varied ranging from 0.01g, 0.025g, 0.05g and 0.1g. Fig. 8-4 presents the exemplary wavelet with amplitude of 0.025 with duration of 5 s (source: DANNEELS, et al. 2008).

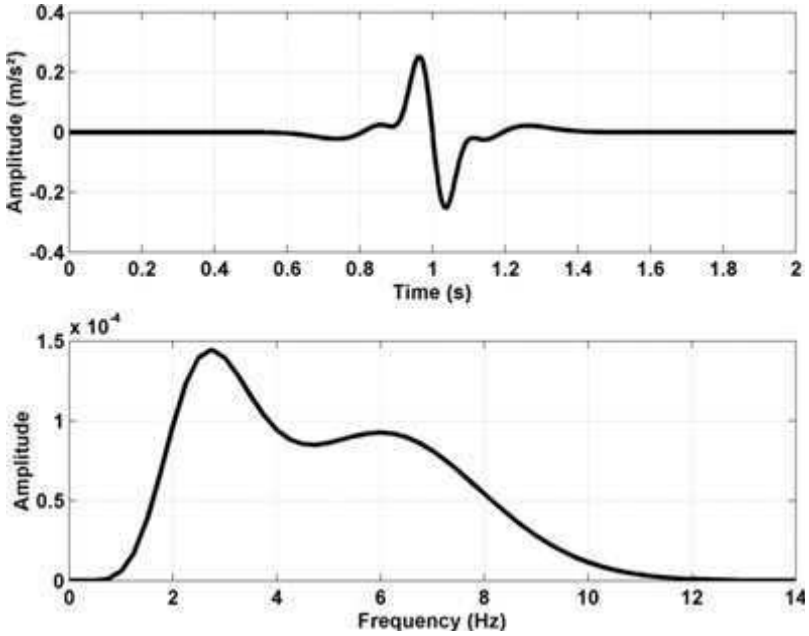

Fig. 8-4: Synthetic signal applied along the base of the model (top plot), and its Fourier amplitude spectrum (Source: DANNEELS, 2008)

8.2.4.5 Wave propagation through model

KUHLEMEYER and LYSMER (1973) showed that the wavelength determines the accuracy for wave propagation problems. According to them, the element size must be smaller than approximately one tenth of the wavelength associated with the highest frequency component that contains appreciable energy:

$$\Delta l \leq \frac{\lambda}{10} \tag{8-8}$$

where λ is the wavelength

The sole restriction when applying velocity or acceleration input to model boundaries is that these boundary conditions cannot be applied along the same boundary as a quiet boundary condition, because the effect of the quiet boundary would be nullified. To input seismic motion at a quiet boundary, a stress boundary condition is used; i.e. a velocity record is transformed into a stress record and applied to a quiet boundary. A wave may be converted to a stress wave using the formula:

$$\sigma_n = 2(\rho C_p)\upsilon_n \tag{8-9}$$

or

$$\sigma_S = 2(\rho C_S)\upsilon_S \tag{8-10}$$

σ_n, σ_S – applied normal and shear stresses
ρ – density of mass
C_p, C_S – speed of *p*- and *s*-wave propagation through medium
υ_n, υ_S – input normal particle velocity

8.3 Seismic impact on slope

8.3.1 Ground motion and reflections into the slope

After applying a seismic signal to a slope, analyses on slope stability for seismic-triggered landslides can be carried out. As mentioned in 8.1 introduction of current chapter eight, seismic shaking resulted ground motion is one of the seismic factors that cause landsliding. To support this theory, MURPHY et al (2002) studied Las Colinas landslide and stated high ground amplifications cause landslides. HAVENITH (2002) studied the influence of site effects on the occurrences of landslides by investigation of earthquake-triggered mass movements such as the Ananevo rockslide in Kyrgyzstan. Field observations and numerical modelling results have shown that the surficial low velocity layer is the key factor controlling ground motions around the rockslide. HAVENITH et al (2003) has also pointed out that the main landslide rupture results from large ground motions induced by wave focusing effects. From such field observations and experiments, it is clear that site amplification causes slope failure. Since regions of Central Asia are prone to earthquakes, the study of seismic ground motion and its anomalies in loess slope is of particular interest.

Putting forward this aim, the first study is carried out to better characterise the site effect influence on a loess slope. Site effects can modify seismic waves in frequency characteristics, amplitude level and time duration, usually resulting in resonance effects of the site and structure or amplification. In a case of slope, high frequencies amplify short slopes rather than higher ones. High slopes are amplified by low frequencies. Frequency characteristics describe at which frequency bands the slope has a strong amplification. In general the natural frequency range is 0.2 to 10 Hz of most subsurface structures (CHO, 2004). Due to earthquake shaking, the natural frequency can be amplified thus resulting to stronger ground motions and in the end to a decrease of slope stability.

To determine the amplification potential of the investigated site, it is necessary to record accelerations on the surface of a slope. Afterwards, these accelerations are transformed into frequency domain. For the studies, elaboration of Fourier amplitude spectra is used. By analysing site effects, strong and weak amplifications are presented in a colour spectrum. The detailed description to get graphs for amplification is presented in the following subchapters.

8.3.2 Site effect analyses

In order to obtain site amplification graphs, it is necessary to locate the receiving points on the surface of a slope some distance from each other. In the example case, these receiving points are located two meters apart (Fig. 8-5). In a slope with a length of 25 m, 16 receiving points are located on the surface of a slope. In Fig. 8-5, only five represent the location of points for

better illustration. This slope constitutes only from bedrock and the properties are given in the Table 8-2.

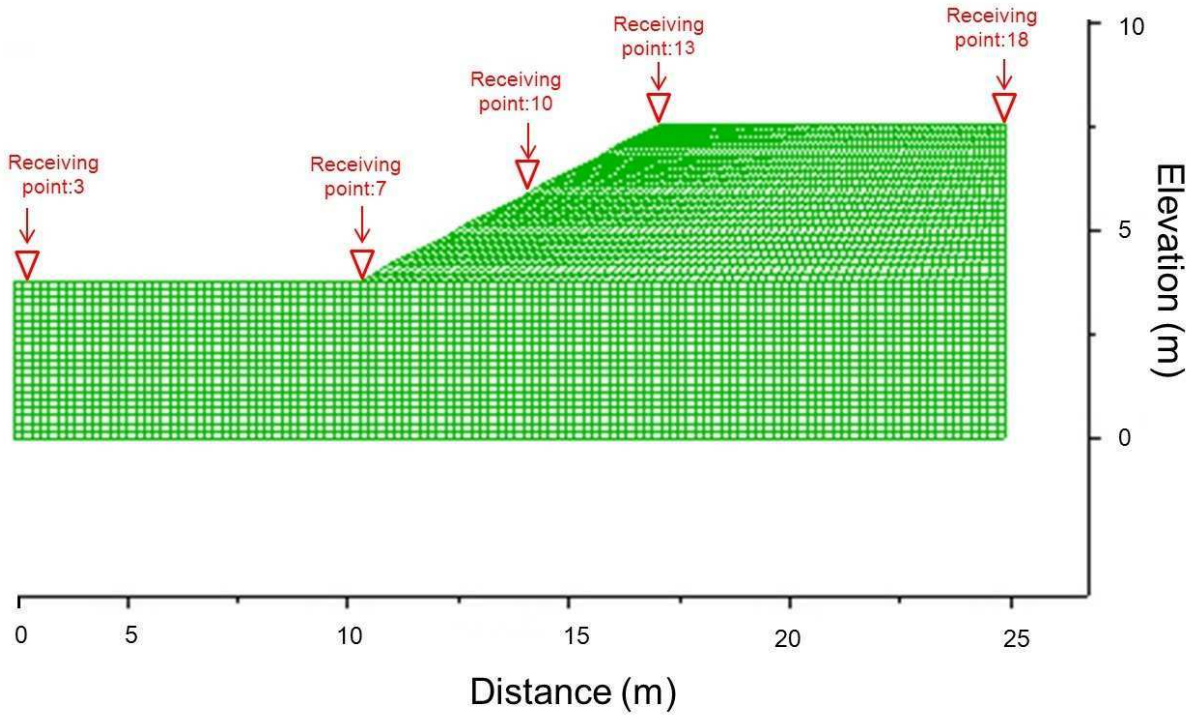

Fig. 8-5: Slope and location of receiving points to record histories of accelerations

In the calculations, to obtain the histories of accelerations in receiving points, the first history is related to time (*his1=time*) and the second to a wave (*his2=wave*). In this case, the third history of acceleration starts from the receiving point three. In Fig 8-5, receiving point three is located on a foot of the slope, receiving point 7 is located on a toe of a slope, point number 10 is on a slope, receiving point 12 is on the crest of the slope and the last point is located on top of a slope at a distance of about 10 m from the crest.

After the allocation of receiving points, a seismic wave is applied to the bottom of a slope. Acceleration is recorded in those receiving points. The acceleration histories of 16 points can be illustrated in the way shown in Fig. 8-6. On the top plot, the slope is presented with receiving points, and in the bottom plot, it is illustrated recorded horizontal acceleration histories in each point in time. A wave can reach the toe and the slope body in about one second, although it reaches the crest in a relatively larger time frame (more than 1 second).

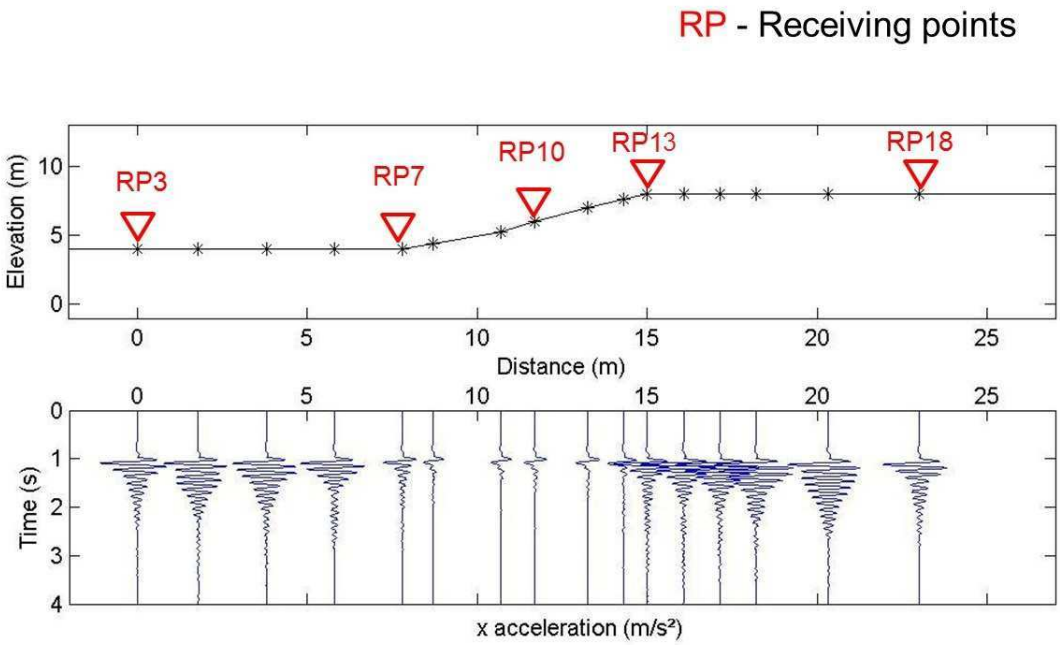

Fig. 8-6: Representation of a slope presenting the receiving points (in red) on the top plot and horizontal acceleration recorded at each receiving point in time (bottom plot)

A more detailed view of horizontal accelerations is illustrated in Fig.8-7. In the top plot, recorded horizontal accelerations for the respective receiving points (RP) are presented in a more detailed way.

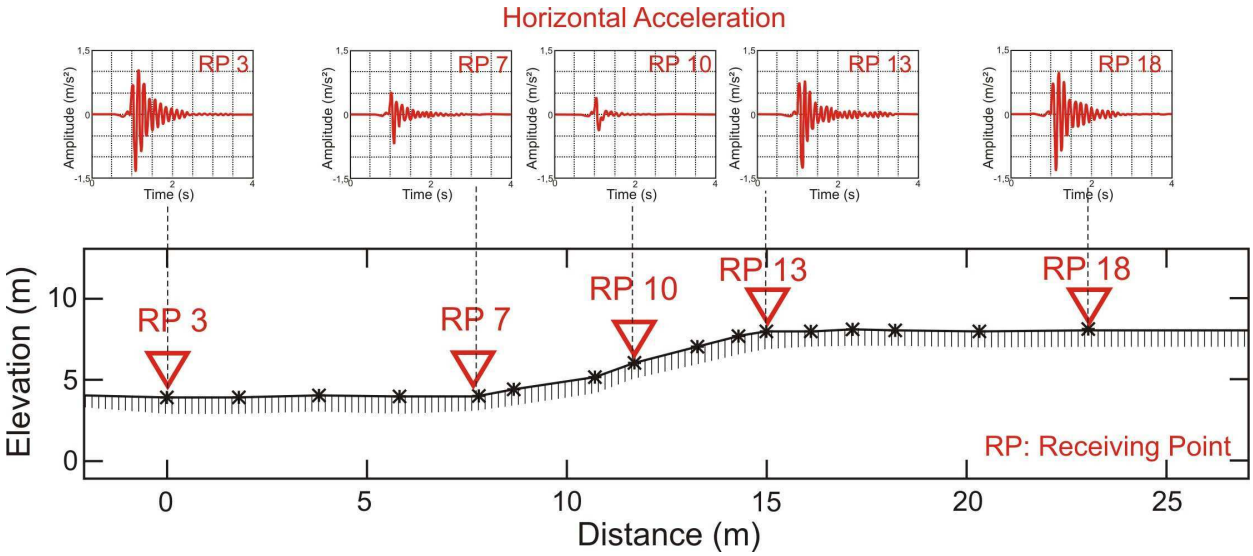

Fig. 8-7: Representation of horizontal accelerations for each receiving points; the top plot shows the accelerations for each receiving point; the bottom plot shows the slope with location of receiving points and recorded accelerations in detail.

These horizontal accelerations can be transformed into the frequency term by using the Fast Fourier transformation in Matlab software. In Fig. 8-8, the slope geometry (top plot) and abovementioned horizontal accelerations (middle plot) are presented. The bottom plot presents the spectral amplification of accelerations that are transformed into a frequency

domain. The colour spectrum is chosen arbitrarily to outline the frequency range. A spectrogram is generated in a form of graph, with representation of time in the horizontal axis, frequency in the vertical axis.
Looking at the lower graph of Fig. 8-8, it can be seen that the toe and the upper part of the slope show the strongest spectral amplifications with a factor of about 1.5 and with central frequencies in the range of 6-8 Hz. These are the frequencies most amplified by the site, therefore if an earthquake occurs in these frequencies, it is probable to cause to seismic failure.

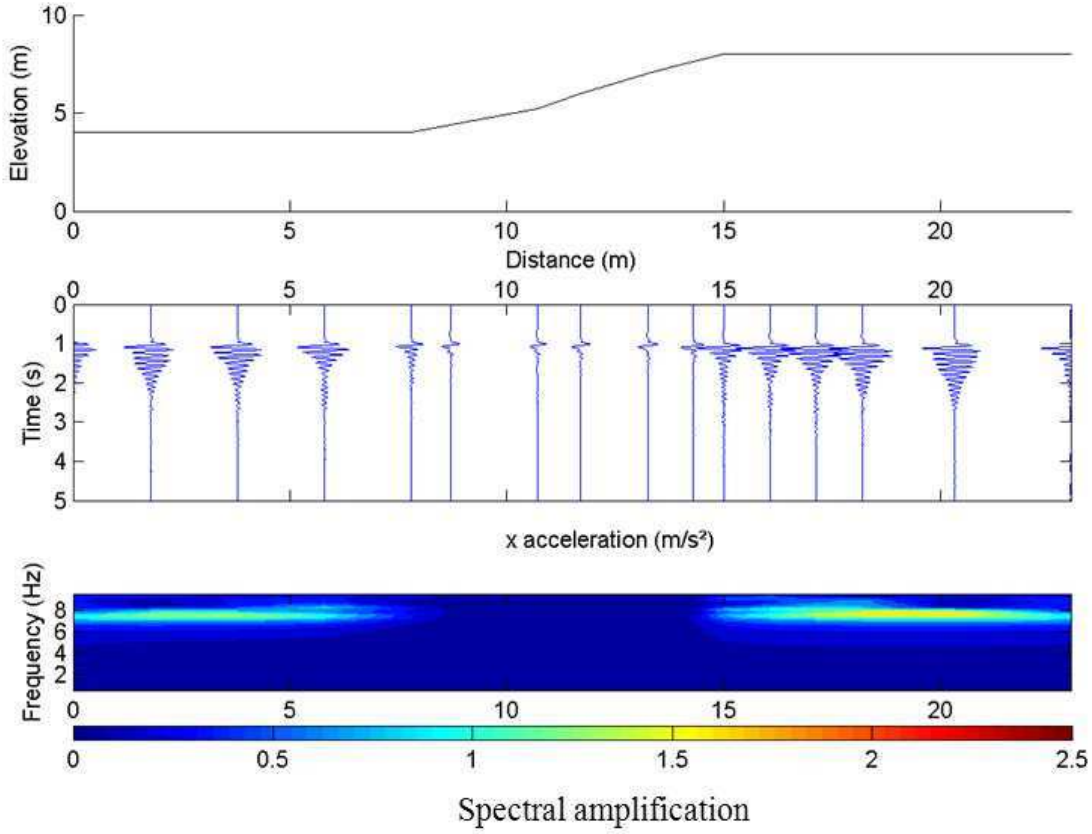

Fig. 8-8: A schematic representation of a slope geometry (top plot), horizontal accelerations recorded at each receiving point (middle plot), computed spectral horizontal amplifications (bottom plot)

8.4 Tension cracks introduction into the slope models

As presented in chapter five related to loess landslides and possible mechanisms of failure, there are cases of unstable slopes with the presence of cracks. Tension cracks which are located in the upper part of a loess slope can facilitate slope instability. In order to understand the behaviour of tension cracks, parametrical studies are undertaken. To study the tension crack impact on slope behaviour in loess deposits, first the following important factors should be mentioned. Tension cracks are simulated as weak zones or weak layers with lower properties than the slope properties. This is adapted due to the observed nets of cracks or nets of fissures that are located in loess slopes. Nets of fissures that are commonly observed in a field are presented in an illustrative sketch in Fig. 8-9. As written in chapter 6, tension cracks

are simulated here as weak zones. These weak zones do not present only one specific crack but rather a whole net of cracks, as shown in Fig. 8-9.

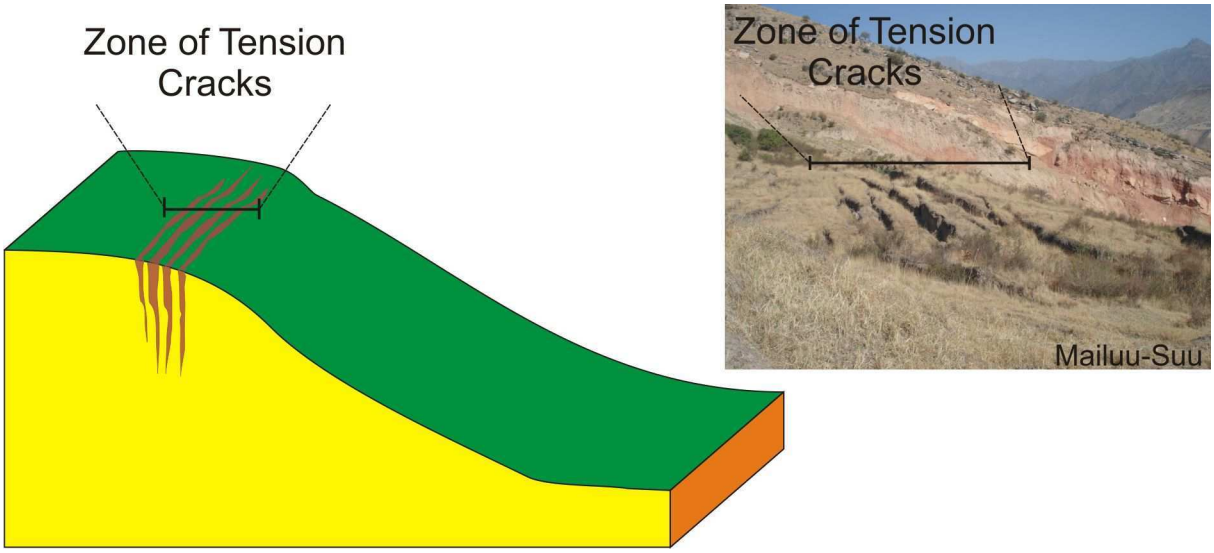

Fig. 8-9: Nets of cracks represented in a numerical slope model (left) and in nature (right)

In the synthetic analyses, two different tension crack geometries are considered, because in the literature there is no concise evidence regarding the locations of tension cracks. However there is some evidence that suggests loess can fail as prismatic discontinuities. This evidence is taken into account to be a probable critical component of inclination of 90 °. Because of time consuming runs, element size is ranged to 4 m. The slope cases in this study were conducted in dry conditions to find the impact of seismic effects on deformation of loess slope.

8.5 Material properties used in the numerical analyses

Questions may appear related to the reliability of slope material properties. As stated, strength parameters from the laboratory tests are attributed in the numerical models. S- and P- wave velocities and material properties of geological layers are obtained from the literature. Namely, DANNEELS et. al. (2008) carried out research on the Kainama landslide that is located in the Alai region of South Kyrgyzstan. This research included geophysical investigations and numerical simulations. This is the only case that gives accurate data about slopes with a superficial loess layer, which are commonly observed in the southern part of Kyrgyzstan. In Table 8-1 and Table 8-2, the parameters of loess and bedrock are shown. Regarding the properties of tension cracks, parameters lower than loess layers are taken, because there are no evident examples from literature. Table 8-3 presents the properties for tension cracks.

Table 8-1: Parameters of loess

Material parameters	Given value	Source
Vs, m/s	420	Literature
Vp, m/s	900	Literature
Density, kg/m^3	1800	Laboratory + Literature
c, kPa	30	Laboratory
φ, °	30	Laboratory

Table 8-2: Parameters of bedrock

Material parameters	Given value	Source
Vs, m/s	1200	Literature
Vp, m/s	2000	Literature
Density, kg/m^3	2300	Literature
c, kPa	2000 (Parametrical studies) 100-200 (Upper Koi-Tash case)	Literature
φ, °	35	Literature

Table 8-3: Parameters of tension cracks

Material parameters	Given value
Vs, m/s	240
Vp, m/s	650
Density, kg/m^3	1300
c, kPa	6
φ, °	30

8.6 Analyses

8.6.1 Parametrical studies: site effects (elastic conditions)

To investigate site amplification in a slope, in which a loess layer covers the upper part of a slope, two values of loess thicknesses are taken. Each case is investigated in terms of site amplifications without presenting of tension cracks within a slope. This case is introduced as a reference case. Two more cases of the same slope configuration with tension crack cases are constructed within the slope. One tension crack is located near the slope with a width of 10 m and another is 20 m. Two slope cases with tension cracks are compared with a reference case, in order to observe the behaviour of cracks within a slope.

Colour spectrum of strong amplification presents the earthquake shakings in the range of frequencies. Amplified areas are shown with different colours, with strong amplification in red to dark red. These are the frequencies most amplified by the site. The strong amplified

zones are more prone to landslide activity due to earthquake shaking. Indeed, if an earthquake occurs in these peak frequencies, large movements are likely to develop and may induce a slope failure in that area.

8.6.1.1 Slope configuration

The slope is characterized with two layers: bedrock and loess. Slope angle is presented to be 30° and loess thickness has two values: 20 m and 40 m. The length of the slope is 1200 m and the height is 400 m (Fig. 8-10).

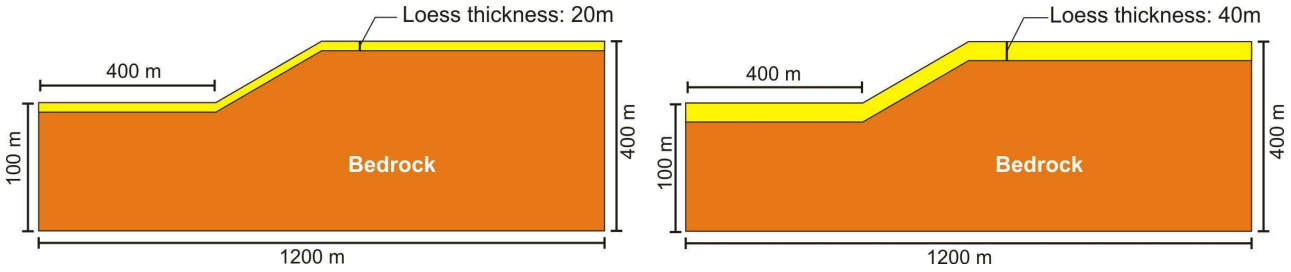

Fig. 8-10: Slope characteristics that are used for site effect assessment. The left-hand graph illustrates the loess slope with loess thickness of 20 m; the right hand graph presents the slope with 40 m loess thickness

8.6.1.2 Material properties

Material properties are shown on Table 8-4.

Table 8-4: Material properties of slope layers

Characteristics	***Vs*, m/s**	***Vp*, m/s**	**Density, kg/m^3**
Loess	420	900	1800
Bedrock	1200	2000	2300
Tension cracks	240	650	1300

8.6.1.3 Grid generation

The element size 4m*4m is used in the numerical slope model. Fig. 8-11 presents the mesh that is used in parametrical analyses.

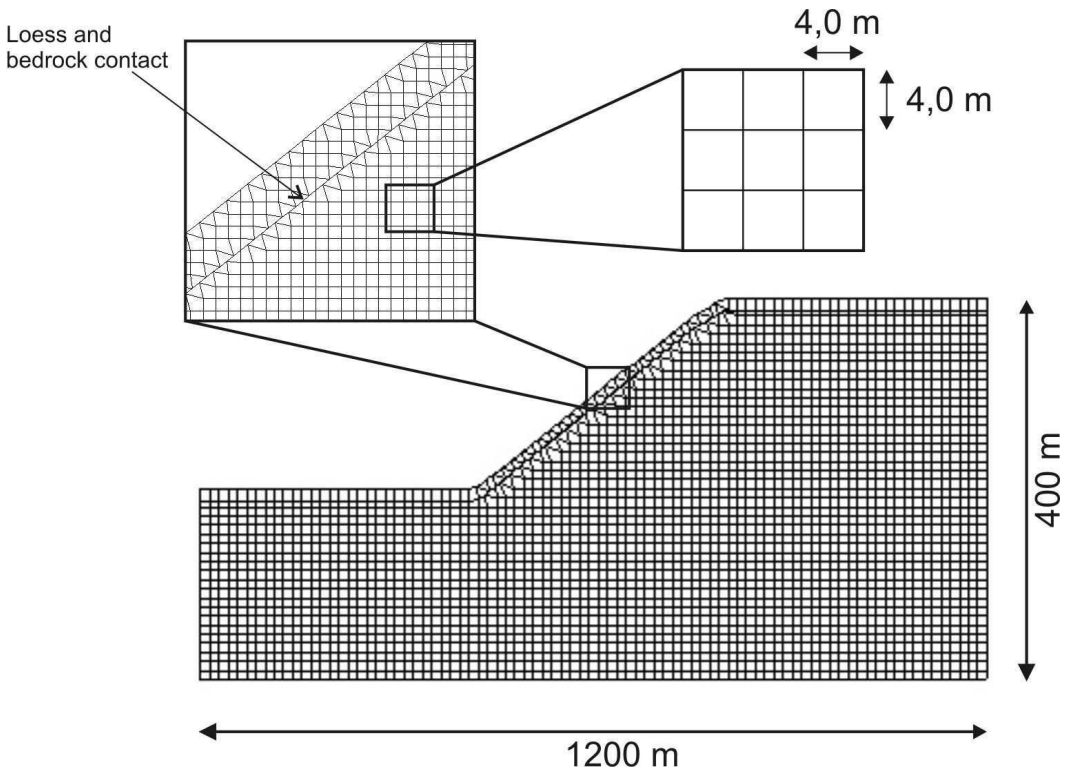

Fig. 8-11: Mesh used for the slope models. Detailed representation presents the element size of 4m*4m

8.6.1.4 Results

The seismic amplification potential of the layers is assessed through numerical simulations. Spectral amplifications along the surface are calculated by dividing the Fourier amplitude spectra of the computed horizontal signals by the Fourier amplitude spectrum of the reference motion. Two configurations of slopes without introducing tension cracks are simulated as the reference cases. The computed spectral amplifications calculated along the ground surface are shown in figures, where strong and weak horizontal amplifications are indicated in red and blue colours, respectively.

Fig. 8-12 shows computed spectral horizontal amplifications. The ***reference case (case 1) with a thin loess layer (20m)*** shows the strongest amplification (with a factor of 5) at the crest of the slope, with a frequency of 4 to 6 Hz. In the middle of the slope, there is hardly any amplification whereas at the bottom of the slope, spectral amplifications are between 3.5 and 4.5 for frequencies in the range of 4–5 Hz.

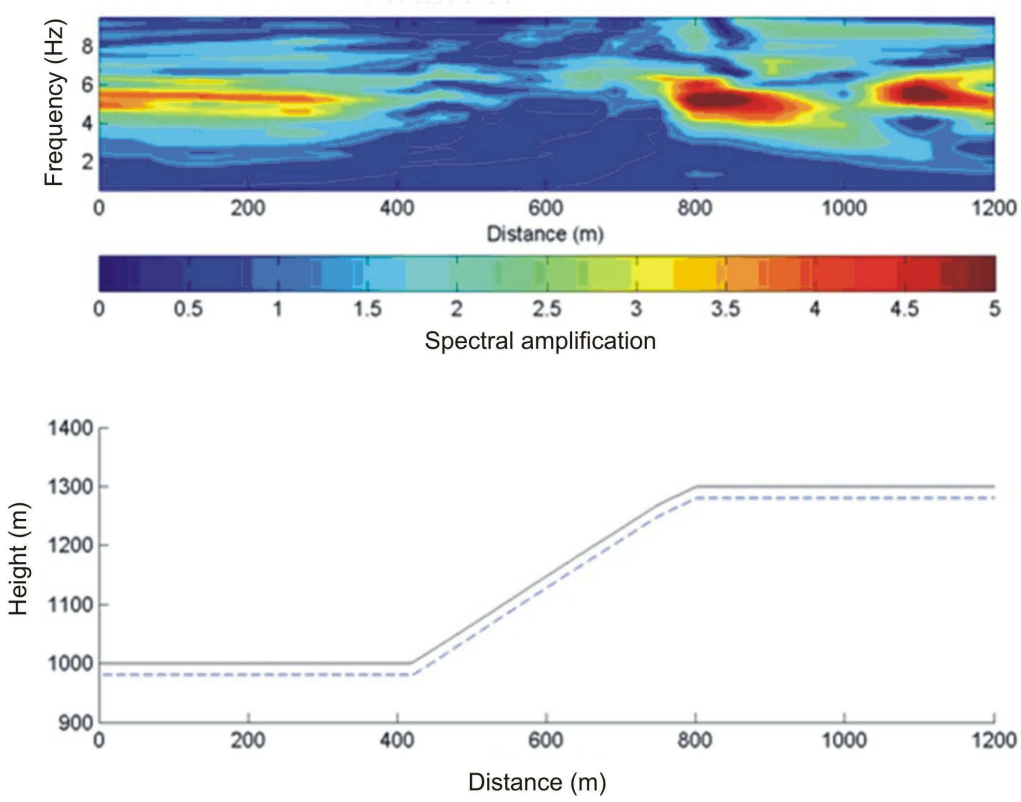

Fig. 8-12: Spectral amplifications of the slope with 20 m thickness of loess layer; reference case (case 1)

For the configuration of a ***slope with a 20m thick loess layer and a 20m thick tension crack (case 1.1)*** the the strongest amplification (with a factor of 5) concentrates close to the location of the crack and near the slope crest (Fig. 8-13). The toe of slope presented similar spectral amplifications observed at the reference case, i.e. amplification ranging 3-4 with a frequency range of 4-6 Hz. In the case of this slope configuration, stronger amplifications are observed with a frequency of more than 8 Hz at the location of the crack.

Spectral amplification in the case of a ***slope with a 20m thick loess layer and a 10m thick crack (thin crack, case 1.2)*** presented similar amplification as a reference case (case 1) and thick crack case (case 1.1) at the bottom of slope (Fig. 8-14). However amplification of 3, with frequencies of 4.5 - 6.5 Hz were observed near the toe of the slope at distances 450 m. Strong amplification was concentrated on the slope crest, on the left hand side of crack and in the *x* location of about 1100 m.

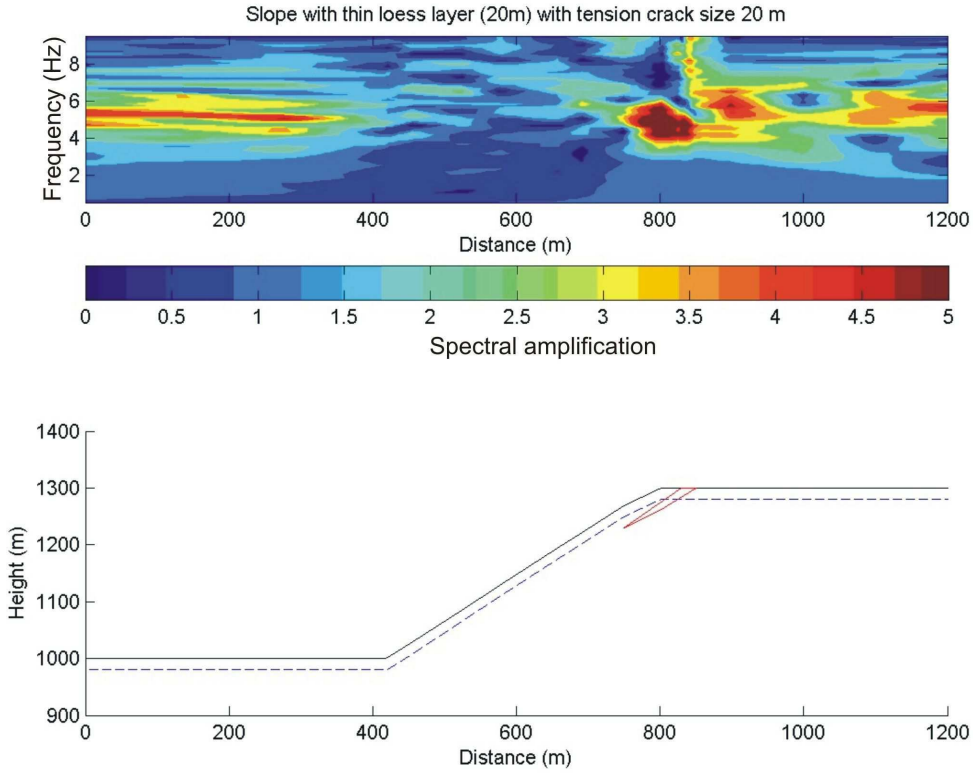

Fig. 8-13: Spectral amplifications of the slope with 20 m thickness of loess layer. In this case the width of the tension crack is 20 m (case 1.1)

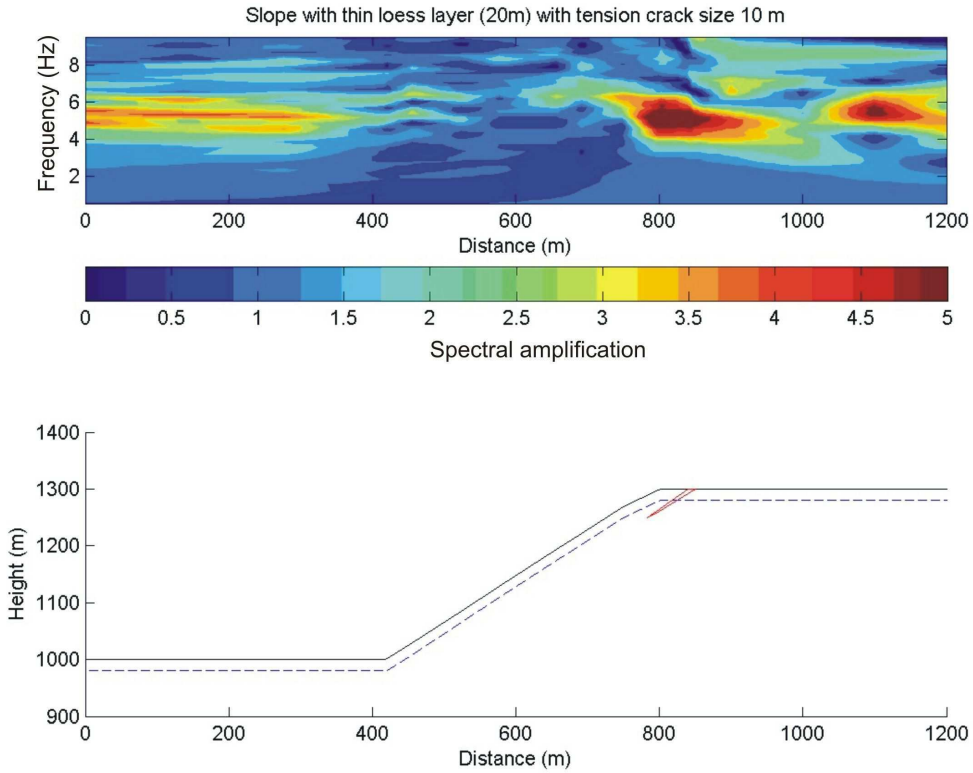

Fig. 8-14: Spectral amplifications of the slope with 20 m thickness of loess layer. In this case the width of the tension crack is 10 m (case 1.2)

A second slope configuration was simulated with 40 m of loess layer (thick loess layer). For comparison with the cases before, a spectral amplification with a range of 0 to 5 was considered. The ***reference case with a 40m thick loess layer (case 2)*** shows strong amplification between 3 – 4 in frequencies ranging from 2 - 4 Hz and 7 - 8 Hz on the bottom of slope. Similar amplifications also occur at the crest of slope (Fig. 8-15).

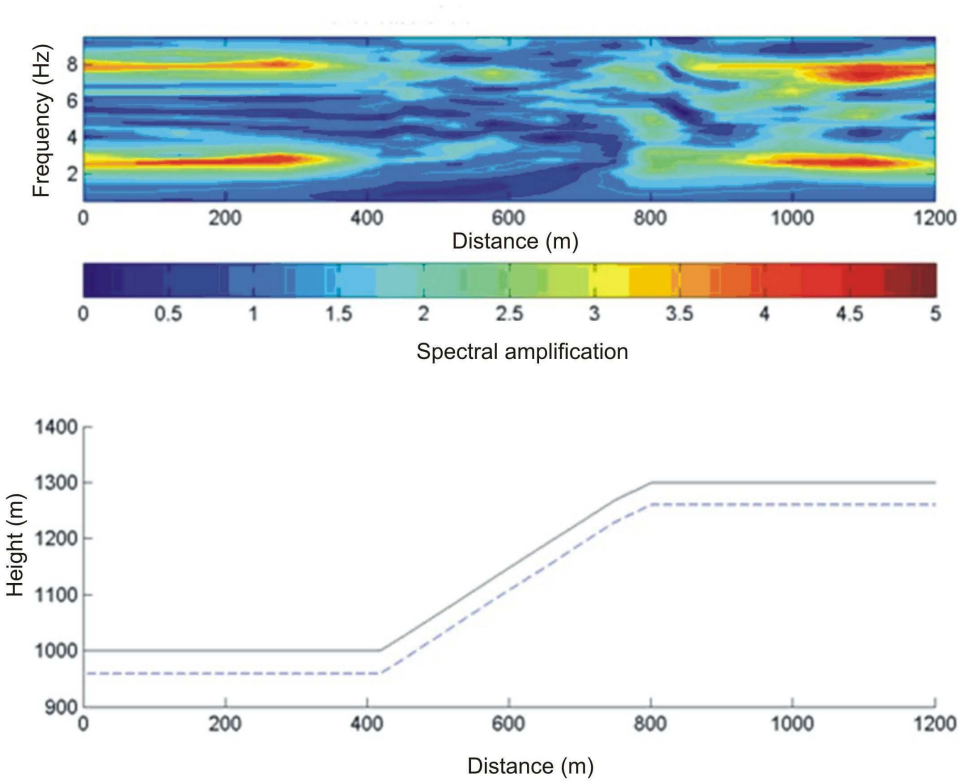

Fig. 8-15: Slope case with a loess thickness of 40 m; reference case

For the configuration of a ***slope with a 40 m thick loess layer and a 20 m thick tension crack (case 2.1)***, it is observed that the size of cracks have an impact on amplification (Fig. 8-16). As the reference case, also stronger amplifications between 3 – 4 in frequencies ranging from 2 - 4 Hz and 7 - 8 Hz can be seen at the bottom and the crest of the slope. In addition, there is also a stronger amplification with 4.5 at the location of the tension crack. On the body of the slope also slightly more amplification is observed than in the reference case. In the area x = 1200 m, the amplification is lower than in the reference case. In comparison with case 1.1 (slope with a 20m thick loess layer and a 20m thick tension crack) the amplification in the crack location is more obvious, even though the amplification is not as strong.

As before, a configuration of the ***slope with a 40 m thick loess layer and only a 10 m thick tension crack (case 2.2)*** was chosen and analysed (Fig. 8-17). In comparison with the reference case 2, slightly stronger amplification is observed at the tension crack location, ranging from 3 – 3.5 in 5Hz. Compared to the slope with the 20m thick tension crack (case 2.1), the amplification at the crack location is smaller. Compared to case 1.2 (slope with a 20m thick loess layer and a 10m thick tension crack) the stronger amplification at the location of the tension crack can be seen better.

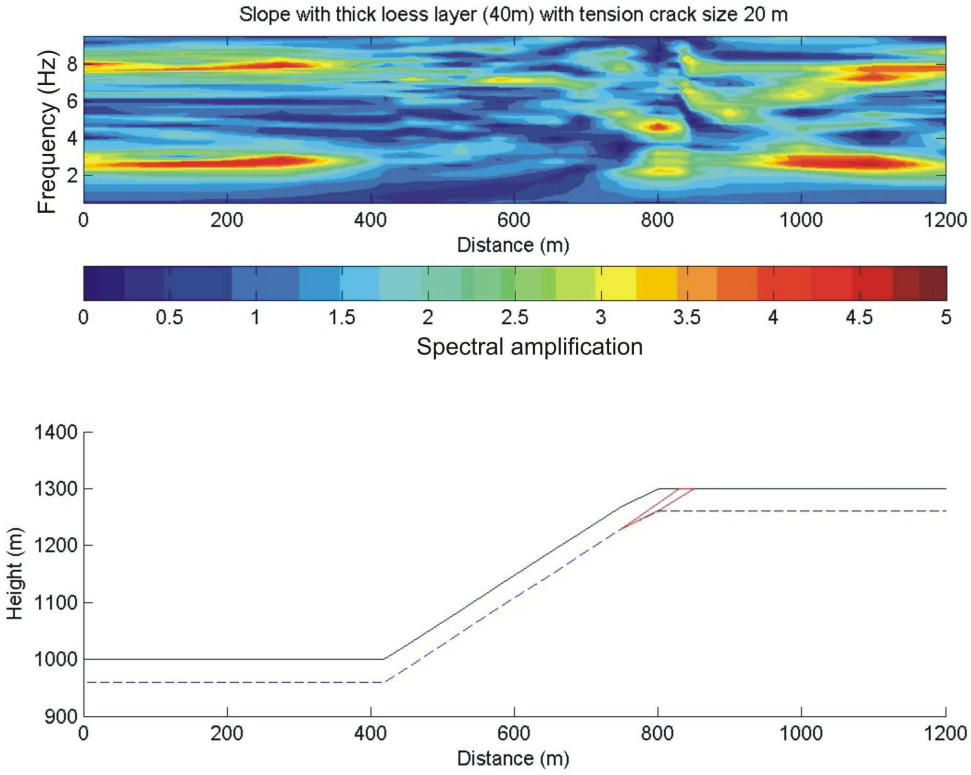

Fig. 8-16: Slope case with loess thickness of 40 m; the case of tension crack width 20m

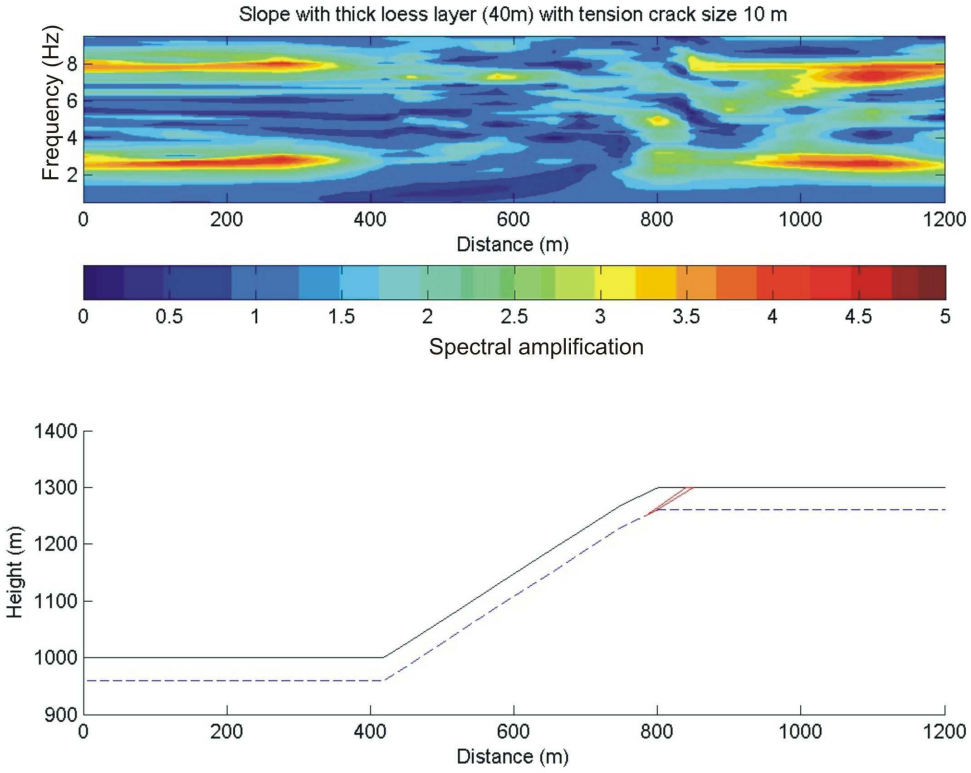

Fig. 8-17: Slope case with loess thickness of 40 m; the case of tension crack width 10m

8.6.1.5 Conclusion to parametrical studies on site effects (elastic condition)

Considering the two slope configurations to study an impact of site effects, it is observed that the thickness of the loess layer can control the amplification within the slope. In the case of a thin loess layer (20 m) the strong amplification ranged in frequencies between 4 and 6 Hz. In the case of thick loess layer (40 m) the frequencies ranged from 2-4 Hz and 7-9 Hz. In the case of tension cracks, it is presented that the crack width ranging to 10 m (case of thin crack) has nearly a similar amplification to the reference cases of slopes. Only a slightly higher amplification was observed in the case with a thicker loess layer.
In the case of thick crack cases (20m) the strong amplification is observed near the slope crest. Thus, according to tension crack and loess thickness stronger amplifications can occur and may have influence on ground motion.

8.6.2 Parametrical studies: Variation of geometries of cracks (Elasto - plastic conditions)

The studies from site effects in loess slopes have shown an impact of tension cracks on the slope in terms of site amplification. Taking into consideration the results of the first parametrical studies, it is in particular interest to concentrate an attention on cracks parameters.

In order to investigate the impact of tension cracks on loess instability, parametrical studies are carried out. From the field observations over a long period, it is observed that landslides in the southern part of Kyrgyzstan can occur in slopes with angle of approximately 30º. The average thickness of loess layer is estimated at about 20 m in such slope cases. Regarding neighboring countries, due to specific geomorphologic features, mass movements in a loess slope occur in a flat slope of 15° and thickness of up to 50 m. To compare two slope sites with a presence of tension cracks and to observe the behavior of a loess slope in dry conditions, numerous models with variations of tension crack parameters are carried out.

8.6.2.1 Slope profiles

For the simulations, the two slope configurations are used. Table 8-6 shows the slope characteristics.

Table 8-6: Slope characteristics

Slope cases	Slope degree (°)	Height (m)	Length (m)	Thickness of a loess layer (m)
1	15	600	2400	20
2	30	600	1535	50

Fig. 8-18 presented the slope case (1) with slope angle 30° and loess thickness of 20 m.

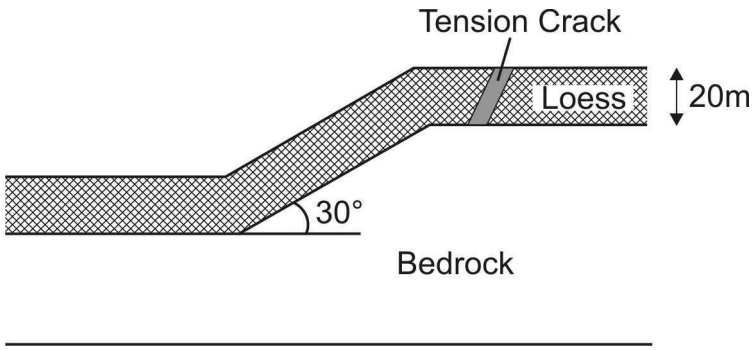

Fig. 8-18: Slope case (1) with angle of 30° and loess thickness of 20 m

The slope case with loess thickness of 50 m is represented in Fig.8-19.

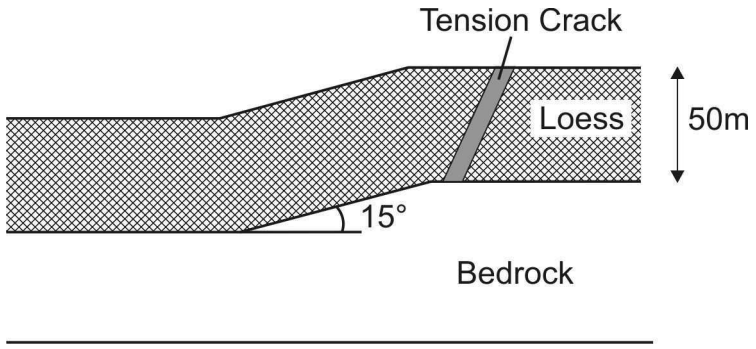

Fig. 8-19: Slope case (2) with angle of 15° and loess thickness is 50 m

8.6.2.2 Tension cracks configurations

For the studies, different parameters of tension cracks included into the slope. Schematically, a slope with parameters of cracks is shown in the Fig. 8-20. Three parameters of distance from the crest are selected. The locations of 10 m, 20 m and the farthest location from the crest is 30 m are selected. Inclination of tension cracks is considered to be 45°, 60° and 90°. 90° and 60° of tension crack inclination is widely observed in loess slopes (KRIGER, 1980). Length of cracks varies from 12 m, 16 and 20 m. In the case of 20 m loess thickness, a 20 m long vertical tension crack reaches loess and bedrock contact.

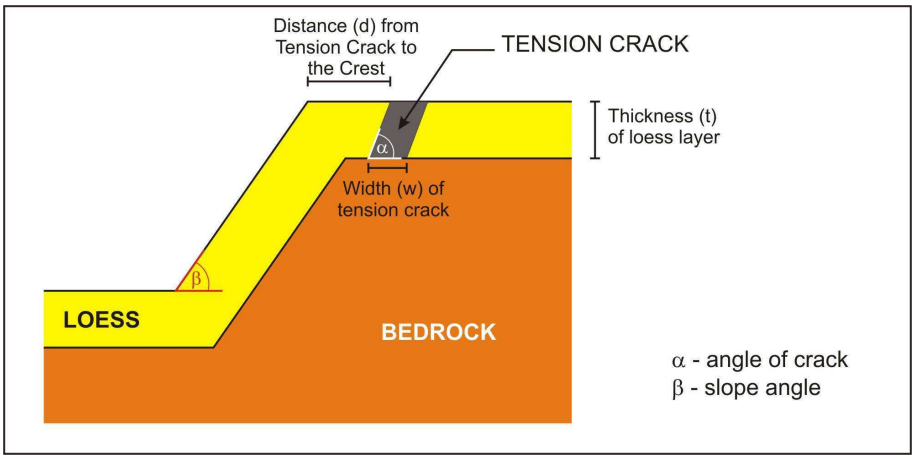

Fig. 8-20: Schematic view of a slope model with tension cracks

Table 8-7 presents the tension cracks variations used for simulations

Table 8-7: Geometrical parameters of tension cracks and given values

Parameters of cracks	Given values		
Length (m)	12	16	20
Inclination (°)	45	60	90
Position (m)	10	20	30

8.6.2.3 Material properties

Material properties are shown in the Table 8-8.

Table 8-8: Material properties used for the numerical analyses

Material	Dry density, kg/m^3	V_S, m/s	V_P, m/s	c', kPa	φ , °
Loess	1800	420	900	30	30
Tension cracks	1300	240	650	6	30
Bedrock	2300	1200	2000	2000	35

8.6.2.4 Grid generation

The adopted grid for the slope case with angle of 15° is shown in Fig. 8-21 in an exemplary way. Element size 2m*2m is used in a zone of interest and 2m*4m size is selected in relation to the bottom of slope.

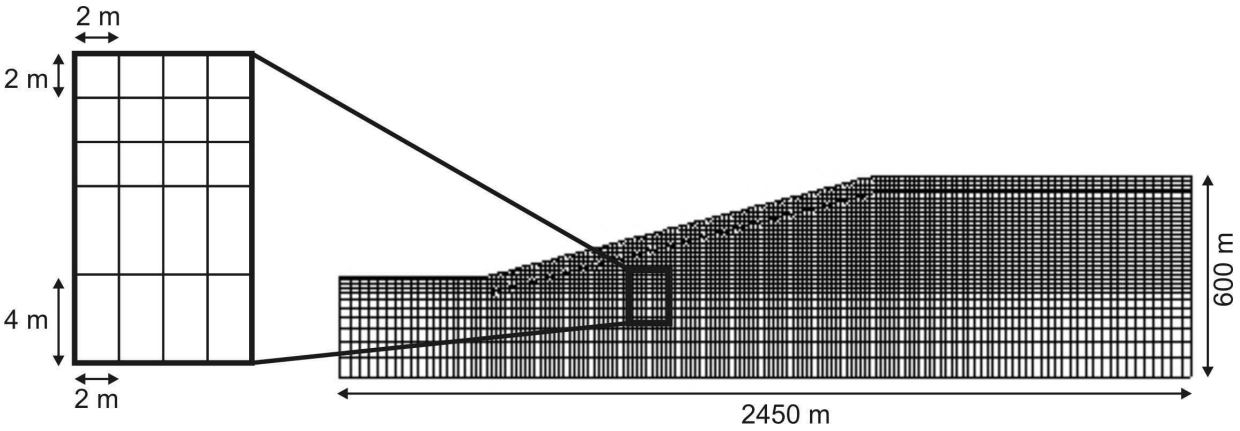

Fig.8-21: Grid used for the slope case with angle 15°, element size 2m*2m, and 2m*4m

8.6.2.5 Results

This analyses aim at defining how the size of a slope failure may be linked to the intensity of the seismic shaking. Therefore material properties, slope geometry and tension cracks with variable parameters are set as defined in tables 8-6, 8-7 and 8-8. Different simulations are carried out while examining the possible failure process. During this process, plots of the

progressive displacement of the slope are made. Displacement vectors in the diagrams show the direction and travelled distance of numerous grid points of the mesh (Fig. 8-22). Areas of displacement define the more unstable part of the slope under earthquake shaking. This area, resulting from displacement vector plots is described here as "unstable mass". In order to better characterize the landslide potential, the unstable mass is calculated for all configurations leading to instability. Fig. 8-22 presents a schematic sketch, showing the definition of the unstable mass.

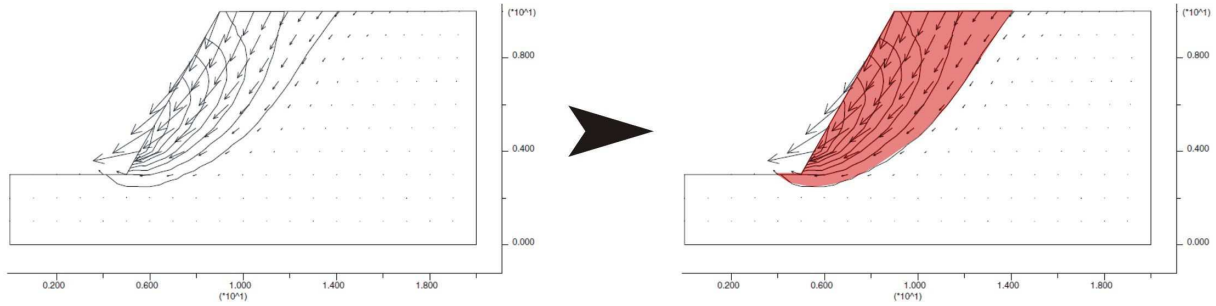

Fig. 8-22: Schematic sketch showing the definition of the unstable mass from the displacement vectors

In a first case a ***slope with an angle of 30° and a loess thickness of 20 m (case 1)*** is studied. At first, a reference scenario without tension cracks is analysed. After that, different simulations are done with variation in geometrical parameters of the tension crack as shown in table 8.7. The different simulations are compared with the reference scenario and the unstable mass is determined for each simulation. All calculated unstable mass values are plotted in one diagram which shows the total area of unstable mass for the different tension crack parameters.

For the case 1, the total area of the unstable mass for all parameters of tension crack cases ranges from 9860 m^2 to 9940 m^2. The area of the reference scenario is 9860 m^2 for this case. Tension cracks with an inclination of 90° show the smallest value that is observed in the runs. Tension cracks located far from the slope crest have no significant impact on the slope stability, as the area of unstable mass value is equal to the reference scenario (about 9860 m²). The biggest area of unstable mass (9940 m²) is located in the crack position of 20 m, crack inclination of 60° and length of 12 m (Fig. 8-23). For the case of length 16 m and 20 m, the area of unstable mass is the same (Fig. 8-24 and Fig. 8-25).

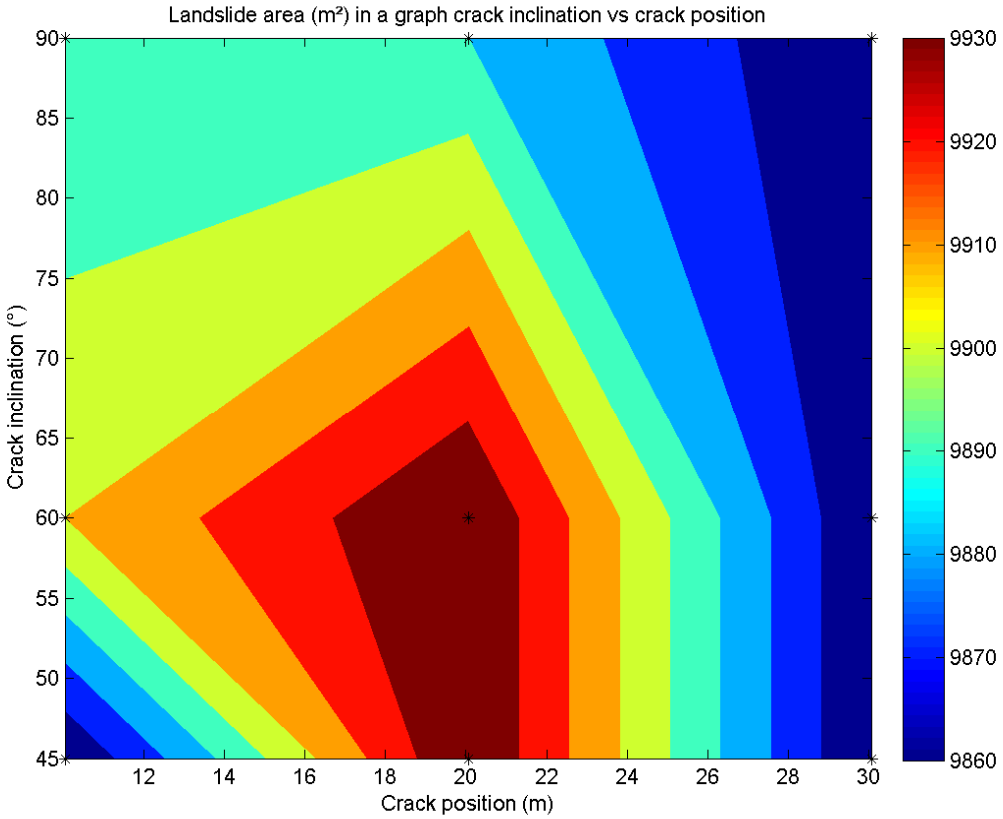

Fig. 8-23: Area of unstable mass in a case with tension crack length of 12m

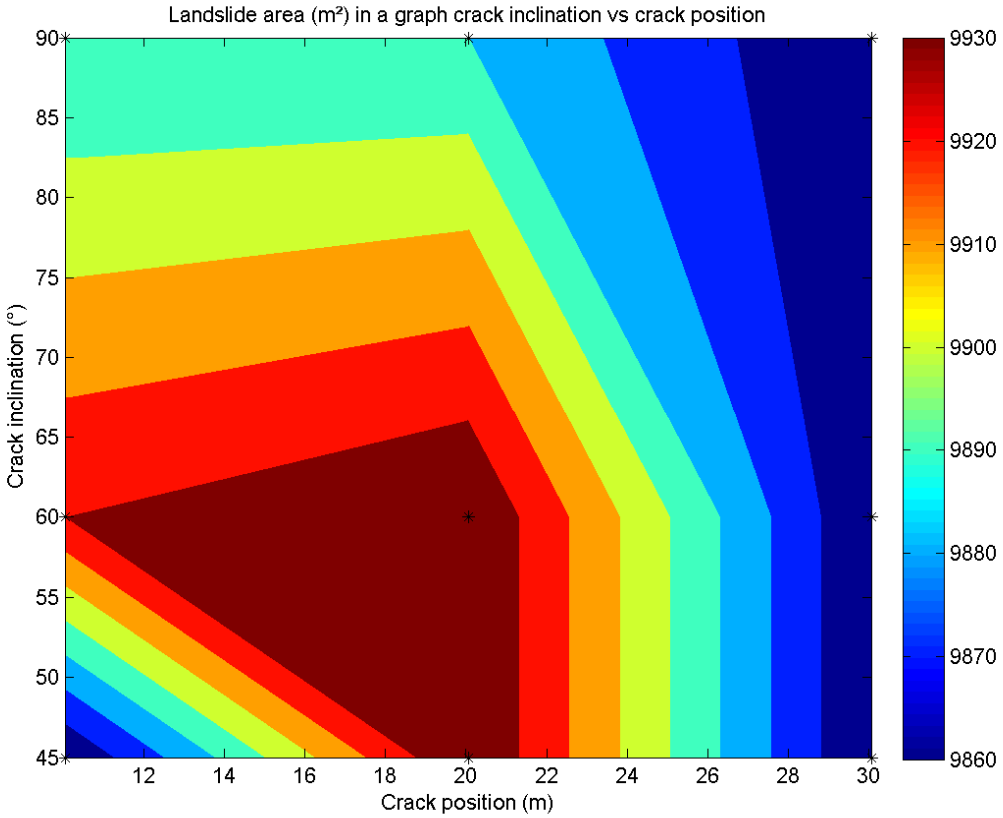

Fig. 8-24: Area of unstable mass in a case with tension crack length of 16m

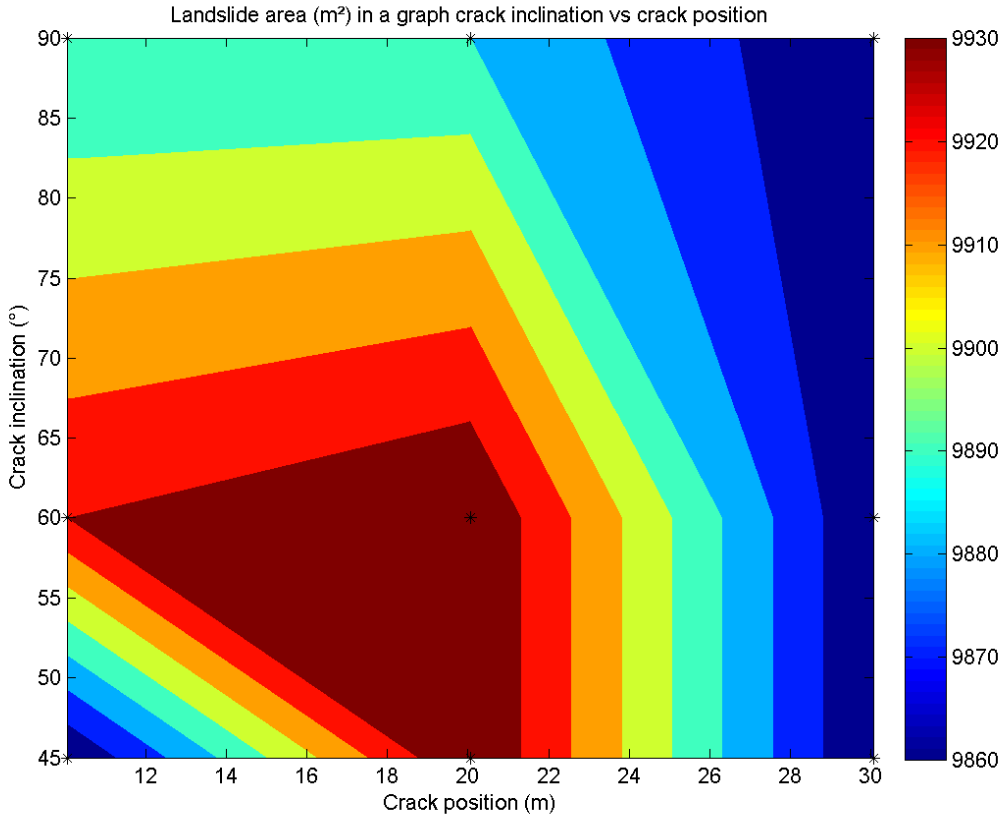

Fig. 8-25: Area of unstable mass in a case with tension crack length of 20m

In a second case a ***slope with an angle of 15° and a loess thickness of 50 m (case 2)*** is analysed. The procedure is the same as before in case 1 and the results are shown as total areas of unstable mass in different diagrams.

The smallest area of unstable mass is 39800 m^2 for the tension cracks characteristics with 10m away from the crest, 12 m in length and an inclination of 45°. Fig. 8-26 shows the area of unstable mass for a tension crack length of 12 m. For this length the biggest area of unstable mass occurs for tension cracks with an inclination around 55° and a position of 18 m to 30 m away from the crest.

Fig. 8-27 presents the area of unstable mass for the crack length of 16 m. For this case, the biggest area is observed at the crack position of 20 m to 30 m with an inclination of 60°. In comparison the shorter tension cracks of only 12 m, the range where the biggest unstable mass occurs is more limited in this scenario. Tension cracks with inclinations higher than 60° show smaller areas of unstable mass.

By comparison, the biggest area of unstable mass for a crack length of 20 m (Fig. 8-28) is observed for the crack position of 20 m to 30 m at an inclination of 60 to 90°. The range where the biggest unstable mass occurs is higher than in scenarios with 16m long tension cracks.

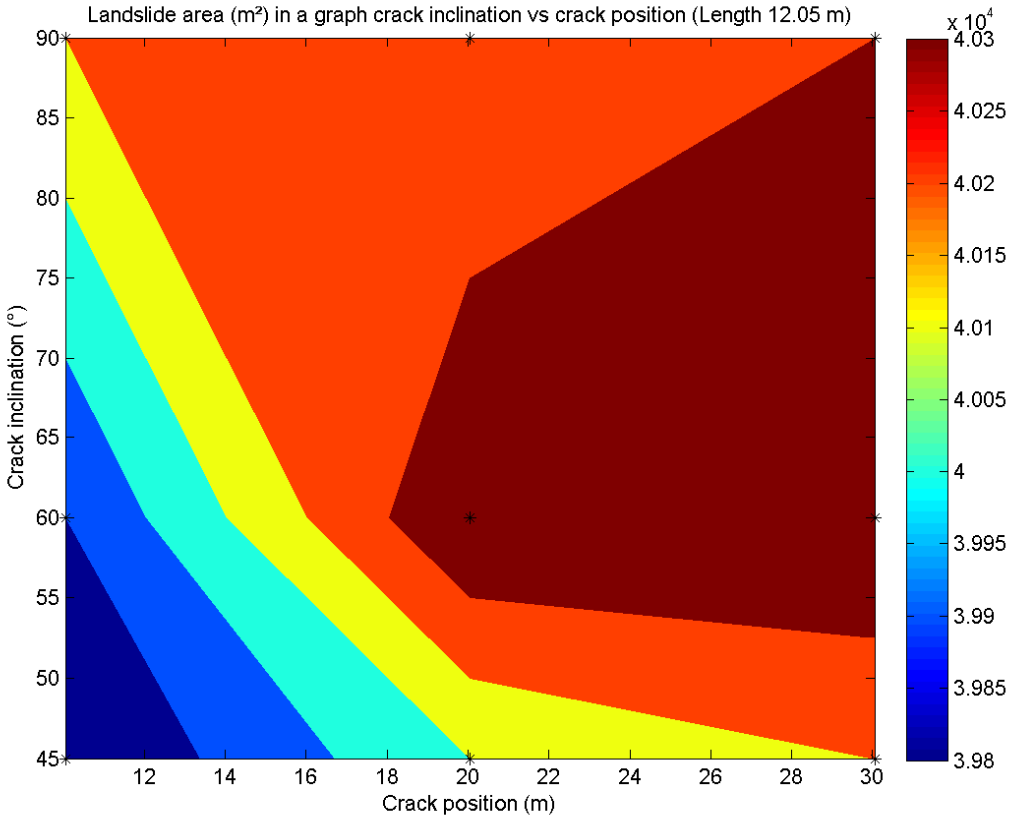

Fig. 8-26: Area of unstable mass in a case with tension crack length of 12m

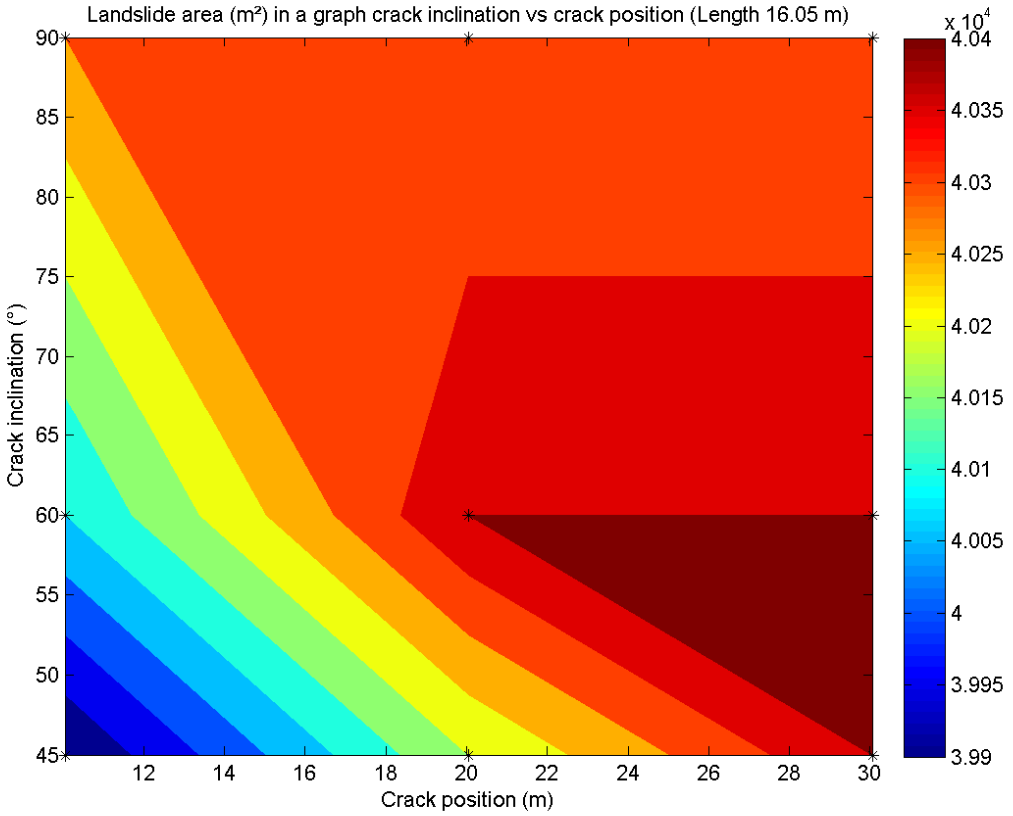

Fig.8-27: Area of unstable mass in a case with tension crack length of 16m

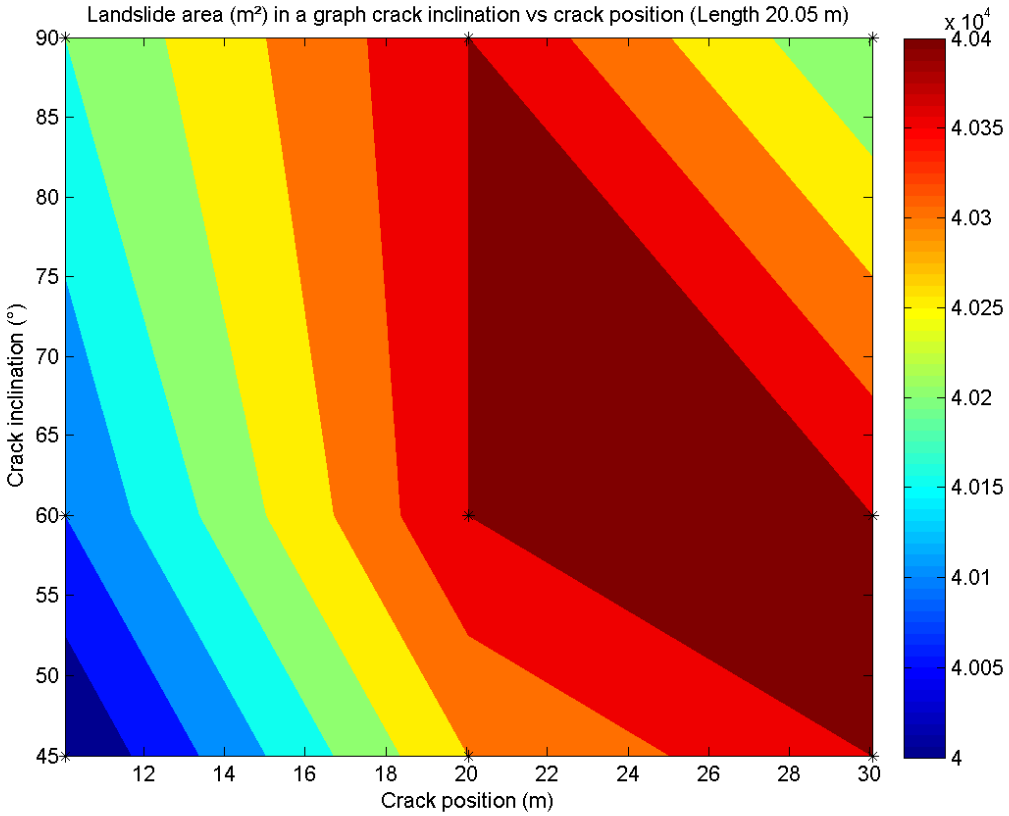

Fig.8-28: Area of unstable mass in a case with tension crack length of 20m

8.6.2.6 Conclusion to the tension cracks impact studies

The following conclusions are drawn from studies on impact of tension cracks on slope instability.

- Areas of unstable mass presented differences, however the range of variations is not broad
- Slope behaviour is affected in the case where a crack is close to the crest
- In general the whole area of unstable mass is larger in the slope case with loess thickness of 50 m than in slope with loess layer of 20 m. In these cases, there is an influence of loess layer on the development of the landslide area.

While comparing results of two slope cases, the following conclusions can be drawn:

- The area of unstable mass depends on tension crack characteristics. However, the range of the variations is not very wide. This means that in dry conditions, slope behavior is much more influenced by slope geometry and geology than by the characteristics of tension cracks.

- There is a critical position above which the presence of the tension crack and its characteristics do not modify slope behavior (which is, in this case, identical to the one obtained without any tension crack).

- The area of unstable mass depends on crack length only when the crack is located close to the crest. Knowing that slope failures are generally quite superficial, controlled by the thickness of the loess layer, it is very likely that only the upper part of the tension crack would modify slope behavior when the crack is located far from the crest i.e. no matter how long the crack is, it would have the same influence on slope stability.

8.6.3 Real case: Upper - Koi-Tash

8.6.3.1 Introduction to the slope

The Upper Koi-Tash landslide is located in the Mailuu-Suu basin. The detailed explanation of this landslide is given at the first part of the current research (chapter two) and its failure history is explained in the part related to loess landslides (chapter five). The aforementioned chapter says that small earthquakes have occurred in the region (Fig. 5-11 in chapter five). In order to observe the behaviour of a slope in case of small seismic shakings, several studies on variation of peak ground accelerations are carried out, in addition to the site amplification cases. Loess covers the top part of the landslide. Fig. 8-29 presents the overall view of the landslide.

Fig. 8-29: Overall view of the landslide Upper Koi-Tash

8.6.3.2 Slope profile

Fig. 8-30 illustrates the satellite image after the landslide occurred, only to show the straight profile that is used to derive the topography. Fig. 8-31 illustrates the topographical profile of the Upper Koi-Tash. The total length is about 1600 m and the height is 830 m. Regarding geological layers, De MARNEFFE (2010) made a detailed geological mapping and layering by using of Digital Elevation Model (DEM) and SPOT Satellite data by importing into GOCAD software. This obtained profile presents the slope before the failure occurred.

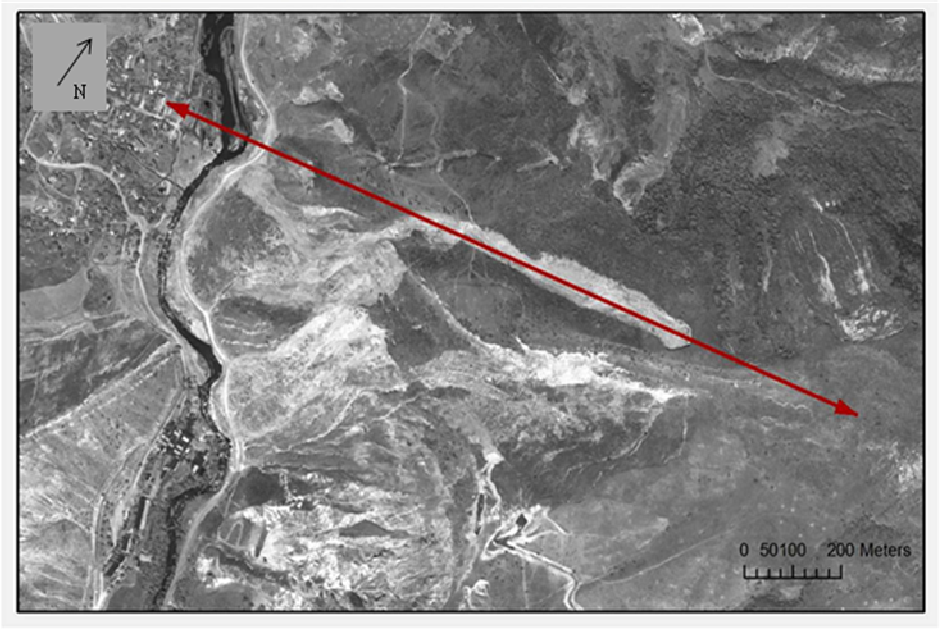

Fig. 8-30: Satellite image of Upper Koi-Tash landslide and a cross section (red line) used to obtain a profile for numerical modelling

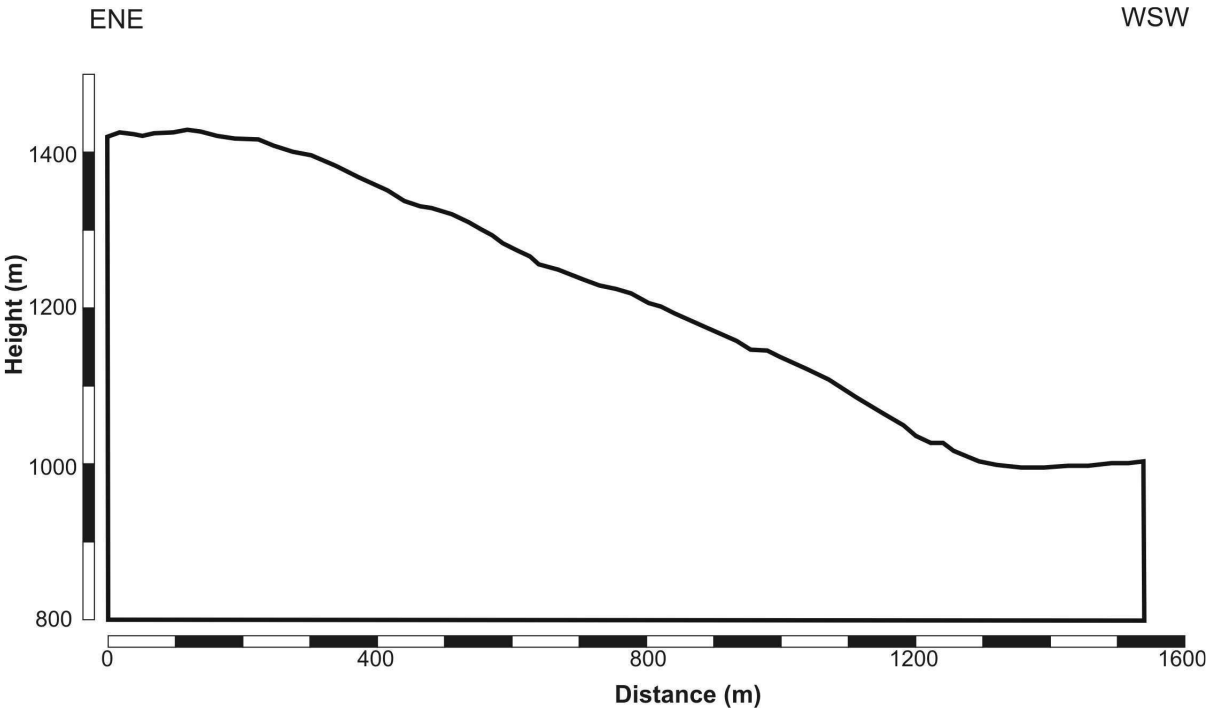

Fig. 8-31: Topographical profile of the Upper Koi-Tash landslide

The geoelectric profile introduced by HAVENITH (2002) in the upper part of the Koi-Tash landslide is in good agreement with the layering. There are uncertainties on the different geological layers since they are based on local information along a few cross sections. These are based on mining data and field work and extrapolations of the information over a wide area (De MARNEFF, 2010).

Fig. 8-32 presents the geological layers of the landslide. It consists of Cretaceous clay and sandstone as bedrock overlaid by Palaeogene limestone. Palaeogene clay and Quaternary loess layer is located as a superficial layer. The loess layer's thickness is approximately 20m and mainly concentrated on the upper part of slope. Loess layer located on the top of slope gets slightly thinner and a small layer is observed.

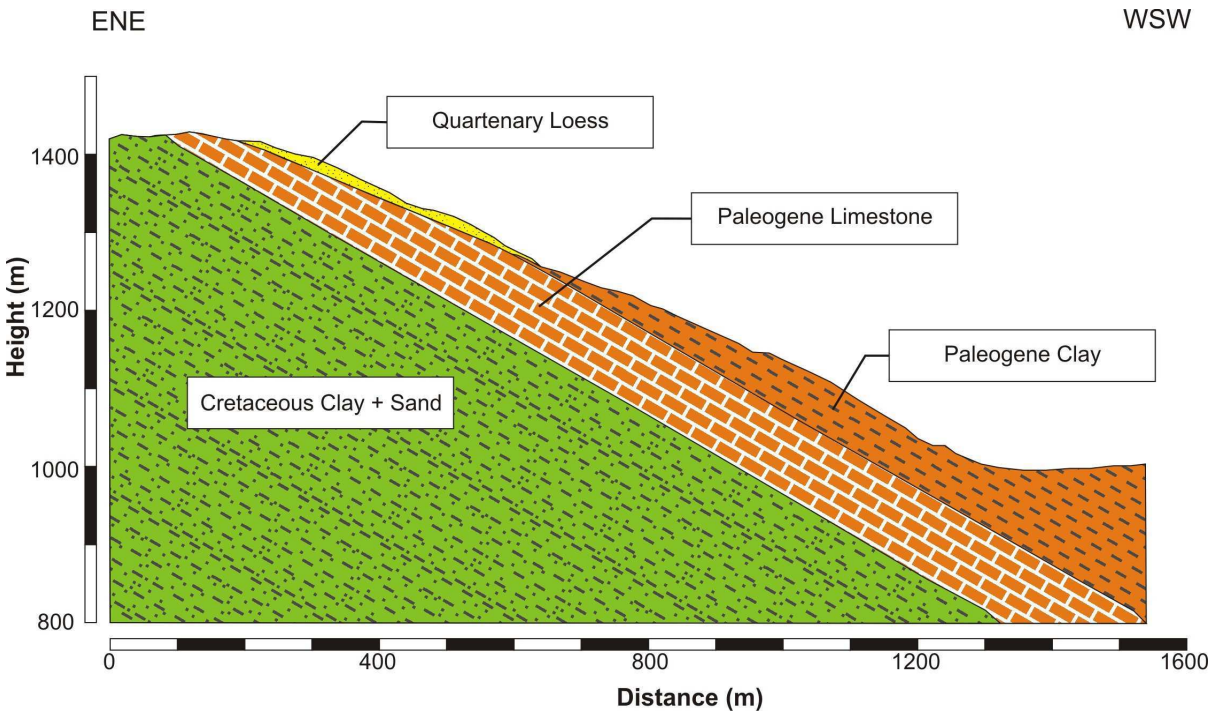

Fig. 8-32: Geological layers of the Upper Koi-Tash landslide

8.6.3.3 Material properties

According to the laboratory analyses from the region and literature comparison, the following material properties are used for simulations (Table.8-9).

Table 8-9: Geotechnical characteristics for soil parameters

Material	Dry density, kg/m^3	V_P, m/s	V_S, m/s	c' , kPa	φ , °
Bedrock	2000	2000	1000	100	35
Limestone	2200	2400	1300	200	35
Clay	1800	1680	800	50	32
Loess	1600	880	400	30	30

The shear (G) and bulk (K) modulus of the rock mass were calculated using the relations (8-1) (8-2), respectively.

8.6.3.4 Grid generation

After obtaining the data on topographic profile and geological layers, a slope model is created to assess the slope stability in dynamic domain. The model consisted of finite difference mesh that is composed of quadrilateral elements. The elements that are the smallest within the mesh

determine the dynamic time step. The element size used in the slope mesh is 2m*2m in zone of interests. In order to decrease the time of computation, the coarser mesh with element size of 2m*4m is used on the bottom of the model. In Fig. 8-33, the grid of a slope is presented. The model contains 64554 elements.

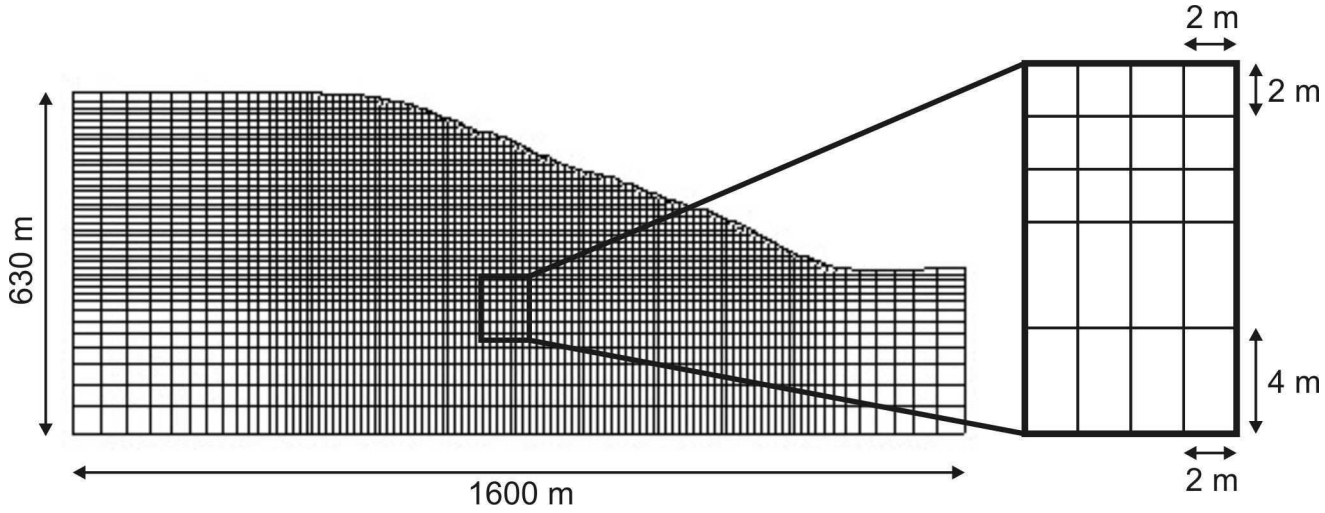

Fig. 8-33: Slope grid representing the landslide Upper Koi-Tash

8.6.3.5 Results: Horizontal acceleration

At first, two cases of slope are considered. The homogeneous slope represents only bedrock and the second case shows a slope with geological layers in the Upper Koi-Tash landslide. The aim of comparing the two cases is to define the role of loess in seismic impact.

In Fig.8-34, the site effects for the homogeneous slope are shown. Input signal reaches the toe of a slope in less than 2 s, in the top of a slope, a time is observed larger than in the bottom of a slope.

Fig. 8-35 presents the site effects in a heterogeneous model of slope. This slope constitutes of four materials that are introduced in the real case. At the location where the loess layer lies, the time of seismic waves represents the long reach. The crest and toe show slightly similar results as a homogeneous slope.

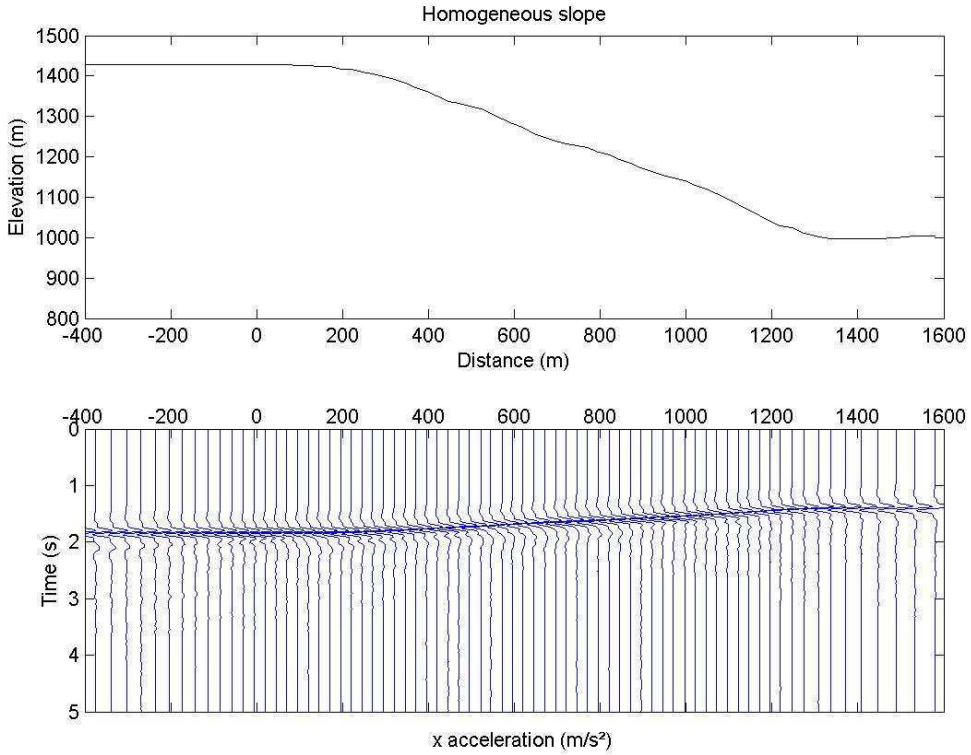

Fig. 8-34: Horizontal accelerations computed every 15 m in homogeneous model

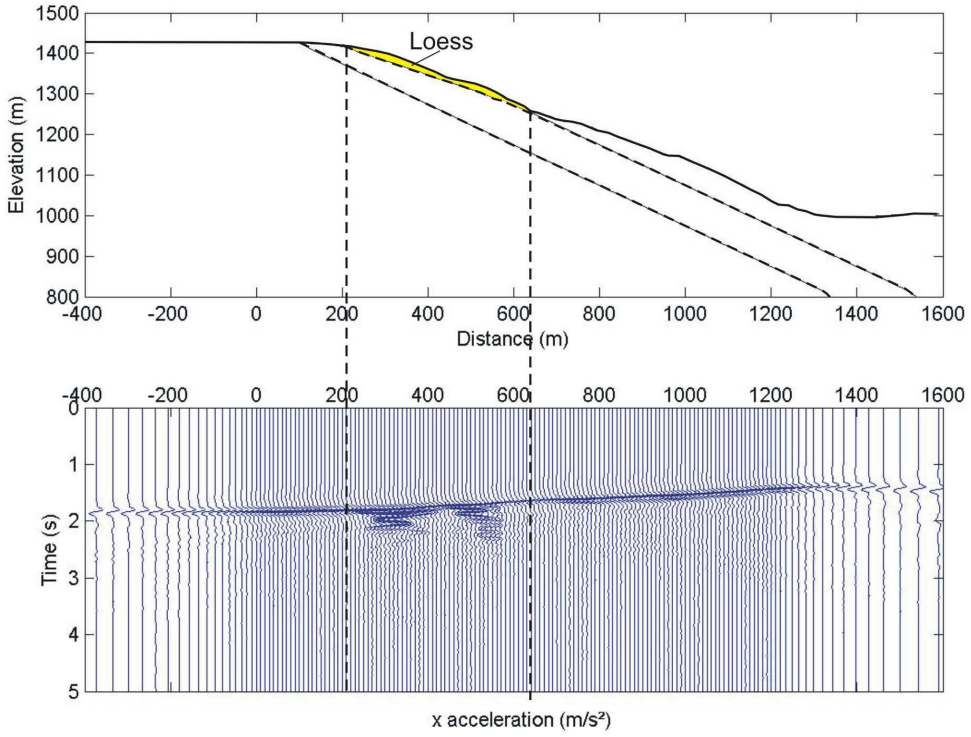

Fig. 8-35: Horizontal accelerations computed every 15 m in heterogeneous slope

8.6.3.6 Results: Topographical site effects and geological site effects

Spectral amplifications along the surface are calculated as described in chapter 8.3.2. To assess the characteristics of pure topographic site effects, one homogeneous model is created. The slope consists only of clay-sandstone material assigned as bedrock. Thus, this first case does not consider loess material.

Geological site effects consider the spectral amplifications inside the slope. The homogeneous slope model is presented in Fig. 8-36. This slope shows no large amplifications, only slightly high amplifications for spectral range up to 1.5 are observed at distances 700 – 1000 m on the slope.

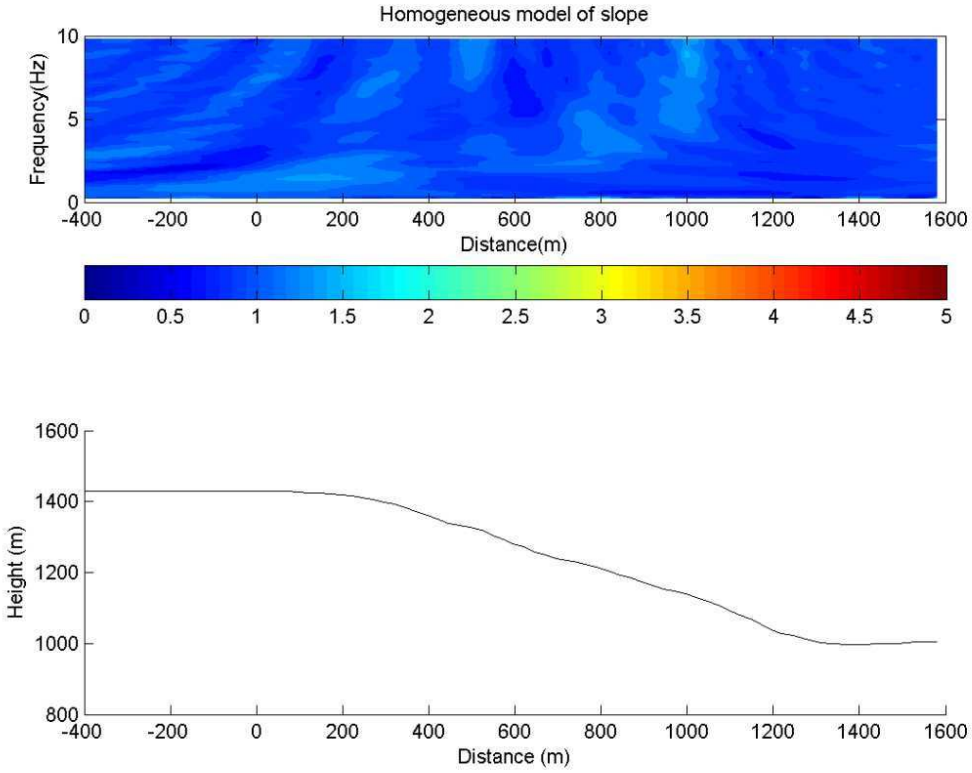

Fig. 8-36: Ground motion amplification in homogeneous slope

The heterogeneous slope is presented in Fig. 8-37 and shows the slope with four layers of materials, with loess on top of the slope as shown in Fig. 8-32. Strong amplification is illustrated in red while low amplification is shown in blue. As it is seen in Fig.8-37, strongly amplified regions are located between 200 m and 400 m of horizontal distance and thus lie in the area where the loess material is sited. On the top of the slope, where surficial loess layer is located, strong amplification in frequencies of 5 to 10 Hz is observed in spectral ranges 3 to 5. In the area, where loess gets thinner, lower amplifications occur and are presented in blue. Inside the slope small amplified zones can be observed. The range is 1 – 1.5.

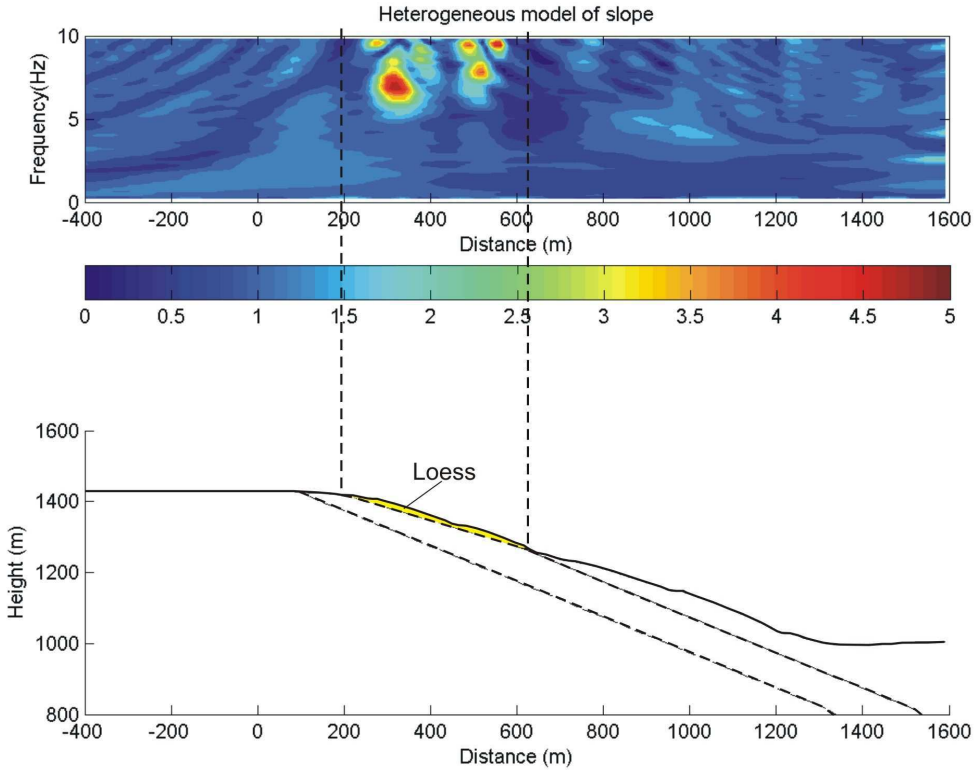

Fig. 8-37: Ground motion amplification in heterogeneous slope

8.6.3.7 Results: Seismic slope deformations

In the following segment, the PGA values are given to observe the seismic impact on a slope. The stability of a slope can also be expressed in terms of development of strains. Hence, the failure of the slopes can also be seen as shear strain rate for each PGA case. The detailed graphs of large concentrations of shear strain rates are shown in detailed graphs. In the following four cases, a shear strain rate is mainly concentrated in a loess layer. However the highest rates are on the toe a slope. For each case a maximum shear strain rate is presented. The smallest amount, PGA=0.01, is the smallest value of shear strain rate represented. This value is increasing gradually, by increasing the PGA.

In a first case the Peak Ground Acceleration is ***PGA = 0.01***. In Fig. 8-38, shear strain rate that developed in a loess layer is presented. The detailed graphs show the high concentration of shear strain on a loess layer. The toe of the slope that consists of the Palaeogene clay is prone to a higher shear strain than a loess layer. Fig. 8-38a represents the total geometry of a slope with shear strain rate. The present case is shown in detail in Fig. 8-38b and illustrates the loess layer. Fig. 8-38c presents the lower part of a slope; the exaggerated graph of the toe shows strong shear strain increment.

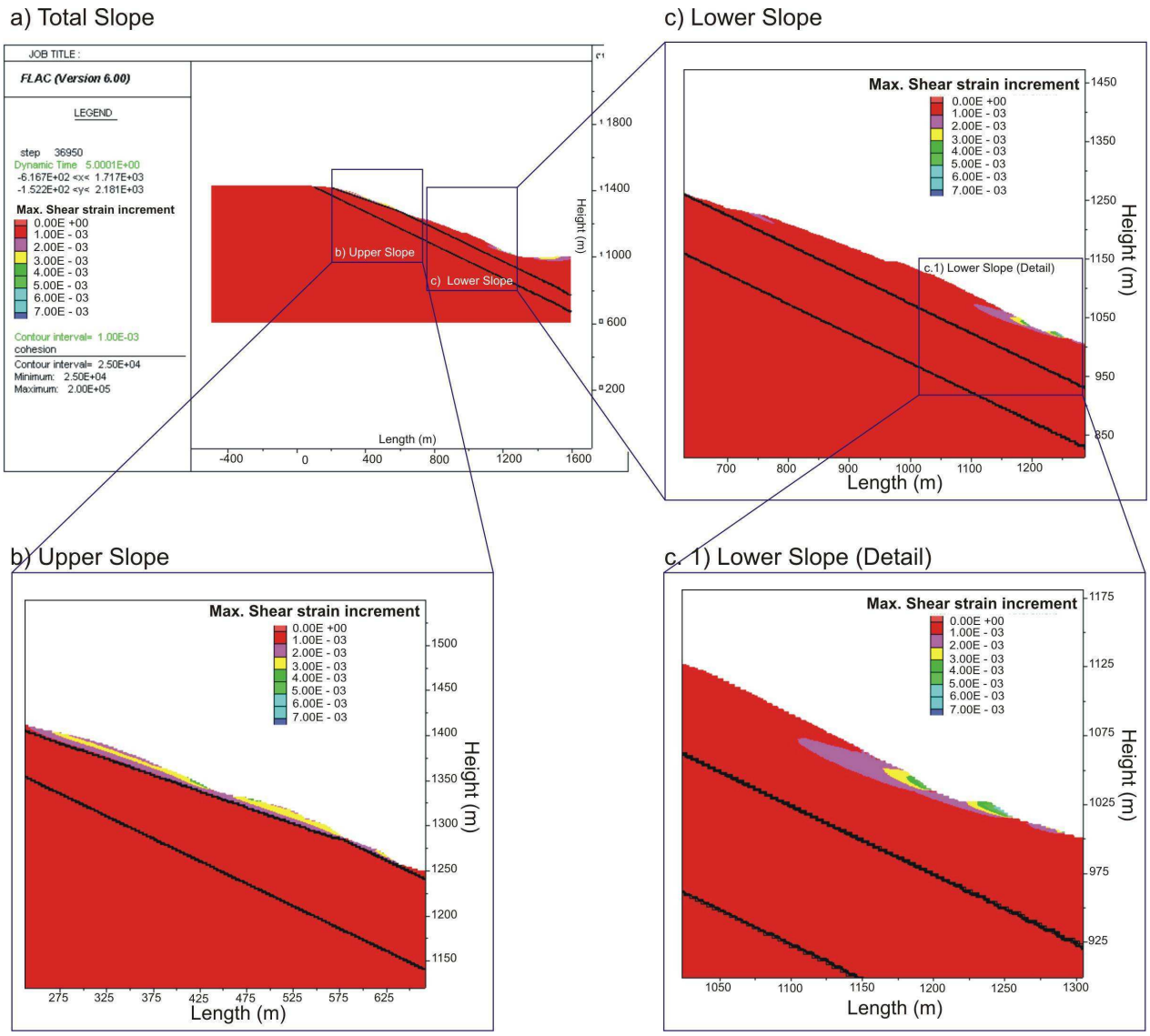

Fig. 8-38: Maximum shear strain increment for the PGA=0.01. a) Total slope geometry is shown in two boxes showing the detailed regions. b) the detailed representation on a loess layer; c) the detailed view on a toe of slope; c) exagerated view to show the shear strain rate concentration on a toe of a slope

In a second case the Peak Ground Acceleration is ***PGA = 0.02.*** Fig. 8-39 presents the case PGA=0.02 and a detailed representation of a loess layer, middle slope and toe of a slope. The area from 275 m to 375 m shows a smaller rate as an area from 375 m to 525 m (Fig. 8-39b). In the toe of a slope, shear strain concentrates in a high range, as a case PGA=0.01 (Fig. 8-39d). The middle part of a slope shows no shear strain rate (Fig. 8-39 c).

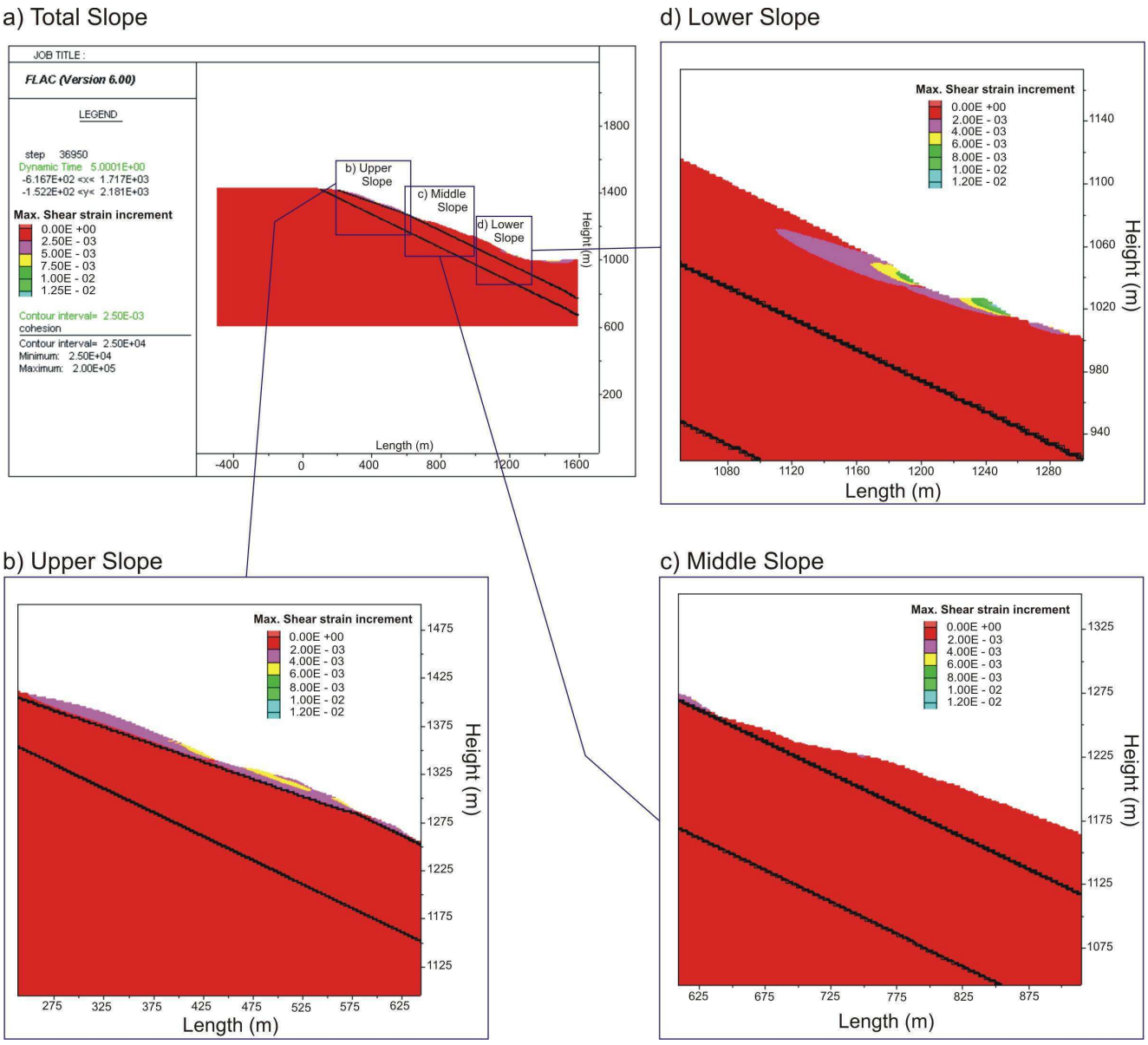

Fig. 8-39: Maximum shear strain increment for a case PGA=0.02; a) The plot shows the total slope with three boxes in black outlining the three regions for a detailed illustration; b) the upper part represents the loess layer; c) the middle part of a slope is shown without any shear strain rate concentration; d) the lower part shows the shear strain rate in toe of a slope.

The third case the Peak Ground Acceleration is ***PGA = 0.05.*** The maximum shear strain rate is presented in Fig. 8-40 and gives a detailed representation of the loess layer, middle of a slope and toe of a slope. In loess, the shear strain rate is observed to be smaller than the previous two cases of PGA (Fig. 8-40a). However, small ranges of rate can be observed in the middle of a slope, in the areas 750 m to 1000 m (Fig. 8-40c). Toe of a slope shows the highest rate of shear strain (Fig. 8-40d).

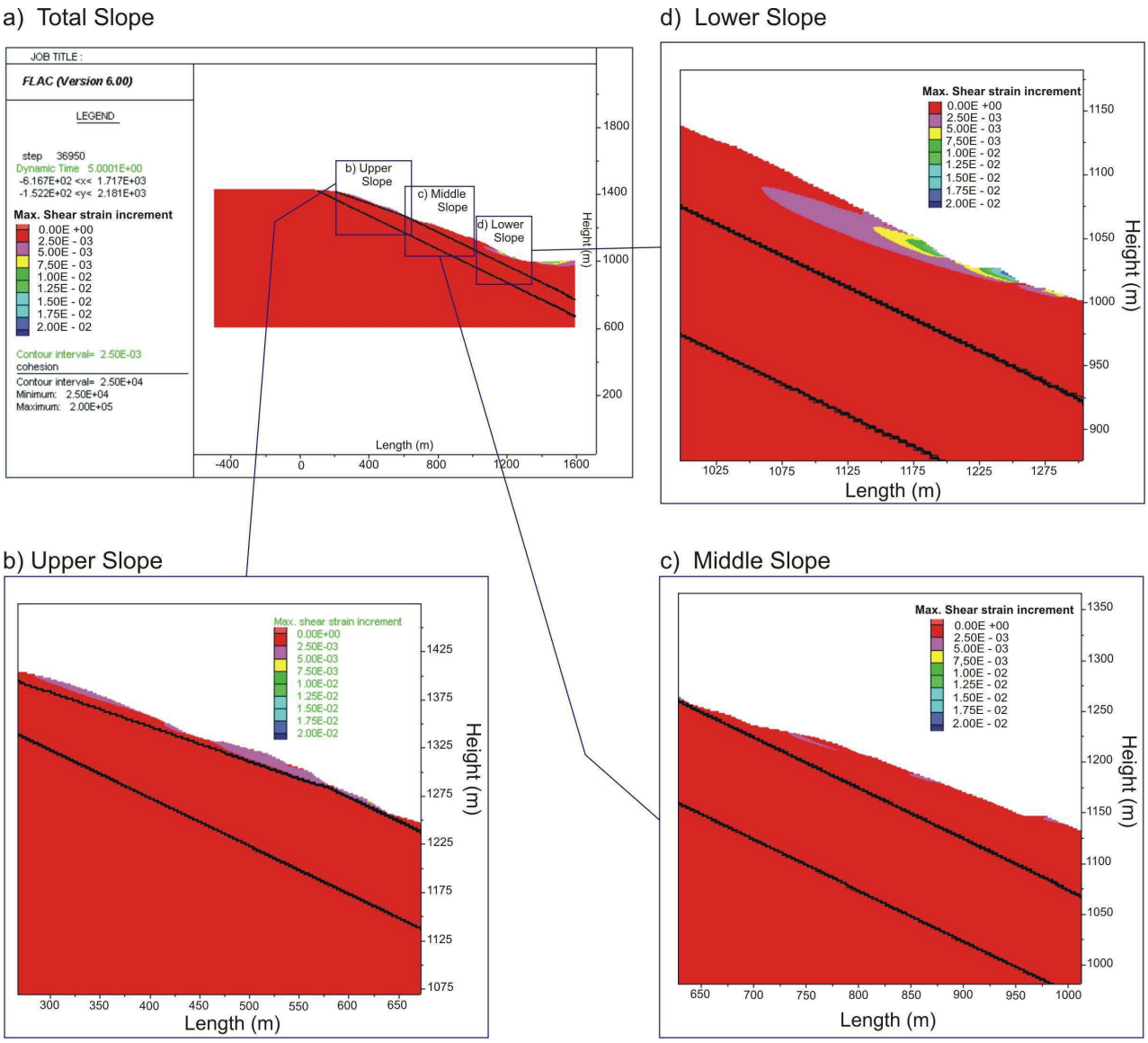

Fig. 8-40: Maximum shear strain increment for a case PGA=0.05. a) The total slope showing three regions, outilined with black boxes, are presented in detail; b) the upper part of slope shown repspresents a loess layer; c) the middle part of a slope is illustrated showing neglible shear strain rates; d) the lower part is illustrated presenting high shear strain rates.

The forth case the Peak Ground Acceleration is ***PGA = 0.1.*** With a PGA=0.1, small shear strain rates are observed on a loess layer, with higher rates between 400 m and 625 m (Fig. 8-41b). The middle part of a slope shows the higher range of shear strains (Fig. 8-41c) and toe of a slope is also susceptible to the highest range of rate (Fig. 8-41d). This case shows that the Palaoegene clay can be susceptible to failure.

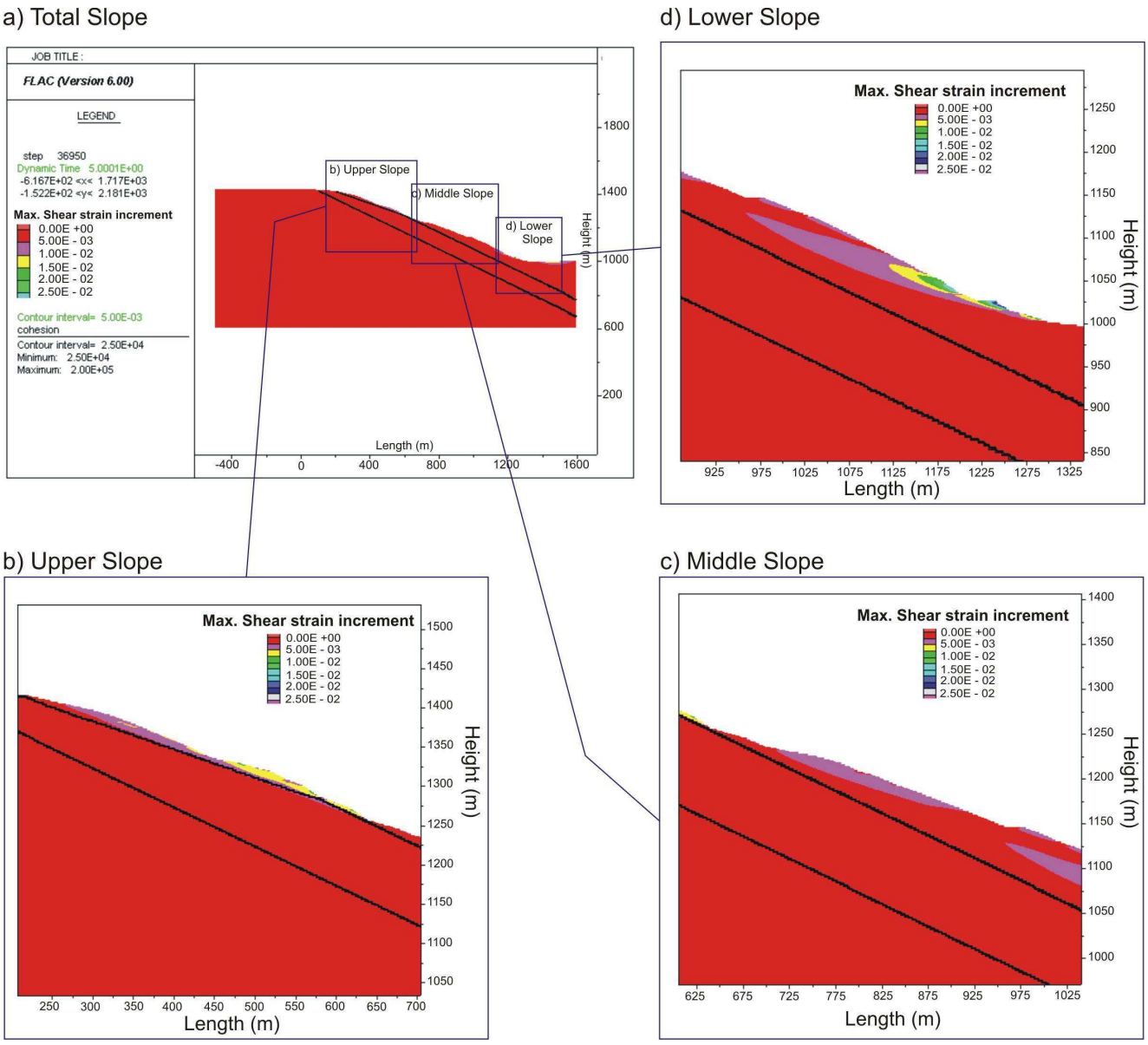

Fig. **8-41**: Maximum shear strain increment for a case PGA=0.1; a) total slope geometry. Three boxes in black show in three regions in a slope for detailed illustration; b) Maximum shear strain increment presented for the upper part of a slope, where loess layer lies; c) the detailed view of a middle view. The shear strain rate developed on the superficial layer Palaeogene clay; d) the toe of a slope is presented with a strong shear strain rate.

For all four cases the maximum displacement is calculated. As it is illustrated in Fig. 8-42, the displacement is increased by increasing PGA.

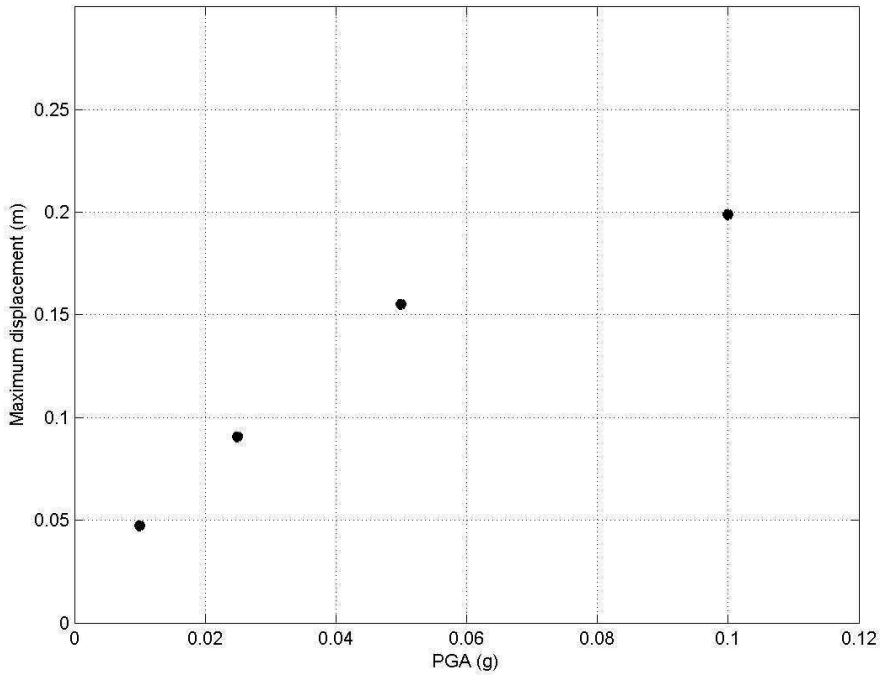

Fig. 8-42: Maximum displacement for each PGA value

8.6.3.8 Conclusion to the Upper Koi-Tash case

The results of the Upper Koi-Tash landslide allow one to say that the thickness of loess can control amplification. By analyzing four values of the PGA in a slope, can be concluded that in two cases (PGA=0.01; PGA=0.02), the shear strain rate developed in a toe of a slope. No significant concentration of a shear strain rate is observed in the middle part of a slope. In the case of PGA=0.05, a smaller shear strain rate is shown in a loess layer that is not observed in the previous two cases. However, some negligible shear strain increment is observed on the middle part of a slope. The last case of PGA=0.1, considered to present the strongest seismic input, presents a relatively larger shear strain rate on superficial layers of the Upper Koi-Tash landslide. In all cases, the toe of slope considered to be most susceptible to failure. All slope models presented a slope case with no water effect. The shear strain rates are negligible, however it can be seen that an increasing PGA can deform the slope and thus the slope becomes unstable.

8.7 Conclusion to chapter

To assess the seismic impact on slope stability, ground motion needs to be taken into consideration. Usually, water can play an important role in causing failure. However, in many cases of research of mass movements, attention has been turned only to water effect on a slope. During this study, the main focus is turned to the behaviour of a slope in seismic conditions.

The first studies concerned the ground motion and site effect analyses in the slope with two different thicknesses of loess layer. The loess layer of about 20 m to 50 m is commonly observed in Central Asian countries. The results of the simulations to assess the site effects showed that in loess thickness of 40 m stronger amplifications are observed than in loess layer with a thickness of 20 m. The case with tension cracks showed that although the thin crack (10 m) has no significant impact on a slope, when the crack is located near the crest, strong amplification is observed. The results of spectral amplifications show a consistency in terms of strong amplification within the loess layer, within results that presented by DANNEELS et al (2008).

The tension cracks are depicted to find deformation within the loess slope in parametrical studies. For this case several variations of tension crack geometries are given. For each case of slope configuration, 27 slope models are created. The results of these studies showed that the loess thickness can control the unstable area in a slope. In a case with loess thickness of 20 m the landslide area is smaller in comparison with a case with loess thickness of 40 m. When the crack is located 20 m from the slope crest, the largest unstable mass is observed. This case can be explained by the following: the first case of tension crack location is 10 m decreasing the slope instability, making it susceptible to deformations, however the loess thickness has a significant role; there is less involved material located from the crest up to tension crack location. The third case of location of tension cracks, 30 m, showed that it has no significant impact on slope instability, because it is located far from the crest.

In both cases the range of the variations is not very broad. In dry conditions, slope behavior is influenced much more by the slope geometry and geology than by characteristics of the tension cracks. It can be said that tension cracks have an impact on slope instability as it can represent a preparatory step where the slope starts to become unstable.

The third study considered is the Upper Koi-Tash landslide. This case needs to be considered as one of the parametrical analyses, rather than a real landslide case. However, the Upper Koi-Tash case is a good example that can be compared with a parametrical case with site effect assessment. The loess thickness is about 10 m to 15 m. The results illustrate that the strong amplification is in a location precisely where the loess lies.

During the numerical analyses, different values of PGA are taken in order to observe the seismic impact on the slope. This case shows the shear strain rate concentrated on the toe of a landslide, in Palaeogene clay. At the contact of Palaeogene limestone and the superficial loess, the shear strain concentration is observed. During field observations in 2003, the failure in contact of bedrock and loess is observed (Internal Reports of Academy of Sciences of Kyrgyzstan, 2004). Some shear strain concentrations are observed in a limestone layer of a slope. In all cases of PGA, it is shown that the toe of a slope is the most susceptible to failure. By increasing PGA the maximum displacement and shear strain rate increases.

CHAPTER 9: Conclusion and recommendations

9.1 Conclusion

Earthquake triggered landslides cause enormous damages to infrastructure and threaten human lives. Usually these seismic types of mass movements take place in the neotectonically sensitive regions. One of such regions is the Tian Shan range, which crosses Central Asian regions that occurred from collision of Pamir-Altai plates. Frequent occurrence of earthquakes in extensive areas of Central and China causes the development of landslides in loess deposits.

Usually earthquake triggered landslides are studied by using of traditional methods as pseudo-static and Newmark methods. Factors like seismic wave distribution within the slope are not included in such methods. Although the seismic wave distribution is one of the important factors within complex topographies. It is observed that strong amplification develops in certain places of topography and can cause deformation of slope together with decrease of slope stability. In this current research the aforementioned traditional methods are not considered. Instead seismic wave distribution within the slope with different local conditions, named site effects, are researched and analysed.

The influence of rainfall on slope stability is already investigated by different projects and research groups all over the world. Apart from intensive rainfall, snow melting or changes in ground-water levels and water level changes along coastlines lead to main water infiltration and thus to slope saturations. However in many currently existing simulations and landslide models, only the infiltration of water and the increase of pore water pressure in the sliding body is analysed and are regarded as main failure processes. Triggering of landslides in loess deposits by precipitation is also investigated in Central Asia and China. Performed research has presented that snow thawing in spring and long lasting rain has more infiltration rate into the loess slope than short heavy rain.

By investigating of loess landslides, researchers observed appearance of cracks on the upper part of the slope. Some research supports the theory of seismic impact on appearance of such cracks. In addition, tension cracks are only regarded as transport or infiltration track into deeper soil layers. Or the water column inside the tension crack is regarded as a further pushing force in slope stability calculations. However, the role of already existed cracks in a slope in dry state is not clear or is underestimated, as this research shows. Thereby the following question arises: Does the presence of tension cracks facilitate the loess slope instability and if yes, how? Placing this issue forwards, the current research is carried out.

Taking into consideration observed and studied cases of loess landslides, a hypothesis of development of failure in loess is presented in the current research. This hypothesis says that from seismic shaking, small tension cracks can develop in loess slope. Further, water

infiltration causes to weaken the loess layer and further seismic shaking to widen the cracks. Climatic factors play a role to cause to erosions and to reduce slope stability. From the hypothesis it is presented that earthquake can have an impact on loess failure. This hypothesis is researched by analysing wave propagation in loess material with numerical simulations.

In this research, it is presented that loess can be affected from the environment and several factors assigned to loess physical and mechanical properties of loess. Soil samples were taken from different loess landslides in the Upper Mailuu-Suu basin of the Kyrgyzstan and were investigated. But some limitations that tackled during the soil sampling are needed to be mentioned. The difficult accessibility of one of the regions around the Kochkor-Ata landslide is one aspect that hampered the soil sampling. The landslide is located in far distances from nearby settlements and roads. Through this, taking samples from three selected locations along the slope was difficult. Due to this issue, it is almost impossible to bring large scale apparatuses to get truly undisturbed samples. Samples that present 'insight' properties obtained manually, waxed and wrapped in a special material. Second limitation is that the structure could be destroyed during transportation to laboratory to Germany. Samples assigned for ring shear tests used remoulded samples.

After transportation to the laboratory, the samples were tested for grain - size analyses, Atterberg limits, water absorption and carbonate content. Strength parameters were obtained by using of direct shear tests, consolidated drained triaxial tests and ring shear tests. The simplest test to get strength parameters of soil specimens is a direct shear test. Loess cohesion ranges from 0.7 to 1.7 kPa and friction angle from 27 to 32° obtained by using of direct shear tests. Triaxial tests have shown the larger cohesion values than direct shear tests, ranging from 27 to 32 kPa with a friction angle of 32°. Remoulded samples were used in ring shear test. Cohesion ranged from 9 to 60 kPa and the friction angle was up to 36°. Soil samples from Upper Koi-Tash were tested in regard to liquefaction potential. According to these tests no liquefaction was observed. This can be interpreted because of the compacted structure of loess. Since triaxial tests presents the natural shear conditions the strength properties of the test were used for slope modelling.

After getting the strength parameters from the samples, the seismic impact on loess slope was assessed by means of the finite difference code named FLAC. Seismic wave distribution was estimated within the loess slope. As described, this research analyses the possible impact of tension cracks and seismic impact, as such research has not yet been done. Due to this parametrical studies were carried out and analysed. Two slope cases were considered for parametrical studies. The slope case with inclination of 30° and loess layer with thickness of 20 m is common in South Kyrgyzstan. The second case of study considered a slope with 15° of angle and loess thickness of 50 m also common in Kyrgyzstan but mainly distributed in Tajikistan.

Topographical and geological site effects were assessed for slope cases and showed that loess thickness has an impact and amplification potential. Different tension crack geometries and site effect variations were studied to see the impact on wave propagation and ground motion. This included cracks with different configurations as location, inclination, length and width. Components of cracks are varied to find out a critical component. This step can be pointed out

as an initial step on tension cracks studies in loess slope. As the studies showed the location is an important criterion, especially when it is located nearby the slope crest. Slope deformation analyses show the thicker the loess the bigger the deformation. The amplification potential is stronger in thick loess layer (in the case of research 50 m) than thin loess layer (20 m). Such amplification potential fluctuating according to loess thicknesses has observed by DANNEELS et al (2008).

Investigations in the current thesis show that the existence of tension cracks in dry conditions can reduce the slope stability, however large displacement doesn't occur. The presence of tension cracks on the slope is regarded to be important, because these cracks play a role as preparatory factor to the slope failure. This is an important point as the existing cracks do not only reduce slope stability even in dry conditions, but also enable water infiltrates into the slope. Through this material strength decreases and thus mass movements can occur.

In summary it can be said that the seismic impact is obvious in loess slope and can develop deformations within the loess slope. The existence of tension cracks can lead to deformations within the slope and thus has an impact on slope stability.

Water should be modelled in slope and inside the tension cracks in order to look at the impact of precipitation in the future research. As described in the hypothesis, water from rain and from snowmelt might play an important role for the development of the landslide and its failure process. As this work concentrates on the seismic impact of ground waves to the slope stability and the occurrence of tension cracks due to seismic activity, the influence of water was neglected. Thus, an implementation of pore water pressure in the slope analyses should be done in future works.

9.2 Recommendations

Since the Mailuu-Suu region is in focus on researchers and stakeholders because of severe ecological problems due to the uranium waste tailings several projects were carried out in the past. One example was the project of the Federal Institute for Geosciences and Natural Resources of Germany (Bundesanstalt für Geowissenschaften und Rohtoffe) in the year 2005 to 2008 that dealt with the reduction of dangers by uranium-mining waste sites in Mailuu-Suu. Especially the distribution of contaminants considering the evaluation of physical and chemical and radiological parameters, together with the risk potential of the different aquifers was evaluated regarding the planned sanitation actions.
Some studies on slope analyses in this region have done by using of literature data, saying the loess is susceptible to liquefaction. The tested loess samples from the Upper Koi-Tash landslide showed no liquefaction, because of the compacted structure of loess. It can be said that the loess has similar properties on liquefaction potential in the Mailuu-Suu basin because of same origin of occurrences of loess. Thus, detailed analyses and field studies are necessary.

Due to hard accessibility of areas of Central Asia, many researches deal by means of Geographic Information Systems (GIS). This tool is convenient since it covers large regions and is a quick way to study landslides. But these researches in most cases ignore tension cracks in various types of mapping as inventory, susceptibility, hazard and risk mapping.

Results of this research presented that tension cracks have an impact to reduce slope stability, as an important preparatory factor to slope instability, and it is necessary to be taken into account especially when doing landslide risk analyses and assessment in loess landslides in Kyrgyzstan.

As described in CHAPTER 1 (Introduction) the general Risk Management framework consists of the three elements Risk Identification, Risk Assessment and Risk Treatment. In the context of loess landslides, the knowledge and identification of composition of material, thickness within a slope and also topographic and geomorphologic parameters are essential. Furthermore, this research showed that also the identification of tension cracks, its existence and distribution are important parameters in earthquake-endangered areas as they influence the slope deformation and should be implemented in this first step of Risk Identification. Detailed field survey and mapping are important in the context of earthquake triggered loess landslides. Thus, as this work showed, information also of distances of tension cracks from the slope edge should be recorded in the field.

Furthermore the obtained results of this work can contribute to the Risk Assessment process of the second step of the Risk Management Framework. Any landslide risk assessment must begin with the collection of information on where landslides are located. This is the goal of landslide mapping. A landslide inventory is the simplest form of a landslide map (GUZETTI, 2003). To determine where protective measures are necessary, scientists and technicians produce landslide inventory and risk assessment maps for many areas around the world. Landslides unfortunately, do not display a clear relationship between magnitude and frequency as do earthquakes and floods. Landslide studies are challenging to scientists, due to the difficulty to represent landslide hazards in quantitative terms over large areas. Interests in determining parameters are the type of movement that has occurred, the degree of present activity of the landslide, and the depth to which movement has occurred.

For landslide analyses and the determination of different maps, as susceptibility mapping or hazard mapping, different so called parameter maps are overlaid and combined with each other (Fig. 9.1). Several methods exist for calculating weightening factors and thus to determine the importance of each factor or the combination of parameters. Most are based on the relationship between the landslide density per parameter class with the landslide density over the entire area (SOETERS et al., 1996). Various parameter maps can be combined into a map of homogenous units, which is then combined with a landslide map.

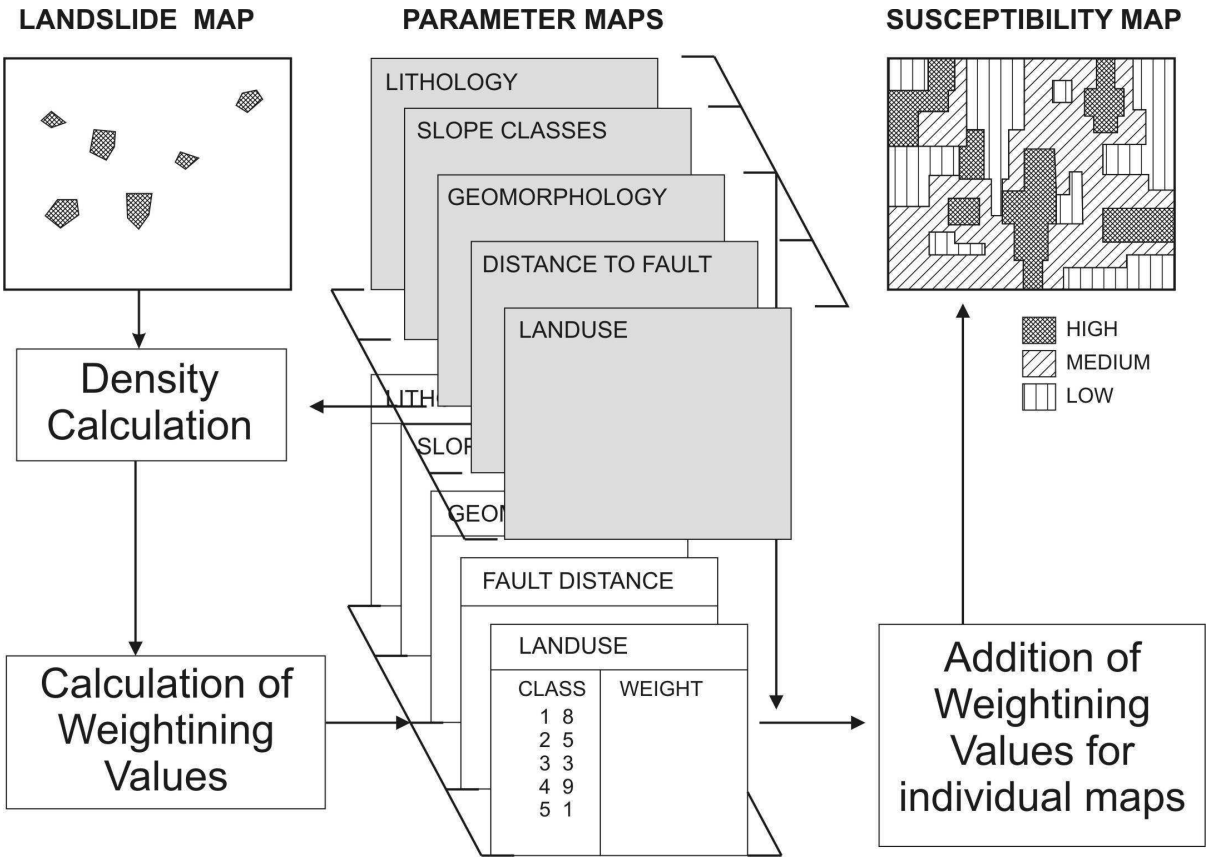

Fig. 9.1: Creation of a susceptibility map by combining different parameter maps (SOETERS et al., 1996)

GIS is a very suitable method to do such map overlaying and combination. A Geographical Information System is ideal for this stage in a landslide investigation because it is capable of handling large amounts of past, present and future data and integrating this data with predictions. Most landslide potential models determine terrain instability by combining slope maps with soils data, then selecting from the resultant soil/slope categories the combinations that are rated for severe erosion potential. Vegetative cover considerations extend the model. When available, maps showing historic landslide sites are added for both establishing and testing landslide potential. As already described, in regions like Kyrgyzstan, main landslide triggering factors are especially earthquakes. As shown in this thesis, parameters about tension crack and thickness of loess have an important influence on earthquake influenced slope stabilities. Thus, tension crack parameter maps should be included in landslide analyze mapping processes (Fig. 9.2). The loess thickness should be included into a lithology map.

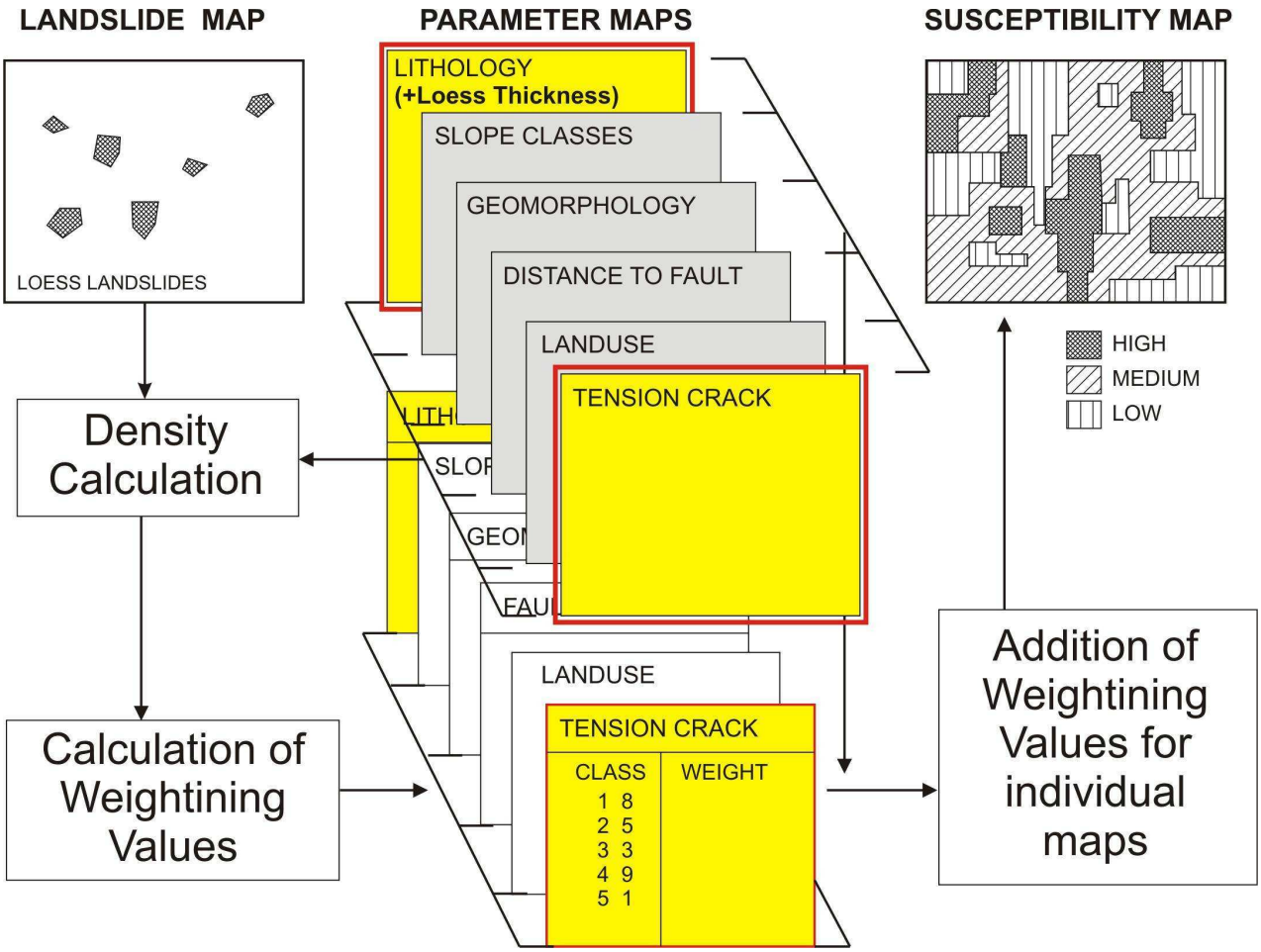

Fig.9.2: Creation of a susceptibility map by combining different parameter maps, including also information about tension cracks and loess thickness in a lithology map

Furthermore, the results of this work can be used for Landslide Hazard Analyze mapping. Landslide hazard maps typically aim to predict where failures are likely to occur without any clear indication of when they are likely to occur. They are useful for providing landslide hazard information needed for planning and protection purposes. The research deals exactly with the aim to analyse components in loess areas that effect slope stability under the influence of ground-motion. The information from the research gives indications of more endangered or areas more prone to landslide movement, and therefore should be implemented in landslide hazard analyses. Landslide hazard (i.e. the probability of a potentially damaging landslide occurring in a unit of time) can be assessed by combining landslide susceptibility with the frequency and magnitude characteristics of landslide types that can cause damage to elements at risk in the area of interest (LEE and JONES, 2004). Thus, landslide hazard can be defined as the probability of occurrence of a landslide event of a given size and can be estimated as the product of susceptibility, frequency and magnitude (LEE and JONES, 2004):

Hazard (H) = Susceptibility (S) x Frequency (F) x Magnitude (M)

Anyhow, the absence of reliable data on landslide frequency and magnitude is often a limitation in landslide hazard assessment (FOURNIADIS, 2007) and thus implicit assumptions have to be made.

One method for landslide hazard analyses is hazard mapping by using multivariate statistical analyses. Thereby, a list of factors or parameters is setup, resulting from different parameter maps. In this list, also factors like distance of tension crack from slope edge, or if possible, information about loess thickness can be included (Fig. 9.3). Parameter maps and land-unit maps can be combined and lead to the creation of a large combination matrix. This matrix is than analysed by using different statistical methods, as multiple regression or discriminant analysis (SOETERS et al.,1996). One possibility is the usage of GIS-tools. Through this, frequency distributions of stable and unstable classified units is possible and thus allows the development of a hazard map, which shows how vulnerable or affected a specific terrain unit is by landslide processes.

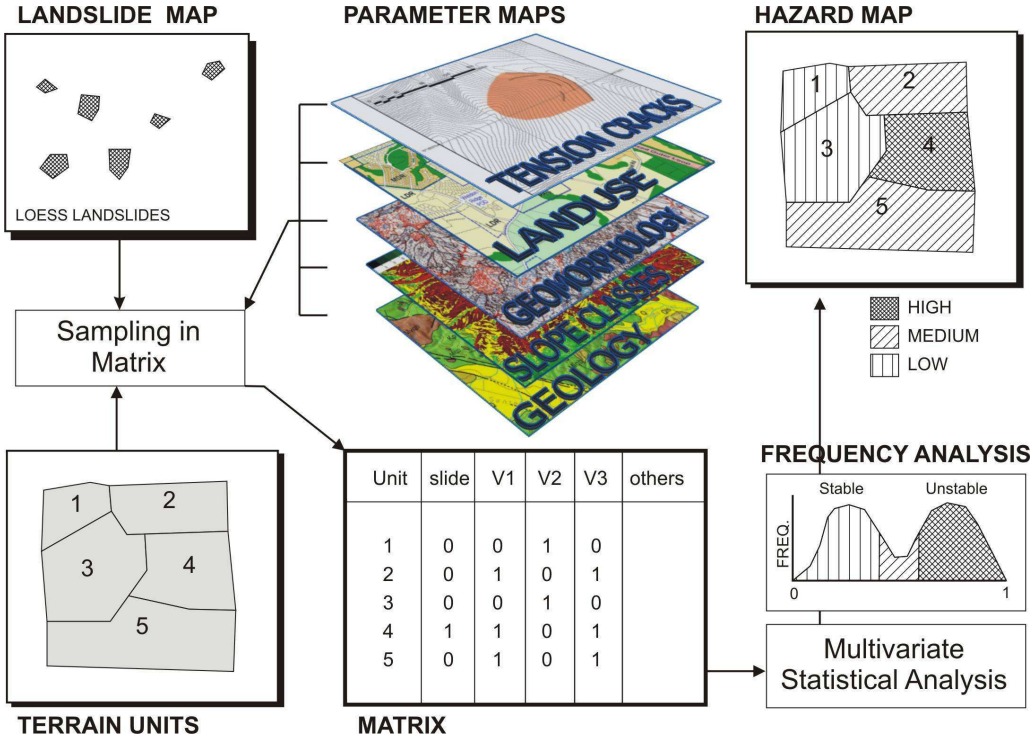

Fig. 9.3: Hazard analyze mapping by integrating of tension crack distribution and parameters.

In addition, the results of this work can be used for monitoring and early warning processes.
In general early warning is understood as advance warning of natural/technological hazards occurrences. In recent years, early warning systems developed to become one of the main pillars of disaster prevention in natural hazards, especially where mitigation strategies are not realizable and thus represent one option to face the danger from landslides.
The four main elements of an early warning system in general are Risk Knowledge, Monitoring & Warning Service, Dissemination & Communication, Response Capability (Fig. 9.4). This chain describes the whole process from risk analyses over the selection of a suitable measuring and monitoring system to detect a specific phenomenon / process, the data analyses and warning tool, the forwarding and understanding of warning messages up to the warning response and reaction according to specific alarm or emergency plans.

Fig. 9.4: Structure of a People-centered Early Warning System (EWC III, 2006)

As already described for the Risk management framework, the identification of a risk and its specific parameters is an important requirement. This definitions and analyses are done in the first element of the early warning chain, the risk knowledge. Concerning landslide, to know the slope stability influencing parameters are a precursor for setting up a functioning early warning system. To detect and classify the landslide, it is important to view the size and contrast of the landslide features and the morphological expression of the topography within and around the landslide. Interests in determining parameters are the type of movement that has occurred, the degree of present activity of the landslide, and the depth to which movement has occurred. Furthermore, in earthquake influenced areas like Kyrgyzstan, the stability of loess slopes is also affected by the loess composition and thickness but also the existence of tension cracks. As this work showed, these parameters also influence slope deformation and thus slope stability. Therefore, these parameters should be included in the Risk Knowledge element of the early warning system.

Monitoring of the landslide activity is the second element of an early warning System. Monitoring is the surveillance of engineering structures either visually or with the aid of instruments (BROWN, 1993). In general monitoring can be regarded as the systematic recording, observing and investigation of activities taking place in a certain structure by means of technical aids or other watching methods. It is a process of routinely gathering information on all aspects of the object (MOORE, 1992). In regard to landslide activity the process if monitoring helps to gather information about landslide activity and thus allows on one side the analyse of possible failure mechanism for further predictions, but on the other side as part of an Early Warning System to provide information about dangerous events and

motions. Monitoring landslide movement involves the comparison of landslide conditions over time, including the aerial extent of the landslide, the speed of movement, and the change in the surface topography. Remote sensing techniques greatly aid in the investigations of landslides, on both a local and regional scale. Remote sensing offers an additional tool from which we can extract information about landslide causes and occurrences. Most importantly, they greatly aid in the prediction of future landslide occurrences, which is very important to those who reside in areas surrounded by unstable slopes. Here, satellite imagery and aerial photography are commonly used in this stage of a landslide investigation. The observation and development of tension cracks is a further important element, as this research work showed. Thereby the comparison of tension crack development and distribution over the time is an important element. The distance from tension crack to the slope edge may change and thus has another impact on wave propagation of earthquake shaking.

New tension cracks may occur, what changes the geometry of the sliding body and thus has also influence on the slope stability. Furthermore, the appearance of new or the widening of old tension cracks is a direct indicator of high activity and movement processes in the landslide area. Instruments especially for the monitoring of tension crack development are on one side remote sensing technologies, as satellite or airborne images. On-site instruments for monitoring of such structures are extensometers or precise crackmeters / fissurometers (Fig. 9.5). Thus the existence of tension cracks and the monitoring of such components can be integrated in the early warning process and has influence on the choice of the measuring instruments. In Mailuu-Suu (Kyrgyzstan) near the Upper Koi-Tash landslide different extensometers were installed at the landslide “Tectonic”. The most of them are not functional any more due to destruction caused by the landslide movement itself.

Fig. 9-5: A fissurometer and a surface-extensometer in action, Traben Trarbach (Germany) (KRAUTER et al. 2004)

In Summary it can be said, that the achieved results of this research work can be used for landslide risk assessment and risk analyses especially in earthquake influenced regions like Central Asia. Especially information about the existence of tension cracks, distribution and properties should be attached more importance as these structures influence wave propagation and thus slope deformations in landslide areas. Information about tension cracks could be mapped and analyzed with other parameter maps, as lithology or geomorphology to get

improved information about landslide vulnerability and susceptibility. All this helps to optimize the risk management process that describes a systematic approach and practice to manage uncertainties to minimize the potential harm and loss (risk mitigation strategy). Through this social and economic losses due to landslides can be reduced by means of effective planning and management.

Appendix 1

Physical and mechanical properties of loess (overview from literature)

Physical and mechanical properties of loess from literature

Literature	Place	place	depth, m	void ratio	water content,%	Plastic limit, %	Liquid limit, %	Plasticity index, %	wet density, g/cm^3	dry density, g/cm^3	degree of saturation	unit weight, kN/m^3	cohesion, kPa	friction angle,°	clay	silt	sand	coeffcient of compress	Compression modu	specific gravity	Type	porosity
CHINA																						
1.Zhang, Z., Wang, L.(1995)	Huihui Chuan landslide, Xiji district			1,038	18,98	21,4	31,1					13,965	44,1	17,2							static triaxial test	
2. Zhao, C., Yang,Z et al (2005)	Qilihe district of Lanzhou city, China				13,03			10	1,42	1,26	30,44				13	72	15			2,71		
3.Zhang,D., Wang,G., et al(2007)	Gaolou village (about 120 km from Xian city)			1,2-1,3											6	92	2			2,73		
4. Wang, L., He,K et al (2002)	Lijiagou village, Gansu province			1,101	9-10	15,7		9,2				14,6-15,0			14	67,7	18,3					
5. Gao,X., Wang J., Zhu,X (2007)			8.5	1,04	8.6	16.9	26.4	9.5														
			17.7	1,031	10.0	17.5	28.2	10.7														
			19.2	0,961	9.3	18.0	28.2	10.2														
			21.7	0,936	12.1	18.1	30.8	12.7														
			23.2	0,939	12.4	18.4	29.0	10.5														
			26.2	0,858	16.7	18.0	30.5	12.5														
			27.5-30.1	0,724	14.8	17.1	27.3	10.2														
			37.4-42.9	0,719	20.1	17.3	27.7	10.2														
			41.8-47.9	0,715	17.5	18.8	28.1	9.4														
6. Xia.J. et al (2009) Engineering Geology	Yanziji in Nanjing, Chin	Palaesol		0,8	26,4			16,3					32,3	14,8				0,24	7,5	2,72		
		Loess		0,69	24			14,1					46,9	15,6				0,19	8,8	2,73		
7. Xia.J. (2005) Engineering geology 78	ancient gravel stratum	Sand 1		0,59	14,7							19,3	51	33								
		Clay 1		0,786	27,5			18,2				19,6	49	3				0,31	6			
		Clay 2		0,758	27			19				19,8	80	12				0,21	10,1			
		Clay 3		0,596	21,7			10,9				20,06	44,9	11,8				0,24	6,6			
8. Ying.J. Liao.H. Yin J. Unsaturated soil, seepage	Baoto district Yanan Shi	ndisturbed loess		0,848	23,57	18,4	30,2	11,8	2,72												direct shear tests	
9. Xia, J. et al (2006) Engineering Geology	Nanjing, China	Flood plain																				
		Upper		0,92	35,2	21,3	36,9	15,6				18,4	22,9	11,6				0,56	3,56		Quick shear test	
		middle		1,16	41,3	22,1	38,6	16,5				17,9	11,7	5,6				0,8	2,7			
		Lower		1,04	35,4	21,6	35,9	14,3				18,2	16,4	7,2				0,59	3,45			
		Riverbed sidebar																				
		Upper		0,98	33,9	20,6	33	12,4				18,4	23,6	10,1				0,51	3,88			
		Lower		0,95	32,3	20,5	32,5	12				18,5	26,2	10,8				0,43	4,53			
																					consolidated quick shear test	
													18	14,5								
													10	12,2								
													15,6	14,7								
													32,2	16,5								
													23,2	14,3								
																					Triaxial test (saturated sample)	
													25	8,5								
													15,6	6,5								
													18,1	7,9								
													11,5	11,7								
													14,3	12,3								
10. Derbyshire et al .(book) (2000)	Malan				5,2-20,6					1,38-1,44			0,6-0,10	33,3-24,8								
	Lishi				5,5-21,0					1,52-1,67			0,80-1,50	31,4-26,5								
	Wucheng				7,0-22,6					1,64-1,81			0,90-2,10	34,9-27,3								
	Neogene argillite				16,4-22,3					1,67-1,97			2,30-2,60	22,9-12,5								

SOUTH AMERICA

11. Franco, M.F. (2007)	Pampas area , Argentina				10,8	5,6	23,5															
					21,3	3,5	24,6															
					11,6	3,6	22,1															
					19,9	4,8	21,8															

USA

12. Higgins (1985)	Iowa loess, USA				19,5					1,37			0,5	28						2,74	triaxial CU	
													21,5	26,9							IBST	
13. Sariosseiri,F., et al. Engineering geology 104 (	soil samples from Wast	Aberdeen			27	42,8	54,2	11,4				14,3								2,75		
		Everett			9,7	29,3	32,5	3,2				18,7								2,7		
		Palouse			17	19,6	33,1	13,6				17,3								2,73		
14. Parsons et al (2005)	Iowa				4-31	17-29	24-53	3-34					0-55, 2-12	28-31, 24-25	12-42	56-85	0-27			2.58-2.72	CU triaxial test, CD direct shear	
	Nebraska					17-28	24-52	1-24					0-460	31-36	11-49	30-71	0-41			2.57-2.69	UU triaxial test	
	Tennessee				12-25	23-26	27-39	1-15							4-30	68-94	1-12			2.65-2.70		
	Mississippi				19-38	17-29	23-43	2-20					14-69,21-55, 0	0-28, 26, 32-33	0-25	75-85	0-8			2.66-2.73	UU triaxial test, CU triaxial test, Direct sh	
	Illinois					18-22	39-58	17-37							35-49	48-54	1-4					
	Alaska				11-49	19-26	22-32	8							3-20	65-93	2-21			2.57-2.79		

CENTRAL ASIA

15. Kojobaev, K.A. (1989)	Tajikistan				23-34		26-28	7-8	1,98-2,00	1,40-161			4-10	20-26	20						
	Kirgisistan				9-24		24-33	8-12	1,35-1,95	1,20-1,58											
16. Kriger, N.I. (1986)	Karaungur region, South Kirgisistan		1	15					1,71	1,5			64	26							
			3	37					1,95	1,73			53	28							
			5	28					1,97	1,73			58	28							
			7	37					2,01	1,71			60	24							
			9	36					2,07	1,76			64	23							
17. Niayzov (1981) Report	Urtaboz, Tajikistan	II- 11	1		11				1,4	1,26			16,6	25					2,69	direct shear	53
			2		14				1,52	1,33			12,7	25					2,68		50
			3		13				1,33	1,18			16,6	24					2,69		56
			4		13				1,36	1,2			15,6	26					2,69		55
			5		15				1,47	1,3			16,6	26					2,68		51
			6		14				1,49	1,3			17,6	26					2,69		51
			8		14				1,45	1,27			17,6	27					2,69		52
			10		22				1,65	1,37			13,7	26					2,68		48
		III - 12	1		18				1,65	1,4			16,6	25					2,69		48
			2		17				1,55	1,32			21,5	23					2,69		51
			3		19				1,55	1,3			15,6	25					2,69		51
			4		24				1,66	1,33			17,6	26					2,68		50
			5		20				1,52	1,26			17,6	24					2,69		53
			6		23				1,6	1,3			15,6	27					2,69		51
			8		22				1,51	1,27			13,7	26					2,68		52
			10		25				1,67	1,32			15,6	27					2,68		50
	Okkuli - Bolo	p-1	1,5		4,6			8,4	1,41	1,35			14,4	28					2,68		49,6
			3		5,3			6,8	1.39-1.43	1.32-1.36			17	27					2,67		50,6
			4		5,4			7,1	1.33-1.40	1.27-1.33			18,7	24					2,57		50,2
			5		5,5			5,6	1,33	1,26			16,7	24					2,68		53
			7		7			6,2	1,37	1,28			11,4	25					2,69		52,4
			10		6,4			7,2	1,42	1,38			19,6	20					2,69		50,5
		p-3	4		18,9			7,1	1,49	1,31			21,2	24-30					2,68		51,1
			6		19,5			6,7	1.62-1.70	1.36-1.42			18,8	25					2,68		47
			3		23			8,2	2,02				7,3	33					2,68		
		III-I	1		20,2			8,9	1,57	1,3			45,6	26,5					2,69		51,3
			2		22,8			8,3	1,66	1,35			42,5	27					2,69		49,8
			3		17,8			8,1	1,6	1,35			51,8	24					2,69		49,8
			4		21,3			5,7	1,72	1,42			44,2	27					2,68		49,8
			5		18,2			6,7	1,67	1,41			43,9	26					2,69		47
		P-1	3		18,6																
			4		18,7																
			5		19,3																
			6		18,2																
		P-4	1,1		17,3				1,58	1,35											
			2,2		17,9				1,56	1,32									2,68		
			3		15,7				1,5	1,3											
			4		18,5				1,6	1,35											
			5		21,6				1.69-1.63	1.30-1.34									2,68		

Appendix 2

MSK Intensity Scale (Source: AGARWAL, SHRIKHANDE, 2006)

Intensity	Description
I	Not noticeable
II	Scarcely noticeable (very slight)
III	Weak, partially observed only
IV	Largely observed
V	Awakening
VI	Frightening
VII	Damage of buildings
VIII	Destruction of buildings
IX	General damage to buildings
X	General destruction of buildings
XI	Destruction
XII	Landscape changes

References

Abdrakhmatov, K., Havenith, H.B., Delvaux, D., Jongmans, D. and Trefois P. (2003): Probabilistic PGA and arias intensity maps of Kyrgyzstan (Central Asia). *Journal of Seismology* 7, pp. 203-220.

Agarwal, P., Shrikhande, M. (2006): Earthquake resistant design of structures. New Deli, 634 pages.

Aki, K. (1993): Local site effects on weak and strong ground motion. Tectonophysics, 218, pp. 93-111.

Aleshyn, Y. G., Torgoev, I. A. and Schmidt G. (2002): Environmental risk management at uranium tailings ponds in Mailuu-Suu, Kyrgyzstan. *In*: Merkel B. J., Planer F. B. and Wolkersdorfer C. (eds.) Uranium in the aquatic environment. Berlin, Springer-Verlag, pp. 881-888.

Assalay, A.M., Rogers, C.D.F., Smalley, I.J. (1997): Formation and collapse of metastable particle packings and open structures in loess deposits. Engineering Geology, 448, pp. 101-115

Assallay, A.M., Rogers, C.D.F. and Smalley, I.J. (1996): Engineering properties of loess in Libya. Journal of Arid Environments, 32, pp. 373-386

Bandyopadhyay, S. S. (1983): Geotechnical evaluation of loessial soils in Kansas. Transportation Research Record 945, Journal of the Transportation Research Board. Washington D.C, pp. 29-36.

Bard, P.Y. (1982): Diffracted waves and displacement field over two-dimensional elevated topographies. Geophys.J.R.astr.Socity, 71, pp. 731-760

Bard, P.-Y. and Bouchon, M. (1980a): The seismic response of sediment-filled valleys. Part 1. The case of incident SH waves. Bull. Seis. Soc. Am., 70, pp. 1263-1286.

Berg, L.S. (1947): Climate and Life. 2nd edition. Moscow, Geographgiz, 356 p. (in Russian)

Borcherdt, R.D. (1970): Effects of local geology on ground motion near San Francisco Bay. Bull. Seis. Soc. Am., 60, pp. 29-61.

Bossu, R. and Grasso, J.R. (1996): Stress analysis in the intraplate area of Gazli, Uzbekistan, from different sets of earthquake focal mechanics. J. Geoph. Res., 101, pp. 645-659.

Brown, E.T. (1993): Geotechnical Monitoring in surface and underground mining – An overview. – Proc. Geotechnical Instrumentation and Monitoring in open Pit and Underbround Mining, Szwedzicki Balkema, Rotterdam, pp. 3 – 11.

Buslov, M. M., De Grave, J., Bataleva, E. A. V. and Batalev V. Y. (2007) : Cenozoic tectonic and geodynamic evolution of the Kyrgyz Tien Shan mountains: a review of geological, thermochronological and geophysical data. Journal of Asian earth sciences 29, pp. 205-214.

Close, U., and McCormick, E. (1922): Where the mountains walked. An account of the recent earthquake in Gansu Province, China, which destroyed 100,000 lives. National Geographic Magazine, (XLI95), pp. 445-464.

Cho, I., Tsurugi, M., Iwata, T., Kagawa, T., Zhao, B. (2004): Modelling of the spectral amplification characteristics at the strong motion observation sites in the Osaka basin, Japan. 13th World Conference on earthquake Engineering. Vancouver, B.C., Canada. Paper No.825.

Cruden, D.M., Varnes, D. J. (1996): Landslide types and processes. In: Turner A.K.; Shuster R.L. (eds) Landslides: Investigation and Mitigation. Transp. Res. Board, Spec. Rep. 247, pp 36–75.

Dai, F.C., Lee, C.F., Ngai,Y.Y. (2002): Landslide risk assessment and management : an overview. Engineering Geology, 64, pp. 65-87.

Danneels G. (2004). Landslide susceptibility assessment in the Maily-Say valley (Kyrgyzstan) by means of remote sensing techniques. Travail de fin d'études, Université de Liège, Liège, non publié, 111 p.

Danneels, G., Bourdeau, C., Torgoev, I. and Havenith, H.B. (2008): Geophysical investigation and numerical modelling of unstable slopes: case-study of Kainama (Kyrgyzstan). Geophysical Journal International, 175, pp. 17-34.

De Marneffe, C. (2010): Cartographie et modélisation 3D de la géologie de la vallée de Mailuu-Suu, Tien Shan. Mémoire en vue de l'obtention du grade de Master en sciences géologiques. Universite de Liege, 126 p.

Delvaux, D., Abrakhmatov, K.E. and Strom, A.L. (2001). Landslides and surface breaks of the 1911 Ms 8.2 Kemin earthquake, Kyrgyzstan. Russian Geology and Geophysics, 42, pp. 1167-1177.

Derbyshire, E. (2001): Geological hazards in loess terrain, with particular reference to the loess regions of China. Earth -Science Reviews, 54, pp. 231-260.

Derbyshire, E., Meng, X.M., Dijkstra, T.A. (2000): Landslides in the thick terrain of North-West China. Chichester: John Wiley

Derbyshire, E., Van Asch, T., Billard, A., Meng, X.M. (1995): Modelling the erosional susceptibility of landslide catchments in thick loess: Chinese variations on a theme by Jan de Ploey. Catena, 25, pp. 315-331.

Derbyshire, E., Dijkstra, T.A., Smalley I.G., Li Y., (1994): Failure mechanisms in loess and the effects of moisture content changes on remoulded strength. Quaternary International, Vol. 24, pp. 5-15.

Derbyshire, E. (1983b): Origin and characteristics of some Chinese loess at two locations in China. Eolian Sediments and Processes (eds. Brookfield, M.E. and Ahlbrandt, T.S.), Elsevier, Amsterdam, pp. 69-90.

Dijkstra, T.A. (2001): Geotechnical thresholds in the Lanzhou loess of China. Quaternary International 76/77, pp. 21-28.

Dijkstra, T.A. (2000): Loess slope instability in the Lanzhou region, China. PhD thesis, University of Utrecht, The Netherlands, p. 301

Dijkstra, T.A., Smalley, I.J., Rogers, C.D.F. (1995): Particle packing in loess deposits and the problem of structure collapse and hydroconsolidation. Engineering Geology, 40, pp. 49-64.

Dijkstra, T.A., Rogers, C.D.F., Smalley, I.J., Derbyshire, E., Jin, L.Y., Meng, X.M. (1994): The loess of north – central China: Geotechnical properties and their relation to slope stability. Engineering Geology, 36, pp. 153-171.

Evans. S.G., Roberts, N., Ischuk, A., Delaney, K., Morozova, G., Tutubalina, O. (2009): Landslides triggered by the 1949 Khait earthquake, Tajikistan, and associated loss of life. Engineering Geology, 109, pp. 195-212.

Faccioli, E. (2000): The importance of earthquake site effects from an engineering point of view. In Proc. Journée d'étude de la Société Suisse du Génie Parasismique et de la dynamique des structures (SGEB) "Prévention sismique en Suisse", pp. 1-11.

Feda, J. (1982): Mechanics of particulate materials. Developments in geotechnical Engineering, 30, Elsevier, Amsterdam, 447 pp.

Feda, J. (1988): Collapse of loess upon wetting. Engineering Geology, 25, pp. 263-269.

Fodor, P. and Kleb, B. (1994): Engineering geological problems in loess regions of Hungary. Quaternary International, Vol.24, pp. 25-30.

Fourniadis, I. G., Liu, J.G., Mason, P. J. (2007): Regional assessment of landslide impact in the Three Gorges area, China, using ASTER data: Wushan-Zigui. – In: Landslides, 4, pp. 267 – 278.

Franco, M.F. (2007): Evaluating the constrained modulus and collapsibility of loess from standard penetration test. Technical Notes. International Journal of Geomechanics, pp. 307-310.

Fukuoka, H., Wang, G., Sassa, K., Wang, F., Matsumoto, T. (2004): Earthquake -induced rapid long traveling flow phenomena: May 2003 Tsukidate landslide in Japan. Landslides, 1, pp. 151-155.

Fukuoka, H., Sassa, K., Wang, G. (2007): Influence of shear speed and normal stress on the shear behavior and shear zone structure of granular materials in naturally drained ring shear tests. Landslides, 4, pp. 63-74

Gao, X-J., Wang, J.-Ch., Zhu, X.-R. (2007): Static load test and load transfer mechanism study of squeezed branch and plate pile in collapsible loess foundation. Journal of Zheijang Univ. Sci. A 2007 8(7), pp. 1110-1117.

Gibbs, H.J. and Bara, J.P. (1962): Predicting surface subsidence from basic soil tests. A.S.T.M. Spec. Tech. Pub., 322, pp. 231--246.

Gibbs, H., Holland, W. (1960): Petrographic and Engineering Properties of Loess. Engineering Monograph, Number 28. U.S. Bureau of Reclamation

Guzzetti, F. (2003): Landslide Hazard Assessment and Risk Evaluation: Limits and Prospectives. Proceedings of the 4th EGS Plinius Conference, Mallorca, Spain.

Hartzell, S., Leeds, A., Frankel, A., and Michael, J. (1996): Site response for urban Los Angeles using aftershocks of the Northridge earthquake. Bulletin of the Seismological Society of America, 86, pp. 168-192.

Havenith, H.B., Bourdeau, C. (2010): Earthquake – induced landslide hazards in mountain regions: a review of case histories from Central Asia. An Inaugural lecture to the society, Geologica Belgica, 13/3, pp. 135-150

Havenith, H. B., Strom, A., Caceres, F. and Pirard, E. (2006a): Analysis of landslide susceptibility in the Suusamyr region, Tien Shan: statistical and geotechnical approach. Landslides 3, pp. 39-50.

Havenith, H. B., Torgoev, I., Meleshko, A., Alioshin, Y., Torgoev, A. and Danneels G. (2006b): Landslides in the Mailuu-Suu valley, Kyrgyzstan - Hazards and impacts. Landslides 3, pp. 137-147.

Havenith, H. B. (2002): Landslides triggered by earthquakes: experimental studies in the Tien Shan mountains (Central Asia) and dynamic modelling. Liège, University of Liège, PhD thesis in applied sciences, 239p, unpublished.

Havenith, H.B., Jongmans, D., Faccioli, E., Abdrakhmatov, K. and Bard, P.- Y. (2002): Site effects analysis around the seismically induced Ananevo rockslide,Kyrgyzstan. Bulletin of the Seismological Society of America, 92, pp. 3190-3209.

Havenith, H. B., Jongmans, D., Abdrakhmatov, K., Trefois, P., Delvaux, D. and Torgoev, I. A. (2000) : Geophysical investigations of seismically induced surface effects: case study of a landslide in the Suusamyr valley, Kyrgyzstan. Surveys in geophysics 21, pp. 349-369.

Head, K.H. (1982): Manual of soil laboratory testing. Vol. 2, Permeability, Shear Strength and Compressibility Tests. Pentech Press, London.

Higgins, J.D., Modeer, V.A. (1996): Landslides: Investigation and mitigation. Chapter 23, pp.585-606.

Higgins, J.D., Fragaszy, R.J. and Beard, L.D. (1989): Engineering geology of loess in Southeastern Washington. Engineering Geology in Washington, Bulletin 78, Washington Division of Geology and Earth Resources, Olympia, Vol.2, pp.887-898

Higgins, J.D., Fragaszy, R.J. and Beard, J.D. (1985): Development of guidelines for cuts in loess soils (Phase 1). Report WA-RD69.1, Washington State Department of Transportation, Olympia, 90 pp.

Holtz, W.G. and Gibbs, H.J. (1951): Consolidation and related properties of loessial soils, Amer.Soc.Testing Mater., Spec.Tech.Pub.126, pp. 9-33.

Hwang, H., Wang, L., Yuan, Z. (2000): Comparison of liquefaction potential of loess in Lanzhou, China and Memphis, USA. Soil dynamics and earthquake engineering 20, pp. 389-395.

Ignatiev, I.V. (1886). Earthquake in the Tokmak district in 1885. In Proc. of the Imperial Russian Geographic Society, 22, issue 2, pp. 150-164. (in Russian)

Internal reports of Ministry Of Emergency of Kyrgyz Republic. 2009.

Internal reports of Institute of physics and rock mechanics. National Academy Sciences in Kyrgyz Republic. 2003. (in Russian)

Ishihara, K., Okusa, S., Oyagi, N., Ischuk, A. (1990): Liquefaction -induced flow slide in the collapsible loess deposit in soviet Tajik. Soils and Foundations, Vol.30, No.4, pp. 73-89.
Itasca. 2000: FLAC 6.0 Manuals. – Minnesota. ITASCA Consulting Group, Inc.

Jibson, R. W. (1993): Predicting earthquake-induced landslide displacements using Newmark's sliding block analysis. *Trans. Res. Rec.* 1411, pp. 9-17.

Kane, H. (1968): A mechanistic explanation of the physical properties of undisturbed loess. Report. Research Project HR-126. Iowa State Highway Commission.

Keefer, D.K. (1984a): Landslides caused by earthquakes. Bull. Geol. Soc. Am., 95, pp. 406-421.

Kojobaev, K.A. (1989): Characteristics of loess in Kyrgyz Republic, Journal of Natural Sciences, pp. 105-114. (in Russian)

Krauter, E., Feuerbach, J., Lauterbach, M. (2004): Risikoabschätzung von Hangbewegungen und Schutzkonzepte.- In.: 10. Internationales Symposium Interpraevent 2004, Riva del Garda / Trient.

Kriger, N.I. (1986): Loess - origin of hydrocompaction properties. Moscow: Izdatelstvo Nauka, 132 pp. (in Russian)

Kriger, N.I., Kojevnikov, A.D. (1983): Velocity of distribution of seismic waves and "paradox interval" of moisture content of disperse soils. Engineering and seismological bases of detailed seismic region and seismic micro region. Tashkent, Fan, pp. 14-16. (in Russian)

Kriger, N.I. (1965): Loess and its properties and relationships to the environment. Moscow: Nauka, 296 pp. (in Russian)

Kuhlemeyer, R. L., Lysmer, J. (1973): Finite element method accuracy for wave propagation problems, Journal of the Soil Mechanics and Foundations Division, ASCE, Vol. 99, No. 5, pp. 421-427.

Lang, D. (2004): Damage potential of seismic ground motion considering local site effects. PhD thesis. Weimar, pp. 206

Larionov, A.K., Dolgaya, P.F. (1963): Dynamics of water dissolved components in relation to loess subsidence. Book Chapter: Construction of infrastructure on loess deposits. Voronezh. Izdatelsztvo Voronezhskogo Universiteta, 2, pp. 44-50 (in Russian)

Lee, E.M., Jones, D.K.C (2004): Landslide Risk Assessment.Thomas Telford Publishing, ASCE Press, London.
Lee, C.-T., Cheng, C.-T., Liao, C.-W. & Tsai, Y.-B. (2001): Site classification of Taiwan free-field strong motion stations. Bulletin of the Seismological Society of America 91, 5, pp. 1283-1297.

Li, T. (1989): Landslides: extent and economic significance in China. Proc. 28th Int.Geol.Congress, Balkema, Rotterdam, 271-288.

Lee, V.W., and Cao, H. (1989): Diffraction of SV waves by circular canyons of various depths, J. Eng.Mech., ASCE, 115(9), pp. 2035-2056.

Leonov, N.N., (1960): The Khait, 1949 earthquake and geological conditions of its occurrence. Izvestia of the Academy of Sciences of the USSR, Geophysical Series, 3, pp. 409–424. (in Russian).

Matalucci, R.V., Abdel-Hady, M., Shelton, J.W. (1970): Influence of microstructure of loess on triaxial shear strength. Engineering Geology, 4, pp. 341-351.

Matalucci, R.V., Shelton, J.W, and Abdel-Hady, M. (1969): Grain orientation in Vicksburg loess. Journ.Sed.Petrol., 39(3), pp. 969-979.

Mayes, R. L., Sharpe, R. L. (1981): Seismic Design Guidelines for Highway Bridges, Report No. FHWA/RD-081-081, Federal Highway Administration, Washington, DC.

Meng, X.M., Derbyshire, E., 1998. Landslides and their control in the Chinese Loess Plateau: models and case studies from Gansu Province, China. In: Maund, J.D., Eddleston, M. Eds.., Geohazards in Engineering Geology. Engineering Geology Special Publications, vol. 15, Geological Society, London, pp. 141–153.

Meng, X.M., Derbyshire, E. and Kemp, R.A. (1997): Origin of the magnetic susceptibility signal in Chinese loess. Quaternary Science Reviews, 16, pp. 833-839.

Milne, J. (1898): Seismology. Ed. 1, Kegan Paul, Trench, Truber, London.

Minetti, L. (2004): Kyrgyz Republic, Proposed natural disaster mitigation project. 1st IDA Preparation Mission, Mission report, Ministry of Environment and Emergency (MEE), Bishkek, 40 p. Unpublished.

Moore, F. A. (1992): Monitoring Building Structures. Blackie and Son Ltd, New York, USA, pp. 155

Münchner Rück (2009): Geo - Natural catastrophes 2008, Analyses, assessments, positions. - Knowledge Series, Number 302-06022, pp. 50.

Nadim, F., Kjekstad, O., Peduzzi, P., Herold, C. and Jaedicke, C. (2006): Global landslide and avalanche hotspots, Landslides, 3, pp. 159–173.

Newmark, N. (1965): Effects of earthquakes on dams and embankments. Geotechnique, 15, pp. 137-160

Norrish, N.I. and Wyllie, D.C. (1996): Rock slope stability analysis, *in* A.K. Turner and R.L. Schuster, editors, *Landslides: Investigation and Mitigation*: Washington, D.C., Transportation Research Board Special Report 247, pp. 391-425.

Nyazov, R. A. (2003): Mudflows of Central Asia, Materials and Geo-environment, Vol.50, No.1, pp. 277-288.

Niyazov, R.A. (1981): Engineering and geological conditions of deposits in Urtaboz. In the Reports of Seismological Institute of Tajikistan. pp. 123-132. (in Russian)

Niyazov, R.A. (1974): Landslides in loess in south west part of Central Asia. Izdatelstvo "Fan", Uzbek SSR. Tashkent, pp. 148. (in Russian)

Papageorgiou, A.S., Kim, J. (1991): Study of the propagation and amplification of seismic waves in Caracas Valley with reference to the 29 July 1967 earthquake: SH Waves. Bulletin of the Seismological Society of America, 81, 6, pp. 2214-2233.

Parsons, R., Johnson, R., Brown, D., Dapp, S., Brennan, J. (2009): Characterization of loess for deep foundations. DFI Journal, 3 No.2, pp. 11-21.

Pecsi, M. (1994): A Landslide type occurring frequently along the loess bluff in the Hungarian Danube section. Quaternary International. 24, pp. 31-33.

Pliefke, T., Sperbeck, S.T., Urban, M., Peil, U., Budelmann, H. (2007): A Standardized Methodology for Managing Disaster Risk – An attempt to Remove Ambiguity. - 5th International Probabilistic Workshop, Ghent, 2007

Popescu, M.E.(1996): From landslide causes to landslide remediation. In K.Senneset (ed.), Landslide. Proc.7th Int. Symp. on Landslides, Trondheim.17-21 June, Rotterdam, Balkema, 1, pp. 75-96

Pye, K. (1995): The nature, origin and accumulation of loess. Quaternary Science Reviews, 14, pp. 653-667.

Razdolskyi, A.G. (1962): Engineering and geological properties of loess like soils in South Kyrgyzstan and methods against the channel deformation in steep slope relief. Academy of Sciences of Kyrg SSR, Frunze, pp. 313

Reports of meteorological station of Kyrgyz Republic (2003). (in Russian)

Richtofen (1877): China: Ergebnisse eigener Reisen und darauf gegründeter Studien. Reimer, Berlin, 5.

Roessner, S.,Wetzel, H.-U., Kaufmann, H., Samagoev, A. (2005): Potential of satellite remote sensing and GIS for landslide hazard assessment in Southern Kyrgyzstan (Central Asia), Natural Hazards, 35, 3, pp. 395-416.

Russell, R. J. (1944a): Lower Mississippi Valley loess. Geological Society of America, Bulletin, 55, pp. 1-40.

Sanchez-Sesma, F. J. (1987a): Site effects on strong ground motion, Soil Dynamics and Earthquake Engineering. 6, pp. 124-132.

Sariosseiri, F., Muhunthan, B., (2009): Effect of cement treatment on geotechnical properties of some Washington State soils: Engineering Geology, 104, pp. 119–125.

Sassa, K., Canuti, P. (2009): Landslides – Disaster Risk Reduction. –Springer Verlag, Berlin Heidelberg 2009.

Sassa, K., Fukuoka, H., Scarascia - Mugnozza, G., Evans, S (1996): Earthquake induced landslides: distribution, motion and mechanisms. Special issue for the great Hanshin Disaster, Soils and Foundations, pp. 53-64.

Sassa, K. (1988): Geotechnical model for the motion of landslides. Special Lecture of 5th International Symposium on Landslides, "Landslides", 1, pp. 37-55

Sassa, K. (1986): The mechanism of debris flows and the forest effect on their prevention. Proc.18th IUFRO World Congress, Div.1, 1, pp. 227-238.

Seed, H. B., Idriss, I. (1969): Influence of Soil Conditions on Ground Motion during Earthquakes, *J. Soil Mech. Found., Div. ASCE*, *95*, pp. 99-137.

Sepulveda, S.A., Murphy, W., Jibson, R.W., Petley, D.N. (2005): Seismically induced rock slope failures resulting from topographic amplification of strong ground motions: The case of Pacoima Canyon, California. Engineering Geology, 80, pp. 336-348.

Schermatov, M.S. (1971): Engineering and geological properties of loess in Chatkal mountain area. Academy of Sciences Uzbek SSR, Tashkent. (in Russian).

Schlögel, R. (2009): Detection of recent landslides in Maily-Say Valley, Kyrgyz Tien Shan, based on field observations and remote sensing data. Travail de fin d'études, Université de Liège, Liège, non publié, pp. 165

Schmertman, J.H. (1976): Measurement of in-situ shear strength. Proceedings of the conference on in-situ measurement of soil properties. American society of civil engineers, New York, pp. 57-137.

Sheeler, J. B. (1968): Summarization And Comparison Of Engineering Properties Of Loess In The United States. Conference On Loess: Design And Construction. Highway Research Record 212. Highway Research Board. Washington, DC, pp. 1-9

Smalley, I.J., Leach, J.A. (1978): The origin and distribution of the loess in the Danube Basin and associated regions of east- Central Europe- A review. Sedimentary Geology, 21, pp. 1-26

Smalley, I.J. (1966): The properties of glacial loess and the formation of loess deposits. Journal of Sedimentary Petrology, 36, pp. 669-676.

Soeters, R., van Westen, C. J. (1996): Slope Instability Recognition, Analysis and Zonation. Turner A.K.; Shuster R.L. (eds) Landslides: Investigation and Mitigation. Transp. Res Board, Spec Rep 247, National Academy Press, Washington, D.C. pp 129 - 177.

Spudich, P., Hellweg, M and Lee, W.H.K. (1996): Directional topographic site response at Tarzana observed in aftershocks of the Northridge, California, earthquake: implications for mainshock motions. Bulletin of the Seismological Society of America, 86, p.193-208

Stewart, J.P., Chiou, S.J., Bray, J.D., Somerville, P.G., Graves, R.W. and Abrahamson, N.A. (2001): Ground motion evaluation procedures for performance based design, Report. No. PEER-2001/09, Pacific Earthquake Engineering Research Center, University of California, Berkeley, pp. 229.

Strokova, L.A., (2003): Characteristics of loess deposits in Tomsk region. Izvestiya of Tomsk politechnical University, 306, 6. (in Russian).

Strom, A. L., Korup, O., Havenith, H. B., Abdrachmatov, K. E. (2006): Extremely large rockslides and rock avalanches in the Tien Shan Mountains, Kyrgyzstan. *Landslides* 3, pp. 125-136.

Strom, A. L., Abdrakhmatov, K. (2004): Rock avalanches and rockslide dams of the northern Kyrgyzstan (Kyrgyz range and Chon-Kemin river valley). Field excursions guidebook, NATO advanced research workshop, security of natural and artificial rockslide dam. Moscow, pp. 26

Strom, A.L. (1996): Some morphological types of long-runout rockslides: effect of the relief on their mechanism and on the rockslide deposits distribution. K. Senneset (Ed.) Landslides. Proc. of the Seventh International Symposium on Landslides, 1996, Trondheim, Norway, Rotterdam, Balkema, pp. 1977-1982.

Sun, P., Peng, J-B., Chen, L-W., Yin,Y-P., Wu,S-R. (2009): Weak tensile characteristics of loess in China – An important reason for ground fissures. Technical note. Engineering geology 108. pp. 153-159.

Sun, J. (1988): Environmental geology in Loess areas of China. Environ. Geol. water sci.,12,1, pp. 49-61

Tan, T.K. (1988): Fundamental properties of loess from northwestern China. Engineering Geology, 25, pp. 103-122.

Terzaghi, K. and Peck, R.B. (1967): Soil mechanics in Engineering Practice, 2nd edition. John Wiley, New York.

Torgoev, I. A., Alioshin Y.G., Havenith H.B. (2002): Impact of uranium mining and processing on the environment of mountainous areas of Kyrgyzstan. In: Merkel, Planer-Friedrich and Wolkersdorfer (eds) Uranium in the aquatic environment. Springer, Berlin Heidelberg New York, pp. 93–98.

Torgoev, I. A., Alioshin, Y. G., Moldobekov, B., Meleshko, A. (1999): Genetic factors of the development of landslides in the Maili-Suu river basin. In: Questions of Geomechanics and Reprocessing of Deposits of Mineral Resources, Ilim, Bishkek. (in Russian).

Trifunac, M.D., Todorovska, M.I. (1998): Amplification of ground motion and damage patterns during the 1994 Northridge, California, Earthquake, proc. ASCE Specialty Conf. on Geotechnical Earthquake Eng. and Soil Dynamics, Seattle, Washington, *Geotech.Special Publ*.No.75, ASCE, 1, pp. 714-725.

Trifunac, M.D. (1980): Effects of site geology on amplitudes of strong motion. Proceedings of Seventh World Conference on Earthquake Engineering, Vol. 2, pp. 145-152.

Vandenhove, H.Q.H., Clerc, J-J., Lejeune, J-M., Sweeck, L., Sillen, X., Mallants, D. and Zeevaert T. (2003): Final report in frame of EC-TACIS Project N°SCRE1/N°38 remediation of uranium mining and milling tailing in Mailuu-Suu District Kyrgyzstan. Mol (Belgium), pp. 614p, unpublished.

UN University News Release (2006): Landslides.-News Release, January 18, 2006, http://www.unu.edu/media/archives/2006/files/mre01-06.pdf

UNISDR (2009): UNISDR Terminology on Disaster Risk Reduction (2009). – United Nations, International Strategy for Disaster Reduction, http://www.unisdr.org/eng/terminology/UNISDR-terminology-2009-eng.pdf

Varnes, D.J. (1978): Slope movement types and processes. In Schuster, R.L.(ed), Landslides: Analyses and control, National Academy of Sciences, pp. 11-33.

Wang, M., Bai, X. (2006): Collapse property and microstructure of loess. Unsaturated soil, seepage and environmental geotechnics, ASCE.

Wang, L., He, K., Shi, Y., Wang, J. (2006): Study on liquefaction of satured loess by in-situ explosion test. Earthquake Engineering and Engineering Vibration, 1, 1, pp. 50-56.

Wang ,L., He, K., Shi, Y., Wang, J. (2002): Study on liquefaction of saturated loess by in-situ explosion test. Earthquake engineering and engineering vibration, Vol.1. No.1, 50-56

World Bank report: Disaster Risk Management Notes for Priority Countries 2009-2015, Europe and Central Asia, pp. 48-52

Xia, J., Han, A. (2009): Cyclic variability in microstructure and physical and mechanical properties of the Xiashu Loess - palaeosol sequence in Nanjing, China. Engineering Geology 104, pp 263-268.

Xia, J. (2005): Soil-rock forming processes and engineering mechanical properties of the ancient gravel stratum near nanjing, China. Engineering Geology, 78, pp 209-214

Xia, J., Huang,G-L., Yan,S-B. (2006): Behaviour and engineering implications of recent floodplain soft soil along lower reaches of the Yangtze River in Western Nanjing, China. Engineering Geology, 87, 1-2, pp. 48-59

Yin,Y., Wang, F., Sun,P. (2009): Landslide hazards triggered by the 2008 Wenchuan earthquake, Sichuan, China. Landslide,6, 2, pp.139-152.

Ying, J., Liao, H., Yin, J. (2006): An experimental study on the shear strength of undisturbed Loess. Unsatured soil, seepage and Environmental Geotechnics (GSP 148), pp.127-135.

Zhang, Z., Wang, L. (1995): Geological disasters in loess areas during the 1920 Haiyuan earthquake, China. Geojournal, 36. 2/3, pp. 269-274

Zhang, D., Wang, G. (2007): Study of the 1920 Haiyuan earthquake - induced landslides in loess (China). Engineering Geology, 94, pp. 76-88

Zhang, D. A. (1996): A study of the mechanism of loess landslides induced by earthquakes. Journal of Natural disaster science, 18, 1, pp. 27-41.

Zhang, Z., Wang, L. (1995): Geological disasters in Loess areas during the 1920 Haiyuan Earthquake, China. Geo-Journal 36, 3, pp. 269-274.

Zhao, C., Yang, Z., Gao, F., Zhang, Y. (2005): Influential factors of loess liquefaction and pore pressure development. Acta Mech. Sinica 21, pp. 129-132.

Zhang, M. and Lui, J. (2009): Controlling factors of loess landslides in western China. Environmental Earth Sciences, 59, 8, pp. 1671-1680.

Zerkal, O.V., Zolotarev, V. (1996): Mechanism of formation and development of deep seismogeneous landslides due to sudden liquefaction of loessial soils. Landslides, Senneset (ed). Balkema Rotterdam. pp. 1055-1059

Zerkal, O.V. (1995): Influence of variability of strength parameters of loess in wet conditions to the landslide slope stability. Geological study and use of soil. Informative collection. pp.14-21. (in Russian).

Zerkal, O.V. (1994): Seismic landslides caused by Gissar earthquake in 1989 (Tajikistan). Geol. Bull. 49, 2, pp. 57-63

Web Links

United States Geological Survey, www.usgs.com

Dave's landslide blog, www.landslideblog.org